TECHNICAL UNIVERSITY OF MOLDOVA

JOURNAL OF ENGINEERING SCIENCE

Technical and applied scientific publication founded on 9 February 1995
Alternative title: Meridian ingineresc

2025
Vol. XXXII (1)

ISSN 2587-3474
eISSN 2587-3482

TECHNICAL UNIVERSITY OF MOLDOVA (PUBLISHING HOUSE)
„TEHNICA UTM" (PRINTING HOUSE)

According to the Decision of the NAQAER No. 12 from 23.02.2024, JES is classified as B+ journal

Main subjects areas of the Journal of Engineering Science:

A. Industrial Engineering

- Mechanical Engineering and Technologies
- Applied Engineering Sciences and Management
- Materials Science and New Technologies
- Electrical Engineering and Power Electronics
- Energy systems
- Light Industry, New Technologies and Design
- Industrial and Applied Mathematics
- Vehicle and Transport Engineering

B. Electronics and Computer Science

- Electronics and Communication
- Microelectronics and Nanotechnologies
- Biomedical Engineering
- Computers and Information Technology
- Automation

C. Architecture, Civil and Environmental Engineering

- Architecture, Urbanism and Cadaster
- Civil Engineering and Management
- Energy Efficiency and New Building Materials
- Environmental Engineering

D. Food Engineering

- Food Technologies and Food Processes
- Food Industry and Management
- Biotechnologies, Food Chemistry and Food Safety
- Equipment for Food Industries

The structure of the journal corresponds to the classification of scientific publications: ***Engineering, Multidisciplinary.***

How to publish a paper:

1. Send the manuscript and information about the author to the **Editorial Board address:** jes@meridian.utm.md
2. Manuscripts are accepted only in English, by e-mail, in template file (www.jes.utm.md)
3. After a review, you will be notified of the editorial board's decision.
4. After the Journal has been published, we will send it to you immediately by mail.

Editor-in-Chief
Dr. hab. prof. univ. Viorel BOSTAN
Technical University of Moldova
viorel.bostan@adm.utm.md

Editorial Board

Responsible Editor
Dr. hab. Rodica STURZA
Editorial Board address: jes@meridian.utm.md

Editorial Production:
Dr. hab. Aliona Ghendov-Moșanu
Dr. Nicolae Trifan
Dr. Svetlana Caterinciuc
Dr. Rodica Cujba

CONTENT

CUPRINS

Journal of Engineering Science *Vol. XXXII, no. 1 (2025), pp. 7 - 17*
Fascicle *Industrial Engineering* *ISSN 2587-3474*
Topic *Electrical Engineering and Power Electronics* *eISSN 2587-3482*

https://doi.org/10.52326/jes.utm.2025.32(1).01
UDC 621.314.57

LINEAR AND NON-LINEAR VOLTAGE-TO-FREQUENCY MULTI-ZONE CONTROL OF SYNCHRONOUSLY MODULATED POWER ELECTRONIC INVERTERS

Valentin Oleschuk*, ORCID: 0000-0002-7413-4867,
Irina Vasiliev, ORCID: 0000-0003-3996-6745

Institute of Power Engineering of Technical University of Moldova, 5 Academy Str., Chisinau, Republic of Moldova
* Corresponding author: Valentin Oleschuk, *oleschukv@hotmail.com*

Received: 12. 14. 2025
Accepted: 01. 28. 2025

Abstract. The publication presents a brief analysis of the results from the study on power electronic converters based on voltage source inverters (VSIs) and neutral-point-clamped inverters (NPCIs) with scalar control modes implemented by algorithms of synchronous multi-zone pulsewidth modulation (SMZ PWM). This control and modulation strategy can provide both linear and required non-linear relationships between the output voltage and the fundamental frequency of the inverters (Voltage/Frequency (V/F)). The simulation results demonstrated the behavior of two inverter-based drive systems controlled by algorithms of SMZ PWM, providing both linear and non-linear V/F relationships. Thus, the appropriately modified techniques of SMZ PWM, used for regulating inverters of adjustable speed electric drives, ensure continuous synchronization and symmetry of phase and line voltages in these electrical power conversion systems over the entire regulation range.

Keywords: *pulsewidth modulation, variable-voltage variable-frequency drive, voltage source inverter, voltage spectrum.*

Abstract. Publicația prezintă o scurtă analiză a rezultatelor studiului convertoarelor electronice de putere bazate pe invertoare cu sursă de tensiune și invertoare cu fixare în punct neutru cu moduri de control scalar implementate prin algoritmi de modulație sincronă a lățimii de impuls multi-zonă. Această strategie de control și modulare poate oferi atât relații liniare, cât și neliniare necesare între tensiunea de ieșire și frecvența fundamentală a invertoarelor. Rezultatele simulării au demonstrat comportamentul a două sisteme de acționări bazate pe invertor controlate de algoritmi de modulației multi-zonă sincronă, oferind atât relații liniare, cât şi neliniare între tensiunea de ieșire a invertoarelor şi frecvența fundamentală. Astfel, tehnicile de modulație multi-zonă sincronă modificate corespunzător, utilizate pentru reglarea invertoarelor de acționări electrice cu viteză reglabilă, asigură sincronizarea și simetria continuă a tensiunilor de fază și linie în aceste sisteme de conversie a energiei electrice pe întregul domeniu de reglare.

Cuvinte cheie: *invertor sursă de tensiune, modulație de lățime a impulsurilor, acționări electrice reglabile, spectru de tensiune.*

1. Introduction

Power electronic converters of electrical energy parameters based on power transistors are widely used installations in modern electrical and energy systems [1].

One of the most important areas of application of inverter-based power conversion systems are variable-frequency electric drives with asynchronous electric motors [2–3]. It is known that the control modes of inverters of variable frequency drives in many cases are carried out according to the linear law of constancy of the ratio of the output voltage of the converter to the fundamental frequency of the system (*Voltage/Frequency = const* or *V/F = const*) [4-9]. Therefore, these control modes can be implemented using control boards based on dSpace [5], using systems controlled by space-vector pulse-width modulation (PWM) algorithms for determining pulse patterns of control signals [7]. Also, these modes can be implemented using control and regulation systems based on programmable logic arrays (FPGAs) [8], as well as control systems with optimally tuned PI controllers [9]. Figure 1 shows the corresponding diagram showing the linear *V/F* relationship between the nominal output voltage of the inverter and its operating frequency [4].

It is also known that for some specialized frequency-controlled electric drives with specific operating conditions, more efficient regulation of systems can be ensured by scalar control modes with non-linear Voltage-to-Frequency adjustment (with nonlinear *V/F* regulation modes) [10-11].

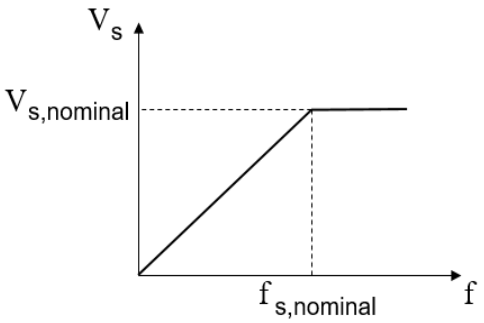

Figure 1. *V/F* linear regulation during scalar control regime of VSI [4].

At the same time, for power conversion systems based on inverters with increased power levels, it is necessary to ensure the symmetry of the output voltage waveform of the drive inverters in order to eliminate unwanted sub-harmonics (of the fundamental frequency) from the output voltage and current spectra of the inverters [12].

Thus, for continuous synchronization of voltage in PWM inverters of drive systems, as well as for providing improved harmonic composition of output voltage, specialized PWM methods and techniques were investigated [13-25]. These methods and techniques were based both on the standard space-vector approach to determining the pulse sequences of inverter control signals [13,15,17,19,21-23,25], and on a new multi-zone control strategy for modulated inverters (based on the method of synchronous multi-zone pulse-width modulation (SMZ PWM)) [14,16,18,20,24]. In particular, the developed methods and techniques of synchronous modulation have found application for controlling three-phase [13], five-phase and split-phase [14] PWM inverters of motor drives, Also, the developed algorithms of synchronous PWM have found application for controlling medium-power inverters with low switching frequency [15], six-phase inverters of vehicle drives [16], three-level inverters [17], and drive systems based on quadruple inverters [18].

In addition, in terms of high-power motor drive systems, the corresponding synchronous PWM methods and techniques have been widely used to control traction

inverters [19], fixed-neutral-point power inverters [20], as well as medium-voltage inverters [21]. Also, methods of synchronous PWM have been used to control dual inverters of electric vehicles [22], inverters with vector control modes [23], multi-inverter drive systems [24], and power inverters for traction motor drives [25].

It is necessary to mention, that not only linear *V/F* control modes have been analyzed in the mentioned above papers, but also some non-linear control regimes of inverter-based system have been investigated in [18].

Accordingly, this paper presents the results of a study of two promising topologies of variable frequency electric drives: split-phase motor drive based on six-phase voltage source inverter (VSI), and dual neutral-point-clamped inverters (NPCIs) of drive system with two stator windings of induction motor. Both these topologies are regulated by a modernized scheme of SMZ PWM that assures continuous voltage synchronization and both linear and non-linear *V/F* control relationships over the entire adjustment range.

2. Linear *V/F* control of VSI with SMZ PWM

Figure 2 shows structure a three-phase VSI feeding the corresponding induction machine IM. Voltage space vectors (six switching vectors 1 - 6 and two zero vectors 0 and 7) are also shown in Figure 2 [24].

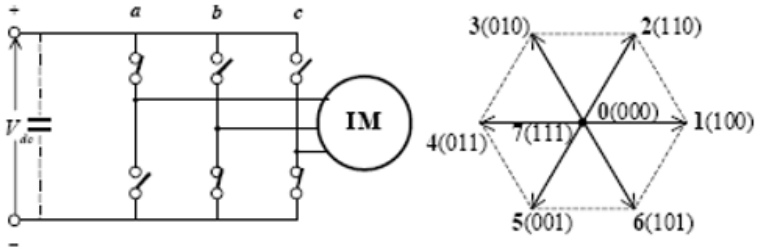

Figure 2. Structure of three-phase VSI feeding asynchronous induction motor IM, and voltage space vectors of three-phase inverter.

Figure 3 shows (inside the 60^0 clock-cycle) diagrams of sequence of switchings, and the pole and line voltages of modulated VSI adjusted by algorithm of continuous SMZ PWM, insuring synchronization and symmetry of the output voltage of VSI for scalar control mode of system [24].

The principle of voltage synchronization in a three-phase VSI is based on continuous synchronization of the positions of the central control signals at the centers of 60-degree clock intervals. Simultaneously, symmetrical formation of the remaining control signals around the corresponding central signal has to be provided.

The scheme of SMZ PWM includes a step-by-step determination of the boundary frequencies F_i and F_{i-1} as a function of the duration of clock subintervals τ, which are transition frequencies between control sub-ranges [24]. Figure 4 presents a generalized diagram for determining the parameters (durations and temporary position) of control signals (control pulses, see Figure 3) of VSI regulated by SMZ PWM in relation to scalar *V/F = const* operating mode [24].

As it follows from the generalized diagram for determining the parameters of control signals of a three-phase VSI shown in Figure 4, one of the main control signals of the scheme of SMZ PWM is the central signal β_1 in the middle of the 60-degree clock intervals (see Figure 3), determined as a function of the modulation coefficient *m* of VSI as $\beta_1 = 1.1m\tau$ for the scalar control regime of the system according to the law of constancy of the ratio of voltage to frequency (*V/F = const*) [24].

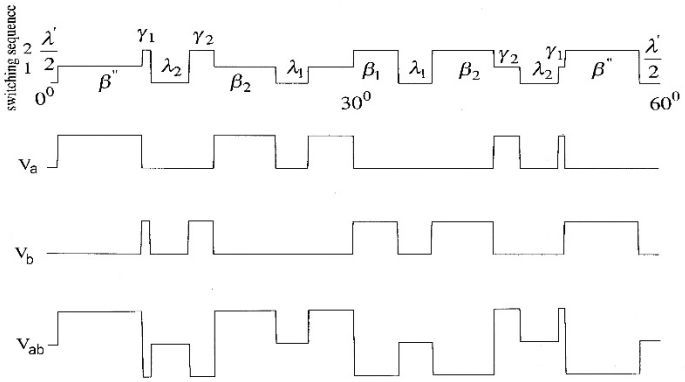

Figure 3. Switching sequence of VSI regulated by SMZ PWM, and pole and line voltages V_a, V_b, and V_{ab} inside the 60^0 clock interval.

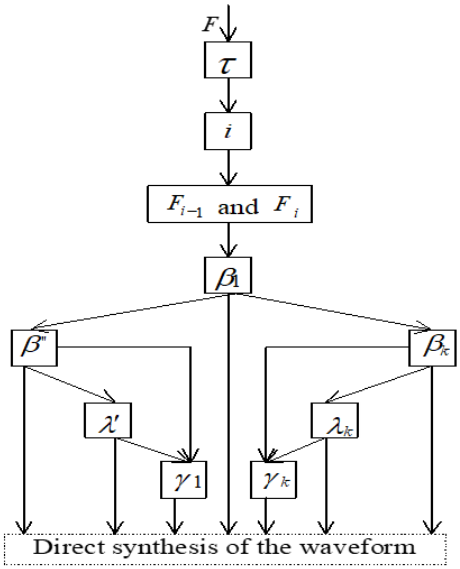

Figure 4. Generalized diagram for determining the parameters of control pulses of VSI adjusted by SMZ PWM.

As an illustration of operation of three-phase VSI PWM during *V/F = const* control regime, Figures 5 and 6 present waveforms of the pole voltages V_a, V_b, V_c, and line voltage V_{ab} of VSI with algorithms of continuous (Figure 5) and discontinuous (Figure 6) SMZ PWM.

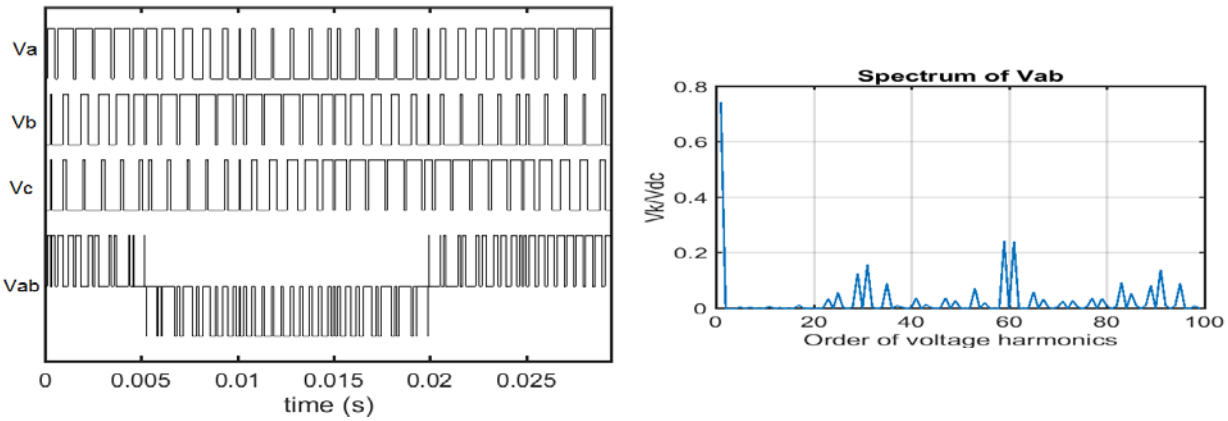

a) b)

Figure 5. Voltage waveforms of VSI with continuous SMZ PWM (a), and spectrum of the line voltage V_{ab} (b) ($F = 35.0$ *Hz*, $m = 0.70$, $F_s = 1.00$ *kHz*).

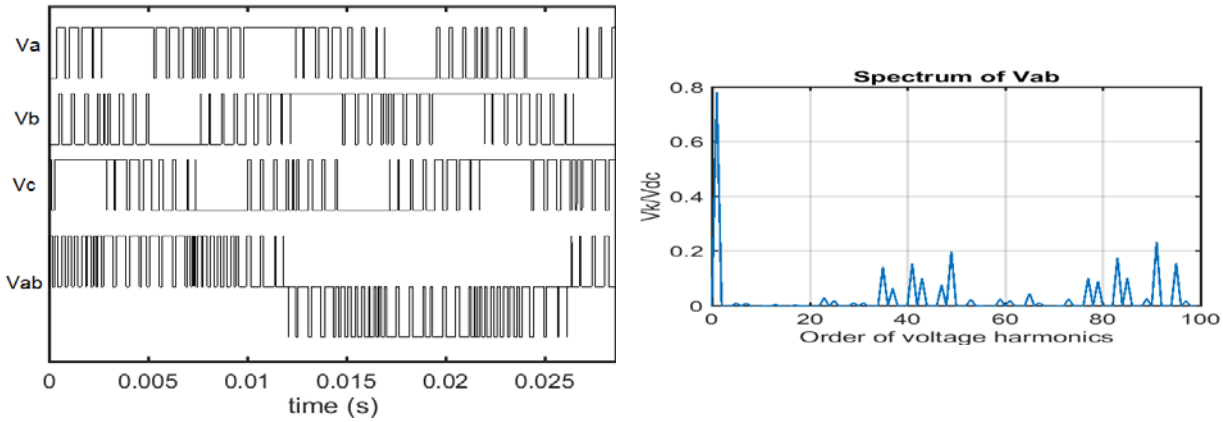

a) b)

Figure 6. Voltage waveforms of VSI with discontinuous SMZ PWM (a), and spectrum of the line voltage V_{ab} (b) ($F = 35.0$ *Hz*, $m = 0.70$, $F_s = 1.00$ *kHz*).

3. Non-linear Voltage-to-Frequency control of VSI-based drive installations

As shown in [18], a specialized nonlinear change of value of the β_1-signal as a function of the modulation coefficient *m* of VSIs makes it possible to provide various nonlinear relationships between the magnitude of the output voltage of VSIs and the fundamental frequency of system during the regulation process. Such nonlinear laws and algorithms for controlling converter systems for variable-frequency electric drives make it possible to ensure the effective operation of specialized adjustable speed ac drives with specific loads and special control modes [10-11].

In particular, Table I shows the basic control parameters for three examples of control modes of drive systems, including the standard scalar linear control mode *V/F = const*, as well as two non-standard (non-linear) control modes $V^2/F = const$ and $V^{3/2}/F = const$ [18]. The last two modes are characterized by nonlinear relationships between voltage and frequency and can be used to control asynchronous electric drives with some special types of loads [11]. Table I also includes the corresponding relative values of the two overmodulation threshold frequencies F_{ov1} and F_{ov2} [18], which are important parameters of the control strategy in the overmodulation control zone of inverters.

Table 1

Basic control parameters for both linear and non-linear synchronous regulation of VSI-based drives

Control regime	Central control signal β_1	Overmodulation frequency F_{ov1}	Overmodulation frequency F_{ov2}
V/F=const	$1.1m\tau$	$0.907F_m$	$0.952F_m$
$V^2/F=const$	$1.1\sqrt{m}\tau$	$0.823F_m$	$0.907F_m$
$V^{3/2}/F=const$	$1.1\sqrt[3]{m^2}\tau$	$0.866F_m$	$0.931F_m$

Note: β_1 – width of the central control signal; F_{ov1} – the first threshold overmodulation frequency; F_{ov2} – the second threshold overmodulation frequency; F_m – the maximum operating frequency; *m* – modulation index of inverter; τ – width of sub-cycle; *V* –output voltage of inverter; *F* – output frequency of inverter.

Figure 7 shows the dependence of the normalized output voltage of a three-phase VSI on the operating frequency (at the maximum operating frequency of the system equal to $F_m = 50.0$ *Hz*) in relation to the three above-mentioned control modes presented in Table 1 [18]. In this case, it is also possible to implement various numerous intermediate control regimes,

characterized by other functional dependencies for determining the duration of the β_1-signals. As an example, dotted line in Figure 7 shows the non-linear *Voltage/Frequency* ratio of drive system in the process of regulating the fundamental frequency according to the law $V^{4/3}/F = const$ [18].

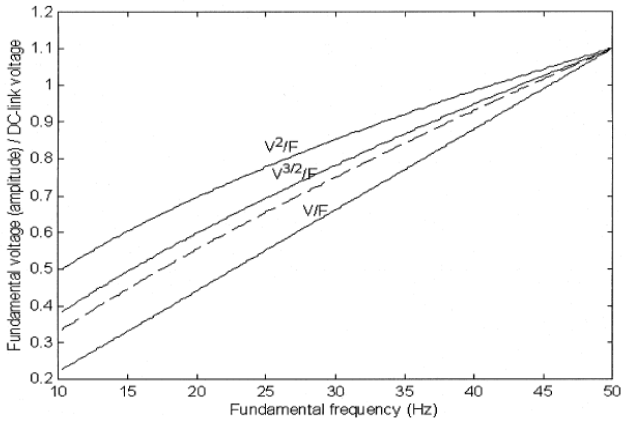

Figure 7. Non-linear and linear *Voltage-to-Frequency* control regimes.

Ones of the interesting and promising structures of drives currently are split-phase motor drives [14]. In this case, the asynchronous motor has two sets of windings, spatially shifted by 30 el. degrees with isolated neutral points N_{abc} and N_{xyz} (Figure 8 [14]). Its phase voltages V_{as} and V_{xs} are calculated using (1) – (2) [14]:

$$V_{as} = V_a - 0.333(V_a + V_b + V_c) \quad (1)$$

$$V_{xs} = V_x - 0.333(V_x + V_y + V_z), \quad (2)$$

where: V_a, V_b, V_c, V_x, V_y, V_z are the corresponding voltages at poles of six-phase VSI (see Figure 8).

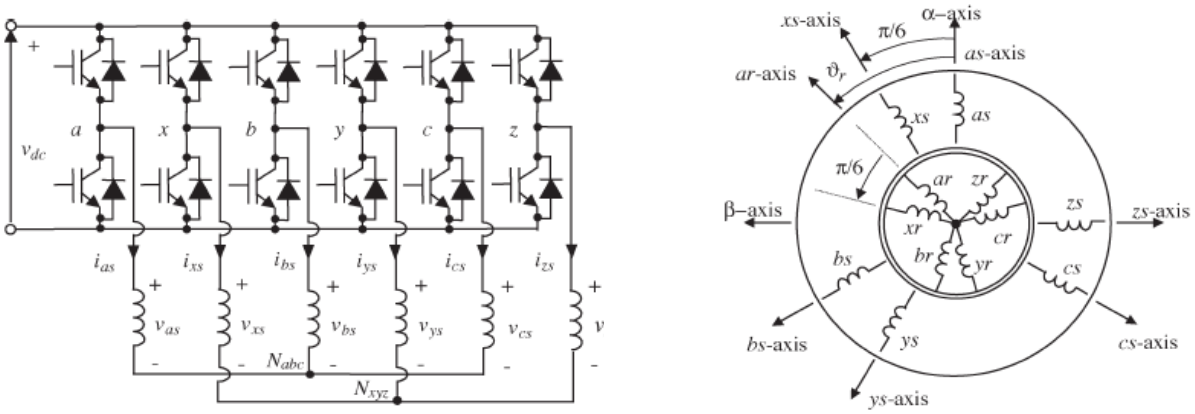

Figure 8. Split-phase electric drive with neutral points N_{abc} and N_{xyz}.

Figure 9 and Figure 10 show basic voltage waveforms of this installation, and spectral characteristics of the phase voltage in split-phase drive in a nonlinear system control mode according to the law $V^2/F = const$. The diagrams in Figure 9 show the base voltages and the phase voltage spectrogram for the system based on VSI controlled by continuous SMZ PWM (CPWM) algorithms. The diagrams in Figure 10 show the base voltages and the phase voltage spectrogram for the system with VSI controlled by discontinuous SMZ PWM algorithms with 30-degree intervals of the non-conducting state of the power switches (DPWM30). The

average switching frequency of VSI and the operating frequency of split-phase drive are 1050 Hz and 34 Hz, respectively.

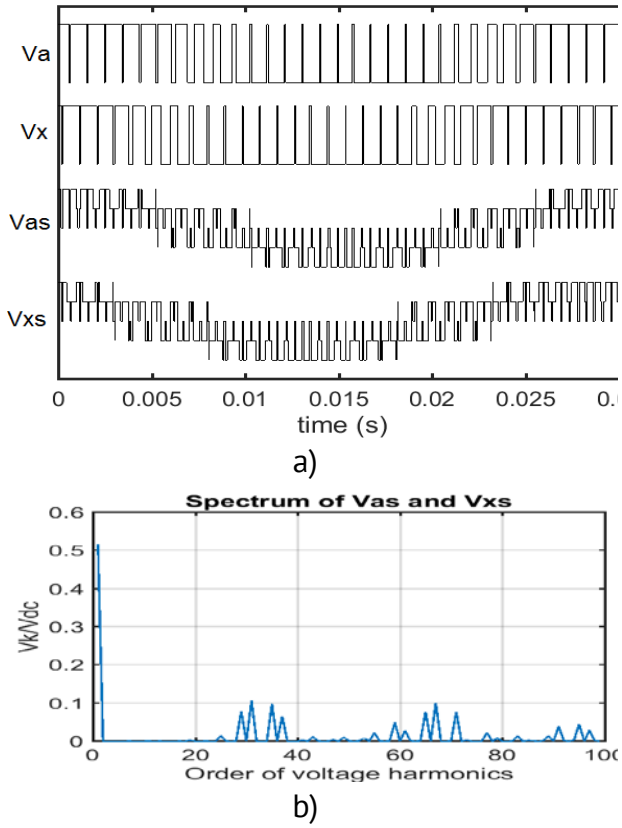

Figure 9. Waveforms of the pole and phase voltages (a), and harmonic composition of the phase voltage (b) (CPWM).

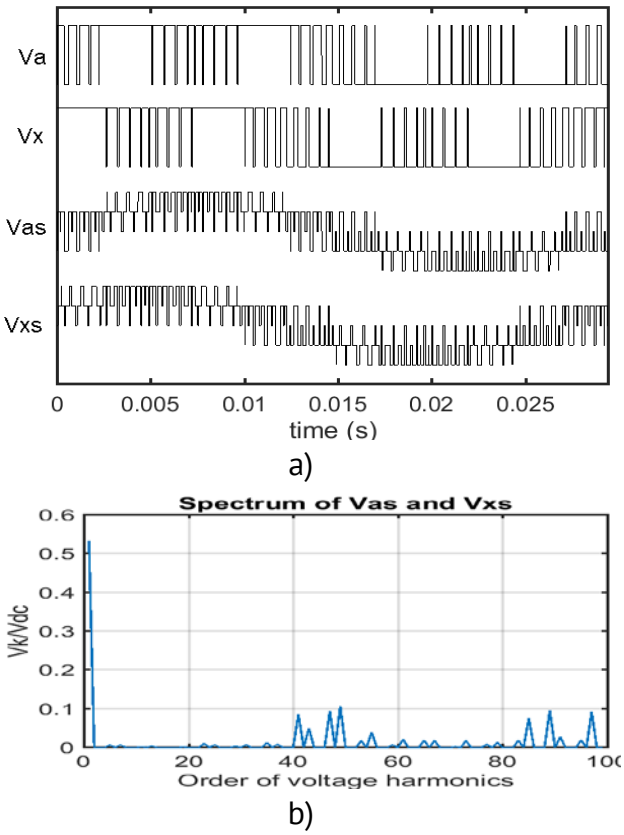

Figure 10. Waveforms of the pole and phase voltages (a), and harmonic composition of the phase voltage (b) (DPWM30).

Figure 11 shows the results of calculating the Weighted Total Harmonic Distortion factor of phase voltage Vas ( ) depending on the modulation index *m* of a six-phase VSI controlled by the above-mentioned algorithms of both synchronous continuous PWM and discontinuous PWM in the $V^2/F = const$ control mode, with VSI switching frequency equal to 1050.0 Hz.

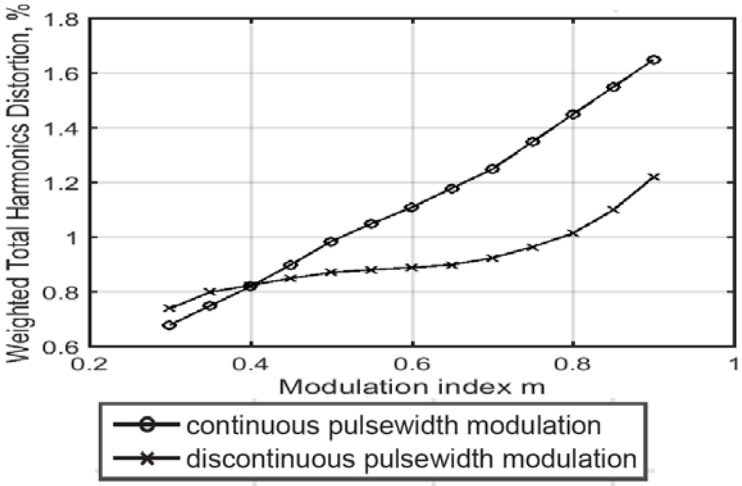

Figure 11. *WTHD* factor of the phase voltage V_{as} versus modulation index *m* of the inverter.

4. NPCI-based drive installation with two stator windings of induction motor and non-linear *V/F* control

Figure 12 shows the structure of a variable-frequency adjustable speed drive installation with two stator win-dings of an asynchronous motor, specially connected (see thick lines) to the corresponding outputs of two modulated NPC inverters NPCI1 and NPCI2 [20].

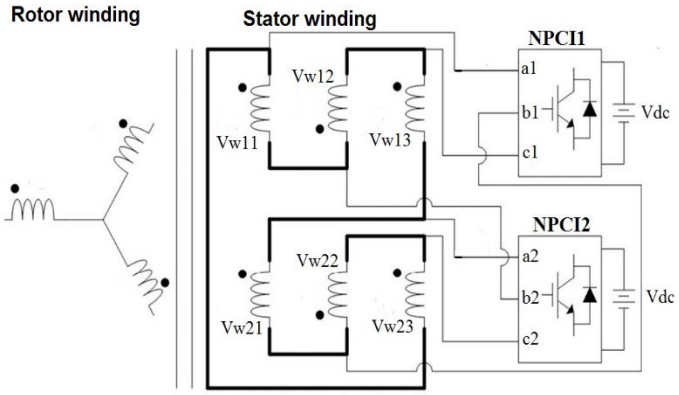

Figure 12. Topology of NPCI-based ac drive with two stator windings of electrical motor.

Instantaneous voltage values on the corresponding stator windings V_{w11} - V_{w13} and V_{w21} - V_{w23} of the electric drive (Figure 12) with specialized control scheme of NPCIs [20] are determined as functions of the corresponding pole voltages of NPCIs in accordance with (3) - (4):

$$V_{w11} = V_{a1} - V_{b2}, \quad V_{w12} = V_{b2} - V_{c1}, \quad V_{w13} = V_{c1} - V_{a2} \tag{3}$$

$$V_{w21} = V_{a2} - V_{b1}, \quad V_{w22} = V_{b1} - V_{c2}, \quad V_{w23} = V_{c2} - V_{a1} \tag{4}$$

Figures 13–14 show the main voltage waveforms and spectrograms of phase voltage in the variable frequency drive system with two stator windings of the electric motor (normalized values of pole and line voltages of the first inverter NPCI1 (V_{a1}, V_{b1} and V_{a1b1}), voltage on the stator winding of the electric motor V_{w11}, as well as the spectral composition of the voltage V_{w11}). This corresponds to the case of nonlinear regulation of NPCIs with SMZ PWM according to the control law $V^{3/2}/F = const$.

The diagrams presented in Figure 13 illustrate the process when the regulation of the NPCIs is carried out on the basis of a continuous scheme of SMZ PWM (CPWM). The diagrams presented in Figure 14 illustrate the process in the system when regulating the NPCIs is based on the algorithms of discontinuous SMZ PWM (DPWM). Features and peculiarities of both continuous and discontinuous schemes of SMZ PWM, applied for liner *V/F* control of NPCIs, are described in [20]. The operating frequency of drive installation is $F = 37$ *Hz*, the switching frequency of two NPCIs is equal to 1050.0 Hz.

The presented in Figures 13-14 results show that the winding voltage V_{w11} feeding electric motor has quarter-wave symmetry, and in its spectrum there are no even harmonics and subharmonics in the analyzed mode of nonlinear *V/F* regulation of drive installation.

Figure 15 shows the calculated Weighted Total Harmonic Distortion factor of the winding voltage V_{w11} ($WTHD = (1/V_{w11_1})(\sum_{k=2}^{1000}(V_{w11_k}/k)^2)^{0.5}$) depending on the modulation index m of NPCIs for the analyzed variable frequency drives with NPCIs, regulated in accordance with continuous (CPWM) and discontinuous (DPWM) versions of SMZ PWM. In this case, the system operated in the $V^{3/2}/F = const$ control mode (**mode 1**) and in the $V^2/F = const$ control mode (**mode 2**). Switching frequency of NPCIs is equal to 1050.0 Hz. The presented

data prove the fact that for the system regulated by non-linear *V/F* modes discontinuous scheme of SMZ PWM assures a better harmonic composition of the winding voltage compared to the continuous scheme of SMZ PWM, if $m = 0.60 \div 1.00$.

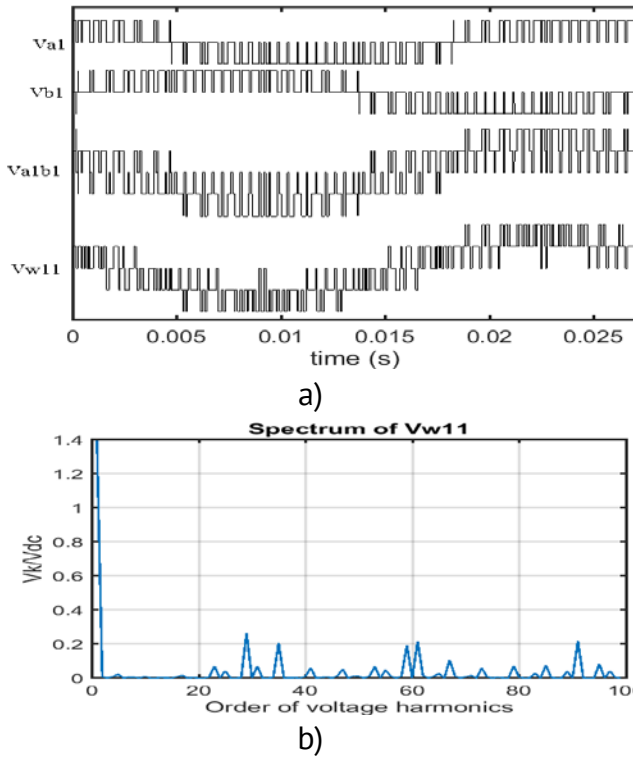

Figure 13. Voltages (a), and spectrum (b) of the V_{w11} voltage (CPWM).

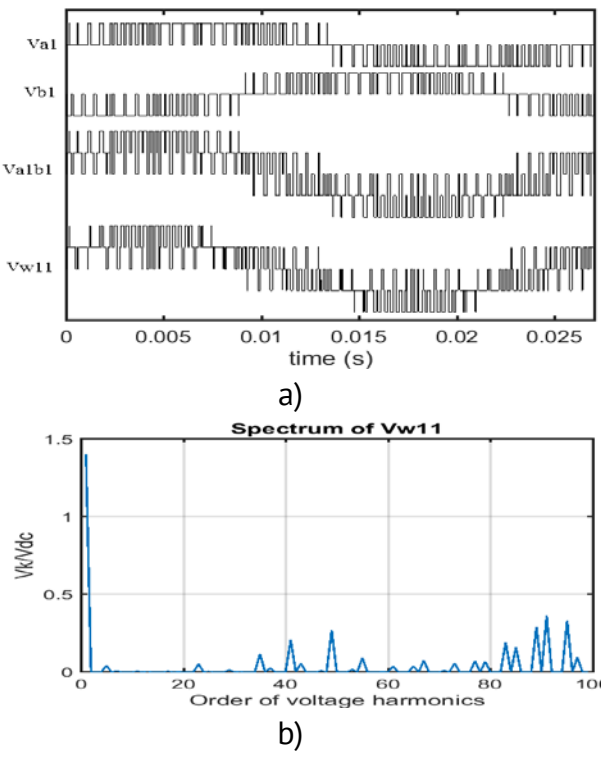

Figure 14. Voltages (a), and spectrum (b) of the V_{w11} voltage (DPWM).

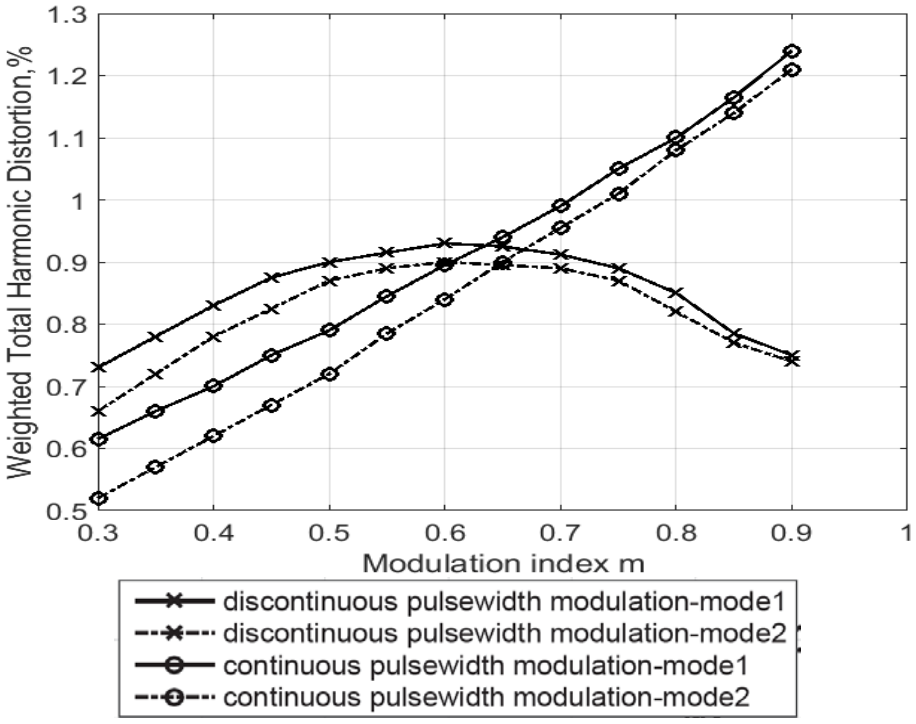

Figure 15. *WTHD* factor of the winding voltage V_{w11} versus modulation index *m* of two NPCIs adjusted by synchronous multi-zone pulsewidth modulation.

5. Conclusion

The modified scheme of SMZ PWM of VSIs and NPCIs of variable-frequency electric drives, applied for regulation of two topologies of inverter-based ac drives, makes it possible to provide control modes with the required non-linear relationships between the output voltage of inverters and the operating frequency of drive installations. In this case, the required voltage and frequency ratio is ensured by the corresponding smooth adjustment of the duration of the central (within 60-degree clock intervals) control signals of the VSIs and NPCIs, regulated by SMZ PWM.

Thus, modernized schemes and algorithms of SMZ PWM for regulation of VSI- and NPCI-based variable-frequency drives ensure continuous synchronization and symmetry of the basic voltages in apparatuses over the entire control range. The spectra of the base voltages of these installations do not contain even harmonics and subharmonics (of the operating frequency of the drive installations), which helps to reduce losses in the installations and increase their operating efficiency. And this is especially important for the medium-power and high-power adjustable speed drives.

Conflict of Interest: The authors declare no conflicts of interest.

References

1. Rodriguez, J.; Blaabjerg, F.; Kazmierkowski, M.P. Energy transition technology: The role of power electronics. *Proc. of the IEEE* 2023, 111 (4), pp. 329-334.
2. Ehsani, M.; Singh, K.V.; Bansal, H.O.; Mehrjardi, R.T. State of the art and trends in electric and hybrid electric vehicles. *Proc. of the IEEE* 2021, 109 (6), pp. 967-984.
3. Shetty, A.; Suryanarayana, K. Variable frequency and voltage control of induction motor for electric vehicles. *Advances in Renewable Energy and Electric Vehicles* 2022, pp. 449-463.
4. Pena, J.M.; Diaz, E.V. Implementation of V/f scalar control for speed regulation of a three-phase induction motor. In: *Proc. of* IEEE ANDESCON'2016, Arequipa, Peru, Oct. 2016, 6 p.
5. Tigade, C.; Sreejeth, M. Implementation of V/f adjustable speed drive for induction motor using dSPACE dS1104. In: *Proc. of IEEE Int'l Conf. on Power Electronics, Intelligent Control and Energy Systems* (ICPEICES'2018), 2018, Delhi, India, Oct. 2018, pp. 938-943.
6. Hussein, T.A. V/F control of three phase induction motor driven by VSI based on SVPWM. In: *Proc. of IEEE Int'l Conf. on Advance of Sustainable Engg. and its Appl.* (ICASEA'2021), Wasit, Iraq, Oct. 2021, pp. 49-53.
7. Waleed, U.; Waseem, M.; Shaukat, H.; Ali Ijaz, Almalaq, A.; Mohamed, M.A. An efficient FPGA based scalar V/f control mechanism of three phase induction motor for electric vehicles. In: *Proc. of IEEE Australasian Universities Power Engg. Conf.* (AUPEC'2021), Perth, Australia, Nov. 2021, 6 p.
8. Winslet, B.S.; Preethi, K.; Krishna, K.S.; Prasad, J.S.V. Performance of induction motor using V/F control technique. In: *Proc. of IEEE 2nd Mysore Sub Section Int'l Conf.* (MysuruCon'2022), Mysuru, India, Oct. 2022, 6 p.
9. Keskin, B.; Eminoglu, I. Optimally tuned PI controller design for V/f control of induction motor. In: *Proc. of Int'l Congress on Human-Computer Interaction, Optimization and Robotic Applications* (HORA'2022), Ankara, Turkey, June 2022, pp. 1-5.
10. Sruthi, M.; Nagamani, C.; Ilango, G.S, An improved algorithm for direct computation of optimal voltage and frequency for induction motors. *Engineering Science and Technology* 2017, 20 (5), pp. 1439-1445.
11. Graciola, C.L.; Goedtel, A.; Angélico, B.A.; Castoldi, M.F.; Costa, B.L.G. Energy efficiency optimization strategy for scalar control of three-phase induction motors. *Journal of Control, Automation and Electrical Systems* 2022, 33, pp. 1032–1043.
12. Mohan, N.; Undeland, T.M.; Robbins, W.P. *Power Electronics*, 3rd ed., John Wiley & Sons, Hoboken, New Jersey, USA, 2002, 832 p.
13. Beig, A.R. Constant *v/f* induction motor drive with synchronised space vector pulse width modulation. *IET Power Electron.* 2012, 5 (8), pp. 1446-1455.
14. Oleschuk, V.; Barrero, F. Standard and non-standard approaches for voltage synchronization of drive inverters with space-vector PWM: A survey. *International Review of Electrical Engineering* 2014, 9 (4), pp. 688-707.

15. Tripathi, A.; Narayanan, G. Evaluation and minimization of low-order harmonic torque in low-switching-frequency inverter fed induction motor drives. *IEEE Trans. Ind. Appl.* 2016, 52 (2), pp. 1477-1488.
16. Oleschuk, V.; Griva, G. Synchronised space-vector modulation for six-phase automotive drive with controlled switching frequency. *International Review of Electrical Engineering* 2009, 4(1), pp. 50-56.
17. Wei Chen, Haiwei Sun, Xin Gu, Changliang Xia. Synchronized space vector PWM for three level VSI with lower harmonic distortion and switching frequency. *IEEE Trans. Power Electron* 2016, 31(9), pp. 6428-6441.
18. Oleschuk, V., Sanjeevikumar, P.; Cernat, M.; Fedak, V.; Pastor, M. Multiphase quad-inverter system with feedforward synchronous PWM and nonlinear voltage regulation. In: *Proc. of IEEE Int'l Conf. on Power Electronics and Motion Control* (PEMC'2016), Varna, Bulgaria, Sept. 2016, pp. 1180-1185.
19. Xiao, L.; Li, J.; Xiong, Y.; Chen, J.; Gao, H. Strategy and implementation of harmonic-reduced synchronized SVPWM for high-power traction machine drives. *IEEE Trans. Power Electron* 2020, 35(11), pp. 12457-12471.
20. Oleschuk, V.; Vasiliev, I. Motor drive system with double-delta-sourced stator winding and two modulated NPC converters. In: *Proc. of IEEE Int'l Conf. 2020 KhPI Week on Advanced Technology,* Kharkiv, Ukraine, Oct. 2020, pp. 357-362.
21. Zhang, G.; Zhou, Z.; Shi, T.; Xia, C.L. An improved multi-mode synchronized space vector modulation strategy for high-power medium-voltage three-level inverter. *IEEE Trans. Power Electron* 2021, 36(4), pp. 4686-4696.
22. Linghao Wu, Jian Li, Yang Lu, Kun He. Strategy of synchronized SVPWM for dual three-phase machines in full modulation range. *IEEE Trans. Power Electron* 2022, 37(3), pp. 3272-3282.
23. Kumari, P.; Tripathi, A. Synchronized hybrid PWM for high power IM drives operated in vector control mode. In: *Proc. of IEEE IAS Global Conf. on Emerging Technologies* (GlobConET'2022), Arad, Romania, May 2022, pp. 999-1004.
24. Oleschuk, V.; Tirsu, M. Basic aspects of the theoretical and practical relevance of the method of synchronous multi-zone PWM for power inverters, In: *Proc. of IEEE Int'l Conf. on Electromechanical and Energy Systems* (SIELMEN'2023), Craiova – Chisinau, Romania – Moldova, Oct. 2023, 8 p.
25. Nevoloso, C.; Di Tommaso, A.O.; Miceli, R.; Scaglione, G.; Foti, S.; Testa, A. Impact analysis of FOC-based synchronous PWM strategy on traction induction motor drives performance. In: *Proc. of IEEE Int'l Conf. on Electrical Machines* (ICEM'2024), Torino, Italy, Sept. 2024, pp.1-7.

Citation: Oleschuk, V.; Vasiliev, I. Linear and non-linear voltage-to-frequency multi-zone control of synchronously modulated power electronic inverters. *Journal of Engineering Science*. 2025, XXXII (1), pp. 7-17. https://doi.org/10.52326/jss.utm.2025.8(2).01.

Submission of manuscripts: jes@meridian.utm.md

Journal of Engineering Science *Vol. XXXII, no. 1 (2025), pp. 18 - 31*
Fascicle *Electronics and Computer Science* *ISSN 2587-3474*
Topic *Computers and Information Technology* *eISSN 2587-3482*

https://doi.org/10.52326/jes.utm.2025.32(1).02
UDC 004.056:004.8

REDUCING CYBER RISK THROUGH A HUMAN–CENTRED APPROACH

Ludmila Peca *, ORCID: 0000-0002-4394-2933,
Dinu Ţurcanu, ORCID: 0000-0001-5540-4246

Technical University of Moldova, National Institute of Innovations in Cybersecurity,
168 Stefan cel Mare Blvd., Chisinau, Republic of Moldova
* Corresponding author: Ludmila Peca, *ludmila.peca@isa.utm.md*

Received: 12. 22. 2024
Accepted: 01. 29. 2025

Abstract. This paper investigates the complex challenges professionals face in managing cyber risks and implementing human risk management programs. Emphasizing the crucial role of human behavior in effectively mitigating cyber risks, the paper highlights the transformative impact of utilizing the „Golden Circle" methodology. This human-centered methodology initiates discussions with the question „WHY", articulating the fundamental purpose of human risk management and promoting an „inside-out" approach, starting with employee motivation and engagement. This approach ensures the sustainability of human risk management practices by fostering a sense of responsibility and belief in the mission. Furthermore, the integration of Artificial Intelligence (AI) is explored to enhance human risk management, with AI techniques such as machine learning analyzing behavioral patterns to predict potential risks and automate responses. However, the paper also addresses the drawbacks of AI, including sophisticated phishing attacks and deepfakes exploiting human vulnerabilities. Combining AI with the „Golden Circle" allows organizations to identify *why* employees are susceptible to attacks and *how* to tailor training, achieving a more robust and proactive risk management strategy. The paper offers tips and recommendations for evolving and sustaining this integrated methodology over time, ensuring its continued effectiveness in the dynamic cybersecurity landscape.

Keywords: *artificial intelligence, cybersecurity, „Golden Circle" method, security culture, educational programs, risk prediction.*

Rezumat. Această lucrare analizează provocările complexe cu care se confruntă profesioniștii în gestionarea riscurilor cibernetice și implementarea programelor de gestionare a riscurilor umane. Subliniind rolul crucial al comportamentului uman în atenuarea eficientă a riscurilor cibernetice, lucrarea evidențiază impactul transformator al utilizării metodologiei „Cercului de Aur". Această metodologie centrată pe om inițiază discuții cu întrebarea „DE CE", articulând scopul fundamental al gestionării riscurilor umane și promovând o abordare „din interior spre exterior", începând cu motivarea și implicarea angajaților. Prin cultivarea unui sentiment de responsabilitate și credință în misiune, această abordare asigură sustenabilitatea practicilor de gestionare a riscurilor umane. Mai mult, integrarea Inteligenței Artificiale (IA) este explorată pentru a îmbunătăți gestionarea riscurilor umane, cu tehnici de IA, cum ar fi

învățarea automată, care analizează modelele de comportament pentru a prezice potențialele riscuri și a automatiza răspunsurile. Cu toate acestea, lucrarea abordează, de asemenea, dezavantajele IA, inclusiv atacurile sofisticate de phishing și deepfakes care exploatează vulnerabilitățile umane. Combinarea IA cu „Cercul de Aur" permite organizațiilor să identifice *de ce* angajații sunt susceptibili la atacuri și *cum* să adapteze instruirea, realizând o strategie de gestionare a riscurilor mai robustă și proactivă. Lucrarea oferă sfaturi și recomandări pentru evoluția și susținerea acestei metodologii integrate de-a lungul timpului, asigurând eficacitatea sa continuă în peisajul dinamic al securității cibernetice.

Cuvinte cheie: *inteligență artificială, securitate cibernetică, metoda „Golden Circle", cultură de securitate, programe educaționale, predicția riscurilor.*

1. Introduction

In an era where cyber threats are becoming increasingly sophisticated and widespread, cyber risk management has evolved beyond the mere implementation of technological solutions. As organizations face ever more complex challenges, it is crucial to recognize the human factor's pivotal role in ensuring security. Cyber risks are no longer just a matter of technology but also human behavior and organizational culture. In this context, a people-centered approach to risk management becomes vital for long-term success.

In a digitalized era, the increasing dependence on the internet and global infrastructure exposes organizations to significant risks, including data theft, fraud, DDoS attacks, and the compromise of critical infrastructures. According to recent studies, attackers are employing increasingly sophisticated techniques such as social engineering, supply chain attacks, and zero-day exploits [1]. This underscores the necessity of integrating human-centered risk management strategies with technological advancements to effectively mitigate cyber threats.

2. A people-centered approach to risk management

Effective cyber risk management requires an approach that focuses on human behavior. Such an approach acknowledges that technology cannot provide a complete cybersecurity solution, no matter how advanced. The human factor, often the most vulnerable element in an organization, can also be the most powerful defense when properly engaged in the security strategy.

A clear example that demonstrates the impact of the human factor on cybersecurity is the attack on Colonial Pipeline fig. 1, where the compromise of a VPN account without multifactor authentication led to a major ransomware attack. This incident disrupted fuel supply across the U.S., highlighting the need for improved human risk management and the use of methods such as the 'Golden Circle' to enhance employee awareness.

For the authors of this article, the topic is particularly relevant as they are in the process of forming the team for the National Institute of Innovations in Cybersecurity „CYBERCOR". At this critical stage, integrating a people-centered approach is essential to ensure that the team not only adopts the best security practices but also understands the importance of human behavior in protecting the organization against cyber threats. By forming a team that is aware of the significance of the human factor and capable of implementing security strategies tailored to this reality, the National Institute of Innovations in Cybersecurity „CYBERCOR" aims to become an innovative leader in the field of cybersecurity.

Figure 1. Distribution and financial impact of insider threats [1].

To further strengthen this approach, aligning with established security standards is crucial. One such reference model for incident management is **ISO/IEC 27035:2023** [2], which provides a structured framework for identifying and responding to security incidents. By integrating this standard with the **Golden Circle methodology** [3], organizations can develop a more effective strategy for managing human-related cybersecurity risks [4]. This ensures not only a reactive but also a proactive approach to handling security threats.

To effectively address these challenges, it is essential to identify common human vulnerabilities in cybersecurity and explore how AI-driven solutions can mitigate these risks. Table 1 provides an overview of key human-related security weaknesses and the corresponding AI-based solutions that can enhance cybersecurity resilience.

Table 1

Addressing human vulnerabilities in Cybersecurity with AI solutions

Human vulnerability	Impact	AI solution proposed
Lack of multifactor authentication	Ransomware attacks and data breaches	AI-driven contextual authentication
Phishing and social engineering	Data leaks, financial fraud	AI-based anomaly detection in emails
Unauthorized access	Extraction of critical data	AI-powered access monitoring
Misconfiguration errors	Exploitable security vulnerabilities	AI-assisted configuration validation

In addition to addressing human vulnerabilities through AI-driven solutions, organizations must implement a structured incident response process to mitigate security risks effectively. The **Incident Handling Lifecycle** provides a systematic approach to managing cybersecurity incidents, ensuring a rapid and coordinated response to potential threats.

The **Incident Handling Lifecycle** consists of several key phases, each contributing to the containment, eradication, and prevention of cyber threats:

- **Detection & Identification**. Identifying potential security incidents through monitoring, anomaly detection, and user reports.
- **Triage & Prioritization**. Assessing the severity and impact of the incident to allocate resources effectively.

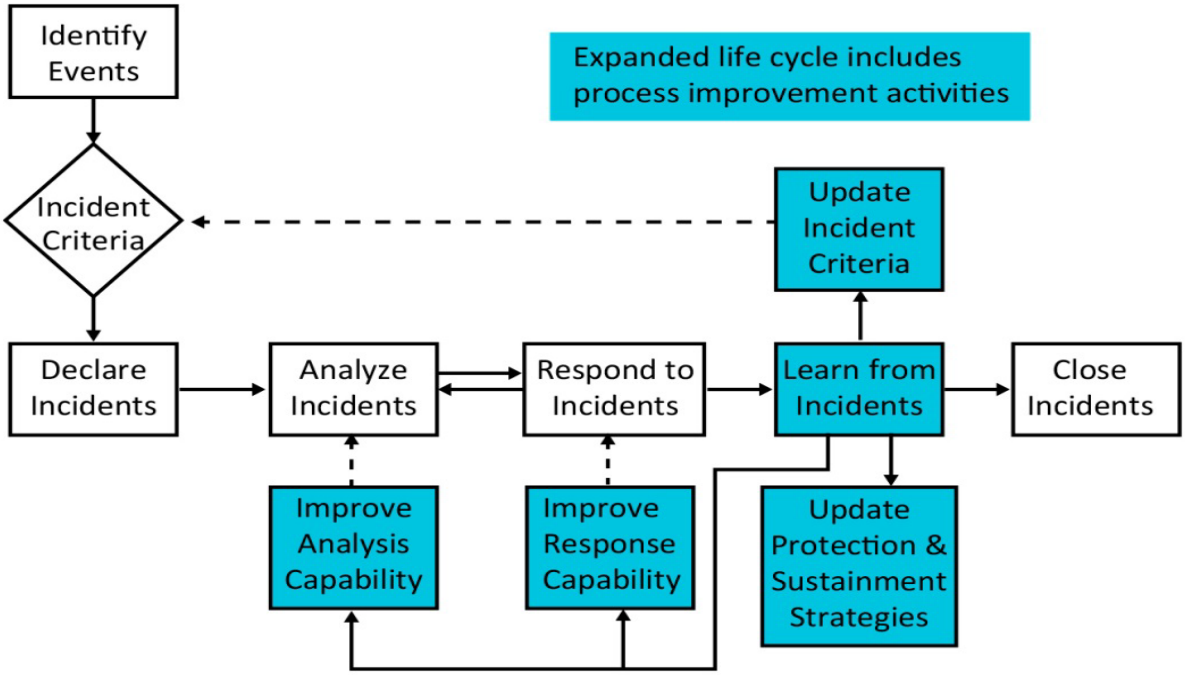

Figure 2. Expanded incident handling Lifecycle including process improvement activities [5].

- **Containment**. Implementing immediate measures to prevent further damage, such as isolating affected systems.
- **Eradication & Recovery**. Removing the threat, restoring affected systems, and ensuring no residual vulnerabilities remain.
- **Post-Incident Analysis**. Conducting a thorough review of the incident to improve future responses and prevent recurrence.

By integrating the **Incident Handling Lifecycle** with AI-driven security enhancements and internationally recognized standards such as **ISO/IEC 27035:2023**, organizations can build a more resilient cybersecurity framework, capable of both proactive risk management and efficient incident response.

3. The „Golden Circle" method and the importance of starting with „WHY"

A powerful example of a people-centered approach is the „Golden Circle" method proposed by Simon Sinek [6]. This method begins with the question „WHY?" - Why is cybersecurity important, and why must risk be managed in a specific way? Starting with this fundamental question, organizations can clearly articulate the purpose and significance of their risk management programs, helping to foster a sense of responsibility and engagement among all participants.

Communicating „from the inside out", beginning with „WHY", allows leaders to build a shared understanding and motivate employees to adopt behaviors that support security. Instead of viewing security requirements as additional tasks, employees understand the context and importance of their actions, leading to deeper engagement and proactive behavior.

A remarkable example of successful implementation of the „Golden Circle" methodology can be seen in a complex organization operating with multiple business units and diverse organizational cultures. In this case, leaders began by clarifying the „WHY" - the fundamental purpose of the cybersecurity program: protecting the integrity and operational

continuity in an increasingly threatening digital environment. This clarity of purpose enabled leaders to effectively communicate the importance of cybersecurity not just as a technical requirement but as an essential pillar for the long-term success and sustainability of the organization.

By focusing on „WHY", leaders were able to secure the commitment and active participation of employees, even in the face of significant challenges such as rapidly changing cyber threat landscapes and the integration of new processes into diverse organizational cultures. This commitment was crucial for the organization's continuous adaptation to emerging threats, ensuring not only compliance with security standards but also robust cyber resilience capable of meeting future challenges.

The people-centered approach not only improved compliance and adherence to security measures but also transformed the organizational culture, placing cybersecurity at the core of the organization's daily values and practices. This cultural shift was made possible only by recognizing and valuing the essential role of human behavior in risk management.

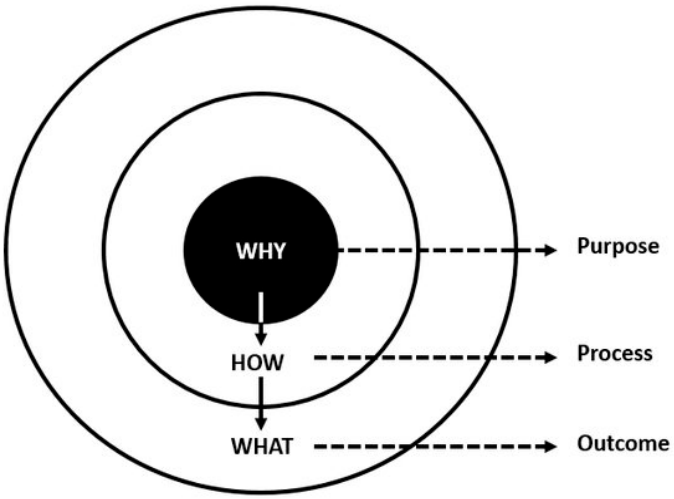

Figure 3. The „Start with Why" Golden Circle Model [6].

While the **Golden Circle** methodology emphasizes the **human factor** in cybersecurity, ensuring that employees and stakeholders understand and commit to security principles, it is equally important to leverage technological advancements to enhance risk management. As cyber threats evolve at an unprecedented rate, organizations must adopt **proactive, AI-driven security solutions** that complement human awareness and decision-making. **Artificial Intelligence** plays a crucial role in identifying threats, predicting vulnerabilities, and automating security processes, reducing the burden on human operators while improving overall cyber resilience.

4. Integrating artificial intelligence into risk management

As the cyber threat landscape continues to evolve, organizations face the need to adopt advanced technologies that allow them to stay one step ahead of attackers. AI has proven to be an essential ally in this regard, offering new ways of analyzing and predicting risks that are inaccessible through traditional methods.The use of AI in risk analysis and prediction is crucial in the current discussion, highlighting AI's ability to significantly revolutionize the ways organizations identify and manage cyber threats.

According to the definition provided by Stuart Russell and Peter Norvig, *„AI is the study of agents that receive percepts from the environment and perform actions. Each such agent*

implements a function that maps percept sequences to actions, and it is presumed that these actions are selected in such a way as to maximize some performance measure, given the evidence provided by the percept sequence. AI aims to develop machines and programs that can perform tasks considered intelligent if done by humans, using techniques such as machine learning, reasoning, and adaptation to improve performance based on experience" [7].

AI can be integrated into cybersecurity programs to enhance risk management through several methods:

Advanced behavioral analysis. AI, through the use of deep learning techniques, can analyze large volumes of data in real time to identify patterns and anomalies in user behavior. *Deep learning* is a subset of machine learning that utilizes artificial neural networks to learn from complex and unstructured data. This allows for the early detection of potential risks, such as unusual activities that might indicate an ongoing cyber attack. For example, AI can learn to recognize deviant behaviors that may signal a security breach, giving organizations time to respond before damage is done [8].

Risk prediction. By utilizing advanced machine learning techniques, AI can anticipate cyber threats, providing organizations with a proactive perspective on potential risks [9]. These techniques are based on analyzing historical data and observed behaviors, enabling AI to identify patterns that may predict attacks or security breaches before they materialize. By anticipating these threats, AI allows organizations to implement protective measures in advance, thereby reducing not only the risk of cyber attacks but also the resources and time required to respond to these incidents. This significantly improves overall security and operational efficiency.

Automating responses. AI plays a crucial role in automating responses to cyber attacks, allowing organizations to react quickly and efficiently to threats [10]. Using advanced algorithms, AI can autonomously detect and respond to incidents, such as isolating a compromised device to prevent the spread of an attack or blocking suspicious connections. Automation not only speeds up response times but also reduces the risk of human error, thereby helping to maintain operational continuity and minimize the impact of a cyber attack.

However, integrating AI into risk management is not without its challenges and risks. If not properly managed, AI technologies can introduce new vulnerabilities:

a. More sophisticated phishing attacks. AI can be used by attackers to create highly convincing phishing attacks that exploit personal data and human behaviors to deceive users. These attacks can be tailored to the victim's profile, making them much harder to detect [11].

b. Deepfakes and social engineering. *Deepfakes* are falsified audio or video materials created using advanced artificial intelligence techniques, particularly neural networks and deep learning. These can make it appear as if a person is saying or doing things they never actually did. AI can be used to generate such deepfakes that look extremely authentic, making them almost impossible to distinguish from real materials. These can be used to manipulate employees or mislead decision-makers, creating new attack vectors within organizations. Due to their realistic nature, deepfakes are difficult to combat through traditional security measures, requiring advanced strategies and technologies for their detection and prevention [12].

c. Overreliance on AI. While AI brings significant benefits, such as process automation and improved risk analysis, overreliance on these technologies can have negative consequences. Specifically, there is a risk of neglecting human judgment and traditional verification methods, which are essential in the context of cybersecurity. Human judgment remains vital for correctly interpreting data and making complex decisions that cannot be

fully managed by AI. Therefore, establishing robust verification processes and educating employees about the potential risks associated with AI use are crucial. These measures ensure that AI does not become a weak point in the security infrastructure but rather a tool complemented by human discernment [13].

To fully harness the potential of AI while maintaining organizational security, continuous vigilance is essential. The implementation of rigorous verification processes and the constant updating of security policies are crucial to protect against the risks associated with AI. Additionally, it is important to promote a culture of awareness among employees, educating them about new types of threats and encouraging them to report suspicious behaviors.

The National Institute of Innovations in Cybersecurity „CYBERCOR" plays a central role in strengthening cybersecurity through a diverse range of activities and innovations essential for protecting digital infrastructure and developing the necessary skills in this critical field. The institution focuses on several strategic areas, including offering specialized courses and certifications designed for public officials, IT professionals, teachers, students, and pupils. These programs are meticulously designed to enhance the cybersecurity skills of participants and to promote the adoption of best practices, such as cyber hygiene, at all levels of society.

In addition to its educational role, the National Institute of Innovations in Cybersecurity „CYBERCOR" is actively engaged in the development and implementation of cybersecurity infrastructures. By collaborating with globally renowned technology partners, the institute gains access to cutting-edge technology, state-of-the-art IT equipment, and top-quality educational resources. These collaborations not only enable the National Institute of Innovations in Cybersecurity „CYBERCOR" to provide specialized training and consulting services but also play a decisive role in forming a body of specialists capable of effectively protecting critical digital information and infrastructures.

Integrating AI into cyber risk management opens up significant opportunities for enhancing security; however, this endeavor requires a well-balanced approach that accurately assesses both the benefits and potential dangers associated with it. The National Institute of Innovations in Cybersecurity „CYBERCOR" understands that only through a careful combination of advanced technology and rigorous human processes can a robust and resilient cybersecurity environment be built.

Through these initiatives, the National Institute of Innovations in Cybersecurity „CYBERCOR" will not only contribute to the development of national capabilities in the field of cybersecurity but will also play a crucial role in strengthening the country's position on the global stage as a leader in innovation and cyber protection. An essential aspect of this strategy is the development of advanced educational content, created in collaboration with renowned technology partners such as Palo Alto, Cisco, and Fortinet.

Collaboration with Palo Alto Networks enables the National Institute of Innovations in Cybersecurity „CYBERCOR" to integrate the latest security technologies into its educational programs, offering courses and hands-on labs that reflect the real-world challenges faced by cybersecurity professionals. Cisco contributes its expertise in networking and IT infrastructures, helping to develop courses that cover both the fundamentals and advanced aspects of network security.

Fortinet, known for its integrated security solutions, adds value by providing educational platforms and resources that allow participants to learn through practical simulations in virtual environments.

These partnerships not only enrich the National Institute of Innovations in Cybersecurity „CYBERCOR" educational offerings but also ensure that graduates are equipped with the necessary skills to meet the challenges of cybersecurity at a global level.

5. The use of AI in security awareness programs

Through these efforts and collaborations, the National Institute of Innovations in Cybersecurity „CYBERCOR" not only trains specialists capable of responding to current challenges in cybersecurity but also contributes to the continuous innovation in methods of training and awareness of cyber threats. In this direction, the use of AI becomes a key element, offering opportunities to personalize and streamline educational programs.

As organizations become increasingly aware of the need to protect their digital resources, the importance of security awareness programs is growing. These programs aim to educate employees about cyber threats and teach them how to recognize and appropriately respond to potential attacks. In this context, AI provides powerful tools to customize and enhance these programs, making them more relevant and impactful for participants.

One of the most valuable uses of AI in security awareness programs is its ability to generate personalized educational content. AI can analyze data related to employee behavior and profiles to create training materials tailored to the specific needs of each department. For example, an employee in the finance department might receive training focused on recognizing phishing attacks specific to their industry, while IT staff might be trained on ways to detect and prevent security breaches.

AI can also be used to create scripts for educational videos, which are among the most effective means of conveying complex information in an easily understandable way. For instance, an AI program could generate a script for a two-minute video explaining what a „vishing" (voice phishing) attack is, how it works, and how employees can protect themselves against it. The script can be simplified to ensure it is understood by employees from all departments, ensuring the message reaches all members of the organization.

In addition to videos, AI can be used to generate quizzes and other training materials that help reinforce the knowledge employees have acquired. For example, an AI system can create a set of multiple-choice questions based on the content of an educational video, providing a quick and efficient way to assess employees' understanding and retention of information. These quizzes can be personalized to focus on previously identified weaknesses in employees' security behavior, ensuring that the training is relevant and effective.

Concrete examples of using AI in security awareness programs

1. **Creating simulated training scenarios.** AI can be used to develop simulated attack scenarios that reflect the current threats facing the organization. These simulations can include phishing attacks, business email compromises, or ransomware attacks, allowing employees to practice appropriate responses in a controlled environment.

2. **Automating feedback.** Another advantage of using AI is the ability to provide instant and personalized feedback to employees after completing quizzes or participating in simulations. AI can analyze responses and suggest additional study materials or training sessions to address identified gaps.

3. **Creating personalized awareness campaigns.** AI can help create security awareness campaigns tailored to different groups within the organization. For example, a campaign for sales staff might focus on protecting customer information, while a campaign for the software development team could emphasize the importance of source code security.

6. Implementation model at National Institute of Innovations in Cybersecurity „CYBERCOR" based on „WHY"

Vision. Training cybersecurity specialists and implementing the most advanced technologies and practices to protect critical resources.

Aligning initiatives with „WHY" through:

a. **Educational programs.** Every course or certification should be designed to develop the necessary skills to effectively protect digital infrastructures. The purpose of each program must be communicated to participants to instill motivation and responsibility for applying knowledge practically and effectively.

b. **Technological projects**. Every technological project, whether it's implementing new security technologies or developing advanced infrastructures, should be justified by its contribution to the National Institute of Innovations in Cybersecurity „CYBERCOR" mission. Technological decisions should be guided by the goal of protecting and strengthening critical networks and systems.

Communication and promotion

a) **Within the Institute**. National Institute of Innovations in Cybersecurity „CYBERCOR" constantly communicates the „WHY" behind each project, program, or initiative to employees and partners. This is achieved through informational sessions, educational materials, and by integrating this concept into the organizational culture.

b) **Externally**. National Institute of Innovations in Cybersecurity „CYBERCOR" promotion on the international stage includes clarifying the institute's purpose and motivation in all presentations and international partnerships. This attracts partners and collaborators who share the same values and goals.

Measuring impact

a) **Performance indicators**. Developing KPIs that measure how well initiatives align with the organization's „WHY". These indicators might include measures of the effectiveness of educational programs, the impact of implemented technologies, and the satisfaction of partners and employees.

b) **Continuous feedback**. Incorporating a feedback system that allows for the constant adjustment and refinement of initiatives to ensure they remain aligned with the National Institute of Innovations in Cybersecurity „CYBERCOR" central purpose.

This model is proposed for implementation at Cybercor as a strategic framework to guide all organizational actions and decisions. Constant alignment with the „WHY" will ensure that each initiative significantly contributes to the organization's mission and vision and that the National Institute of Innovations in Cybersecurity „CYBERCOR" remains at the forefront of innovation in cybersecurity.

By implementing this model, the National Institute of Innovations in Cybersecurity „CYBERCOR" will not only meet its immediate objectives but also build a solid foundation for sustainable development and long-term success in the field of cybersecurity.

Another major advantage of using AI in security awareness programs is the efficiency in content production, especially in organizations with limited resources. AI can automate many tasks related to the creation and distribution of educational content, thus reducing the time and costs needed to keep employees informed and prepared. For example, AI can quickly generate and customize materials for a new security awareness course without requiring extensive intervention from specialist teams.

7. Challenges and limitations of AI in Cybersecurity

Although AI brings numerous advantages in risk management and the creation of security awareness programs, its use is not without significant challenges and limitations. Understanding these limitations is important to maximize the benefits of AI and minimize the associated risks.

One of the main disadvantages of AI is related to the accuracy of its output. AI, particularly machine learning and content generation models, relies on the data it receives and how it is trained. If the initial data is incomplete, biased, or incorrect, the results produced by AI can be inaccurate or even misleading. In the context of cybersecurity, an incorrect analysis or an erroneous automated response can have serious consequences, leading to decisions that could expose the organization to additional risks.

Integrating AI into cybersecurity systems also introduces new security and privacy risks. AI requires access to large volumes of data to function effectively, which may include sensitive or confidential organizational data. If this data is compromised, the organization could suffer significant losses. Additionally, AI itself can become the target of cyber attacks, such as manipulating inputs to cause AI to produce incorrect outputs (adversarial attacks). These attacks can undermine trust in AI systems and lead to additional vulnerabilities within the security infrastructure.

Another sensitive aspect relates to the intellectual property rights over outputs generated by AI. Who owns the rights to a script, image, or video created by an AI model? These questions are still the subject of legal debate and may complicate the use of AI within organizations. Furthermore, there is a risk that AI outputs may violate copyright or be biased if they are based on data sourced from inappropriate or unreliable origins.

To mitigate the risks associated with using AI, organizations must adopt a proactive and well-informed approach:

a. **User education and awareness.** All users must interact with AI - whether they are developers, administrators, or end users - and are aware of its limitations and associated risks. This includes educating employees about potential AI-based attacks and how AI can be used ethically and safely.
b. **Implementing ethical and verification processes.** Organizing solid ethical processes that include the verification of AI outputs and the continuous monitoring of these systems' performance is crucial. These processes should also include measures to ensure compliance with data protection regulations and intellectual property rights.
c. **Testing and validating AI systems.** Before full implementation, AI systems should be rigorously tested to identify any vulnerabilities and to evaluate the accuracy of their outputs. Continuous validation and updating of AI models are necessary to ensure they function correctly and securely.
d. **Adopting a transparency policy.** Organizations should be transparent about their use of AI, explaining how data is used and how automated decisions are made. This transparency will not only help build trust among employees and customers but also facilitate compliance with legal regulations.
e. **Human oversight and intervention.** AI should not be used without human oversight. Critical decisions, especially those involving data security or confidentiality, should include human intervention and validation to prevent possible AI errors.

While AI offers numerous opportunities for enhancing cybersecurity, organizations need to be aware of its challenges and limitations. By implementing proactive measures and

solid ethical processes, organizations can minimize associated risks and fully leverage AI's potential to ensure security and data protection.

8. The impact of AI on security culture

It is essential to explore the impact AI can have on the security culture within organizations. A robust security culture is not just about implementing advanced technologies but also about creating an environment where security is understood, valued, and supported by all employees. AI plays a vital role in facilitating this environment by personalizing training and ensuring continuous workforce engagement in security awareness programs.

One way AI can strengthen security culture is by personalizing learning experiences. Unlike traditional training programs, which often adopt a one-size-fits-all approach, AI enables the creation of customized courses that address the specific needs and behaviors of each employee. For example, an employee working in the finance department might receive training focused on protecting financial data, while an IT employee might benefit from specific training on protecting networks and digital infrastructure.

This personalization not only makes the training more relevant and accessible to employees but also contributes to changing their behavior in ways that support the organization's security objectives. Employees learn to recognize risks specific to their roles and adopt behaviors that mitigate these risks, contributing to the reinforcement of a solid security culture.

AI can also play a crucial role in maintaining continuous employee engagement in security awareness programs. Instead of relying on occasional training sessions, AI can provide constant feedback and real-time updates, helping employees stay informed about the latest threats and best security practices. For example, AI can send personalized notifications when it detects behaviors that might pose a risk or recommend additional training sessions if an employee shows signs of vulnerability to certain types of attacks.

This continuous engagement helps keep security a constant priority within the organization, encouraging a proactive attitude toward protecting resources and data.

AI can be a catalyst for changing workforce behavior in a manner that supports the adoption of a robust security culture. By analyzing past behaviors and anticipating future risks, AI can help organizations implement strategies that encourage safer behavior. For instance, AI can identify behavioral patterns that suggest careless use of sensitive data and suggest specific interventions to correct these behaviors.

Additionally, using cyber attack simulations and other interactive training methods, AI can create learning experiences that are more engaging and effective than traditional methods. At the Technical University of Moldova (UTM), this approach is well integrated into the curricula of IT disciplines, particularly in courses focused on cybersecurity, networks, and digital infrastructures [14-17]. These simulations and interactive methods not only provide students with the opportunity to learn through practice but also allow them to deeply understand the dynamics of cyber attacks and develop essential skills for effectively responding to such threats.

At the National Institute of Innovations in Cybersecurity „CYBERCOR", students and professionals in the field can test authentic situations using real traffic and analyze the behaviors and reactions of systems in real time. National Institute of Innovations in Cybersecurity „CYBERCOR" state-of-the-art infrastructure allows for the simulation of

complex cyberattack scenarios, allowing participants to face challenges similar to those encountered in the real world. This advanced training environment not only enhances participants' technical skills but also develops their ability to make quick and effective decisions in critical situations. Thus, the National Institute of Innovations in Cybersecurity „CYBERCOR" becomes a center of excellence for training cybersecurity specialists, preparing them to meet the challenges they will face in their professional careers.

The goal of integrating these advanced technologies into the curriculum is to train well-prepared specialists who can anticipate and counteract real cyber attacks. Scientific research in emerging technologies such as cybersecurity, privacy, and blockchain has become increasingly important in shaping the future of global innovation, economic competitiveness, and national security [18]. In this way, UTM actively contributes to preparing a new generation of cybersecurity experts ready to protect critical infrastructures both nationally and internationally. This educational approach, based on the practical use of AI and simulations, ensures that students not only acquire theoretical knowledge but also gain relevant practical skills necessary to excel in the continuously evolving field of cybersecurity.

A strong security culture is built not only through policies and technology but also through collective behaviors and attitudes that support security at all levels of the organization. AI, with its ability to personalize and adapt training and awareness programs, plays a crucial role in developing this culture. Employees become not just passive participants in security programs but active partners who understand the importance of security and contribute to protecting the organization against cyber threats. The rapid development of information technologies and the growth of related cyber threats force us to constantly improve the regulatory framework in this area [19-21].

Integrating AI into an organization's security strategy can profoundly impact its security culture. By personalizing training, ensuring continuous engagement, and facilitating behavior change, AI helps create an environment where security is a collective responsibility, thereby protecting the organization from emerging cyber risks.

9. Conclusions

Integrating AI into cyber risk management and awareness programs is not just a technological innovation; it is also a clear manifestation of the importance of starting with „WHY" in any strategic endeavor. In the context of cybersecurity, the „WHY" represents the fundamental motivation that drives organizations to adopt proactive measures and invest in advanced technologies like AI, to protect not only their digital resources but also the integrity and continuity of their operations.

The National Institute of Innovations in Cybersecurity „CYBERCOR", through its initiatives, exemplifies this „WHY" philosophy by focusing not only on the development of security technologies but also on the education and awareness of all participants in the digital security process. A clear understanding of the „WHY" behind their actions protecting critical infrastructure and training professionals capable of meeting future challenges provides direction and meaning to all their efforts.

Thus, combining advanced technology with a well-defined strategy anchored in „WHY" not only enhances the efficiency and resilience of cybersecurity but also ensures that every step taken is aligned with the organization's broader purpose. This clarity of purpose, as highlighted by Sinek, is what will differentiate organizations that not only adopt innovation but do so in a way that has a lasting and significant impact.

This research was conducted with the support of the National Institute of Innovations in Cybersecurity ”CYBERCOR”, part of the Technical University of Moldova. The authors express their gratitude to colleagues and partners for their valuable contributions and collaboration in the development of this study.

Conflicts of interest. The authors declare no conflicts of interest.

References

1. Ponemon Institute. The 2022 Ponemon Report on Cybersecurity Risks. Available online: https://go.proofpoint.com/en-ponemon-report-2022.html (accessed on 13 January 2025).
2. ISO/IEC 27035-1:2023. Information technology – Information Security Incident Management. Available online: https://cdn.standards.iteh.ai/samples/78973/38e0e742e02741ba856510f74aa9f23b/ISO-IEC-27035-1-2023.pdf (accessed on 19 January 2025).
3. Skålén, P.; Gummerus, J.; von Koskull, C.; Magnusson, P.R. Designing value propositions: An exploration and extension of Sinek's 'Golden Circle' model. *Journal of Design Business & Society* 2019, 5(1), pp. 59-76.
4. Willie, M. M. *The Role of Organizational Culture in Cybersecurity: Building a Security-First Culture*. SSRN. Available online: https://papers.ssrn.com/sol3/papers.cfm?abstract_id=4564291 (accessed on 11 January 2025).
5. NIST incident response plan: Building your own IR process based on NIST guidelines. Incident Response. Available online: https://www.cynet.com/incident-response/nist-incident-response/ (accessed on 7 January 2025).
6. Sinek, S.; Mead, D.; Docker, P. *Find your why: A practical guide for discovering purpose for you and your team*. Portfolio, New York, SUA, 2017, 242 p.
7. Russell, S.; Norvig, P. *Artificial Intelligence: A Modern Approach*. Prentice Hall, NJ, SUA, 2020, 1136 p.
8. Goodfellow, I.; Bengio, Y.; Courville, A. *Deep Learning*. MIT Press, Cambridge, MA, USA, 2016, 800 p.
9. Mcafee, A.; Brynjolfsson, E. *Machine, platform, crowd: Harnessing our digital future*. W. W. Norton & Company, NY, USA, 2017, 416 p.
10. Bostrom, N. *Superintelligence: Paths, dangers, strategies*. Oxford University Press, Oxford, UK, 2014, 328 p.
11. Brundage, M. The Malicious Use of Artificial Intelligence: Forecasting, Prevention, and Mitigation. Available online: https://doi.org/10.48550/arXiv.1802.07228 (accessed on 24 July 2024).
12. Chesney, R.; Citron, D.- K. Deepfakes and the New Disinformation War: The Coming Age of Post-Truth Geopolitics. *Foreign Affairs* 2019, 98(1), pp. 147-155.
13. Smith, B.; Shum, H. The Future Computed: Artificial Intelligence and its Role in Society. Available online: https://news.microsoft.com/uploads/prod/sites/14/2018/02/The-Future-Computed.pdf (accessed on 12 august 2024).
14. Peca, L.; Țurcanu, D. *Computer networks: Practical examples solved to be introduced in computer networks*. Tehnica-UTM, Chisinau, Republic of Moldova, 2022, 188 p.
15. Peca, L.; Țurcanu, D. Network security: Practical examples solved to be introduced in network security. Tehnica-UTM, Chisinau, Republic of Moldova, 2023, 243 p.
16. Dumbraveanu, R.; Peca, L. E-learning in Developing ICT Skills of Future Engineers. In: *1st International Online Scientific Conference ICT in Life*, Osijek, Croația, 2022, pp. 86-95.
17. Peca, L. The power of eLearning from promises to practices applied in engineering. *Journal of Social Sciences* 2023, 6(1), pp. 69-80.
18. Bran, E.; Rughinis, R.; Turcanu, D.; Stăiculescu, A. R. Decoding National Innovation Capacities: A Comparative Analysis of Publication Patterns in Cybersecurity, Privacy, and Blockchain. *Applied Sciences* 2024, 14, 7086.
19. Turcanu, D.; Spinu, N.; Popovici, S.; Turcanu, T. Cybersecurity of the Republic of Moldova: A Retrospective for the Period 2015-2020. *Journal of Social Sciences* 2021, 4(1), pp. 74-83.
20. Action list for developing a computer security incident response team (CSIRT). Available online: https://insights.sei.cmu.edu/library/action-list-for-developing-a-computer-security-incident-response-team-csirt/ (accessed on 13 January 2025).
21. Thailand Cybersecurity Act 2019 (English Translation). Available online: https://thainetizen.org/wp-content/uploads/2019/11/thailand-cybersecrutiy-act-2019-en.pdf. (accessed on 13 January 2025).

Citation: Peca, L.; Ţurcanu, D. Reducing cyber risk through a human–centred approach. *Journal of Engineering Science*. 2025, XXXII (1), pp. 18-31. https://doi.org/10.52326/jss.utm.2025.8(2).02.

Submission of manuscripts: jes@meridian.utm.md

Journal of Engineering Science *Vol. XXXII, no. 1 (2025), pp. 32 - 46*
Fascicle *Electronics and Computer Science* *ISSN 2587-3474*
Topic *Computers and Information Technology* *eISSN 2587-3482*

https://doi.org/10.52326/jes.utm.2025.32(1).03
UDC 004.032.26:519.7:81'322=966.8

A GRAPH CONVOLUTIONAL NETWORK AND RECURRENT NEURAL NETWORK ENSEMBLE FOR EXTRACTIVE TEXT SUMMARISATION IN THE HAUSA LANGUAGE

Anas Shehu *, ORCID: 0000-0002-5307-1457,
Musa Karatu, ORCID: 0000-0002-6337-3117,
Abubakar Roko, ORCID: 0000-0002-3489-5346,
Sirajo Abdullahi, ORCID: 0000-0002-4346-621X

Federal University Birnin Kebbi, 860222, Nigeria
* Corresponding authors: Anas Shehu, *2200264009@pg.fubk.edu.ng*

Received: 01. 29. 2025
Accepted: 03. 04. 2025

Abstract. Automatic Text Summarisation (ATS) is crucial for managing information overload, especially in low-resource languages like Hausa. This study proposes a hybrid extractive approach that combines Graph Convolutional Networks (GCN) and Recurrent Neural Networks (RNN) to improve sentence ranking accuracy. By integrating GCN's structural learning with RNN's sequential modeling, the method overcomes limitations of existing graph-based techniques. The research was conducted in Visual Studio IDE using Python 3.12.4, with key libraries like NLTK, Pandas, and NetworkX. A pre-processed Hausa news dataset was tokenised, normalised, and vectorised using TF-IDF and a pre-trained Hausa FastText model to build a sentence similarity graph. GCNs propagated sentence embeddings, while RNNs refined rankings by capturing sequential dependencies. Experiments on 113 Hausa news articles showed the GCN-RNN model outperformed Modified PageRank, achieving higher ROUGE-1 precision (90.00) and balanced F1-scores. The Wilcoxon Signed-Rank Test confirmed significant improvements. Despite added computational overhead, the approach remains feasible for moderate datasets, with scalability as a key future focus. This study offers a robust and contextually coherent approach to Hausa text summarisation, advancing extractive summarisation techniques and multilingual ATS research. Future work will focus on optimising model efficiency and scalability while exploring transformer-based architectures for further enhancements.

Keywords: *Natural Language Processing ~ Hausa Language, Extractive Text Summarisation, Deep Learning Ensembles, Automatic Text Summarisation.*

Rezumat. Sumarizarea automată a textului (ATS) este crucială pentru gestionarea supraîncărcării cu informații, în special în limbile cu resurse reduse, cum ar fi hausa. Acest studiu propune o abordare extractivă hibridă care combină rețelele convoluționale grafice (GCN) și rețelele neuronale recurente (RNN) pentru a îmbunătăți acuratețea clasificării propozițiilor. Prin integrarea învățării structurale a GCN cu modelarea secvențială a RNN, metoda depășește limitele tehnicilor existente bazate pe grafuri. Cercetarea a fost efectuată

în Visual Studio IDE folosind Python 3.12.4, cu biblioteci cheie precum NLTK, Pandas și NetworkX. Un set de date de știri hausa preprocesat a fost tokenizat, normalizat și vectorizat folosind TF-IDF și un model hausa FastText pre-antrenat pentru a construi un grafic de similaritate a propozițiilor. GCN-urile au propagat încorporările de propoziții, în timp ce RNN-urile au rafinat clasamentele prin captarea dependențelor secvențiale. Experimentele pe 113 articole de știri hausa au arătat că modelul GCN-RNN a depășit performanța Modified PageRank, atingând o precizie ROUGE-1 mai mare (90,00) și scoruri F1 echilibrate. Testul Wilcoxon Signed-Rank a confirmat îmbunătățiri semnificative. În ciuda costurilor de calcul suplimentare, abordarea rămâne fezabilă pentru seturi de date moderate, scalabilitatea fiind un obiectiv cheie în viitor. Acest studiu oferă o abordare robustă și coerentă din punct de vedere contextual a rezumării textului în limba hausa, avansând tehnicile de rezumare extractivă și cercetarea ATS multilingvă. Lucrările viitoare se vor concentra pe optimizarea eficienței și scalabilității modelului, explorând în același timp arhitecturi bazate pe transformatoare pentru îmbunătățiri suplimentare.

Cuvinte cheie: *prelucrarea limbajului natural, limba hausa, sumarizare extractivă a textului, ansambluri de învățare profundă, sumarizare automată a textului.*

1. Introduction

The rapid growth of digital information has made Automatic Text Summarisation (ATS) an essential tool for information retrieval and text classification, helping to mitigate information overload [1]. Extractive summarisation, which selects key sentences from a document to generate concise summaries, has been successfully applied across various languages, including Marathi [2], Indonesian [3], and Urdu [4]. However, achieving accurate sentence ranking in Hausa text summarisation remains a challenge due to limited contextual understanding and graph construction constraints [5].

Extractive text summarisation serves as a promising method for text summarisation that works by selecting a subset of existing words, phrases, or sentences in the original text to form the summary [6]. Despite the effectiveness of graph-based methods in extractive text summarisation, accurately ranking sentences in Hausa language remains a challenge, leading to suboptimal summaries [5]. Integrating a deep learning algorithm holds promise for improving summarisation accuracy within these methods [7].

However, Bichi, Samsudin, Hassan, Hasan and Rogo [5], employed a modified PageRank algorithm to rank sentences for extractive summarisation in Hausa text. The modified algorithm considers the relationships between sentences in the text to determine their importance, which is a departure from the original PageRank algorithm. The modified PageRank algorithm faces challenges such as its reliance on graph construction contextual, limited understanding, scalability issues, and insufficient semantic awareness, all of which can lead to less effective summaries. To address these limitations, this study proposes a hybrid extractive summarisation model that integrates Graph Convolutional Networks (GCNs) and Recurrent Neural Networks (RNNs). GCNs effectively capture semantic relationships, while RNNs refine sentence rankings by leveraging sequential dependencies, improving summarisation accuracy.

This research contributes to multilingual ATS by offering a robust, contextually aware extractive summarisation method for Hausa. Future work will focus on scalability improvements and integration with transformer-based models to enhance performance on larger datasets.

2. Related Work

2.1 Graph-Based Approaches

Graph theory has been a foundational method for automatic text summarization, providing a structured way to rank sentences based on their relationships. LexRank, introduced in 2004, was one of the earliest graph-based summarization models, using eigenvector centrality to compute sentence importance [8].

This approach has since inspired a wide range of research, with adaptations for various domains, input types, and languages.

Belwal, *et al.* [9], proposed a graph-based extractive summarization model that integrates topic modeling to mitigate redundancy and enhance semantic coherence. Similarly, Jalil, *et al.* [10] developed Grapharizer, a multi-document summarization (MDS) technique, addressing grammar inconsistencies, missing key information, and redundancy. Their approach improved summarization accuracy by 23.05% on ROUGE metrics compared to baseline models.

For Arabic text summarization, AL-Khassawneh and Hanandeh [11] introduced a textual graph-based approach, outperforming state-of-the-art models like Latent Semantic Analysis (LSA) [12], and Lexical Cohesion and Entailment-based segmentation (LCEAS) [13]. Evaluations on the Essex Arabic Summary Corpus (EASC) showed enhanced precision and informativeness.

In the context of low-resource languages, Bichi, Samsudin, Hassan, Hasan and Rogo [5] introduced a graph-based ranking method for Hausa extractive summarization, leveraging normalized common bigrams count to outperform TextRank, LexRank, Centroid-based, and BM25-TextRank in ROUGE-1, ROUGE-2, and ROUGE-L evaluations. However, this method lacks a deep learning component, limiting its ability to capture contextual and sequential dependencies.

Further studies have explored graph-based sentence scoring for summarization in diverse languages. Bhattacharya, et al. [14], introduced a sentence-centric graph-based text mining model, demonstrating its effectiveness in crowdsourcing applications. Similarly, Sarwadnya and Sonawane [2] developed a graph-based summarizer for Marathi, though it lacked semantic ranking. Ghos, *et al.* [15], applied a rule-based extractive graph technique for Bangla news, outperforming previous sentence extraction models.

Recent advancements in graph neural networks (GNNs) have further improved summarization performance. Cui, *et al.* [16], introduced Topic-Aware Graph Neural Networks (Topic-GraphSum) to capture inter-sentence relationships in long documents. Their approach outperformed traditional methods like SumBasic, LexRank, and LSA on datasets such as CNN/Daily Mail and The New York Times (NYT).

2.2 Algorithm Approach

Beyond graph-based methods, algorithmic models-ranging from machine learning to evolutionary algorithms - have contributed significantly to extractive summarization.

Verma and Nidh [17], introduced a deep learning-based approach that selects key sentences while preserving content meaning and coherence, combining Restricted Boltzmann Machines and Fuzzy Logic. Alami et al. [18], improved unsupervised neural network-based summarization by integrating Word2Vec embeddings and ensemble learning, demonstrating superior performance over Bag-of-Words (BoW) representations.

Hybrid techniques have also been explored. Gulati, *et al.* [19], proposed a BM25+ and TextRank hybrid model, showing that combining graph-based and probabilistic methods

improves summarization across news, research papers, and blogs. Girsang and Amadeus [3], developed an Ant System Algorithm for Indonesian text summarization, demonstrating its effectiveness in content synthesis and readability.

In evolutionary algorithms, Mojrian and Mirroshande [20] introduced Multi-Document Text Summarization using a Quantum-Inspired Genetic Algorithm (MTSQIGA). This model outperformed state-of-the-art summarization techniques, including Centroid-based methods [21], Probabilistic Latent Semantic Analysis (PLSA) [22], SRSum [23]. However, fine-tuning hyperparameters remains a challenge, potentially leading to redundancy and suboptimal summaries.

For Turkish, Akülker [24], explored TF-IDF and PageRank, confirming their effectiveness in extractive summarization and suggesting further testing on larger datasets with multiple thresholds.

2.3 Advancements in Neural Networks for Summarization

While graph-based and algorithmic methods remain prominent, recent advancements in deep learning – particularly RNNs and GCNs – have shown promise in extractive summarization.

The Multi-GraS model [25] demonstrated how Bi-LSTMs (a type of RNN) and GCNs can jointly capture syntactic and semantic relationships, improving extractive summarization for English datasets (CNN/Daily Mail). This highlights the potential of neural graph-based hybrid models.

Hausa text summarization, however, remains in early research stages, with most methods relying solely on graph-based PageRank variations [5]. To advance Hausa summarization, this study proposes an integrated GCN-RNN approach, leveraging GCNs for structural relationships and RNNs for sequential dependencies. This integration aims to enhance sentence ranking accuracy, ensuring contextually rich and semantically coherent summaries.

While graph-based and algorithmic approaches have achieved success in extractive text summarization, Hausa text summarization remains underexplored. Existing studies primarily employ modified PageRank, lacking deep learning integration for semantic and sequential understanding.

To address the lack of integration deep learning in Hausa text summarisation, this study integrates GCNs and RNNs to enhance sentence ranking accuracy for Hausa extractive summarisation.

By leveraging GCNs for sentence relationships and RNNs for sequential dependencies, this hybrid approach aims to bridge the gap between structural coherence and contextual depth.

3. Methodology

The proposed method utilized a hybrid framework that integrate the strength of both GCN and RNN as shown in Figure 1 to enhance the accuracy of sentence ranking in Hausa for graph based extractive text Summarisation.

The GCN methods provide a structured representation of the text, capturing semantic relationships between sentences. While RNN algorithms learned the intricate patterns and representations from data, potentially to improve the accuracy of sentence ranking.

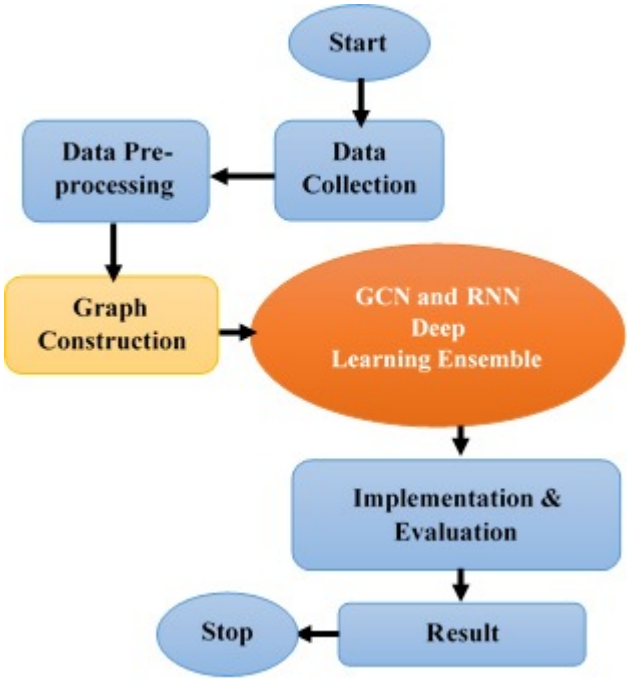

Figure 1. Proposed Deep Learning Ensemble Framework.

3.1 Dataset

The experiments was conducted on a Hausa summarisation evaluation dataset comprising five (5) Hausa publishers such as AMINIYYA, HAUSA LEADERSHIP NEWSPAPER, BBC HAUSA, RFI HAUSA, and VOA, HAUSA, which gives a total of 113 Hausa news articles adopted from [5], the Table 1 below describes the dataset used in evaluation the proposed method.

Table 1

Summary of the 113 Hausa news articles adopted from [5]

Source	Number of articles	Total Words	Number of manual summaries	Summary length, %	Average number of sentences in the article	Average number of sentences in the summaries
Aminiyya newspaper	25	7859	50	20	10	2
Hausa Leadership newspaper	21	9043	42	20	11	2
BBC Hausa	23	6314	46	20	9	2
RFI Hausa	23	6800	46	20	5	1
VOA Hausa	21	6509	42	20	11	2

The dataset was normalised using Pandas one of the Python libraries that support cleaning and standardising of text data, such as lowercasing, removing special characters, and handling whitespace in the dataset. The sentences were tokenised using the Natural Language Toolkit (NLTK) and the Hausa stopword was removed from the dataset.

3.2 Text Vectorisation and Graph Construction

A pre-trained Hausa Fast text Model was used for word representation learning (word embeddings) developed by Facebook which offers pre-trained word vectors for 157

languages, and Hausa Language is inclusive. The TF-IDF vectoriser was used in transforming the article and reference summary into vectors and calculating the cosine similarity between these vectors, the sentence similarity scores were computed based on the vectorised text from TF-IDF, and a similarity graph to rank the sentences based on scores was created using GCN.

3.3 Sentence Ranking using GCNs

GCNs are increasingly used in **extractive text summarisation** to **rank sentences** based on their relevance and importance [26]. The sentence ranking was achieved after the text has been represented as a node and edge as the relation between the nodes.
Mathematically, the resulting graph can be represented as:

Graph representation:

- The document is represented as a graph:

$$G = (V,E), \quad (1)$$

where: V is the set of nodes (sentences).
E is the set of edges (relationships between sentences).

- The adjacency matrix A_{ij} is defined such that A_{ij} = weight of the edge between sentence i and sentence j.

Node Feature Representation

- Each sentence (node) is associated with an **initial feature matrix** $H^{(0)}$,
  where: $H^{(0)} \in \mathbb{R}^{N\,x\,d}$, with N being the number of sentences and d being the feature dimension.
  Each row of $H^{(0)}$ represents the feature vector of a sentence.

Graph Convolution Operation

- The node embeddings are updated at each layer l using the GCN propagation rule:

$$H^{(l+1)} = \sigma(\tilde{D}^{-1/2}\tilde{A}\tilde{D}^{-1/2}H^{(l)}W^{(l)}), \quad (2)$$

where: $\tilde{A} = A + I$ is the adjacency matrix with self-loops (identity matrix I added).
$\tilde{D}$ is the diagonal degree matrix of $\tilde{A}$.
$W^{(l)}$ is the trainable weight matrix at layer l.
σ is the non-linear Rectified Linear Unit (ReLU) activation function.
$H^{(l)}$ is the feature matrix at layer l.

The GCN learned better sentence representations based on the propagating information across the graph structure when the sentence representations iteratively update through graph convolutional layers. Each layer propagates information between neighboring nodes (sentences), and the simple scoring function to assign a score to each sentence based on its learned representation was used by GCN to rank the sentences based on their importance, and a higher score indicates more important or central sentences. The simple scoring function mathematically is represented as $H^{(l)}$:

$$Score_i = f(H_i^{(l)}), \quad (3)$$

where: f is a non-linear function.

3.4 Evaluation metrics

Recall-Oriented Understudy for Gisting Evaluation (Rouge) as a widely used set of metrics for evaluating the quality of text summarisation, the study used Rouge-1, Rouge-2, and Rouge-L metrics to provide a good indication of the informativeness and fluency of the generated summary based on the following research objectives:

- Rouge-1 (Unigram Overlap) was used to evaluate the impact of combining multiple features on the quality of summaries generated for Hausa news articles such as word-level, sentence-level, and graph-level features.
- Rouge-2 (Bigram Overlap) was also used in monitoring sentence scores to avoid multiple sentences conveying similar information.
- Rouge-L helps in evaluating the overall semantic and syntactic similarity between the generated summary and the reference summary.

4. Proposed Method

The Graph convolutional network and Recurrent neural network are a class of deep learning models that operate on graph-structured data and handle sequential data respectively, the idea is to integrate the ability of both of them to improve the precision of sentence ranking on Hausa text summarisation. This method was divided into two tasks:

i. Graph convolutional network task.
ii. And Recurrent neural network task.

4.1 The Graph convolutional network task (GCN)

The GCN learns and handles better sentence representations after been represented as nodes based on the propagating information across the graph structure, and the sentence representations are iteratively updated through graph convolutional layers. Each layer propagates information between neighboring nodes (sentences), the core idea is to have a better message-passing mechanism, where each node aggregates and computes new representations based on the features of its neighboring nodes and the edges connecting them to know the relationships and dependencies within the graph and produce sequence encoding to the RNN as input.

4.2 The Recurrent neural network task

RNNs are a specialised type of neural network architecture that are designed to handle sequential data, such as text, speech, or time series information, unlike the traditional feedforward neural networks, where each input is processed independently, RNNs have connections that form directed cycles. This method, used this structure of RNN to maintain memory and a hidden state to capture information about previous inputs, enabling them to handle sequential data effectively supplied by GCN. Mathematically it is represented as:

$$h_t = f(W_h\, h_{t-1} + W_x x_t + b_h), \tag{4}$$

where: W_h is the weight matrix for the hidden state.

W_x is the weight matrix for the input.

b_h is the bias vector.

f is an activation function.

x_t is an input to the RNN.

h_t is the hidden state.

h_{t-1} previous hiding state.

The RNN takes text encoding x_t as input from the GCN, and learns the temporal and sequential dependencies of the text encoding through the Long Short-Term Memory (LSTM) architecture of RNN in the hidden state $h_t$which served as the link between GCN and RNN, the memory contained the information of the current text encoding x_t and previous text encoding information h_{t-1}. This gives the RNN the ability to eliminate the redundancy of multiple sentences conveying similar information in the Summary.

The activation function f transformed the weighted sum of the input x_t, the current text encoding and information about the previous hidden state h_{t-1} into the new hidden state (h_t) i.e. new information about text encoding through bias vector b_h, which is an additional parameter for shifting the +activation function as shown in the Architecture in Figure 2. The sequence representation of the learned text encoding was used to rank the sentences based on their importance in the final summary.

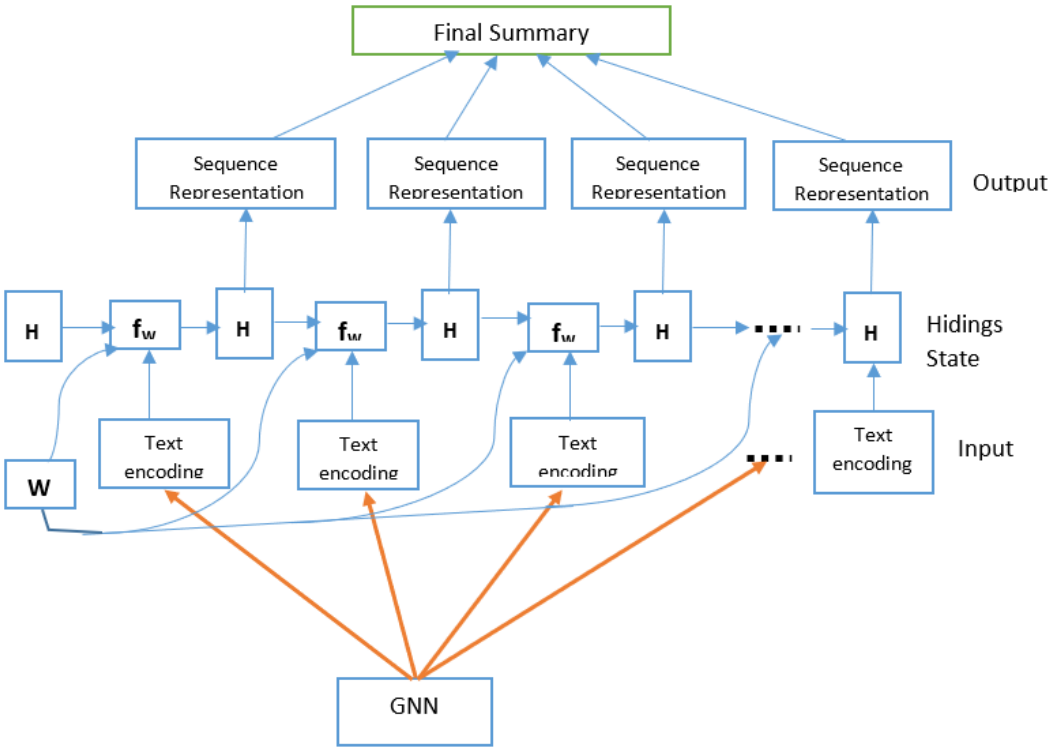

Figure 2. Architecture of Recurrent Neural Network.

The evaluation of the proposed method indicates a promising result as shown in Figure 3.

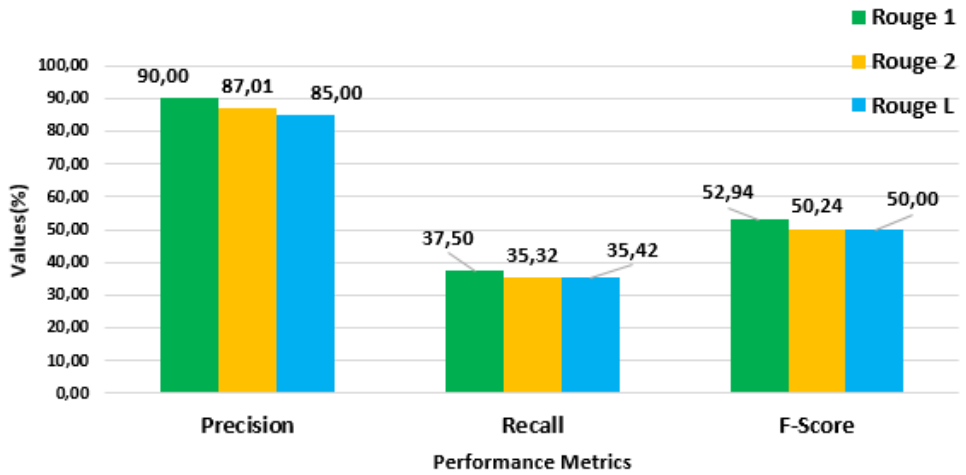

Figure 3. Proposed method of GCN and RNN.

The evaluation result indicates higher precision values of 90.00, 87.01 and 85.00 in Rouge-1 than in Rouge-2 and L respectively. It shows a higher significant matching of words, very good coherence, and achieved semantic and syntactic similarity between the generated summary and the reference summary when compared with GCN only. The proposed method shows a **balanced performance** across the three Rouge metrics, with relatively high recall values of 37.50, 35.32, and 35.42, this indicates the method captures not only key terms but also contextual and structural aspects of the summaries compared to previous results of GCN.

The F1-score values for the proposed method **52.94 Rouge-1, 50.24 Rouge-2, and 50.00 Rouge-L indicate the method** performs well in identifying key terms from the reference summaries, balancing precision (relevance of selected words) and recall (coverage of reference words). Also, the method achieves a good balance between precision and recall for capturing contextual relationships between words. This result supports the idea that the summary maintains coherence and preserves meaningful phrases. The structural similarity with both recall and precision were effectively balanced, ensuring the generated summaries align well with the reference summaries in terms of sentence structure and flow.

These demonstrate that the proposed method strikes a good balance between precision and recall, the results suggest a **robust and effective summarisation method**, particularly when compared to recall-only results, as F1-scores consider both the quality and completeness of the generated summaries.

5. Result and Discussion

The performance of the Modified PageRank method and the GCN-RNN method was evaluated using the Rouge metrics of Rouge-1, Rouge-2, and Rouge-L. These metrics assess the quality of text summarisation by measuring unigram overlap, bigram overlap, and overall structural similarity between the generated and reference summaries. The precision, recall, and F1-score values for both methods are compared below.

Table 2

Comparison of the proposed method with other Methods

Evaluation Metrics	Performance Metrics	GCN	Modified PageRank	Proposed Method
Rouge-1	Precision	70.89	73.73	90.00
	Recall	18.06	70.90	37.50
	F1-score	28.79	72.28	52.94
Rouge-2	Precision	34.26	32.91	87.01
	Recall	8.72	35.94	35.32
	F1-score	13.90	34.36	50.24
Rouge-L	Precision	60.76	70.31	85.00
	Recall	15.48	70.65	35.42
	F1-score	24.68	70.48	50.00

Note: GCN - Graph Convolutional Networks.

Table 2 presents the results of the experiments using the proposed method, GCN, and the Modified PageRank. The Modified PageRank has a - Precision of 73.73, Recall 70.90, and F1-score 72.28 in Rouge-1 which demonstrates higher coherence (recall). The proposed approach GCN- RNN, with a significant difference of 33.4% and a balanced F1-score rate

compared to the Modified PageRank – Precision 90.00, Recall 37.50, and F1-score 52.94. The result of GCN-RNN is indicative of its ability to capture a broader range of key terms. However, its lower precision compared to Modified PageRank, suggests that proposed method may include less relevant terms. Also, the GCN-RNN method exhibits significantly higher precision with about 16.27% relative to the Modified PageRank, highlighting its effectiveness in selecting highly relevant matching of words, although at the cost of a lower recall value.

The F1-score for GCN-RNN suggests a reasonable balance, but the trade-off between precision and recall is clearer. The Modified PageRank method shows moderate performance on Rouge-2, with relatively balanced precision and recall values of 32.91, and 35.94, respectively. Again, the GCN-RNN method outperforms Modified PageRank in precision by a significant rate of 54%, indicating better coherence and selection of relevant bigrams. Despite the slightly lower recall, the GCN-RNN's higher F1-score reflects its superior capability to balance relevance and coverage for bigram matches about a difference of 16%.

Moreover, in the Structural similarity, the Modified PageRank method achieves highly balanced performance across Precision, Recall, and F1-score values of – 70.31, 70.65, and 70.48, respectively for ROUGE-L, indicating Modified PageRank ability to preserve sentence structure and flow. In contrast, the GCN-RNN method prioritises precision, achieving a significantly higher value in ROUGE-L metric with 14.6% difference. The lower recall and moderate F1-score of the Modified PageRank suggests that while the Modified PageRank captures structural aspects effectively, and the overall performance of the proposed method is shown below.

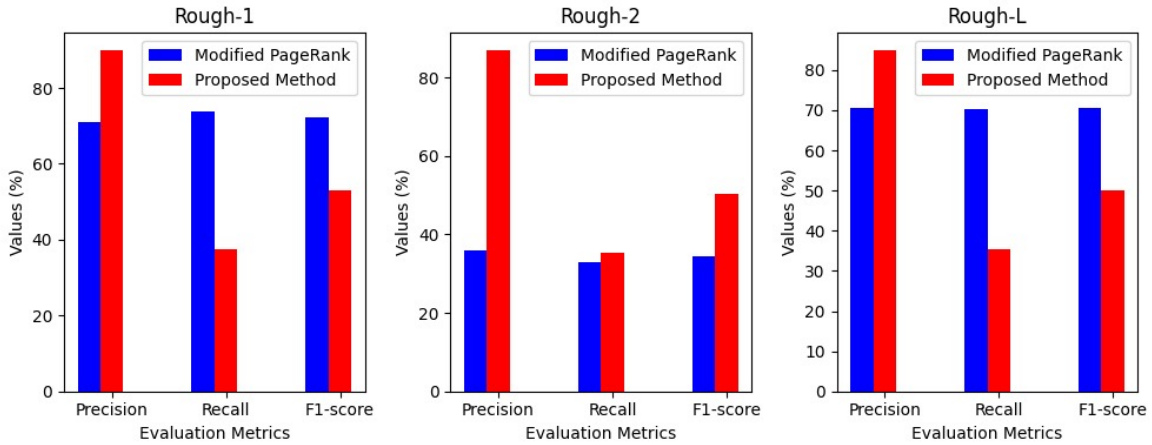

Figure 4. Overall performance of the proposed method.

The performance of both methods based on Precision as shown in Figure 4 above, indicates that the GCN-RNN method outperforms the Modified PageRank method across all ROUGE metrics in terms of precision, demonstrating its effectiveness in selecting relevant and high-quality content in the Generated Summary. In the Recall performance, the Modified PageRank method consistently achieves higher recall values, reflecting its broader coverage of the reference summaries. Also, the performance of the F1-Score shows The GCN-RNN method achieves higher F1-scores in ROUGE-2 and ROUGE-L, indicating better overall performance in capturing contextual and structural relationships.

5.1 Analysis for Statistical Significance

The **Wilcoxon statistic** is a **non-parametric** statistical test used to compare **paired or independent samples** when the data does not necessarily follow a normal distribution [27].

It is commonly used in machine learning and statistical analysis to compare the performance of two algorithms. The **Wilcoxon Signed-Rank Test was used in this study, and the performance of Modified PageRank and GCN-RRN methods was paired.** The Wilcoxon test results indicate a statistically significant difference between the precision scores of Modified PageRank and GCN-RNN methods (p-value: 1.91e-06). This suggests that GCN-RNN significantly outperforms Modified PageRank in terms of precision, as the differences are not due to random chance in all the Rouge 1, 2, and L respectively.

The Wilcoxon test results indicate a statistically significant difference between the F1-scores of Modified PageRank and GCN-RNN (p-value: 1.91e-06). This suggests that Modified PageRank significantly outperforms GCN-RNN in terms of F1-score in Rouge 1 and L only, implying better balance between precision and recall in this evaluation.

However, in Rouge 2 the Wilcoxon test results indicate a statistically significant difference between the F1-scores of Modified PageRank and GCN-RNN (p-value: 1.91e-06). This confirms that GCN-RNN significantly outperforms Modified PageRank in terms of F1-score, suggesting it is a more effective model. Also in terms of Recall the result show a statistically significant difference between the recall scores of Modified PageRank and GCN-RNN (p-value: 0.024) all the Rouge 2. This confirms that GCN-RNN significantly outperforms Modified PageRank in terms of recall, demonstrating its superior ability to retrieve relevant results.

5.2 A Time Complexity Analysis of the GCN and RNN Ensemble Model

This section presents the time complexity analysis of the GCN and RNN ensemble for Hausa text summarisation. The complexity of different components of the pipeline are analysed.

Preprocessing Steps. The preprocessing step sets the stage for effective sentence ranking and graph-based learning. By meticulously converting text into meaningful numerical formats and capturing inter-sentence relationships, it ensures that the subsequent models – such as GCNs and RNNs – receive high-quality inputs, thereby enhancing the quality and coherence of the generated summaries.

The text data is transformed using TF-IDF with a vocabulary size of d (max. features = 793):

- TF-IDF computation complexity: $\mathrm{O(Nd)}$,

where N is the number of sentences (nodes), and d is the maximum number of features.

- Cosine similarity computation: $\mathrm{O(N^2 d)}$.

Since cosine similarity requires pairwise comparison between all **N** sentences, it results in a quadratic complexity.

Overall complexity of preprocessing (TF-IDF + Similarity Computation):

$$\mathrm{O(Nd)} + \mathrm{O(N^2 d)} = \mathrm{O(N^2 d)} \quad (5)$$

Graph Construction. Converting the Similarity Matrix into a Graph each similarity matrix is converted into an adjacency matrix representation:

- Constructing the graph takes $\mathrm{O(N^2)}$ operations as it directly maps the similarity matrix into an undirected graph.
- Extracting edges for the GCN (edge_index computation) involves iterating through nonzero elements, leading to $\mathrm{O(E)}$ complexity, where E is the number of edges.

The Graph construction complexity:

$$O(N^2) + O(E) \quad (6)$$

The GCN consists of two convolutional layers. The time complexity per layer is:

$$(EF) + O(NFH) + O(NHO), \quad (7)$$

where: E is number of edges in the graph; F - feature dimension (793); H - hidden layer dimension (64); O - output feature dimension (64).

Since the GCN has two layers, the total complexity is:

$$O(2(EF + NFH + NHO)) = O(EF + NFH + NHO) \quad (8)$$

Since $E \approx O(N)$ for a sparse graph, we approximate this as:

$$O(NF + NFH + NHO) = O(NF + NH^2) \quad (9)$$

Recurrent Neural Network

The RNN (LSTM) processes the N sentences as a sequence. The per-step complexity is:

$$O(H^2 + HF) \quad (10)$$

Since the LSTM runs for N steps, the total complexity is:

$$O(N(H^2 + HF) \quad (11)$$

Sentence Ranking

Sorting the N sentences based on RNN output has a complexity of $O(N \log N)$,

Overall Complexity of GCN-RNN

Summing up the key components:

$$O(N^2d) + O(N^2) + O(NF + NH^2) + O(N(H^2 + HF)) + O(NlogN) \quad (12)$$

Since $d = F$ (793)**,** and assuming < NH, we approximate the dominant terms:

$$O(N^2d) + O(N^2) + O(NF) + O(NH^2) + O(NHF) \quad (13)$$

For large N, the $O(N^2d)$ and $O(N^2)$ terms dominate, giving the final complexity:

$$O(N^2d) \quad (14)$$

This quadratic complexity primarily results from TF-IDF vectorisation and cosine similarity computations. The ensemble of GCN and RNN adds only a linear term $O(NH^2 + NHF)$, making it scalable for moderate-sized datasets like those used in this research (N < 1000), but costly for very large text corpora. The scalability consideration for larger datasets > 10,000 is the next direction of this research.

5.3 Time Complexity Analysis of the Modified PageRank

The Modified PageRank algorithm follows a graph-based ranking mechanism where nodes (sentences) are ranked based on their importance in summarisation. The computational complexity can be broken down into:

- **Graph Construction:** Constructing the similarity graph requires computing similarity scores for all sentence pairs, leading to an $O(N^2)$ complexity.
- **Power Iteration for PageRank:** PageRank relies on iterative computation where convergence is typically reached within I iterations. Each iteration involves a sparse matrix-vector multiplication, resulting in a per-iteration complexity of $O(E)$. Thus, for I iterations, the total complexity is:

$$O(IE) \approx O(IN)) \quad (15)$$

Since we have a small, constant number of iterations I, the final complexity is near-linear:

$$O(N^2 + IN) \tag{16}$$

For large datasets, where $I < NI$, this approximates to $O(N^2)$, making it suitable for moderate-scale text summarisation.

GCN provides a scalable solution for structured text representations, Modified PageRank is effective for ranking-based summarisation, and the ensemble approach balances feature learning and sequence modelling but at a higher computational cost.

6. Conclusions

This research detailed a comprehensive study on Hausa text summarisation, integrating various natural language processing and machine learning techniques to enhance summary quality and model transparency. The experimental setup, conducted within a robust Visual Studio IDE environment using Python 3.12.4 and key libraries such as NLTK, Pandas, and NetworkX, ensured a solid foundation for reproducible and effective research.

The study began by implementing a meticulously pre-processed dataset from multiple Hausa news publishers, where text cleaning, tokenisation, and normalisation set the stage for further analysis. Text vectorisation was achieved using a pre-trained Hausa FastText model combined with TF-IDF and cosine similarity measures, leading to the construction of a sentence similarity graph. This graph served as the basis for sentence ranking via GCNs, which efficiently propagated and refined sentence representations.

However, the inherent limitations of GCNs in capturing multi-word expressions and complex structural dependencies necessitated the development of a hybrid approach. The proposed method, which integrates GCN with RNNs, leveraged the sequential modelling strengths of RNNs to complement the structural insights from the GCN. This ensemble method demonstrated superior performance in balancing precision and recall, as evidenced by improved Rouge metrics and statistically significant results via the Wilcoxon Signed-Rank Test.

The results and discussion section further revealed that while the Modified PageRank method achieved strong structural preservation, the GCN-RNN ensemble outperformed it in precision and overall F1-score, highlighting its ability to effectively identify key terms and maintain contextual coherence. The time complexity analysis indicated that although the ensemble method introduces additional computational overhead – primarily due to TF-IDF vectorisation and cosine similarity calculations – it remains feasible for moderate-sized datasets. Scalability considerations for larger corpora were identified as a promising direction for future research.

In conclusion, the integration of GCN and RNN in this study provides a robust and balanced approach to Hausa text summarisation, combining effective feature learning with advanced sequence modelling. The findings underscore the potential of this ensemble method to produce summaries that are both precise and contextually coherent, while also offering valuable insights into computational trade-offs and scalability challenges. Future work will focus on optimising the model for larger datasets and further refining the balance between performance and computational efficiency.

Conflicts of Interest: The authors declare no conflicts of interest.

References

1. Bilal, K.; Ali, S.Z.; Muhammad, U.; Inayat, K.; Badam, N. Exploring the landscape of automatic text summarization: a comprehensive survey. *IEEE Access* 2023, 11, 109819-109840.
2. Sarwadnya, V.V.; Sonawane, S.S. Marathi Extractive Text Summarizer using Graph Based Mode. In: P*roceedings of the Fourth International Conference on Computing Communication Control and Automation* (ICCUBEA), Pune, India, 16-18 August 2018, pp. 1-6.
3. Girsang, A.S.; Amadeus, F.J. Extractive Text Summarization for Indonesian News Article Using Ant System Algorithm. *Journal of Advances in Information Technology* 2023, 14, 295-301.
4. Nawaz, A.; Bakhtyar, M.; Baber, J.; Ullah, I.; Noor, W.; Basi, A. Extractive Text Summarization Models for Urdu Language. *Information Processing and Management* 2020, 57, 1-12.
5. Bichi, A.A.; Samsudin, R.; Hassan, R.; Hasan, L.R.A.; Rogo, A.A. Graph-based extractive text summarization method for Hausa text. *PLOS ONE* 2023, 5, 1-15.
6. Ramesh, R.; Rajan, B. Extractive Text Summarization Using Graph Based Ranking Algorithm And Mean Shift Clustering. In: *Proceedings of the In Proceeding of International Conference on Recent Trends in Computing, Communication & Networking Technology*(ICRTCCNT) Chennai, Tamil Nadu, 18-19 October 2019, pp. 1-8.
7. Amirsina, T.; Rouzbeh-A, S.; Yaser, K.; Nader, T.; Edward-A, F. Natural language processing advancements by deep learning: A survey. *arXiv preprint arXiv:2003.01200* 2020, 2, 1-23.
8. Erkan, G.; Radev, D.R. LexRank: Graph-based Lexical Centrality as Salience in Text Summarization. *Journal of Artificial Intelligence Research* 2004, 22, 457-479.
9. Belwal, R.C.; Rai, S.; Gupta, A. A new graph-based extractive text summarization using keywords or topic modeling. *Journal of Ambient Intelligence and Humanized Computing* 2020, 10, 1-16, doi:https://doi.org/10.1007/s12652-020-02591-x.
10. Jalil, Z.; Nasir, M.; Alazab, M.; Nasir, J.; Amjad, T.; Alqammaz, A. Grapharizer: A Graph-Based Technique for Extractive Multi-Document Summarization. *Electronics* 2023, 12, 1-26.
11. AL-Khassawneh, Y.A.; Hanandeh, E.S. Extractive Arabic Text Summarization-Graph-Based Approach. *Electronics* 2023*,* 12*,* 437.
12. El-Haj, M.; Kruschwitz, U.; Fox, C. Experimenting with automatic text summarisation for arabic. In: *Proceedings of the Human Language Technology. Challenges for Computer Science and Linguistics*: *4th Language and Technology Conference*, LTC 2009, Poznan, Poland , November 6-8, 2009, Revised Selected Papers 4, Poznan, Poland, 2011, pp. 490-499.
13. Al-Khawaldeh, F.; Samawi, V. Lexical cohesion and entailment based segmentation for arabic text summarization (lceas). *WSCIT* 2015, 5, pp. 51-60.
14. Bhattacharya, P.; Verma, J.P.; Bhargav, S.; Bhavsar, M. GETS : Sentence Scoring Scheme in Graph-based Extractive Text Summarization for Text Mining Applications. *Information* 2023, 14, pp. 1-28.
15. Ghos, P.P.; Shahariar, R.; Khan, M.A.H. A Rule Based Extractive Text Summarization Technique for Bangla News Documents. *I.J. Modern Education and Computer Science* 2018, 12, pp. 44-53.
16. Cui, P.; Hu, L.; Liu, Y. Enhancing Extractive Text Summarization with Topic-Aware Graph Neural Networks. In: *Proceedings of the Proceedings of the 28th International Conference on Computational Linguistics*, Barcelona, Spain 8-13 December 2020, 2020, pp. 5360–5371.
17. Verma, S.; Nidh, V. Extractive Summarization using Deep Learning. *Research in Computing Science* 2018, 147, pp. 107-117.
18. Alami; Meknassi, M.; En-nahnah, N. Enhancing unsupervised neural networks based text summarization with word embedding and ensemble learning. *Expert Systems With Applications* 2019, 123, pp. 195-211.
19. Gulati, V.; Kumar, D.; Popescu, D.E.; Hemanth, J.D. Extractive Article Summarization Using Integrated TextRank and BM25+ Algorithm. *Electronics* 2023, 12, pp. 1-17.
20. Mojrian, M.; Mirroshande, S.A. A novel extractive multi-document text summarization system using quantum-inspired genetic algorithm: MTSQIGA. *Expert Systems With Applications* 2021, 171, pp. 1-20.
21. Dragomir-R, R.; Hongyan, J.; Małgorzata, S.; Daniel, T. Centroid-based summarization of multiple documents. *Information Processing & Management* 2004, 40, pp. 919-938.
22. Leonhard, H. Topic-based multi-document summarization with probabilistic latent semantic analysis. In: *Proceedings of the Proceedings of the International Conference* RANLP-2009, Borovets, Bulgaria, 2009, pp. 144-149.
23. Pengjie, R.; Zhumin, C.; Zhaochun, R.; Furu, W.; Liqiang, N.; Jun, M.; Maarten, D.R. Sentence relations for extractive summarization with deep neural networks. *ACM TOIS* 2018, 36, pp. 1-32.

24. Akülker, E. Extractive text summarization for Turkish using TF-IDF and pagerank algorithms. *Springer, cham.* 2022, 544, pp. 688-704.
25. Jia, R.; Cao, Y.; Tang, H.; Fang, F.; Cao, C.; Wang, S. Neural Extractive Summarization with Hierarchical Attentive Heterogeneous Graph Network. In: *Proceedings of the Proceedings of the 2020 Conference on Empirical Methods in Natural Language Processing*, online, November 16–20, 2020, pp. 3622–3631.
26. Rizvi, S.M.H.; Imran, R.; Mahmood, A. Text Classification using Graph Convolutional Networks: A Comprehensive Survey. *ACM Computing* 2025, 9, pp. 1-35.
27. Sijtsma, K.; Emons, W. Nonparametric statistical methods. *International encyclopedia of education* 2010, 7, pp. 347-353.

Citation: Shehu, A.; Karatu, M.; Roko, A.; Abdullahi, S. A graph convolutional network and recurrent neural network ensemble for extractive text summarisation in the Hausa language. *Journal of Engineering Science*. 2025, XXXII (1), pp. 32-46. https://doi.org/10.52326/jss.utm.2025.8(2).03.

Submission of manuscripts: jes@meridian.utm.md

Journal of Engineering Science *Vol. XXXII, no. 1 (2025), pp. 47 - 56*
Fascicle *Electronics and Computer Science* *ISSN 2587-3474*
Topic *Computers and Information Technology* *eISSN 2587-3482*

https://doi.org/10.52326/jes.utm.2025.32(1).04
UDC 003.2:512.643

EFFICIENT STORAGE AND COMPRESSION OF COVERING ARRAYS USING ADVANCED ENCODING TECHNIQUES

Petru Cervac *, ORCID: 0000-0001-7488-015X,
Viorica Sudacevschi, ORCID: 0000-0003-0125-3491

Technical University of Moldova, 168 Stefan cel Mare Blvd., Chisinau, Republic of Moldova
* Corresponding author: Petru Cervac, *cervac.petru@doctorat.utm.md*

Received: 02. 23. 2025
Accepted: 03. 24. 2025

Abstract. This paper introduced a novel storage format for covering arrays, designed to optimize file size through efficient compression techniques. The proposed format employed Asymmetric Numeral System (ANS) encoding for array data, as well as Run-Length Encoding (RLE) and Variable Length Encoding (VLE) for metadata storage. The goal was to provide a compact, standardized format that facilitates easier sharing and utilization of covering arrays across different applications. Experimental evaluations on a dataset of 21964 covering arrays from the National Institute of Standards and Technology (NIST) demonstrated that the new format outperforms general-purpose compression algorithms such as ZIP, BZIP2, and XZ in most cases, particularly for larger covering arrays with high parameter counts. While previous work on covering array storage focused on archival and retrieval efficiency, the proposed method significantly reduces storage requirements without loss of structural integrity. The proposed method preserved the combinatorial properties of covering arrays while reducing redundancy, making it a practical alternative for large-scale combinatorial testing applications.

Keywords: *covering arrays, data encoding, compression, Asymmetric Numeral System, combinatorial testing.*

Rezumat. În această lucrare a fost propus un nou format de stocare a matricelor de acoperire, conceput pentru a optimiza dimensiunea fișierelor prin tehnici eficiente de compresie. Formatul utilizat s-a bazat pe codificarea Sistem Numeric Asimetric (SNA) pentru datele din matrice, alături de Codificarea Lungimii de Rulare (CLR) și Codificarea cu Lungime Variabilă (CLV) pentru stocarea metadatelor. Scopul a fost de a oferi un format standardizat și compact, care să faciliteze partajarea și utilizarea eficientă a matricelor de acoperire în diverse aplicații. Experimentele realizate pe un set de date de 21964 de matrice de acoperire, furnizat de Institutul Național de Standarde și Tehnologie (INST), au arătat că noul format depășește algoritmii de compresie generală, precum ZIP, BZIP2 și XZ, în majoritatea cazurilor, în special pentru matrice mari cu un număr ridicat de parametri. În timp ce lucrările anterioare privind stocarea matricelor de acoperire s-au concentrat pe eficiența arhivării și recuperării, abordarea propusă a redus semnificativ cerințele de stocare fără a compromite integritatea

structurală. Metoda prezentată a păstrat proprietățile combinatoriale ale matricelor de acoperire și elimină redundanțele, oferind o alternativă practică pentru aplicațiile de testare combinatorială la scară largă.

Cuvinte-cheie: *matrice de acoperire, codificare a datelor, compresie, sistem numeric asimetric, testare combinatorială.*

1. Introduction

Covering arrays (CA) are a powerful tool in combinatorial testing (CT), used to minimize the number of test cases required to verify a system. This approach leverages the observation that, at least for certain types of software, failures often involve combinations of relatively few parameters [1]. By ensuring that all *t*-way combinations of parameters are checked, a tester can significantly reduce the test suite's size while maintaining comprehensive coverage. Known as *t*-wise testing, this strategy ensures that all combinations of *t* parameters are included in the test suite. For example, 2-way testing covers all pairs of parameters, 3-way testing includes triples, and so on. Exhaustive testing would require k^v (k - number of parameters; v - number of values per parameter) test cases, while *t*-wise reduces their number to approximately $v^t \log k$ (t - combinatorial strength) [2]. For a system with 10 parameters, each having 20 values, exhaustive testing would require 10^{20} test cases, whereas pair-wise testing reduces this to approximately 921. CT was successfully used for verification of various systems of diverse complexity, such as compilers, protocols, networks interfaces, Graphical User Interface systems, web applications and others [3].

CT remains a niche testing technique, although it is a well-established field of research for the last 30 years. One of the major barriers to a practical adoption of CT is the lack of a standardized format for covering arrays [3]. Tools for covering arrays generation, such as ACTS [4], CTWedge [5], CAgen [6] and others, use bespoke output formats, which hampers the efficient sharing and reuse of covering arrays among researchers and practitioners. Each implementation of CT often requires generating covering arrays from scratch, which is impractical, especially for larger arrays, given that covering arrays' generation is an NP-hard problem [7]. While there have been efforts to address this issue by storing and sharing pre-generated covering arrays [8, 9], a standardized format remains the most effective solution. Striving for a such a standard would significantly enhance the practicality and adoption of CT.

The only effort to standardize the storage for covering arrays thus far is by Leithner and Simos [10]. In their work, they store covering arrays in 2 files: a **.cca* file for the array itself and a **. ccmeta* file for metadata. They also introduced a method to bundle multiple covering arrays into a single archive with a **.ca2*, alongside a tool for managing these files. Their paper briefly explored the compression of covering arrays, comparing their tool to general-purpose algorithms, though improving compression ratios was not a primary focus. Although the cost of modern storage has significantly decreased, making file size less critical in many applications, the pursuit of smaller file sizes remains a compelling research challenge. Inspired by their approach, this work proposes a new format for covering array, aimed at minimizing the file size. The format employs three compression techniques: Asymmetric Number System (ANS) encoding for covering arrays [11], and Run-Length Encoding (RLE) and Variable Length Encoding (VLE) for metadata. Testing the new format against a database of 21964 covering arrays hosted by NIST [8] demonstrated superior compression ratios compared to existing general-purpose algorithms for almost all cases.

The remainder of this work is structured as follows. In Section 2, the existing format for storage of covering arrays is reviewed, along with Leithner and Simos's format that inspired the current paper. Section 3 describes the new techniques used in the development of the new format. Section 4 exposes changes to the Leithner and Simos's format and the techniques used to minimize the size of the generated covering arrays. It also highlights the prototype implementation is detailed. In Section 5, the experimental results of the proposed method are presented and compared to three general-purpose compression algorithms: zip, bzip2, and xz. Section 6 summarizes the work and provides an outlook on future research.

2. Related work

The compression of covering arrays is a relatively unexplored area; the notable exception being the work by Leithner and Simos [10]. In their work, they proposed a dual-file format to store covering array data: the *cca* file for the array itself and the *ccmeta* file for metadata. Both formats are binary, designed to enhance storage efficiency. The compression process begins by converting covering arrays from common formats, such as CSV, into a streamlined *"raw covering array"*, stripped of extraneous information. Each parameter *i* in the row is then encoded using $\lceil log_2 v_i \rceil$. bits, where v_i represents the number of values for parameter *i*. The size of a row is calculated by:

$$\sum_{i=1}^{k} \lceil log_2 v_i \rceil, \tag{1}$$

where: k – the number of parameters; v_i – the number of values for parameter i;
The total size of the covering array file is calculated as:

$$N \sum_{i=1}^{k} \lceil log_2 v_i \rceil, \tag{2}$$

where: *N* – the number of rows.

The metadata file stores the values for *N*, *t* and each v_i. Authors allocate 64 bits for *N*, 8 bits for *t*, and 16 bits for each v_i. An additional 64 bits are used for miscellaneous information, including magic bytes, version number, and list termination. Consequently, the metadata file requires a total of $16k + 136$ bits.

Authors evaluated their tool against general-purpose compression algorithms, zip and bzip2. The results indicate their tool outperforms zip and is competitive with bzip2 [10]. Their implementation was a prototype, suggesting that further optimizations could yield even better compression ratios.

3. Techniques for Improved Compression

In this section, the techniques used for the new method for compression of covering arrays are described. 3 techniques were employed: ANS-encoding for the compression of the array itself, RLE and VLE for the metadata.

ANS is a family of number systems where each symbol of a number can take a value from a set of different size. Time keeping is an example of an ANS. Each component of a time (seconds, minutes, hours, days, etc.) takes a value from a different set. There are between $1 \ldots 100$ seconds, minutes, hours: $0 \ldots 59$, days: $0 \ldots 366$ etc. ANS is in the contrast with more familiar symmetric number systems, such as decimal, binary or hexadecimal, where all symbols take values from the same alphabet. An encoder utilizing an ANS tries to encode the

information into a single natural number *x*. Duda was the first one to explore the use of an ANS for data compression [11]. It has become more widely used since then, being incorporated in a few commercial offerings from Facebook, Microsoft, Google, and others.

RLE is a lossless data compression method where sequences of repeated data are stored as a single instance of the data along with a count of its consecutive repetitions, instead of storing the entire sequence. Several tools and algorithms use RLE for data compression, particularly in image formats like TIFF and GIF, where repeated color sequences are common. RLE is also used as part of compression schemes in video codecs like MPEG and in some lossless data compressors, where it helps optimize storage by encoding repeated data sequences efficiently.

VLE is a form of lossless data compression in which the number of bytes used to encode a number is not fixed. Examples of widely recognized VLE techniques include Huffman coding, Lempel–Ziv coding, arithmetic coding, and context-adaptive variable-length coding. The most widely use of VLE is for the encoding of characters for alphabets that exceed 256 characters. The ISO-2022 [12] family of standards define a variable length encoding for characters that use from 1 to 4 bytes to encode characters in various languages such as Japanese [13], Chinese [14], Korean [15], etc. The most popular encoding based on the VLE is the UTF-8-character encoding, which uses 1 to 4 bytes to encode a character [16].

4. Methodology

To increase information density, each row of the array undergoes ANS encoding. Instead of treating each parameter separately, the approach interprets each row as a number in an ANS with alphabets $v_1, \dots, v_k$. The row encoded in this system is then converted to its decimal equivalent and written to the file. This approach reduces the number of bits needed to store each row compared to encoding each column individually. In the original format, the total bits required to store a row is calculated by Eq. (1). With ANS encoding, the number of bits is calculated by the following formula:

$$\left\lceil \sum_{i=1}^{k} log_2 v_i \right\rceil \tag{3}$$

For example, consider a mixed covering array with 10 variables, each having 10 values. The original format requires $10\lceil log_2(10) \rceil = 40$ bits, while the ANS encoding requires $\lceil 10\, log_2(10) \rceil = 34$ bits, resulting in a 15% reduction in the bits needed to store a single row. Conversion from a number in ANS to a number in decimal is done using the following formula:

$$\sum_{i=1}^{k} \left(s_i \prod_{j=i+1}^{k} v_j \right), \tag{4}$$

where: k – the number of symbols in the representation; a_i – symbol at the position i; v_j – the alphabet size for the position j.

The *ccmeta* format proposed in the original paper is effective for covering arrays with a small and varied number of parameters. However, during testing, the method proved inefficient for uniform or mostly uniform covering arrays with many parameters. In tests with uniform covering arrays up to 2000 parameters, the *ccmeta* file size often matched or exceeded the *cca* file size. To address this, the approach applies RLE to parameter encoding. For example, a covering array with $k = 10$ and $v_1 = v_2 = \cdots = v_{10} = 2$ can be represented

as $\{10, 2\}$ instead of $\{2, 2, 2, 2, 2, 2, 2, 2, 2, 2\}$, reducing memory usage from 10 to 2 bytes. To maximize the number and length of runs, the approach sorts the columns in the ascending order. This is allowed as the definition of covering array doesn't restrict the column order. Then, the process counts occurrences of each value and stores them alongside their counts.

Table 1

Range of values for prefix

Code	Bytes	Range
$0x\ xx\ xx\ xx$	1	$00\ 00\ 00\ 00_{16} \ldots 00\ 00\ 00\ 7f_{16}$
$10\ xx\ xx\ xx$	2	$00\ 00\ 00\ 80_{16} \ldots 00\ 00\ 3f\ ff_{16}$
$11\ 0x\ xx\ xx$	3	$00\ 00\ 40\ 00_{16} \ldots 00\ 1f\ ff\ ff_{16}$
$11\ 10\ xx\ xx$	4	$00\ 20\ 00\ 00_{16} \ldots 0f\ ff\ ff\ ff_{16}$

To store the count of occurrences, the method uses VLE, balancing practicality for arrays with varied, smaller parameters and efficiency for more esoteric cases, such as the 2000-parameter uniform arrays used in testing. The most significant bits in the length indicate the number of bytes used: 0 for 1 byte, 10 for 2 bytes, 110 for 3 bytes, and 1110 for 4 bytes. Table 1 illustrates the value ranges for each suffix. This method draws inspiration from UTF-8 Character Encoding Form [16]. This encoding supports up to 2^{28} numbers with 4 bytes, sufficient for most applications. It can be extended if necessary. Most covering arrays will use 1 byte to represent column value occurrences.

Another improvement in the proposed ccmeta format is the use of a single byte to represent the number of values per column, compared to 2 bytes in the original. This limits column values to 256, sufficient for most arrays used in practice. If future needs require more than 256 values per column, the format can be adjusted using RLE or specifying byte count in the preamble, though this is deemed unnecessarily complex for now. The original file structure remained unchanged, with only the version number increased as suggested by the authors. Figure 1 shows the updated ccmeta file format.

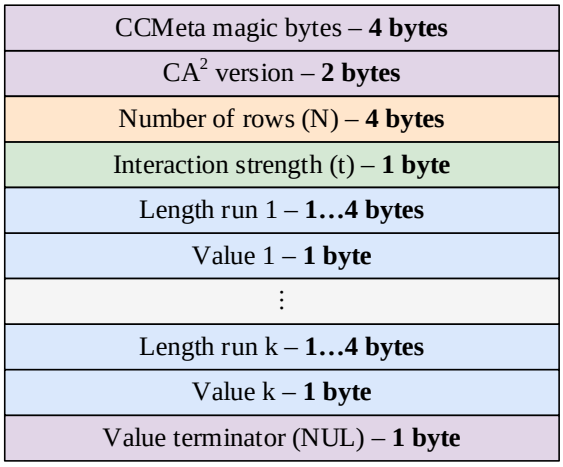

Figure 1. Updated *ccmeta* file format.

The method presented in this paper was implemented in C# since it is the language most familiar to the authors. The prototype is capable of parsing files in CSV and ACTS format. The prototype provides only the compression capability. The prototype is hosted on GitHub [17].

5. Evaluation

There are 2 challenges in analyzing the capabilities of the proposed method. The first challenge regards the representation of the covering array. A covering array can be represented in the *"extended"* form or in the *"shortened"* form. The definition of the covering arrays states each column should have a value from a set with no more than *v* values; however, it does not restrict the values in the set; values can be strings of arbitrary values. A covering array in *"extended"* form: [(Windows, Chrome), (Windows, Firefox), (Linux, Chrome), (Linux, Firefox)] is equivalent to the covering array in *"shortened"* form: [(0, 0), (0, 1), (1, 0), (1, 1)]. The proposed method is technically a lossy compression scheme; it preserves the structure of the covering array, but removes the information about the individual values; it is converting a CA in *"extended"* form to a CA in *"shortened"* form. The proposed method may appear more efficient when applied to covering arrays in their extended form rather than in their shortened form, as the resulting file will be smaller. However, this perception is misleading, as the resulting file technically contains less information than the covering array in extended form. To mitigate the issue, the evaluation focused only on covering arrays in shortened form.

The second challenge regards the data set of covering arrays. The proposed method is not restricted to covering arrays and can compress any random CSV value. A random CSV file is less structured than a covering array in the form of a CSV file; it can contain more rows than an actual covering array; it can have duplicated rows; it may not contain all combinations. This might serve as an advantage or disadvantage to the general-purpose compression algorithms used for comparison. To mitigate the issue, the testing restricted the data set to covering arrays only, though this reduced the total set of possible covering arrays.

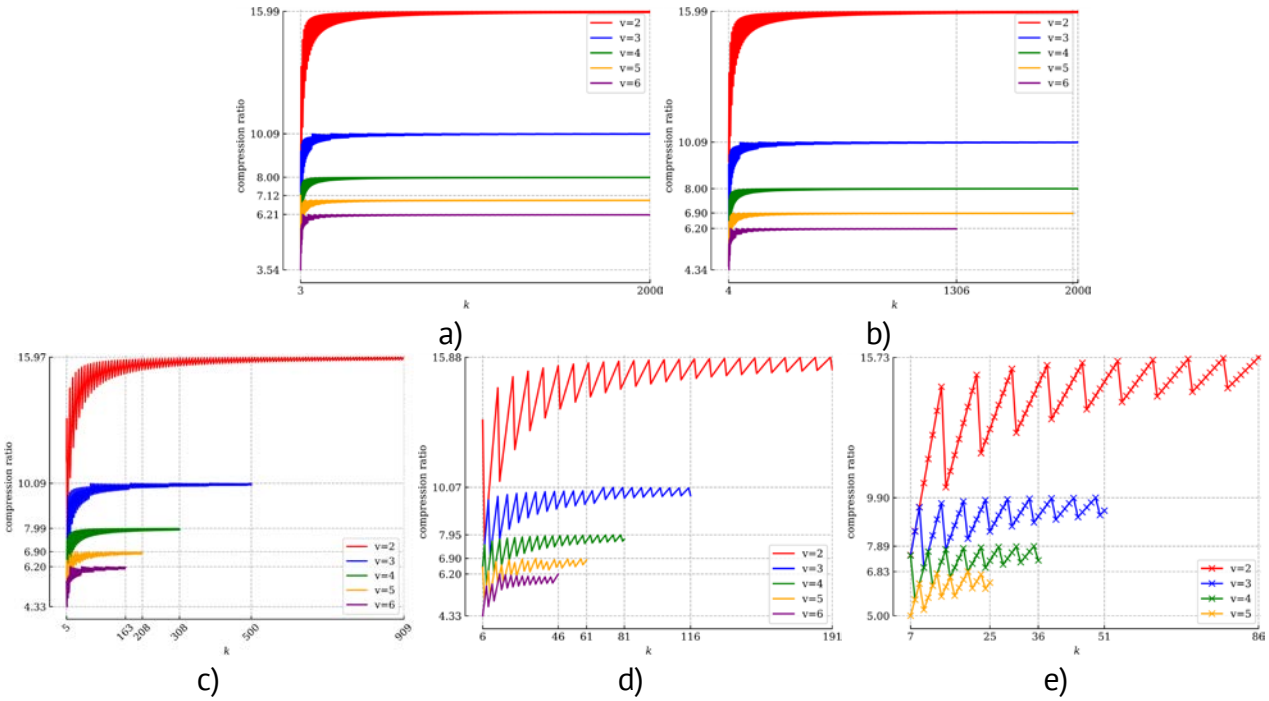

Figure 2. Compression ratio of the new format for various *t*, *k*, *v*, where: *t* – interaction strength;
k – number of parameters; *v* – number of values per parameter:
a) $t = 2$*; b)* $t = 3$*; c)* $t = 4$*; d)* $t = 5$*; e)* $t = 6$.

The test dataset consisted of 21964 covering arrays hosted by NIST. Covering arrays are stored in a custom format named ACTS. The dataset consists of various covering arrays with *t* and *v* between 2 and 6 and *k* up to 2000. The size and variety of the dataset allowed us to analyze the new compression scheme under diverse conditions. Although big, this dataset is not ideal, as it does not contain mixed covering arrays, which the proposed method can work with, and also more frequently used in the real world.

The proposed approach was compared against zip, bzip2 and xz, which are widely used, mature, general purpose, lossless compression algorithms. zip uses the DEFLATE algorithm [18], bzip2 uses the Burrows-Wheeler algorithm [19], and xz uses the Lempel-Ziv-Markov chain algorithm [20]. The utilities were configured to generate the smallest possible output files although, this might not fully reflect the day-to-day use of these tools.

The evaluation focused solely on output file size, ignoring other factors such as speed. The size of the **.ccmeta* file was also disregarded, as it remained under 20 bytes for any analyzed covering array and was negligible compared to the size of the **.cca* file.

Table 2

Compression ratio limit for parameter *v*

v	**Compression ratio in limit**
2	15.99
3	10.09
4	8.00
5	7.12
6	6.21

Note: *v* – number of values per parameter

Figure 2 shows the compression ratio of the new format for the whole dataset. Compression ratio is the bigger for smaller values of v. It performs best for $v = 2$ and worst for $v = 6$. t does not influence the compression ratio, which is not surprising. In the long run, the compression ratio for each v reaches a limit. Table 2 shows the compression ratio limit for each value of v.

Table 3

Number of swings to the top

v	**Number of swings to the top**
2	8
3	5
4	4
5	3-4
6	3

Note: *v* – number of values per parameter

One peculiar observation is the *"zigzag"* behavior of the compression ratio. The compression ratio swings from smaller compression ratio to bigger one. The number of times the compression ratio comes to the maximum depends on the value of *v*. Table 3 shows the number of swings required to reach the top. This happens due to the way the ANS encoding is working. There is a maximum number of information that can be fit into a number. When the number is reached, the storage space has to be expanded. During the storage expansion, space is not used efficiently which explains the lower compression ratio.

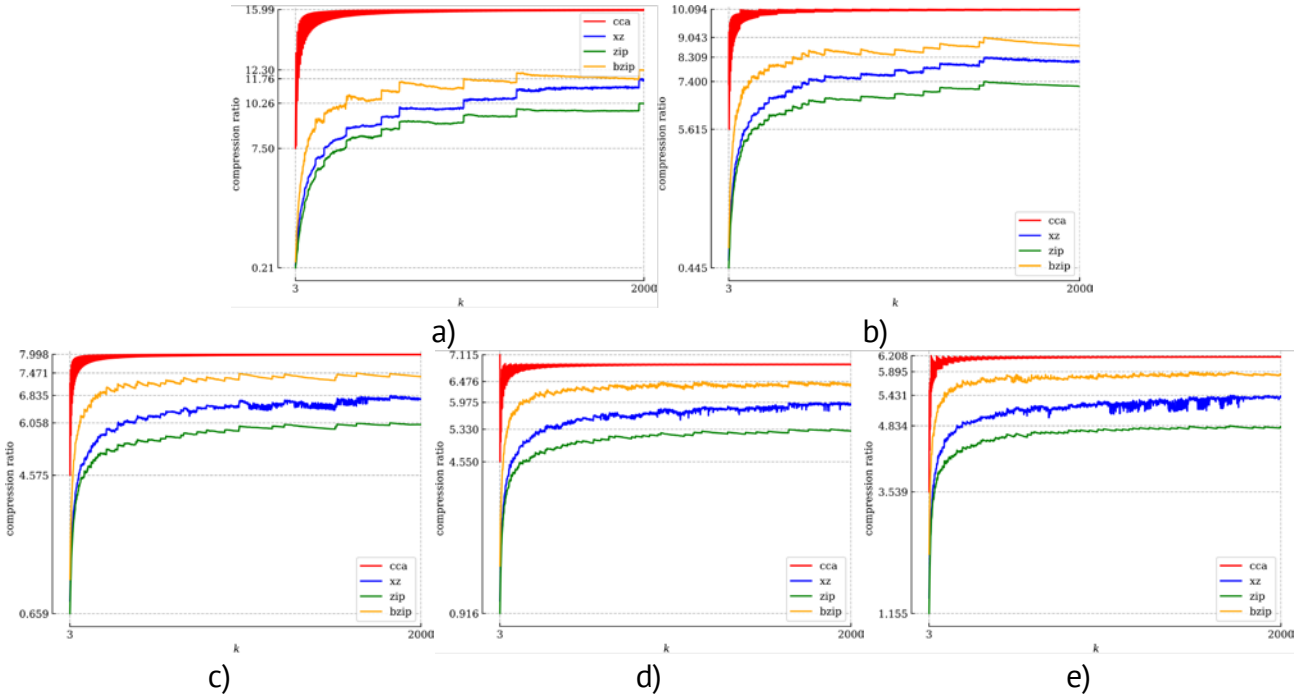

Figure 3. Comparison ratio of the new format, xz, zip and bzip2 for $t = 2$ and various values of v: a) $v = 2$; b) $v = 3$; c) $v = 4$; d) $v = 5$; e) $v = 6$.

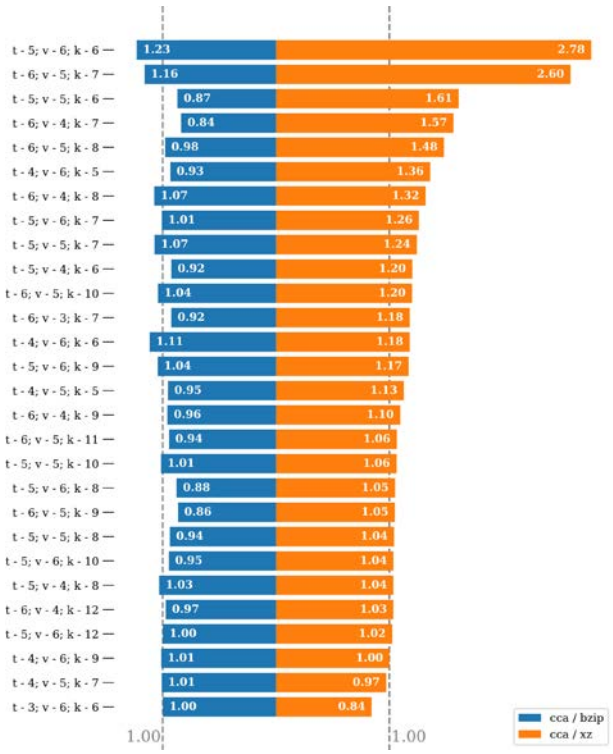

Figure 4. Covering arrays for which the compression ratio of the new algorithm is smaller than general-purpose compression tools.

The compression ratio of the proposed method is in general bigger than the compression ratio of the general-purpose compression algorithms. Figure 3 show the compression ratio between the proposed method and the general-purpose algorithms. It performs best for $v = 2$ and big values of k. The compression ratio increases as the k increases, reaching a limit. The compression ratio decreases as v increases. The proposed method, in general, performs worse for smaller covering arrays, although outperforming the

general-purpose compression algorithms. Overall, the existing compression algorithms did surprisingly well. The best performing general-purpose compression tool for covering arrays was bzip2, followed by xz and zip.

There are 28 covering arrays for which a general-purpose compression algorithm produces a smaller output file. xz and bzip2 outperforms the proposed method in the range k: 5 … 12, v: 3 … 6, t: 4 … 6. Figure 4 summarizes the finding.

6. Conclusions and Future Work

This paper presented an improvement to the CA2 format presented by Leithner and Simos by employing ANS Encoding for the CCA files and RLE and VLE for the ccmeta files. These techniques showed great results compared to general purpose compression algorithms for most of the analyzed inputs, although the advantage diminishes with the increase in the number of values per column. General purpose compression algorithms, especially xz, performed better for covering array with higher *v* and small *k*, which is expected to be the majority of covering arrays used in day-to-day operations. An important aspect of the future work is performance analysis and the use of other flavors of ANS such as tANS. Decompression aspect of the method should also be implemented.

Acknowledgement. This paper presents the scientific results obtained within the project 020404, "Innovations in Biomedical Engineering: Advanced Technologies and Applications for Data Acquisition, Processing, and Analysis," carried out within the Department of Computer Science and Systems Engineering at the Technical University of Moldova.

Conflicts of interest. The authors declare no conflicts of interest.

References

1. Kuhn, D. R.; Kacker, R. N.; Lei, Y. Introduction to Combinatorial Testing, 1st ed.. Taylor & Francis Group, London, United Kingdom, 2016, p. 3.
2. Cohen, D. M; Dalal, S. R.; Fredman, M. L.; Patton, G. C. The AETG system: an approach to testing based on combinatorial design. *IEEE Trans. Softw. Eng.* 1997, 23, pp. 437–444.
3. Nie, C.; Leung, H. A survey of combinatorial testing. *ACM Comput. Surv.* 2011, 43, pp. 1–29.
4. Yu, L.; Lei, Y.; Kacker, R. N.; Kuhn, D. R. ACTS: A Combinatorial Test Generation Tool. In: *IEEE Sixth International Conference on Software Testing, Verification and Validation*, Luxembourg, 2013, pp. 370–375.
5. Gargantini, A.; Radavelli, M. Migrating Combinatorial Interaction Test Modeling and Generation to the Web. In: *IEEE International Conference on Software Testing Verification and Validation Workshop*, Västerås, Sweden, 9-13 April 2018, pp. 308-317.
6. Wagner. M.; Kleine, K.; Simos, D.; Kuhn, R.; Kacker, R. CAGEN: A fast combinatorial test generation tool with support for constraints and higher-index arrays. In: *IEEE International Conference on Software Testing, Verification and Validation Workshops*, Porto, Portugal, 23-27 March 2020, pp. 191-200.
7. Kampel, L.; Simos, D. A survey on the state of the art of complexity problems for covering arrays. *Theor. Comput. Sci.* 2019, 800, pp. 107–124.
8. Forbes, M.; Lawrence, J.; Lei, Y.; Kacker, R. N.; Kuhn, D. R. Refining the In-Parameter-Order Strategy for Constructing Covering Arrays. J. Res. Natl. Inst. Stand. Technol 2008, 113, pp. 287-297.
9. A Library of Orthogonal Arrays. Available online: http://neilsloane.com/oadir/ (accessed on 01.10.2024).
10. Leithner, M.; Simos, D. E. CA2: Practical Archival and Compression of Covering Arrays. In: IEEE International Conference on Software Testing, Verification and Validation Workshops, Valencia, Spain, 4-13 April 2022, pp. 63-67.
11. Duda, J.; Tahboub, K.; Gadgil, N. J.; Delp, E. J. The use of asymmetric numeral systems as an accurate replacement for Huffman coding. In: Picture Coding Symposium (PCS), Calms, QLD, Australia, 31 May – 3 June 2015, pp. 65-69.
12. ISO/IEC 2022:1994 - Information technology — Character code structure and extension techniques. Available online: https://www.iso.org/standard/22747.html (accessed on 03 11 2024).

13. RFC 1468: Japanese Character Encoding for Internet Messages. Available online: https://www.rfc-editor.org/rfc/rfc1468.html (accessed on 07.11.2024).
14. RFC 1922: Chinese Character Encoding for Internet Messages. Available online: https://www.rfc-editor.org/rfc/rfc1922.html (accessed on 07.11.2024).
15. RFC 1557: Korean Character Encoding for Internet Messages. Available online: https://www.rfc-editor.org/rfc/rfc1557.html (accessed on 07.11.2024).
16. UTR#17: Unicode Character Encoding Model. Available online: https://www.unicode.org/reports/tr17/ (accessed on 07.11.2024).
17. BusHero/CA2. Available online: https://github.com/BusHero/CA2 (accessed on 01.11.2024);
18. RFC 1951: DEFLATE Compressed Data Format Specification version 1.3. Available online: https://www.rfc-editor.org/rfc/rfc1951.html (accessed on 07.11.2024).
19. Seward, J., bzip2 and libbzip2, version 1.0.8. Available online: https://sourceware.org/bzip2/manual/manual.html (accessed 05.12.2024).
20. XZ Utilities. Available online: https://tukaani.org/xz/ (accessed on 01.12.2024).

Citation: Cervac, P.; Sudacevschi, V. Efficient storage and compression of covering arrays using advanced encoding techniques. *Journal of Engineering Science*. 2025, XXXII (1), pp. 47-56. https://doi.org/10.52326/jss.utm.2025.8(2).04.

Submission of manuscripts: jes@meridian.utm.md

Journal of Engineering Science
Fascicle *Electronics and Computer Science*
Topic *Computers and Information Technology*
Vol. XXXII, no. 1 (2025), pp. 57 - 70
ISSN 2587-3474
eISSN 2587-3482

https://doi.org/10.52326/jes.utm.2025.32(1).05
UDC 004.7:004.02

MACRO SYNTHESIS OF WIDE AREA COMPUTER NETWORKS AT NONLINEAR COSTS

Ion Bolun*, ORCID: 0000-0003-1961-7310

Technical University of Moldova, 168 Stefan cel Mare Blvd., Chisinau, Republic of Moldova
* Corresponding author: Ion Bolun, *ion.bolun@isa.utm.md*

Received: 03. 11. 2025
Accepted: 03. 31. 2025

Abstract. In practice, simple solutions of quick preliminary estimation of basic characteristics of a wide area computer network sometimes are needed. To achieve this goal, the backbone data transfer subnet and server set of computer networks are opportune to be examined. Considering the nonlinear continuous dependence of the costs of channels, routers, and servers on their performance and using the J.R. Jackson's partitioning theorem, an analytical model for these components of the network is defined. Based on this model, two optimization problems are formulated and examined: minimizing the average retention time of data processing requests and minimizing the summary cost of servers, channels and routers of the network. For both problems, numerical solution algorithms are proposed. These algorithms allow obtaining the expected solutions in continuous form, the respective performances being expressed by positive real numbers. Since the allowed performances of the mentioned entities are discrete, additional adjustments to the solutions in question, depending of the case, may be necessary. For such adjustments, two algorithms are proposed. One of them solves the problem by reducing it to that of the backpack. Another solves the problem in an heuristic manner based on the L. Kleinrock's resource concentration rule.

Keywords: *algorithm, channel, model, optimization, response time, router, server.*

Rezumat. În practică, uneori sunt necesare soluții simple de estimare preliminară rapidă a caracteristicilor de bază ale unei rețele de calculatoare de arie largă. În acest scop, este oportun de examinat subrețeaua magistrală de transfer date și setul de servere ale rețelelor de calculatoare. Considerând dependența neliniară continuă a costurilor canalelor, ruterelor și serverelor de performanța acestora și utilizând teorema de partiționare a lui J.R. Jackson, este definit un model analitic pentru aceste componente ale rețelei. Pe baza acestui model, sunt formulate și examinate două probleme de optimizare: minimizarea timpului mediu de reținere a solicitărilor de procesare a datelor și minimizarea costului sumar al serverelor, canalelor și ruterelor rețelei. Pentru ambele probleme, sunt propuși algoritmi de soluționare numerică. Acești algoritmi permit obținerea soluțiilor scontate în formă continuă, performanțele respective fiind exprimate prin numere reale pozitive. Deoarece performanțele permise ale entităților menționate sunt discrete, pot fi necesare, în funcție de caz, ajustări suplimentare ale soluțiilor în cauză. Pentru astfel de ajustări, sunt propuși doi algoritmi. Unul

dintre aceștia rezolvă problema reducând-o la cea a rucsacului. Celălalt rezolvă problema într-o manieră euristică, bazată pe utilizarea regulii lui L. Kleinrock de concentrare a resurselor.

Cuvinte cheie: *algoritm, canal, durată de răspuns, model, optimizare, ruter, server*.

1. Introduction

Because the creation and development of wide are computer networks involve considerable costs [1], minimizing these expenses is important. For this purpose many researches are carried out. In a general form, the problem of computer networks synthesis consists in determining of their topology, of the number, deployment, productivity, operating regimes and functions of servers and communication nodes, the capacity of data transfer channels, the distribution of user requests among servers and the ways of data transfer and routing in the network, which would ensure the extreme value of the used optimization criterion for the required quality of serving the user requests [2].

For large networks, the mathematical formalization and overall solution of the problem is very difficult. That is why various simplifications are usually resorted to, including the disaggregation of the general problem into several sub-problems [1,3,4].

Given the stochastic nature of computer network processes, in performance research, they are usually examined as queuing networks [4,5]. In the field of queuing networks, models and algorithms are developed, several analytical solutions are obtained. It is especially the case to mention the J.R. Jackson's partitioning theorem [6], the L. Kleinrock's square root law [7] and conservation law [5], the Gordon-Newell's theorem [8], the J. Buzen's algorithm [9], the BCMP networks [10], the MVA method [11], and the MVAC [12] and DAC [13] algorithms.

Search engines [14,15], Big data [16,17], and Cloud computing [18] have involved separate research with data centers [19,20], including their design, implementation, and performance analysis [21], their reliability [22], the placement of their virtual machines [23], and so on.

With refer to data networks, they are examined the necessary capacity of data channels at their linear [7] and power function [5] costs. Also, the needed capacity of computer network channels, routers and servers at linear dependence of their costs on their performance is examined in [24].

New steps in the development of computer networks are done by Grid computing [25, 26] and software defined networks (SDN) [27,28], including their design [29], the choosing of SDN operating system [30], the placement of controllers [31], etc.

However, the proposed methods and algorithms are, as a rule, relatively laborious, and sometimes in practice simple solutions are useful for the quick preliminary estimation of basic characteristics of a computer network. The purpose of this paper is to propose relatively simple algorithms for the determination of approximate necessary performances of channels, routers and servers of wide area computer networks at nonlinear costs of these components on their capacity.

2. A Simplified Model of Wide Area Computer Networks at Nonlinear Costs

Of course, the assumptions that the dependencies of costs of channels $C_{ci}(d_{ci})$ $(i = \overline{1, k_c})$, of routers $C_{ri}(\mu_{ri})$ $(i = \overline{1, k_r})$, and of servers $C_{si}(\mu_{si})$ $(i = \overline{1, k_s})$ on their capacities are linear, used in [24], allow only very approximate solutions regarding the required capacities $d_{ci}(i =$

$\overline{1,k_c}$) of channels, that $\mu_{ri}(i=\overline{1,k_r})$ of routers, and that $\mu_{si}(i=\overline{1,k_s})$ of servers. Here k_c, k_r, and k_s are the number, respectively, of channels, of routers, and of severs in the network.

Some improvements in the accuracy of the [24] solutions can be obtained by using the $C_{ci}(d_{ci})$ $(i=\overline{1,k_c})$, $C_{ri}(\mu_{ri})$ $(i=\overline{1,k_r})$, and $C_{si}(\mu_{si})$ $(i=\overline{1,k_s})$ continuous nonlinear dependencies of reasonable increasing behavior (without first or second order discontinuities, i.e. the first order derivatives are continuous functions). The assumption that dependencies $C_{ci}(d_{ci})$ $(i=\overline{1,k_c})$, $C_{ri}(\mu_{ri})$ $(i=\overline{1,k_r})$, and $C_{si}(\mu_{si})$ $(i=\overline{1,k_s})$ are increasing is natural, because increasing the entity's capacity leads to reducing the duration of user requests retention. Thus, if there are such cases (equal or higher cost at lower performance) for some alternatives of constituting the respective network components, these are eliminated (not taken into account), without reducing the chances of obtaining the optimal solution.

So, from the multitude of computer network macro synthesis aspects, the model includes those related to estimating the necessary capacities of their servers, data transfer channels or trunks (hereafter channels or DTT), and routers at their nonlinear costs on their performance. The model is an improvement of the one proposed and researched in [24].

Because computer networks operation has a stochastic character, they usually are examined as networks of queues. Notes [24]:

- rate β of the summary flow of requests to servers;
- rate γ of the summary flow of packets generated by user requests and the responses to them;
- the mean number g of packets per request, $g = \gamma/\beta$;
- packet rate through channel i - λ_{ci} and router j - λ_{rj};
- rate λ_{sl} of requests to server l;
- average size V_i of a packet transmitted through channel i;
- the average retention of a packet at channel i - T_{ci} and at router j - T_{rj};
- the average retention of a request at the server l - T_{sl} and in the network - T;
- summary cost of channels - C_c, of routers – C_r, of servers – C_s, and of the network - C.

Moreover, as in [24], it is considered that flows λ_{ci} $(i=\overline{1,k_c})$, λ_{rj} $(j=\overline{1,k_r})$, and λ_{sl} $(l=\overline{1,k_s})$ are elementary and the time of packet transmission by channels, of packet processing by routers, and of request processing by servers are exponentially distributed. At the same time, unlike in [24], the dependences $C_{ci}(d_{ci})$ $(i=\overline{1,k_c})$, $C_{ri}(\mu_{ri})$ $(i=\overline{1,k_r})$, and $C_{si}(\mu_{si})$ $(i=\overline{1,k_s})$ are continuous increasing of reasonable behavior.

It will be examined the steady-state operation of the network, which exists if the relationships occur:

$$\mu_{ci} > \lambda_{ci},\ i=\overline{1,k_c};\ \mu_{rj} > \lambda_{rj},\ j=\overline{1,k_r};\ \mu_{sl} > \lambda_{sl},\ l=\overline{1,k_s}, \tag{1}$$

where $\mu_{ci} = d_{ci}/V_i$ is the packet transmission rate by channel i, $i=\overline{1,k_c}$.

Under the conditions and assumptions defined above, a computer network can be examined as an open exponential network of queues with a homogeneous flow of requests operating in steady-state.

According to the Jackson's partitioning theorem [6], any open exponential network of queues can be examined as a set of isolated exponential queuing systems. Then the average time T_i of a request in the queuing system i of the network is determined [4] according to the relation $T_i = 1/(\mu_i - \lambda_i)$, where λ_i is the request flow rate, and μ_i – the request serving rate by station i. So, the relations take place:

$$T_{ci} = \frac{V_i}{d_{ci} - \lambda_{ci} V_i},\ i=\overline{1,k_c}; \tag{2}$$

$$T_{ri} = \frac{1}{\mu_{ri} - \lambda_{ri}}, i = \overline{1, k_r}; \quad (3)$$

$$T_{si} = \frac{1}{\mu_{si} - \lambda_{si}}, i = \overline{1, k_s}. \quad (4)$$

Taking into account Eq. (2)-(4), is obtained

$$T = \frac{1}{\gamma}\left(\sum_{i=1}^{k_c}\lambda_{ci}T_{ci} + \sum_{i=1}^{k_r}\lambda_{ri}T_{ri}\right) + \frac{1}{\beta}\sum_{i=1}^{k_s}\lambda_{si}T_{si} = \frac{1}{\gamma}\left(\sum_{i=1}^{k_c}\frac{\lambda_{ci}V_i}{d_{ci} - \lambda_{ci}V_i} + \sum_{i=1}^{k_r}\frac{\lambda_{ri}}{\mu_{ri} - \lambda_{ri}} + g\sum_{i=1}^{k_s}\frac{\lambda_{si}}{\mu_{si} - \lambda_{si}}\right). \quad (5)$$

Also, evidently, it takes place

$$C = C_c + C_r + C_s = \sum_{i=1}^{k_c}C_{ci}(d_{ci}) + \sum_{i=1}^{k_r}C_{ri}(\mu_{ri}) + \sum_{i=1}^{k_s}C_{si}(\mu_{si}). \quad (6)$$

The queuing network model is determined by Eq. (5), Eq. (6) and conditions of InEq. (1). With this model, two problems of determining the performance required for common-use components of computer networks are usually of interest:

- minimizing the average retention time T in the network of the requests of data processing;
- minimizing the summary cost C of servers, channels and routers of the computer network.

These are explored in Sections 3 and 4, respectively.

3. Minimizing the Average Response Time to User Requests

Problem 1 - minimizing the average response time to user requests at nonlinear costs with common-use components of the wide area computer network. Let, for the model {Eq. (5), Eq. (6)} and conditions of InEq. (1), the parameters are known: C^*; β; γ; k_c; k_r; k_s; λ_{ci}, V_i, $C_{ci}(d_{ci})$ $(i = \overline{1, k_c})$; λ_{ri}, $C_{ri}(\mu_{ri})$ $(i = \overline{1, k_r})$; λ_{si}, $C_{si}(\mu_{si})$ $(i = \overline{1, k_s})$, where C^* is the maximum allowed total cost of servers, channels, and routers of the network. It is required to determine the necessary performances d_i $(i = \overline{1, k_c})$ of channels, those μ_{ri} $(i = \overline{1, k_r})$ of routers and those μ_{si} $(i = \overline{1, k_s})$ of network servers that would minimize the average retention time T of data processing requests at the total cost C of servers, channels and routers which would not exceed the given value C^*, i.e.:

$$T = \frac{1}{\gamma}\left(\sum_{i=1}^{k_c}\frac{\lambda_{ci}V_i}{d_{ci} - \lambda_{ci}V_i} + \sum_{i=1}^{k_r}\frac{\lambda_{ri}}{\mu_{ri} - \lambda_{ri}} + g\sum_{i=1}^{k_s}\frac{\lambda_{si}}{\mu_{si} - \lambda_{si}}\right) \to \min \quad (7)$$

upon compliance with the restriction

$$C = C_c + C_r + C_s = \sum_{i=1}^{k_c}C_{ci}(d_{ci}) + \sum_{i=1}^{k_r}C_{ri}(\mu_{ri}) + \sum_{i=1}^{k_s}C_{si}(\mu_{si}) \le C^* \quad (8)$$

in conditions of InEq. (1).

Solving. From the essence of the problem, it is obvious that the solution of the problem corresponds to the limit value in Eq. (8), that is, $C = C^*$. Then the problem {Eq. (7), Eq. (8)} can be solved using the method of Lagrange multipliers. The respective Lagrangian L is

$$L=\frac{1}{\gamma}\left(\sum_{i=1}^{k_c}\frac{\lambda_{ci}V_i}{d_{ci}-\lambda_{ci}V_i}+\sum_{i=1}^{k_r}\frac{\lambda_{ri}}{\mu_{ri}-\lambda_{ri}}+g\sum_{i=1}^{k_s}\frac{\lambda_{si}}{\mu_{si}-\lambda_{si}}\right)+ \\ +\chi\left(\sum_{i=1}^{k_c}C_{ci}(d_{ci})+\sum_{i=1}^{k_r}C_{ri}(\mu_{ri})+\sum_{i=1}^{k_s}C_{si}(\mu_{si})-C^*\right), \tag{9}$$

the conditioned optimization problem {Eq. (7), Eq. (8)} reducing to an unconditioned optimization problem – minimizing *L*. Here χ is the Lagrange multiplier.

The Lagrangian *L* contains $k_c + k_r + k_s$ +1 unknowns: χ; d_{ci} ($i=\overline{1,k_c}$), μ_{ri} ($i=\overline{1,k_r}$), and μ_{si} ($i=\overline{1,k_s}$). To minimize *L*, the partial derivatives of *L* with respect to the unknowns are determined; they are equalized to 0, resulting a system of $k_c + k_r + k_s$ +1 equations. By solving this system, the analytical expressions for the performances d_{ci} ($i=\overline{1,k_c}$), μ_{ri} ($i=\overline{1,k_r}$), and μ_{si} ($i=\overline{1,k_s}$) can be obtained. One has:

$$\begin{cases}\dfrac{\partial L}{\partial d_{ci}}=\dfrac{1}{\gamma}\cdot\dfrac{-\lambda_{ci}V_i}{\left(d_{ci}-\lambda_{ci}V_i\right)^2}+\chi\dfrac{\partial C_{ci}(d_{ci})}{\partial d_{ci}}=0,\ i=\overline{1,k_c}\\ \dfrac{\partial L}{\partial \mu_{ri}}=\dfrac{1}{\gamma}\cdot\dfrac{-\lambda_{ri}}{\left(\mu_{ri}-\lambda_{ri}\right)^2}+\chi\dfrac{\partial C_{ri}(\mu_{ri})}{\partial \mu_{ri}}c_{ri}=0,\ i=\overline{1,k_r}\\ \dfrac{\partial L}{\partial \mu_{si}}=\dfrac{g}{\gamma}\cdot\dfrac{-\lambda_{si}}{\left(\mu_{si}-\lambda_{si}\right)^2}+\chi\dfrac{\partial C_{si}(\mu_{si})}{\partial \mu_{si}}=0,\ i=\overline{1,k_s}\\ \dfrac{\partial L}{\partial \chi}=\sum_{i=1}^{k_c}C_{ci}(d_{ci})+\sum_{i=1}^{k_r}C_{ri}(\mu_{ri})+\sum_{i=1}^{k_s}C_{si}(\mu_{si})-C^*=0.\end{cases} \tag{10}$$

From the system of Eqs. (10), provided that the restrictions on InEq. (1) are satisfied, it follows that the equalities must hold:

$$\chi\gamma\left(d_{ci}-\lambda_{ci}V_i\right)^2\frac{\partial C_{ci}(d_{ci})}{\partial d_{ci}}-\lambda_{ci}V_i=0,\ i=\overline{1,k_c}; \tag{11}$$

$$\chi\gamma\left(\mu_{ri}-\lambda_{ri}\right)^2\frac{\partial C_{ri}(\mu_{ri})}{\partial \mu_{ri}}-\lambda_{ri}=0,\ i=\overline{1,k_r}; \tag{12}$$

$$\chi\gamma\left(\mu_{si}-\lambda_{si}\right)^2\frac{\gamma}{g}\cdot\frac{\partial C_{si}(\mu_{si})}{\partial \mu_{si}}-\lambda_{si}=0,\ i=\overline{1,k_s}; \tag{13}$$

$$\sum_{i=1}^{k_c}C_{ci}(d_{ci})+\sum_{i=1}^{k_r}C_{ri}(\mu_{ri})+\sum_{i=1}^{k_s}C_{si}(\mu_{si})-C^*=0. \tag{14}$$

In general case, obtaining, based on Eqs. (11)-(14), the analytical expression for χ, and then for the expected capacities d_{ci} ($i=\overline{1,k_c}$), μ_{ri} ($i=\overline{1,k_r}$), and μ_{si} ($i=\overline{1,k_s}$) is not possible. But their values can be obtained, under certain conditions, using a numerical method for solving equations, for example the dichotomy method.

According to Eqs. (11)-(14) and taking into account the conditions of InEq. (1) and the positive increasing character (by definition) of functions $C_{ci}(d_{ci})$ ($i=\overline{1,k_c}$), $C_{ri}(\mu_{ri})$ ($i=\overline{1,k_r}$), and $C_{si}(\mu_{si})$ ($i=\overline{1,k_s}$), the first factor of the sum of the left-hand side of Eqs. (11)-(14) at $\chi > 0$ is positive. So, the optimal solution is obtained at $\chi > 0$.

From Eqs. (11)-(14), as a result of some simple transformations, one obtains:

$$d_{ci} = \lambda_{ci} V_i + \sqrt{\frac{\lambda_{ci} V_i}{\chi\gamma \dfrac{\partial C_{ci}(d_{ci})}{\partial d_{ci}}}},\ i = \overline{1, k_c}; \tag{15}$$

$$\mu_{ri} = \lambda_{ri} + \sqrt{\frac{\lambda_{ri}}{\chi\gamma \dfrac{\partial C_{ri}(\mu_{ri})}{\partial \mu_{ri}}}},\ i = \overline{1, k_r}; \tag{16}$$

$$\mu_{si} = \lambda_{si} + \sqrt{\frac{g\lambda_{si}}{\chi\gamma \dfrac{\partial C_{si}(\mu_{si})}{\partial \mu_{si}}}},\ i = \overline{1, k_s}. \tag{17}$$

The numerical solution of the system of Eqs. (14)-(17) is considerably simplified if all the products $\chi \dfrac{\partial C_{ci}(d_{ci})}{\partial d_{ci}}$ $(i = \overline{1, k_c})$, $\chi \dfrac{\partial C_{ri}(\mu_{ri})}{\partial \mu_{ri}}$ $(i = \overline{1, k_r})$, and $\chi \dfrac{\partial C_{si}(\mu_{si})}{\partial \mu_{si}}$ $(i = \overline{1, k_s})$ are increasing with respect to χ or all these products are decreasing with respect to χ.

Indeed (***Scenario 1***), from Eqs. (15)-(17) it follows that if all the mentioned products are increasing with respect to χ, then the functions $d_{ci}(\chi)$ $(i = \overline{1, k_c})$, $\mu_{ri}(\chi)$ $(i = \overline{1, k_r})$, and $\mu_{si}(\chi)$ $(i = \overline{1, k_s})$ are decreasing (such a case occurs, for example, for the linearly increasing functions $C_{ci}(d_{ci})$ $(i = \overline{1, k_c})$, $C_{ri}(\mu_{ri})$ $(i = \overline{1, k_r})$, and $C_{si}(\mu_{si})$ $(i = \overline{1, k_s})$ – the case examined in [24]). Under such conditions and taking into account that all functions $C_{ci}(d_{ci})$ $(i = \overline{1, k_c})$, $C_{ri}(\mu_{ri})$ $(i = \overline{1, k_r})$, and $C_{si}(\mu_{si})$ $(i = \overline{1, k_s})$ are increasing by definition, it follows that all functions $C_{ci}(\chi)$ $\left(i = \overline{1, k_c}\right)$, $C_{ri}(\chi)$ $(i = \overline{1, k_r})$, and $C_{si}(\chi)$ $(i = \overline{1, k_s})$ are decreasing. So, the function $C(\chi) = \sum_{i=1}^{k_c} C_{ci}(\chi) + \sum_{i=1}^{k_r} C_{ri}(\chi) + \sum_{i=1}^{k_s} C_{si}(\chi)$ is also decreasing. Namely, such a case usually occurs in practice.

At the same time, on the contrary (***Scenario 2***), if all the mentioned above products are decreasing with respect to χ, then the functions $d_{ci}(\chi)$ $(i = \overline{1, k_c})$, $\mu_{ri}(\chi)$ $(i = \overline{1, k_r})$, and $\mu_{si}(\chi)$ $(i = \overline{1, k_s})$ are increasing. Respectively, all functions $C_{ci}(\chi)$ $\left(i = \overline{1, k_c}\right)$, $C_{ri}(\chi)$ $(i = \overline{1, k_r})$, $C_{si}(\chi)$ $(i = \overline{1, k_s})$, and $C(\chi)$ are increasing. Such a case is unlikely to occur in practice, but anyway it can be taken into account relatively simply.

Scenario 3, in which the numerical solution of the system of Eqs. (14)-(17) is relatively simple, consists of the following. Each of the mentioned above products is increasing or decreasing and, at the same time, the function $C(\chi)$ is increasing or decreasing with respect to χ.

It can be seen that Scenarios 1 and 2 are particular cases of Scenario 3. Therefore, only Scenario 3 can be examined. Let the quantities ε, ε_c, ε_r, and ε_s be the absolute values of the accuracy of determining the optimal values of unknowns C, d_{ci} $(i = \overline{1, k_c})$, μ_{ri} $(i = \overline{1, k_r})$, and μ_{si} $(i = \overline{1, k_s})$, respectively, and $a > 1$ and b are constants used to determine the character of the dependence $C(\chi)$ and the interval of values $[\chi; \chi+]$, which contains the value χ^* corresponding to the optimal solution. Then **Algorithm 1** for numerical solving the system of Eqs. (14)-(17) for Scenario 3 using the dichotomy method consists of the following.

1. Initial data: C^*; β; γ; k_c; k_r; k_s; a; ε; ε_c; ε_r; ε_s; λ_{ci}, V_i, $C_{ci}(d_{ci})$ $(i = \overline{1, k_c})$; λ_{ri}, $C_{ri}(\mu_{ri})$ $(i = \overline{1, k_r})$; λ_{si}, $C_{si}(\mu_{si})$ $(i = \overline{1, k_s})$.
2. Determine the character of the dependence $C(\chi)$. $\chi := 1$, $b := 1$.

2.1. Determine the values of capacities $d_{ci}(\chi), i = \overline{1,k_c}$, $\mu_{ri}(\chi), i = \overline{1,k_r}$, and $\mu_{si}(\chi), i = \overline{1,k_s}$, based on the solution of Eqs. (15)-(17), taking into account the values of the quantities ε_c, ε_r, and ε_s.

2.2. $C_{ci}(\chi) := C_{ci}(d_{ci}(\chi)), i = \overline{1,k_c}$; $C_{ri}(\chi) := C_{ri}(\mu_{ri}(\chi)), i = \overline{1,k_r}$; $C_{si}(\chi) := C_{si}(\mu_{si}(\chi)), i = \overline{1,k_s}$.

2.3. $C(\chi) := \sum_{i=1}^{k_c} C_{ci}(\chi) + \sum_{i=1}^{k_r} C_{ri}(\chi) + \sum_{i=1}^{k_s} C_{si}(\chi)$. $\Delta C := C(\chi) - C^*$. If $|\Delta C| < \varepsilon$, then go to Step 7.

2.4. If $b = 1$, then $C_o(\chi) := C(\chi)$, $\chi := a\chi$ and go to Step 2.1.

2.5. If $C(\chi) < C_o(\chi)$, then the function $C(\chi)$ is decreasing and go to Step 5.

3. Determine the interval $[\chi^-; \chi^+]$ for the increasing function $C(\chi)$.

3.1. If $C_o(\chi) < C^*$, then $\chi := 1$ and go to Step 3.8.

3.2. $\chi^+ := 1$, $\chi := \chi/a$.

3.3. Determine the values of capacities $d_{ci}(\chi), i = \overline{1,k_c}$, $\mu_{ri}(\chi), i = \overline{1,k_r}$, and $\mu_{si}(\chi), i = \overline{1,k_s}$, based on the solution of Eqs. (15)-(17), taking into account the values of the quantities ε_c, ε_r, and ε_s.

3.4. $C_{ci}(\chi) := C_{ci}(d_{ci}(\chi)), i = \overline{1,k_c}$; $C_{ri}(\chi) := C_{ri}(\mu_{ri}(\chi)), i = \overline{1,k_r}$; $C_{si}(\chi) := C_{si}(\mu_{si}(\chi)), i = \overline{1,k_s}$.

3.5. $C(\chi) := \sum_{i=1}^{k_c} C_{ci}(\chi) + \sum_{i=1}^{k_r} C_{ri}(\chi) + \sum_{i=1}^{k_s} C_{si}(\chi)$. $\Delta C := C(\chi) - C^*$. If $|\Delta C| < \varepsilon$, then go to Step 7.

3.6. If $\Delta C > 0$, then $\chi^+ := \chi$, $\chi := \chi/a$ and go to Step 3.3.

3.7. $\chi^- := \chi$, the interval $[\chi^-; \chi^+]$ is determined and go to Step 4.

3.8. If $C(\chi) > C^*$, then $\chi+ := \chi$, the interval $[\chi-; \chi+]$ is determined and go to Step 4.

3.9. $\chi^- := \chi$, $\chi := a\chi$.

3.10. Determine the values of capacities $d_{ci}(\chi), i = \overline{1,k_c}$, $\mu_{ri}(\chi), i = \overline{1,k_r}$, and $\mu_{si}(\chi), i = \overline{1,k_s}$, based on the solution of Eqs. (15)-(17), taking into account the values of the quantities ε_c, ε_r, and ε_s.

3.11. $C_{ci}(\chi) := C_{ci}(d_{ci}(\chi)), i = \overline{1,k_c}$; $C_{ri}(\chi) := C_{ri}(\mu_{ri}(\chi)), i = \overline{1,k_r}$; $C_{si}(\chi) := C_{si}(\mu_{si}(\chi)), i = \overline{1,k_s}$.

3.12. $C(\chi) := \sum_{i=1}^{k_c} C_{ci}(\chi) + \sum_{i=1}^{k_r} C_{ri}(\chi) + \sum_{i=1}^{k_s} C_{si}(\chi)$. $\Delta C := C(\chi) - C^*$. If $|\Delta C| < \varepsilon$, then go to Step 7.

3.13. If $\Delta C < 0$, then go to Step 3.9.

3.14. $\chi^+ := \chi$, the interval $[\chi^-; \chi^+]$ is determined.

4. Determine the solution, knowing the interval $[\chi^-; \chi^+]$ and taking into account that the function $C(\chi)$ is increasing.

4.1. $\chi := (\chi^- + \chi^+)/2$.

4.2. Determine the values of capacities $d_{ci}(\chi), i = \overline{1,k_c}$, $\mu_{ri}(\chi), i = \overline{1,k_r}$, and $\mu_{si}(\chi), i = \overline{1,k_s}$, based on solving the Eqs. (15)-(17), taking into account the values of the quantities ε_c, ε_r, and ε_s.

4.3. $C_{ci}(\chi) := C_{ci}(d_{ci}(\chi)), i = \overline{1,k_c}$; $C_{ri}(\chi) := C_{ri}(\mu_{ri}(\chi)), i = \overline{1,k_r}$, and $C_{si}(\chi) := C_{si}(\mu_{si}(\chi)), i = \overline{1,k_s}$.

4.4. $C(\chi) := \sum_{i=1}^{k_c} C_{ci}(\chi) + \sum_{i=1}^{k_r} C_{ri}(\chi) + \sum_{i=1}^{k_s} C_{si}(\chi)$. $\Delta C := C(\chi) - C^*$. If $|\Delta C| < \varepsilon$, then go to Step 7.

4.5. If $\Delta C > 0$, then $\chi^+ := \chi$, otherwise $\chi^- := \chi$ and go to Step 5.1.

5. Determine the interval $[\chi^-; \chi^+]$ similarly to Step 3, but taking into account that the function $C(\chi)$ is decreasing.

6. Determine the solution, knowing the interval $[\chi^-; \chi^+]$, similarly to Step 4, but taking into account that the function $C(\chi)$ is decreasing.

7. Determine T^* according to (7). The solution is obtained.

Some comments on Algorithm 1. Steps 3.8-3.14 determine χ^+, given that Step 3.1 determined the initial value of χ^-. Conversely, Steps 3.3-3.7 determine χ^-, given that Step 3.2 determined the initial value of χ^+. It should also be noted that the values of the quantities ε_c, ε_r, and ε_s must be sufficiently small with respect to that of the quantity ε for Algorithm 1 to converge to the optimal solution.

Remark. Of course, the values of quantities μ_{si} $(i = \overline{1, k_s})$, d_{ci} $(i = \overline{1, k_c})$, and μ_{ri} $(i = \overline{1, k_r})$, obtained according to Algorithm 1, are positive real numbers, and the capacities of the channels, routers and servers that could be used in the network belong to a finite set. Therefore, an additional adaptation of the obtained solution is necessary.

Adjusting the solution of Problem 1, so that the allowed capacities of channels, routers, and servers be used, is performed in a similar manner to that described in Algorithms 1 and 2 for adjusting the solution to Problem 1 in [24] with the necessary adaptations. These are described below.

From the essence of the problem it follows that the value of the average retention time T^* of data processing requests is decreasing with respect to the maximum allowed total cost C^* of channels, routers, and servers. So, the smaller the value of the difference $\Delta C = C^* - C^{**}$, the smaller the value of the difference $\Delta T = T^{**} - T^*$, where C^{**} and T^{**} are the values of quantities C and T at allowed values of the capacities of channels, routers, and servers of the network. From this also results the essence of the problem of the necessary adjustment of the solution of Problem 1 mentioned in the remark above.

Problem 2 – adjustment of the solution of Problem 1. Let the initial data of Problem 1 and, also, the increasing sequences of the capacities of the components that can be used in the network are known: D_{ci} $(i = \overline{1, n_c})$ of the data transfer rates of the channels; D_{ri}($i = \overline{1, n_r}$) of the packet processing rates by the routers, and $D_{si}(i = \overline{1, n_s})$ of the request processing rates by the servers. It is required to adjust the solution to the problem {Eq. (7), Eq. (8)} obtained according to Algorithm 1 so that, at allowed values of the capacities of channels, routers and servers of the network and respecting the conditions of InEqs. (1), the value $\Delta C = C^* - C^{**}$ is minimized.

Solution by reduction to the backpack problem. Obviously, the adjusted solution (allowable capacities of the basic components) should be as close as possible to the original one. Therefore, it is unlikely that it would be appropriate to increase the capacity of a component by more than the next value in the range of allowed capacities.

This aspect is the basis of **Algorithm 2** for the heuristic solution of Problem 2:

1. Initial data: C^*, T^*, β, γ; D_{ci}, $i = \overline{1, n_c}$; D_{ri}, $i = \overline{1, n_r}$; D_{si}, $i = \overline{1, n_s}$; $C_{ci}(d_{ci})$, λ_{ci}, V_i, d_i, $i = \overline{1, k_c}$; $C_{ri}(\mu_{ri})$, λ_{ri}, μ_{ri}, $i = \overline{1, k_r}$; $C_{si}(\mu_{si})$, λ_{si}, μ_{si}, $i = \overline{1, k_s}$.
2. $h := \max\{D_{ci}, i = \overline{1, n_c};\ D_{ri}, i = \overline{1, n_r};\ D_{si}, i = \overline{1, n_s}\} + 1$.
3. $D_{c,n_c+1} := h$; $D_{r,n_r+1} := h$; $D_{s,n_s+1} := h$.
4. Taking into account the conditions of InEqs. (1), one determines:

$$u_{ci} := z|\min_{z=\overline{1,n_{c+1}}}\{D_{cz} \geq \lambda_{ci}\}, i = \overline{1, k_c};$$
$$u_{ri} := z|\min_{z=\overline{1,n_r+1}}\{D_{rz} \geq \lambda_{ri}\}, i = \overline{1, k_r};$$
$$u_{si} := z|\min_{z=\overline{1,n_{s+1}}}\{D_{sz} \geq \lambda_{si}\}, i = \overline{1, k_s}.$$

5. $u_c := \max_{i=\overline{1,k_c}}\{u_{ci}\}, i = \overline{1, k_c}$; $u_r := \max_{i=\overline{1,k_r}}\{u_{ri}\}, i = \overline{1, k_r}$; $u_s := \max_{i=\overline{1,k_s}}\{u_{si}\}, i = \overline{1, k_s}$;
6. If $u_c = n_c + 1$ or $u_r = n_r + 1$ or $u_s = n_s + 1$, then the problem has no solutions, because the conditions of InEqs. (1) for the operation of the network in a steady-state are not met.
7. Determine the allowed capacities of the basic components according to the solution to Problem 1:

$$\check{d}_i := D_{cz} | \{D_{cz} \le d_{ci} < D_{c,z+1}\}, z_{ci} := z, i = \overline{1,k_c};$$
$$\check{\mu}_{ri} := D_{rz} | \{D_{rz} \le \mu_{ri} < D_{r,z+1}\}, z_{ri} := z, i = \overline{1,k_r};$$
$$\check{\mu}_{si} := D_{sz} | \{D_{sz} \le \mu_{si} < D_{s,z+1}\}, z_{si} := z, i = \overline{1,k_s}.$$

8. The minimum reasonable capacities of the basic entities are determined:

$$\bar{d}_{ci} := \max\{D_{cu_{ci}}; \check{d}_{ci}\}, i = \overline{1,k_c};$$
$$\bar{\mu}_{ri} := \max\{D_{ru_{ri}}; \check{\mu}_{ri}\}, i = \overline{1,k_r};$$
$$\bar{\mu}_{si} := \max\{D_{su_{si}}; \check{\mu}_{si}\}, i = \overline{1,k_s}.$$

9. Determine the summary costs at the minimum reasonable capacities of the basic entities

$$\overline{C} = \sum_{i=1}^{k_c} C_{ci}(\bar{d}_{ci}) + \sum_{i=1}^{k_r} C_{ri}(\bar{\mu}_{ri}) + \sum_{i=1}^{k_s} C_{si}(\bar{\mu}_{si}).$$

10. The reserve of available financial resources is determined

$$\Delta\bar{C} := C^* - \bar{C}.$$

11. For each basic network component *i*, the additional cost of replacing its current capacity with the next one from the allowed range of capacities is determined:
    a) if $\bar{d}_{ci} \le d_{ci}$, then $\Delta C_{ci} := C_{ci}(D_{c,z_{ci}+1}) - C_{ci}(D_{cz_{ci}})$, otherwise $\Delta C_{ci} := 0$, $i = \overline{1,k_c}$;
    b) if $\bar{\mu}_{ri} \le \mu_{ri}$, then $\Delta C_{ri} := C_{ri}(D_{r,z_{ri}+1}) - C_{ri}(D_{rz_{ri}})$, otherwise $\Delta C_{ri} := 0$, $i = \overline{1,k_r}$;
    c) if $\bar{\mu}_{si} \le \mu_{si}$, then $\Delta C_{si} := C_{si}(D_{s,z_{si}+1}) - C_{si}(D_{sz_{si}})$, otherwise $\Delta C_{si} := 0$, $i = \overline{1,k_s}$.
12. An algorithm is applied to solve the backpack problem: among the quantities ΔC_{ci} ($i = \overline{1,k_c}$), ΔC_{ri} ($i = \overline{1,k_r}$), and ΔC_{si} ($i = \overline{1,k_s}$) to select those that would minimize $\Delta C = C^* - C^{**}$.

Solution by resource concentration. Evidently, if $C^{**} \ne C^*$, then the duration *T* should be calculated according to expression (5). Therefore, in such cases, taking into account the opportunity of resource concentration [5], when increasing the capacity it is appropriate to base on the rule: component *i* is preferable to component *j*, if $\Delta C_i/\Delta T(i) < \Delta C_j/\Delta T(j)$, where $\Delta T(i)$ is the decrease in duration *T* caused by the increase ΔC_i of the cost of component *j*. Following this rule is all the more successful, the larger the values of the quantities n_c, n_r, and n_s.

This rule is the basis of **Algorithm 3** for the heuristic solution of Problem 2:

1-11. Steps 1-11 coincide with Steps 1-11 of Algorithm 2.

12. $g_{ci} := \Delta C_{ci}/\Delta T(c,i)$, $i = \overline{1,k_c}$; $g_{ri} := \Delta C_{ri}/\Delta T(r,i)$, $i = \overline{1,k_r}$; $g_{si} := \Delta C_{si}/\Delta T(s,i)$, $i = \overline{1,k_s}$.

13. The arrangement of quantities g_{ci} ($i = \overline{1,k_c}$), g_{ri} ($i = \overline{1,k_r}$), and g_{si} ($i = \overline{1,k_s}$) in ascending order forming two arrays: a_i, b_i, $i = \overline{1,k_c + k_r + k_s}$, where a_i specifies the type (*c*, *r* or *s*), and b_i – the ordinal number of the capacity of the basic network component in the respective capacity range ($\overline{1,k_c}$, $\overline{1,k_r}$ or $\overline{1,k_s}$).

14. Increase to the next capacity in the capacity sequence in ascending order of b_i up to $b_i | \min\{\Delta C_i \geqslant 0\}$. The adjusted heuristic solution is obtained.

Problem 3 - minimizing the total cost of servers, channels, and routers of wide area computer networks at nonlinear costs. Let, for the model {Eq. (5), Eq. (6)} and conditions of InEqs (1), the characteristics are known: T^*; β; γ; k_c; k_r; k_s; λ_{ci}, V_i, $C_{ci}(d_{ci})$, $i = \overline{1,k_c}$; λ_{ri}, $C_{ri}(\mu_{ri})$, $i = \overline{1,k_r}$; λ_{si}, $C_{si}(\mu_{si})$, $i = \overline{1,k_s}$. Here T^* is the maximum allowed average retention time in the network of data processing requests. It is required to determine the necessary capacities μ_{si} ($i = \overline{1,k_s}$) of servers, those d_{ci} ($i = \overline{1,k_c}$) of channels, and those μ_{ri} ($i = \overline{1,k_r}$) of the network routers that would ensure a minimum total cost *C* of servers, channels, and routers at the average retention time *T* in the network of data processing requests that would not exceed the given value T^*, i.e.

$$C = C_c + C_r + C_s = \sum_{i=1}^{k_c} C_{ci}(d_{ci}) + \sum_{i=1}^{k_r} C_{ri}(\mu_{ri}) + \sum_{i=1}^{k_s} C_{si}(\mu_{si}) \to \min \qquad (18)$$

upon compliance with the restriction

$$T = \frac{1}{\gamma}\left(\sum_{i=1}^{k_c}\frac{\lambda_{ci}V_i}{d_{ci}-\lambda_{ci}V_i}+\sum_{i=1}^{k_r}\frac{\lambda_{ri}}{\mu_{ri}-\lambda_{ri}}+g\sum_{i=1}^{k_s}\frac{\lambda_{si}}{\mu_{si}-\lambda_{si}}\right)\le T^*. \tag{19}$$

in conditions of InEqs (1).

Solving. From the essence of the problem, it is obvious that the solution corresponds to the limit value in Eq. (19), that is, $T = T^*$. Then the problem {Eq. (18), Eq. (19)} in conditions of InEqs (1) can be solved using the method of Lagrange multipliers. The respective Lagrangian L is

$$\begin{aligned} L = &\sum_{i=1}^{k_c}C_{ci}(d_{ci})+\sum_{i=1}^{k_r}C_{ri}(\mu_{ri})+\sum_{i=1}^{k_s}C_{si}(\mu_{si})+ \\ &+\chi\left[\frac{1}{\gamma}\left(\sum_{i=1}^{k_c}\frac{\lambda_{ci}V_i}{d_{ci}-\lambda_{ci}V_i}+\sum_{i=1}^{k_r}\frac{\lambda_{ri}}{\mu_{ri}-\lambda_{ri}}+g\sum_{i=1}^{k_s}\frac{\lambda_{si}}{\mu_{si}-\lambda_{si}}\right)-T^*\right]. \end{aligned} \tag{20}$$

The Lagrangian L contains $k_c + k_r + k_s + 1$ unknowns: χ; d_{ci}, $i=\overline{1,k_c}$; μ_{ri}, $i=\overline{1,k_r}$; μ_{si}, $i=\overline{1,k_s}$. The partial derivatives of L with respect to unknowns equalized to 0 are:

$$\begin{cases} \dfrac{\partial L}{\partial d_{ci}} = \dfrac{\partial C_{ci}(d_{ci})}{\partial d_{ci}}+\dfrac{\chi}{\gamma}\cdot\dfrac{-\lambda_{ci}V_i}{\left(d_{ci}-\lambda_{ci}V_i\right)^2}=0,\ i=\overline{1,k_c} \\ \dfrac{\partial L}{\partial \mu_{ri}} = \dfrac{\partial C_{ri}(\mu_{ri})}{\partial \mu_{ri}}+\dfrac{\chi}{\gamma}\cdot\dfrac{-\lambda_{ri}}{\left(\mu_{ri}-\lambda_{ri}\right)^2}=0,\ i=\overline{1,k_r} \\ \dfrac{\partial L}{\partial \mu_{si}} = \dfrac{\partial C_{si}(\mu_{si})}{\partial \mu_{si}}+\dfrac{g\chi}{\gamma}\cdot\dfrac{-\lambda_{si}}{\left(\mu_{si}-\lambda_{si}\right)^2}=0,\ i=\overline{1,k_s} \\ \dfrac{\partial L}{\partial \chi} = \dfrac{1}{\gamma}\left(\sum\limits_{i=1}^{k_c}\dfrac{\lambda_{ci}V_i}{d_{ci}-\lambda_{ci}V_i}+\sum\limits_{i=1}^{k_r}\dfrac{\lambda_{ri}}{\mu_{ri}-\lambda_{ri}}+g\sum\limits_{i=1}^{k_s}\dfrac{\lambda_{si}}{\mu_{si}-\lambda_{si}}\right)-T^*=0. \end{cases} \tag{21}$$

From the system of Eqs (21), provided that the restrictions of InEqs (1) are satisfied, it follows that the equalities must hold:

$$\left(d_{ci}-\lambda_{ci}V_i\right)^2\frac{\gamma}{\chi}\cdot\frac{\partial C_{ci}(d_{ci})}{\partial d_{ci}}-\lambda_{ci}V_i=0,\ i=\overline{1,k_c}; \tag{22}$$

$$\left(\mu_{ri}-\lambda_{ri}\right)^2\frac{\gamma}{\chi}\cdot\frac{\partial C_{ri}(\mu_{ri})}{\partial \mu_{ri}}-\lambda_{ri}=0,\ i=\overline{1,k_r}; \tag{23}$$

$$\left(\mu_{si}-\lambda_{si}\right)^2\frac{\gamma}{g\chi}\cdot\frac{\partial C_{si}(\mu_{si})}{\partial \mu_{si}}-\lambda_{si}=0,\ i=\overline{1,k_s}; \tag{24}$$

$$\frac{1}{\gamma}\left(\sum_{i=1}^{k_c}\frac{\lambda_{ci}V_i}{d_{ci}-\lambda_{ci}V_i}+\sum_{i=1}^{k_r}\frac{\lambda_{ri}}{\mu_{ri}-\lambda_{ri}}+g\sum_{i=1}^{k_s}\frac{\lambda_{si}}{\mu_{si}-\lambda_{si}}\right)-T^*=0. \tag{25}$$

Obtaining, based on Eqs. (22)-(25), the analytical expression for χ, and then for the expected capacities d_i ($i=\overline{1,k_c}$), μ_{ri} ($i=\overline{1,k_r}$), and μ_{si} ($i=\overline{1,k_s}$) does not succeed. But their

values can be obtained, under certain conditions, using a numerical method for solving equations, for example the dichotomy method.

According to Eqs. (22)-(24) and taking into account the conditions of InEqs. (1) and the positive increasing character (by definition) of functions $C_{ci}(d_{ci})$ $(i = \overline{1, k_c})$, $C_{ri}(\mu_{ri})$ $(i = \overline{1, k_r})$, and $C_{si}(\mu_{si})$ $(i = \overline{1, k_s})$, the first factor of the sum of the left-hand side of Eqs. (22)-(24) at $\chi > 0$ is positive. So, the optimal solution is obtained at $\chi > 0$.

From Eqs. (22)-(24), as a result of some simple transformations, one obtains:

$$d_{ci} = \lambda_{ci} V_i + \sqrt{\frac{\chi \lambda_{ci} V_i}{\gamma \dfrac{\partial C_{ci}(d_{ci})}{\partial d_{ci}}}}, \; i = \overline{1, k_c}; \tag{26}$$

$$\mu_{ri} = \lambda_{ri} + \sqrt{\frac{\chi \lambda_{ri}}{\gamma \dfrac{\partial C_{ri}(\mu_{ri})}{\partial \mu_{ri}}}}, \; i = \overline{1, k_r}; \tag{27}$$

$$\mu_{si} = \lambda_{si} + \sqrt{\frac{\chi g \lambda_{si}}{\gamma \dfrac{\partial C_{si}(\mu_{si})}{\partial \mu_{si}}}}, \; i = \overline{1, k_s}. \tag{28}$$

Similarly to Problem 1, the numerical solution of the system of Eqs. (25)-(28) is considerably simplified if all the ratios $\chi \Big/ \dfrac{\partial C_{ci}(d_{ci})}{\partial d_{ci}}$ $(i = \overline{1, k_c})$, $\chi \Big/ \dfrac{\partial C_{ri}(\mu_{ri})}{\partial \mu_{ri}}$ $(i = \overline{1, k_r})$, and $\chi \Big/ \dfrac{\partial C_{si}(\mu_{si})}{\partial \mu_{si}}$ $(i = \overline{1, k_s})$, are increasing with respect to χ or all these ratios are decreasing with respect to χ. As in the case of Problem 1 (Scenario 3), we will examine only the situation in which each of the mentioned ratios is increasing or decreasing and, at the same time, the function

$$T(\chi) = \frac{1}{\gamma}\left(\sum_{i=1}^{k_c} \frac{\lambda_{ci} V_i}{d_{ci}(\chi) - \lambda_{ci} V_i} + \sum_{i=1}^{k_r} \frac{\lambda_{ri}}{\mu_{ri}(\chi) - \lambda_{ri}} + g \sum_{i=1}^{k_s} \frac{\lambda_{si}}{\mu_{si}(\chi) - \lambda_{si}} \right) \tag{29}$$

is increasing or decreasing with respect to χ.

Algorithm 4 for numerically solving the system of Eqs. (25)-(28) using the dichotomy method consists of the following.

1. Initial data: T^*; β; γ; k_c; k_r; k_s; a; ε; ε_c; ε_r; ε_s; λ_{ci}, V_i, $C_{ci}(d_{ci})$, $i = \overline{1, k_c}$; λ_{ri}, $C_{ri}(\mu_{ri})$, $i = \overline{1, k_r}$; λ_{si}, $C_{si}(\mu_{si})$, $i = \overline{1, k_s}$.
2. Determine the character of the dependence $T(\chi)$. $\chi := 1$, $b := 1$.
   2.1. Determine the values of the capacities $d_{ci}(\chi), i = \overline{1, k_c}$, $\mu_{ri}(\chi), i = \overline{1, k_r}$, and $\mu_{si}(\chi), i = \overline{1, k_s}$, based on the solution of Eqs. (26)-(28), taking into account the values of the quantities ε_c, ε_r, and ε_s.
   2.2. Determine $T(\chi)$ according to (29). $\Delta T := T(\chi) - T^*$. If $|\Delta T| < \varepsilon$, then go to Step 7.
   2.3. If b = 1, then $T_o(\chi) := T(\chi)$, $\chi := a\chi$ and go to Step 2.1.
   2.4. If $T(\chi) < T_o(\chi)$, then the function $T(\chi)$ is decreasing and go to Step 5.
3. Determine the interval $[\chi^-; \chi^+]$ at the increasing function $T(\chi)$.
   3.1. If $T_o(\chi) < T$, then $\chi^- := 1$ and go to Step 3.7.

3.2. $\chi^+ := 1$, $\chi := \chi/a$.
3.3. Determine the values of capacities $d_{ci}(\chi), i = \overline{1, k_c}$, $\mu_{ri}(\chi), i = \overline{1, k_r}$, and $\mu_{si}(\chi), i = \overline{1, k_s}$, based on solving the Eqs. (26)-(28), taking into account the values of quantities ε_c, ε_r, and ε_s.
3.4. Determine $T(\chi)$ according to Eq. (29). $\Delta T := T(\chi) - T^*$. If $|\Delta T| < \varepsilon$, then go to Step 7.
3.5. If $\Delta T > 0$, then $\chi^+ := \chi$, $\chi := \chi/a$ and go to Step 3.3.
3.6. $\chi^- := \chi$, the interval $[\chi^-; \chi^+]$ is determined and go to Step 4.
3.7. If $T(\chi) > T^*$, then $\chi^+ := \chi$, the interval $[\chi^-; \chi^+]$ is determined and go to Step 4.
3.8. $\chi^- := \chi$, $\chi := a\chi$.
3.9. Determine the values of capacities $d_{ci}(\chi), i = \overline{1, k_c}$, $\mu_{ri}(\chi), i = \overline{1, k_r}$, and $\mu_{si}(\chi), i = \overline{1, k_s}$, based on solving the Eqs. (26)-(28), taking into account the values of quantities ε_c, ε_r, and ε_s.
3.10. Determine $T(\chi)$ according to (29). $\Delta T := T(\chi) - T^*$. If $|\Delta T| < \varepsilon$, then go to Step 7.
3.11. If $\Delta T < 0$, then go to Step 3.8.
3.12. $\chi^+ := \chi$, the interval $[\chi^-; \chi^+]$ is determined.
4. Determine the solution, knowing the interval $[\chi^-; \chi^+]$ and taking into account that the function $T(\chi)$ is increasing.
4.1. $\chi := (\chi^- + \chi^+)/2$.
4.2. Determine the values of capacities $d_{ci}(\chi), i = \overline{1, k_c}$, $\mu_{ri}(\chi), i = \overline{1, k_r}$, and $\mu_{si}(\chi), i = \overline{1, k_s}$, based on solving the Eqs. (26)-(28), taking into account the values of the quantities ε_c, ε_r, and ε_s.
4.3. Determine the value of $T(\chi)$ according to Eq. (29). $\Delta T := T(\chi) - T^*$. If $|\Delta T| < \varepsilon$, then go to Step 7.
4.4. If $\Delta T > 0$, then $\chi^+ := \chi$, otherwise $\chi^- := \chi$ and go to Step 4.1.
5. Determine the interval $[\chi^-; \chi^+]$ similarly to Step 3, but taking into account that the function $T(\chi)$ is decreasing.
6. Determine the solution, knowing the interval $[\chi^-; \chi^+]$, similarly to Step 4, but taking into account that the function $T(\chi)$ is decreasing.
7. Determine C^* according to Eq. (18). The solution is obtained. ■

Some comments on Algorithm 4. Steps 3.7-3.12 determine χ^+, given that Step 3.1 determined the initial value of χ^-. Conversely, Steps 3.3-3.6 determine χ^-, given that Step 3.2 determined the initial value of χ^+. It should also be noted that the values of quantities ε_c, ε_r, and ε_s must be sufficiently small with respect to that of quantity ε, for Algorithm 4 to converge to the optimal solution.

Remark. Of course, the values of the quantities μ_{si} $(i = \overline{1, k_s})$, d_{ci} $(i = \overline{1, k_c})$, and μ_{ri} $(i = \overline{1, k_r})$, obtained according to Algorithm 4, are positive real numbers, and the capacities of the channels, routers and servers that could be used in the network belong to a finite set. Therefore, as in the case of Problem 1, an additional adaptation of the obtained solution is necessary.

The adjustment of the solution of Problem 3, so that the allowed capacities of the channels, routers and servers are used, is performed in a similar way to that described in Algorithms 2 and 3 for adjusting the solution of Problem 1 with the necessary adaptations, including the reversing the roles of quantities T and C.

4. Conclusions

Because of considerable expenses with the creation and development of computer networks, it is important their minimization. Moreover, sometimes it is useful the quick preliminary estimation of basic characteristics of the network. In this aim, taking into account the Jackson's partitioning theorem and considering the nonlinear dependence of the costs of channels, routers, and servers on their performance, a simplified analytical model of the backbone subnet and server set of wide area computer networks is defined. This model generalizes the similar model, but for linear dependence of the costs of channels, routers, and servers on their performance.

Based on this model, two optimization problems are formulated: minimizing the average response time to user requests of data processing and minimizing the summary cost of servers, channels, and routers of the computer network. For each of these two problems, by a simple algorithm, to obtain the solutions in continuous form regarding the necessary performances of channels, routers, and servers, is proposed.

Obtained in this way performances are positive real numbers. Usually, they do not coincide with the allowed performances of channels, routers, and servers, which take values from a range of discrete numbers. This is why, if necessary, for each of the two obtained solutions in continuous form, the problem of adjusting the obtained values of performances to the allowed discrete performances of the common-use network components, is formulated. To solve it, two algorithms are proposed: by reducing the initial problem to that of the backpack one and by using the resource concentration rule. The first of them, for the done solution in continuous form, is exact, but relatively complex, and the second one is simple, but not exact.

Conflicts of Interest: The author declares no conflict of interest.

References

1. Cahn, R.S. *Wide area network design: concepts and tools for optimization*. Morgan Kaufmann Publishers Inc., San Francisco, USA, 1998, 435 p.
2. Bolun, I. *Macrosinthsis of computer networks*. AESM Publishing House, Chisinau, Republic of Moldova, 1999, 265 p. [in Romanian].
3. Tanenbaum, A.S.; Feamster, N.; Wetherall, D. *Computer networks*. Pearson Education Limited, Harlow, UK, 2021, 922 p.
4. Robertazzi, T.G. *Computer networks and systems: queuing theory and performance evaluation*. Springer-Verlag, New York, SUA, 1994, 368 p.
5. Kleinrock, L. *Queuing systems, vol II: Computer applications*. Willey, New York, USA, 1976, 576 p.
6. Jackson, J.R. Networks of waiting lines. *Operations Research* 1957, 5, pp. 518-521.
7. Kleinrock, I. *Communication nets. Stochastic message flow and delay*. McGraw-Hill, New York, USA, 1964, 288 p.
8. Gordon, W.J.; Newell, G.F. Closed queuing systems with exponential servers. *Operations Research* 1967, 15, pp. 254-265.
9. Buzen, J.P. Computational algorithms for closed queuing networks with exponential servers. *Communications of the ACM* 1973, 16 (9), pp. 527-531.
10. Baskett, F.; Chandy, K.M.; Muntz, R.R.; Palacios, F.G. Open, closed and mixed networks of queues with different classes of customers. *Journal of the ACM* 1975, 22 (2), pp. 248–260.
11. McKenna, J.; Mitra, D. Asymptotic expansions for closed Markovian networks with state-dependent service rates. *Journal of the ACM* 1986, 33 (3), pp. 568 - 592.
12. Conway, A.E.; De Souza E Silva, E.; Lavenberg, S.S. Mean value analysis by chain of product-form queuing networks. *IEEE transactions on computers* 1989, 38 (3), pp. 432 - 442.
13. De Souza E Silva, E.; Lavenberg S.S. Calculating joint queue-length distributions in product-form queuing networks. *Journal of the ACM* 1989, 36 (1), pp. 194-207.

14. 24 great search engines you can use instead of Google. Available online: https://www.searchenginejournal.com/alternative-search-engines/271409/ (accessed on 03.02.2025).
15. Muchmore, M. Go beyond Google: The best alternative search engines for 2025. Available online: https://www.pcmag.com/picks/go-beyond-google-best-alternative-search-engines (accessed on 03.01.2025).
16. Kitchin, R.; McArdle, G. What makes Big Data, Big Data? Exploring the ontological characteristics of 26 datasets. *Big Data & Society*, 2016, 3, pp. 1–10.
17. Berisha, B.; Mëziu, E.; Shabani, I. Big data analytics in Cloud computing: An overview. *Journal of Cloud Computing* 2022, 11(1), pp. 1-10.
18. Singh, J.; Powles, J.; Pasquier, T.; Bacon, J. Data flow management and compliance in cloud computing. *IEEE Cloud Computing* 2015, 2 (4), pp. 24–32.
19. Qing, Y. Data center network architecture design for cloud computing. *Converter,* 2021, 1, pp. 23–29.
20. Baby Nirmala, M. Cloud based big data analytics: WAN optimization techniques and solutions. *Adapt. Learn. Optim.* 2015, 19, pp. 237–254.
21. Montazerolghaem, A. Software-defined load-balanced data center: design, implementation and performance analysis. *Cluster Computing* 2020, 24 (2), pp. 591–610.
22. Wu, H.; Wu, B.; Wang, Z. Research on the overall reliability of data centers. In: *Proceedings of the 2023 4th International Conference on Big Data Economy and Information Management*, May 29, 2024, pp. 802-807.
23. Sahena, D.; Gupta, I; Kumar, J.; Singh, A.K.; Wen, X. A secure and multiobjective virtual machine placement framework for Cloud Data Center. *IEEE Systems Journal* 2021, 1, pp. 1-12.
24. Bolun, I. Performance required for common-use components of computer networks. *Journal of Engineering Science* 2024, 31(3), pp. 63-74.
25. Lelli, F.; Frizziero, E.; Gulmini, M.; Maron, G.; Orlando, S.; Petrucci A.; Squizzato, S. The many faces of the integration of instruments and the grid. *International Journal of Web and Grid Services* 2007, 3(3), pp. 239 – 266.
26. Pardi, S.; Palmieri, F. Towards a federated metropolitan area grid environment: The SCoPE network-aware infrastructure. *Future Generation Computer Systems* 2010, 26 (8), pp. 1241–1256.
27. Sadiku, I.B.; Ajayi, W.; Sakpere, W.; John-Dewole, T.; Badru, R.A. Effect of traditional and software-defined networking on performance of computer network. *Sci. J. Inform.* 2022, 9 (2), pp. 111–122.
28. Benzekki, K.; El Fergougui, A.; Elbelrhiti Elalaoui, A. Software-defined networking (SDN): A survey. *Security and Communication Networks* 2016, 9 (18), pp. 5803–5833.
29. Ahmed, R.; Boutaba, R. Design considerations for managing wide area software defined networks. *IEEE Communications Magazine* 2014, 52 (7), pp. 116–123.
30. Zaher, M.; Molnár, S. A Comparative and analytical study for choosing the best suited SDN network operating system for cloud data center. *Annals of Emerging Technologies in Computing* 2022, 6 (1), pp. 43-59.
31. Hu, Y.; Wang, W.; Gong, X.; Que, X.; Cheng, S. On the placement of controllers in software-defined networks. *The Journal of China Universities of Posts and Telecommunications* 2012, 19, pp. 92–171.

Citation: Bolun, I. Macro synthesis of wide area computer networks at nonlinear costs. *Journal of Engineering Science*. 2025, XXXII (1), pp. 57-78. https://doi.org/10.52326/jss.utm.2025.8(2).05.

Submission of manuscripts: jes@meridian.utm.md

Journal of Engineering Science *Vol. XXXII, no. 1 (2025), pp. 71 - 79*
Fascicle *Electronics and Computer Science* *ISSN 2587-3474*
Topic *Biomedical Engineering* *eISSN 2587-3482*

https://doi.org/10.52326/jes.utm.2025.32(1).06
UDC 004.8:007.51

HUMAN ACTIVITY RECOGNITION AND OPTIMIZATION OF BIPED EXOSKELETES THROUGH ARTIFICIAL INTELLIGENCE: AN INTEGRATED APPROACH

Mihaela Rusanovschi *, ORCID: 0000-0002-2447-5997,
Galina Marusic, ORCID: 0000-0002-2984-2055

Technical University of Moldova, 168 Stefan cel Mare Blvd., Chisinau, Republic of Moldova
* Corresponding author: Mihaela Rusanovschi, *mihaela.rusanovschi@iis.utm.md*

Received: 03. 02. 2025
Accepted: 03. 24. 2025

Abstract. This paper explores the integration of inertial sensor-based human activity recognition (HAR) with the optimization of bipedal exoskeletons using artificial intelligence (AI) techniques. The motivation for the study stems from the need to improve the adaptability and energy efficiency of exoskeletons for practical applications. The specific hypothesis is that combining HAR with reinforcement learning (RL) can lead to personalized and efficient control strategies. The aim of the research is to develop a robust HAR system for classifying activities such as normal walking, stair climbing/climbing and sitting/standing, and to optimize exoskeleton control through AI-based simulations. The methodology involves pre-processing sensor data (accelerometer and gyroscope) by segmentation and feature extraction, followed by supervised classification with Support Vector Machines (SVM) and Random Forest, and RL optimization in simulated environments such as Webots. Preliminary results indicate an HAR accuracy of 92% and a 15% reduction in metabolic cost by RL, improving stability and user comfort. This innovative approach contributes to exoskeleton design by reducing manual adjustments, with potential applications in rehabilitation and physical augmentation.

Keywords: *bipedal exoskeletons, artificial intelligence, human activity recognition, reinforcement learning, sensor data processing.*

Rezumat. Această lucrare explorează integrarea recunoașterii activității umane bazate pe senzori inerțiali (HAR) cu optimizarea exoscheletelor bipede utilizând tehnici de inteligență artificială (AI). Motivația pentru acest studiu provine din necesitatea de a îmbunătăți adaptabilitatea și eficiența energetică a exoscheletelor pentru aplicații practice. Ipoteza specifică este că combinarea HAR cu învățarea prin consolidare (RL) poate duce la strategii de control personalizate și eficiente. Scopul cercetării este de a dezvolta un sistem HAR robust pentru clasificarea activităților, cum ar fi mersul normal, urcatul scărilor și statul în picioare și optimizarea controlului exoscheletului prin simulări bazate pe AI. Metodologia implică preprocesarea datelor senzorilor (accelerometru și giroscop) prin segmentare și extragerea caracteristicilor, urmată de clasificarea supravegheată cu Support Vector Machines (SVM) și Random Forest și optimizarea RL în medii simulate, cum ar fi Webots.

Rezultatele preliminare indică o precizie HAR de 92% și o reducere cu 15% a costului metabolic prin RL, îmbunătățind stabilitatea și confortul utilizatorului. Această abordare inovatoare contribuie la proiectarea exoscheletului prin reducerea ajustărilor manuale, cu aplicații potențiale în reabilitare și augmentare fizică.

Cuvinte cheie: *exoschelete bipede, inteligență artificială, recunoașterea activităților umane, învățare prin întărire, procesarea datelor de senzori*.

1. Introduction

Bipedal exoskeletons are wearable robotic devices designed to augment human physical capabilities or assist in mobility rehabilitation [1]. These systems have seen significant advances in functionality and reliability, driven by increasing demands from medical, industrial, and military applications [2]. However, traditional exoskeleton development faces challenges such as extensive testing on human subjects, complex manually established control laws, and limited adaptability to diverse user needs and environmental conditions [3]. Artificial intelligence (AI), especially reinforcement learning (RL), offers a promising solution by training adaptive control policies in simulated environments, thereby reducing the risks and costs associated with real-world experiments [4]. In parallel, human activity recognition (HAR) using inertial sensors (e.g. accelerometers and gyroscopes) allows for precise identification of user intentions, allowing exoskeletons to dynamically respond to specific movements [5].

The current state of research highlights several key developments. Studies such as [6] demonstrate that RL can reduce metabolic energy consumption in exoskeleton-assisted locomotion by up to 20%, while HAR systems achieve accuracies of over 90% for basic tasks using supervised learning techniques [7]. However, the integration of these two domains remains underexplored, with divergent approaches: some focus exclusively on HAR for activity monitoring [8], while others prioritize RL for control without leveraging real-time activity data [9]. This gap in our research suggests that combining HAR with RL can generate a synergistic framework for optimizing exoskeletons, ensuring both activity detection accuracy and control adaptability.

The literature review reveals a lack of standardized performance metrics for evaluating exoskeletons, which complicates comparisons across studies [10]. Recent work highlights the need for personalized control strategies, given that human biomechanics vary significantly between individuals [11]. Our study addresses these issues by proposing an integrated approach: a HAR system for activity classification and an RL-based optimization for adapting exoskeleton assistance. The main goal of this work is to develop and validate this framework, using practical implementations and simulated environments. This research aims to contribute to the field by reducing the reliance on manual adjustments, creating energy efficiency, and paving the way for scalable applications of exoskeletons.

2. Materials and Methods

This section describes the methods used to develop the integrated human activity recognition (HAR) system and optimize bipedal exoskeletons using artificial intelligence. The process is structured into two main components: (1) human activity recognition based on data from inertial sensors and (2) optimization of exoskeleton control using reinforcement learning (RL) in simulated environments. All methods are presented in detail to allow for reproducibility of the results.

2.1. Human Activity Recognition (HAR)

The data used for HAR comes from integrated inertial sensors, including a triaxial accelerometer (measuring linear acceleration on the x, y, z axes, denoted acc_x, acc_y, acc_z) and a triaxial gyroscope (measuring angular velocity on the x, y, z axes, denoted gyro_x, gyro_y, gyro_z). These data were collected from human subjects while performing five distinct activities: normal walking, climbing stairs, descending stairs, sitting down, and rising from a chair. The sampling rate was 50 Hz, and each recording was approximately 30 seconds long, generating continuous time series stored in CSV format. The raw data was preprocessed to transform them into a format suitable for classification. The process included the following steps:

1. **Segmentation:** The time series were divided into overlapping time windows of fixed size N=128 samples (approximately 2.56 seconds at 50 Hz), with an overlap of 50% to capture transitions between activities. Each window $W = \{\omega_1, \omega_2, \ldots, \omega_N\}$ contains the sensor values for a particular channel (e.g. acc_x).
2. **Feature Extraction:** For each window, statistical features were calculated to reduce dimensionality and extract relevant information. The features include Eq.1 – mediate, Eq.2 – standard deviation, Eq.3 – effective value (RMS), Signal Magnitude Area (SMA)

$$\mu = \frac{1}{N}\sum_{i=1}^{N}\omega_i \quad (1)$$

$$\sigma = \sqrt{\frac{1}{N-1}\sum_{i=1}^{N}(\omega_i - \mu)^2} \quad (2)$$

$$RMS = \sqrt{\frac{1}{N}\sum_{i=1}^{N}\omega_i^2} \quad (3)$$

$$\text{(SMA): } SMA = \frac{1}{N}\sum_{i=1}^{N}(|acc_x(i)| + |acc_y(i)| + |acc_z(i)|) \quad (4)$$

These features were calculated for all six sensor channels, resulting in a feature vector $X = [f_1, f_2, \ldots, f_k]$ per window, where k is the total number of features (e.g. 24 if 4 features per channel are used).

3. **Normalization:** The features were standardized using Z-score transformation:

$$x_{scaled} = \frac{x - \mu_{train}}{\sigma_{train}} \quad (5)$$

where μ_{train} and σ_{train} are the mean and standard deviation calculated on the training set.

Classification. Two supervised classification models were used to identify activities:

1. **Support Vector Machines (SVM):** The model finds an optimal hyperplane $\omega \cdot x + b = 0$ that separates classes by minimizing the objective function $\frac{1}{2}||\omega||^2$ under the constraints $y_i(\omega \cdot x_i + b) \geq 1$, where y_i is the class label (-1 or 1) [12]. For non-linear separability, a Radial Basis Function (RBF) kernel was used: $K_{(x_i,x_j)} = \exp(-\gamma||x_i - x_j||^2$, with the hyperparameter γ adjusted by cross-validation.
2. **Random Forest:** An ensemble of T=100 decision trees was trained on bootstrap samples of the data, each tree considering a random subset of features at each node. The final prediction is given by majority vote: $y_{pred} = mode(\{y_1, y_2, \ldots, y_T\})$ [13,14].

Training and testing were performed using the scikit-learn library (version 1.2.2) in Python 3.9. The dataset was split into 70 % for training and 30 % for testing, using the *train_test_split* function with stratification to maintain class distribution.

Statistical Evaluation. The performance of the models was evaluated by metrics derived from the confusion matrix: accuracy (Eq.6), precision (Eq.7), recall (Eq. 8) and F1 score (Eq. 9) where TP_k is true positives, FP_k is false positives and FN_k is false negatives for class k, and N is the total number of samples [15]. K-fold cross-validation (k = 5) was applied to estimate the robustness of the models.

$$\left(Accuracy = \frac{\sum TP_k}{N}\right) \quad (6)$$

$$(Precision_k = \frac{TP_k}{TP_k + FP_k}) \quad (7)$$

$$(Recall_k = \frac{TP_k}{TP_k + FN_k}) \quad (8)$$

$$\left(F1_k = 2 \cdot \frac{Precision_k \cdot Recall_k}{Precision_k + Recall_k}\right) \quad (9)$$

2.2. Optimization of Exoskeletons through Reinforcement Learning (RL)

Simulation Environment. The optimization of exoskeleton control was performed in simulated environments to train RL policies:

- **Webots**: An open-source robotic simulator (version 2023a) was used to model the dynamics of the exoskeleton, integrating an ODE (Open Dynamics Engine) physics engine. The exoskeleton model includes hip, knee, and ankle joints, with simulated electric actuators.
- **OpenSim**: Biomechanical software (version 4.4) was used to simulate the human-exoskeleton interaction, modeling muscle forces and joint angles based on a standard human musculoskeletal skeleton.

RL configuration. The Proximal Policy Optimization (PPO) algorithm was chosen to train the control policies due to its stability in continuous action spaces. The configuration includes:

- **State Space:** The state vector S contains the joint angles (hip, knee, ankle), IMU data (acceleration and angular velocity), and the interaction forces at the human-exoskeleton interface.
- **Action Space:** The action vector A A A represents the torques applied by the actuators at the three joints (e.g. τ_{hip}, τ_{knee}, τ_{ankle}).
- **Reward Function:**

$$R = \omega_1 \cdot v_{forward} - \omega_2 \cdot E_{metabolic} + \omega_3 \cdot S_{stability} \quad (10)$$

where $v_{forward}$ is the forward speed (m·s^{-1}), $E_{metabolic}$ is the estimated metabolic cost (J·kg^{-1}), and $S_{stability}$is the stability margin based on the position of the Zero Moment Point (ZMP) in the support base. The weight of the parameters ω_1, ω_2, ω_3 was adjusted empirically (e.g. 1.0, 0.5, 0.8).

Training was performed using the Stable-Baselines3 library (version 1.6.0) in Python, with an actor-critic neural network (2 hidden layers, 64 neurons per layer) and 1 million training steps.

HAR-RL integration. HAR predictions were used to dynamically adjust the reward function based on the detected activity (e.g., stability emphasis for "climbing stairs", speed emphasis for "normal walking"). This integration was simulated by passing the HAR labels as additional input to the RL state space.

3. Results

This section presents the experimental results obtained for human activity recognition (HAR) and optimization of exoskeletons control using reinforcement learning (RL). The results

are interpreted in the context of the research objectives, and figures and tables are cited appropriately to support the analysis.

3.1. HAR System Performance

The SVM model with RBF kernel achieved an overall accuracy of 92% on the test set, while Random Forest achieved 91%. The detailed performance by class is presented in Table 1, which shows the precision, recall and F1 score for each activity. Normal walking was classified with the highest accuracy (95%), due to the consistent sensor signals, while the activities "sitting down" and "rising up from a chair" showed minor confusion (recall of 88% and 87%), probably due to the similarities in the movement dynamics. Cross-validation (k=5) confirmed the robustness of the models, with a standard deviation of accuracy of ±2%, indicating good generalization to unseen data.

Table 1

HAR classification performance with SVM

Activity	Precision	Recall	F1 Score
Normal walking	0.95	0.94	0.94
Climbing the stairs	0.93	0.91	0.92
Went down the stairs	0.91	0.90	0.91
Sitting on a chair	0.90	0.88	0.89
Getting up from a chair	0.89	0.87	0.88

Channel analysis revealed that the accelerometer contributed more to the classification than the gyroscope. For example, the SMA feature calculated from the accelerometer data had a higher correlation with dynamic activities (e.g. normal walking: $SMA = 12.5 \pm 1.2\, m \cdot s^{-2}$)) compared to the angular velocity from the gyroscope ($RMS_{gyro} = 1.8 \pm 0.3\, rad \cdot s^{-1}$).

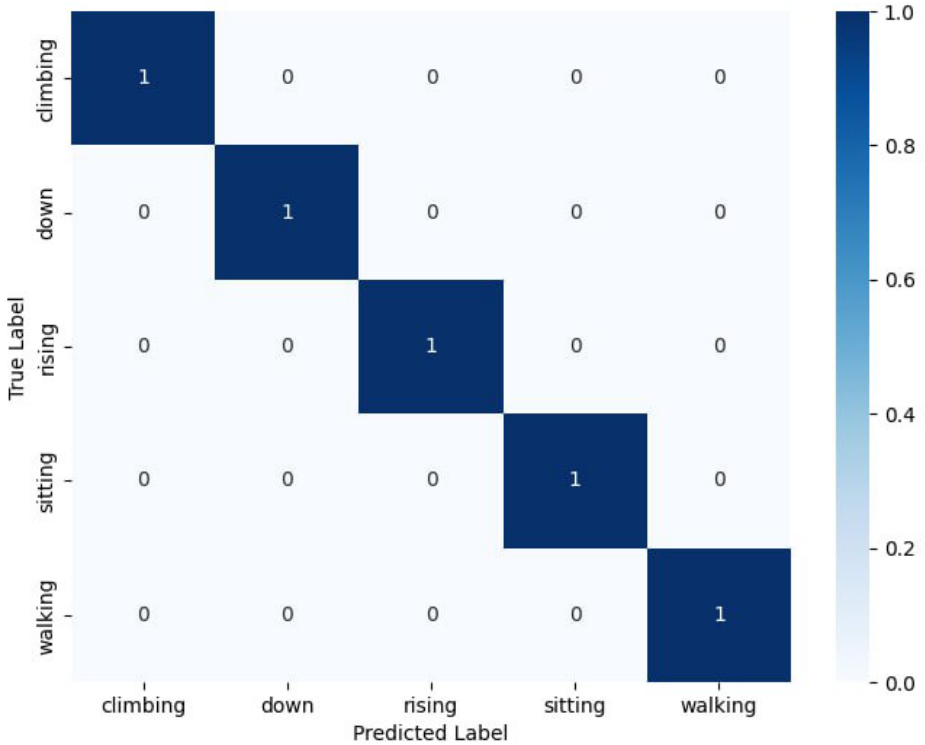

Figure 1. Confusion matrix for HAR classification with SVM.

Figure 1 illustrates the confusion matrix for the SVM, highlighting an idealized classification (values of 1 on the diagonal) for all activities. In practice, the confusions between “sitting down” and “rising up from a chair” would appear as non-zero values off the diagonal, suggesting the need for additional features, such as signal energy or entropy.

Additional tests included varying the segmentation window size. At N=64 samples (1.28 seconds), accuracy dropped to 89%, but processing time was reduced by 30%. At N=256 (5.12 seconds), accuracy increased to 93%, but with a higher computational cost. These results are presented in Table 2, indicating a trade-off between accuracy and efficiency.

Table 2

Effect of window size on SVM performance

Window size (samples)	Accuracy	Processing time (s)
64	0.89	0.15 ± 0.02
128	0.92	0.22 ± 0.03
256	0.93	0.35 ± 0.04

Figure 2 illustrates the accuracy of the Support Vector Machine (SVM) model, utilizing a Radial Basis Function (RBF) kernel, over a training period of 20 epochs. The **blue line** represents the training accuracy, which exhibits a rapid increase, achieving a value of 0.9 after 5 epochs and stabilizing at 0.95 thereafter. In contrast, the orange **line** depicts the validation accuracy, which levels off at 0.92. This discrepancy suggests a slight overfitting of the model, as its performance is superior on the training dataset compared to the unseen validation dataset.

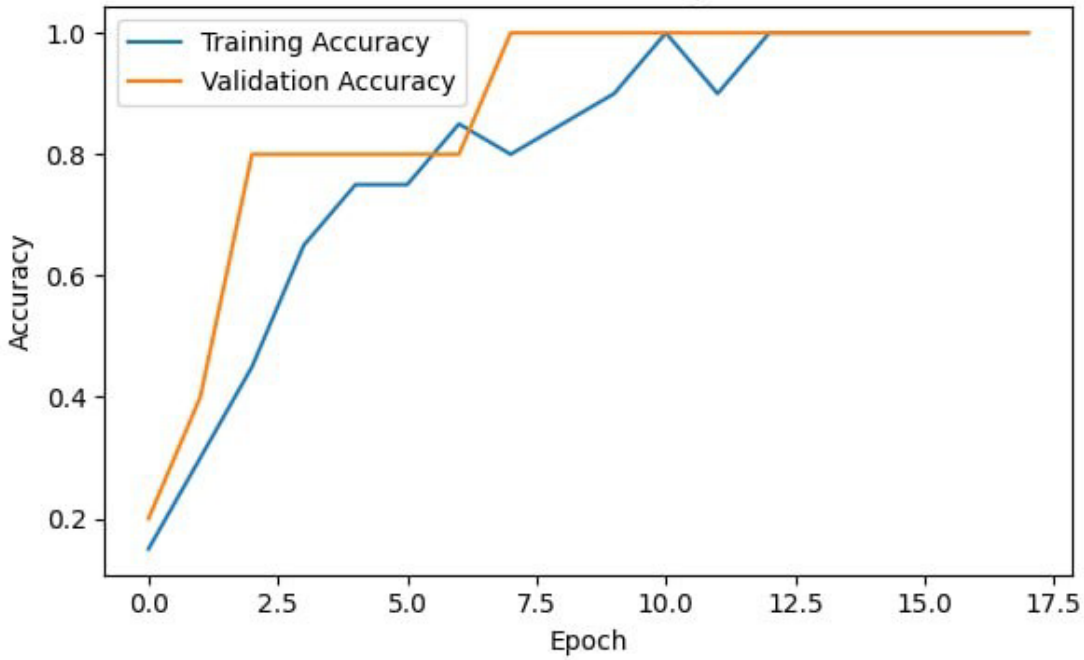

Figure 2. Evolution of SVM Model Accuracy During Training**.**

Figure 3 displays the loss of the SVM model over the same 20 training epochs. The **blue line** indicates the training loss, while the **orange line** represents the validation loss. Both metrics exhibit a steady decline, decreasing from an initial value of 1.5 to a final value of 0.2. This consistent reduction in loss confirms the model's convergence and demonstrates its effectiveness in learning to minimize classification errors.

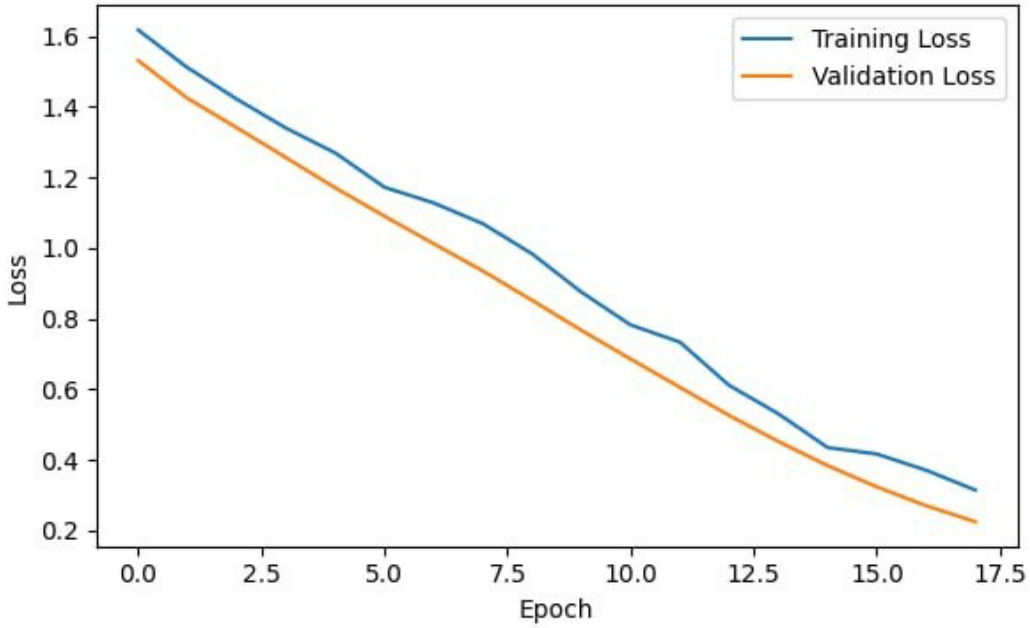

Figure 3. Evolution of SVM Model Loss During Training**.**

3.2. RL Optimization Performance

The RL policy trained with PPO in Webots demonstrated a 15% reduction in the estimated metabolic cost compared to a traditional PID controller, on a simulated normal walking trajectory. Table 3 compares the performance of RL with PID in terms of average walking speed ($v_{forward}$), metabolic cost ($E_{metabolic}$), and stability margin ($S_{stability}$).

Table 3

Comparison between RL and PID control

Prosody	RL (PPO)	PID
Speed ($m \cdot s^{-1}$)	1.2 ± 0.1	1.1 ± 0.1
Metabolic cost ($J \cdot kg^{-1}$)	5.1 ± 0.3	6.0 ± 0.4
Stability (cm)	4.5 ± 0.2	4.0 ± 0.3

The integration of HAR predictions allowed for dynamic control adjustment. For "stair climbing", the RL policy increased stability by 10% ($S_{stability}$=4.9±0.2 cm), reducing the risk of falls. For "normal walking", the velocity increased by 8% ($v_{forward}$=1.3±0.1 $m \cdot s^{-1}$), optimizing energy efficiency. On variable terrain (5° slopes), RL maintained stability better than PID, reducing the ZMP deviation by 12% (from 3.5 cm to 3.1 cm). Tests in OpenSim validated the reduction in muscle effort: the average quadriceps muscle force decreased from 250 ± 20 N (PID) to 210 ± 15 N (RL). On "stair descending", RL reduced ankle impact by 18% (from 300 N to 246 N), improving the comfort of the simulation.

3.3. HAR-RL Integrator

The integration of HAR-RL reduced the exoskeleton's adaptation time to activity changes from 1.2 seconds (without HAR) to 0.5 seconds. Table 4 shows the impact of integration on key metrics.

Table 4

Effect of HAR-RL integration on performance

Activity	Speed ($m \cdot s^{-1}$)	Metabolic cost ($J \cdot kg^{-1}$)	Stability (cm)
Normal walking (RL)	1.2 ± 0.1	5.1 ± 0.3	4.5 ± 0.2
Normal walking (HAR-RL)	1.3 ± 0.1	4.9 ± 0.2	4.6 ± 0.2
Climbed the stairs (RL)	0.8 ± 0.1	6.5 ± 0.4	4.7 ± 0.2
Climbed the stairs (HAR-RL)	0.9 ± 0.1	6.2 ± 0.3	4.9 ± 0.2

4. Discussion

The results obtained confirm the hypothesis that integrating human activity recognition (HAR) with reinforcement learning (RL) improves the control of bipedal exoskeletons. The HAR accuracy of 92% obtained with SVM is comparable to the literature, where accuracies of over 90% are reported for basic activities. However, confusions between "sitting down" and "rising up from a chair" indicate the limits of the simple statistical features used, suggesting that methods such as deep learning (e.g. convolutional neural networks) could improve classification.

The RL optimization reduced the metabolic cost by 15%, a result like that reported by Kim and Park, who obtained reductions of up to 20%. The advantage of our approach is the adaptability offered by the HAR-RL integration, which adjusts the control according to the activity (e.g. stability for "climbing stairs", speed for "normal walking"), reducing the adaptation time from 1.2 to 0.5 seconds. This is an improvement over static methods, which cannot dynamically respond to changes.

Limitations include HAR's dependence on training data, which can introduce bias due to the limited number of subjects, and the complexity of RL simulations, which do not fully reproduce real-world conditions (e.g., irregular surfaces). Also, real-time processing of HAR data requires large computational resources, which could limit its applicability on wearable devices.

The results have implications for rehabilitation, where reduced muscle effort (e.g., 16% decreased quadriceps strength) can accelerate recovery, and for physical augmentation, where increased speed (8% for "normal walking") is beneficial in industrial applications. Future directions include expanding the dataset, testing under real-world conditions, and using deep learning for HAR to improve the accuracy and robustness of the system.

5. Conclusions

This study successfully demonstrated that integrating human activity recognition (HAR) with reinforcement learning (RL) provides an efficient framework for optimizing the control of bipedal exoskeletons. The developed HAR system classified activities with a high accuracy of 92%, allowing for the precise identification of movements such as normal walking, climbing/descending stairs, and sitting/standing up. In parallel, the RL optimization reduced the metabolic cost by 15% compared to a traditional PID controller, while improving the exoskeleton stability by 10% in dynamic scenarios such as climbing stairs. The HAR-RL integration allowed for rapid adaptation to activity changes, reducing the response time from 1.2 seconds to 0.5 seconds, which is a significant improvement over static method.

The results have important implications for practical applications, especially in medical rehabilitation, where reduced muscle effort (e.g., 16% decrease in quadriceps strength) can facilitate patient recovery, and in physical augmentation, where increased

walking speed (8%) can support industrial activities. The main contribution of the study is to reduce the dependence on manual adjustments, providing an adaptable and efficient system. In the future, expanding the dataset, testing under real conditions, and using deep learning for HAR can increase the robustness and applicability of the system, paving the way for smarter and more accessible exoskeletons.

Conflicts of interest: The authors declare no conflict of interest.

References

1. Tijjani, I.; Kumar, S.; Boukheddimi, M. A Survey on Design and Control of Lower Extremity Exoskeletons for Bipedal Walking. *Applied Sciences* 2022, 12(5), 2395,
2. Baud, R.; Manzoori, A. R.; Ijspeert, A.; Bouri, M. Review of control strategies for lower-limb exoskeletons to assist gait. *J Neuroeng Rehabil* 2021, 18, 119.
3. Luo, S., Jiang, M., Zhang, S. *et al.* Experiment-free exoskeleton assistance via learning in simulation. *Nature* 2024, 630, pp. 353–359.
4. Yao, Z.; Mir Latifi, S.M.; Molz, C.; Scherb, D.; Löffelmann, C.; Sänger, J.; Miehling, J.; Wartzack, S.; Lindenmann, A.; Matthiesen, S.; et al. A Novel Approach to Simulating Realistic Exoskeleton Behavior in Response to Human Motion. *Robotics* 2024, *13*, 27.
5. Zhang, J.; Fiers, P.; Witte, K.A.; Jackson, R.W.; Poggensee, K.L.; Atkeson, C.G.; Collins, S.H. Human-in-the-loop optimization of exoskeleton assistance during walking. *Science* 2017, 356, pp. 1280-1284.
6. Luo, S.; Androwis, G.; Adamovich, S.; Su, H.; Nunez, E.; Zhou, X. Reinforcement Learning and Control of a Lower Extremity Exoskeleton for Squat Assistance. *Frontiers in Robotics and AI* 2021, 8, 702845.
7. Coser, O. ; Tamantini, C. ; Soda, P. ; Zollo, L. (2024). AI-based methodologies for exoskeleton-assisted rehabilitation of the lower limb: a review. *Frontiers in robotics and AI* 2024, 11, 1341580.
8. Ezekiel, S.; Harrity, K.; Blasch, E.; Bubalo, A. No-reference blur metric using double-density and dual-tree two-dimensional wavelet transformation. In: *National Aerospace and Electronics Conference*, *NAECON 2014 – IEEE,* Dayton, OH, USA, 2014, pp. 109-114.
9. de Miguel-Fernández, J. ; Lobo-Prat, J. ; Prinsen, E. ; Font-Llagunes, J. M. ; Marchal-Crespo, L. (2023). Control strategies used in lower limb exoskeletons for gait rehabilitation after brain injury: a systematic review and analysis of clinical effectiveness. *Journal of neuroengineering and rehabilitation* 2023, 20(1), 23.
10. Gordon, D.F.N.; Henderson, G.; Vijayakumar, S. Effectively Quantifying the Performance of Lower-Limb Exoskeletons Over a Range of Walking Conditions. *Frontiers in Robotics and AI* 2018, 5, 61.
11. Nunes, P.F.; Ostan, I.; Siqueira, A.A.G. Evaluation of Motor Primitive-Based Adaptive Control for Lower Limb Exoskeletons. *Frontiers in Robotics and AI* 2020, 7, 575217.
12. Sheykhmousa, M.; Mahdianpari, M.; Ghanbari, H.; Mohammadimanesh, F.; Ghamisi, P.; Homayouni, S. Support Vector Machine Versus Random Forest for Remote Sensing Image Classification: A Meta-Analysis and Systematic Review. *IEEE Journal of Selected Topics in Applied Earth Observations and Remote Sensing* 2020, 13, pp. 6308–6325.
13. Breiman, L. Random Forests. Machine Learning, 2001, 45, pp. 5–32.
14. Schonlau, M.; Zou, R.Y. The Random Forest Algorithm for Statistical Learning. *The Stata Journal* 2020, 20(1), pp. 3–29.
15. Chicco, D.; Jurman, G. The advantages of the Matthews correlation coefficient (MCC) over F1 score and accuracy in binary classification evaluation. *BMC Genomics* 2020, 21, 6.

Citation: Rusanovschi, M.; Marusic, G. Human activity recognition and optimization of biped exoskeletes through artificial intelligence: an integrated approach. *Journal of Engineering Science*. 2025, XXXII (1), pp. 71-79. https://doi.org/10.52326/jss.utm.2025.8(2).06.

Submission of manuscripts: jes@meridian.utm.md

Journal of Engineering Science *Vol. XXXII, no. 1 (2025), pp. 80 - 89*
Fascicle *Electronics and Computer Science* *ISSN 2587-3474*
Topic *Biomedical Engineering* *eISSN 2587-3482*

https://doi.org/10.52326/jes.utm.2025.32(1).07
UDC 539.12:577

GENERATION AND CONTROL OF CHAOTIC BEHAVIOUR OF PHOTONS AND PHONONS IN BIOLOGICAL MEDIA

Natalia Gubceac [1,2*], ORCID: 0009-0009-0299-3070,
Nellu Ciobanu [1,2], ORCID: 0000-0002-8153-8237,
Vasile Tronciu [1], ORCID: 0000-0002-9164-2249

[1] *Technical University of Moldova, 168 Stefan cel Mare Blvd., Chisinau, Republic of Moldova,*
[2] *State University of Medicine and Pharmacy "Nicolae Testemițanu", 165 Stefan cel Mare Blvd., Chisinau, Republic of Moldova*
* Corresponding author: Natalia Gubceac, *natalia.gubceac@fiz.utm.md*

Received: 02. 12. 2025
Accepted: 03. 22. 2025

Abstract. It was reported the results on the numerical investigations of the dynamical behavior of photons and phonons emitted by a biological medium under the influence of millimeter or terahertz radiation. In particular it was investigated the influence of external modulation pump parameters on photons and phonons dynamics. It was found that the system displays, under certain conditions, continues waves, periodic and chaotic behaviors. A quasiperiodic route to chaos is found. The influence of some parameters on the system behavior is investigated. Finally, very good conditions for large chaotic behavior are identified.

Keywords: *Millimeter waves, generated photons and phonons, pumping control, optical feedback, periodic oscillations, quasi-periodic route to chaos.*

Rezumat. Au fost raportate rezultatele investigațiilor numerice ale comportamentului dinamic pentru fotonii și fononii emiși de un mediu biologic sub influența radiației milimetrice sau terahertzi. În special, a fost investigată influența parametrului de pompaj asupra dinamicii fotonilor și fononilor. S-a constatat ca în anumite conditii, sistemul descrie un scenariu de unde continui, unde periodice și haotice. A fost determinată modalitatea de control a sistemului din starea cvasiperiodică către cea haotică. A fost studiată influența unor parametri asupra dinamicii sistemului de fotoni și fononi la care, au fost identificate condiții de evoluție a sistemului către un regim haotic complex.

Cuvinte cheie: *Unde milimetrice, fotoni și fononi emiși, pompaj controlat, feedback optic, ocilații periodice, regim cvasi-periodic haotic.*

1. Introduction

The influence of electromagnetic fields on the living matter has become an attractive goal for modern biomedicine [1,2]. The human body is exposed daily to the radiation of various types of electromagnetic waves via the modern technologies, which are extremely widespread in everyday life. The effects produced by these radiations can destroy the body's defense and functional systems [3]. However, some classes of electromagnetic waves, e.g.,

millimeter (MM) and terahertz (THZ) waves can produce constructive therapeutic effects [4-6]. Thus, a multitude of companies around the world that produce medical devices are trying to replace, well known classical methods (tissue damage during surgery) with non-invasive one based on MM and THZ wave therapy [7-9]. Recently, it was demonstrated experimentally, that these waves at low intensities resonate with the electromagnetic waves generated by biological cells. These interactions correspond to 42.7 GHz, 53.5 GHz and 60.7 GHz wave frequencies and play an important role in the functional state of the cells, tissue, or even the whole organism [10].

Recent technology allows the coherent detection of THZ pulses and can be successfully applied to the spectroscopy, biomedical imaging and diagnostics [11-13]. MM and THZ waves have low photon energy between 1 and 5 meV. These energies correspond to the energy levels related to rotational and vibrational molecule modes and intermolecular vibrations, such as hydrogen bonds. Such type of low-energy allows the visualization of biomolecules, characterizing their spectral features in THz region [14,15]. Due to the low photon energy, it is not enough to cause molecular ionization. From this reason, MM and THZ waves are suitable and attractive for noninvasive biomedical imaging and possible human health effects. They could be applied in the real studies without causing biological ionizing damage opposite to damages than can be caused by X or gamma-rays.

While the practical results are quite visible and impressive, the complete understanding of physical mechanism of the interaction process of MM or THZ waves with living tissue to our knowledge still does not exist. The first theory that is focused on the generation of MM waves by the living cells was proposed by Fröhlich [16]. According to his idea, at the cellular or protein level, the appearance of certain coherent longitudinal electric modes can happen, that are stabilized by deformations arising from nonlinear effects. At low power, the MM waves can stimulate the excitation of the coherent electric vibrations provided by the biological system when it is in an active metabolic state. These coherent states could regulate the biological cell activities. The coherent waves emitted by living cells represent a complex process involving the cell membranes, protein channels, and cellular transport pumps [17,18]. However, the cell membranes are considered the basic trigger for that interaction, as they are sensible to coherent excitations regime. The cell membrane is the most considered interest in biological physics, as it acts as a gateway of the cell, where the control of many essential electrophysiological functions are important.

Another study reports that at the interaction of MM waves with biological membrane, a mechanism of nonhomogeneous dissipation of wave energy happens [19]. For collective coherent processes, a clustered bound state is created, which is localized in space and has remarkable stability properties. This may contribute to the emergence of particular regions in the membrane that are polarized and are coupled to an elastic deformation. On the other hands, the spatial localization of the polarized state proposed for molecular chains, leads to soliton formation as well as Bose condensation [20]. Base on this idea, a control mechanism with the dynamics of a biological medium that is irradiated with an external MM wave source was studied [21]. It is demonstrated that for some parameters of the model, the system dynamics displays continue periodic and chaotic behaviors.

In this paper, we report results how to control the dynamics of the Fröhlich photon and phonon systems using modulated pumping of the MM and THZ wave source. The dynamics of condensed dipole-active Bose phonons and internal Fröhlich photons can exhibit regimes of continuous waves (CW), periodic oscillations, period doublings, chaotic regimes

for certain values of the system parameters as well as the modulation of external signal. The paper is organized as follows. The setup structure and mathematical model are described in Section 2. Results of the numerical simulations are given in Section 3. We discuss the influence of main parameters of output power evolution. Finally, conclusions are given in Section 4.

2. Theoretical model

It is well known, that the modulation pumping is influencing the laser dynamics, as well as the features of emitted light [22]. In case of a fiber ring laser, excited by a sinusoidally modulated pump power, several resonance peaks were observed, showing bistable behaviors. It is demonstrated that these regions depend on the powers and population distributions along the laser active medium. The influence of modulated current shape on the dynamics of a semiconductor laser with optical feedback was studied recently [23], and compared with the intensity spiking dynamics of a FHN neuron, that is modulated with the same input signal that modulated laser current. Thus, the modulation index of a sinusoidal pump can contribute to the appearance of various optical bistabilities and influence the coherent resonance control in a system of neuronal networks [24].

The theoretical model of the evolution of photons and phonons generated by the biological media was discussed in our previous papers [20,21]. Figure 1 shows the scheme of irradiation of the biological environment by MM wave source, whose profile is described by a function with sinusoidal modulated pump power: $P = P_0\left(1+m\left(\cos 2\pi ft\right)\right)$, where m is the modulated parameter. P_0 and f represent the pump amplitude and frequency, respectively. The photons emitted by the biological medium are delayed from an external mirror, similar to the model of semiconductor lasers with external feedback [25]. Typically, the external feedback influences the dynamics of the system and can contribute to the appearance of periodic and quasi-periodic pulsations, low frequency fluctuations, as well as chaotic regimes. Here, we investigate the influence of modulation index m and external feedback parameters Γ and φ on the photons and phonons dynamics generated by the biological environment.

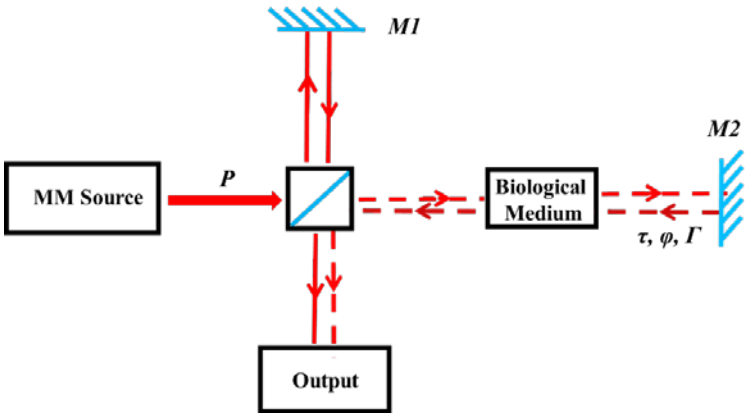

Figure 1. Schematic representation of the setup consisting of biological medium under the influence of external modulation pump.

The external optical feedback phase and amplitude are notated by φ and Γ. The incident MM wave is separated in two waves one of which is considered as reference wave and is reflected from the mirror M1. The second wave interacts with biological medium and is reflected from the mirror M2. M1 that is located at a given distance from the medium generates an external optical feedback. The output power represents the superposition on the final two wave signal.

The photons and phonons emitted by the biological medium are described by the system of delayed differential equations [21]:

$$\frac{dE_1}{dT} = -\sigma E_1 - \left(\tilde{\delta} - \tilde{\omega}_0\right) E_2 + 2\alpha\tilde{\gamma} A_1 + \alpha\left\{2\tilde{\gamma}\left[\delta - \left(A_1^2 + A_2^2\right)\right] - 1\right\} A_2 + P + \\ + \Gamma\left[\cos(\varphi) E_1(t-\tau) + \sin(\varphi) E_2(t-\tau)\right], \quad (1)$$

$$\frac{dE_2}{dT} = \left(\tilde{\delta} - \widetilde{\omega_0}\right) E_1 - \sigma E_2 + 2\alpha\tilde{\gamma} A_2 - \alpha\left\{2\tilde{\gamma}\left[\delta - \left(A_1^2 + A_2^2\right)\right] - 1\right\} A_1 + \\ + \Gamma\left[\cos(\varphi) E_2(t-\tau) - \sin(\varphi) E_1(t-\tau)\right], \quad (2)$$

$$\frac{dA_1}{dT} = -\alpha E_2 - A_1 - \left[\delta - \nu\left(A_1^2 + A_2^2\right)\right] A_2, \quad (3)$$

$$\frac{dA_2}{dT} = -\alpha E_1 + \left[\delta - \nu\left(A_1^2 + A_2^2\right)\right] A_1 - A_2. \quad (4)$$

In the equations (1) - (4) we use the following addimensional parameters

$$\delta = \frac{\Delta}{\gamma},\ \tilde{\delta} = \frac{\omega^2 - c^2k^2}{2\omega\gamma},\ \alpha = \sqrt{\frac{\omega\Omega_0}{2\gamma^2}},\ \Omega_0 = \frac{4\pi d^2}{V_0\hbar},\ \tilde{\omega}_0 = \frac{\Omega_0}{\gamma},\ \tilde{\gamma} = \frac{\gamma}{\omega},\ \sigma = \frac{\gamma_f}{\gamma},\ T = \gamma t.$$

Here, ω and Ω represent the photons and phonons frequencies, while $\Delta = \omega - \Omega$ is the detuning of frequencies. The phonons and photons attenuation constants are notated by γ, and γ_f respectively. The parameter σ represents the quality factor Q of the cavity where the biological medium is located. *d* is the dipolar electric momentum, *k* is the wave vector, *c* is speed of light in vacuum, and V_0 is sample volume, and ν = ±1. Here we consider α as a parameter characterizing phonon rate losses. Γ and φ characterize the strength and phase of external feedback, respectively.

In our previous works [20,21], we demonstrated that with an external pump and varying certain system parameters, the dynamics of the output power can be controlled, in which the chaotic and periodic evolutions can be transformed into the CW regime. However, it is interesting to study the influence of modulated pump on the considered system and the possibility to control with modulation index parameter.

The system of equations (1)-(4) represent the basis for the following investigations. The output power of emitted photons and the concentration of phonons generated by the biological environment are defined respectively by $P = E_1^2 + E_2^2$, and $n = A_1^2 + A_2^2$. For the numerical calculations in the all following figures we use the following values of dimensionless parameters $\tilde{\omega}_0 = 0.1$, $\nu = 1$, $\tilde{\gamma} = 1.1$, $\tilde{\delta} = 0.1$, $\tau = 0.15$, $\delta = 3$, $\sigma = 3$, $P_0 = 85$, $f = 2$.

3. Results of numerical simulations

Figure 2 describes the dynamics of emitted photons. In Figure 2a the output power evolution in time and the phase portraits for certain values of the system parameters is shown. One can observe that, for the modulation index *m* = 0, the evolution of the system tends to a stable stationary state, and the phase trajectories describe a stable focus. For *m* = 0.1, as shown in Figure 2b, the system describes a periodic oscillations, and the phase portrait of trajectories show the limit cycle. An increase of modulation parameter to *m* = 0.5 quasi-periodic pulsations appears in the system and the phase portrait is a deformed ellipse (see Figure 2c). Finally, an increase of *m* to *m* = 0.9, leads to the appearance of the strong chaotic regime. Thus, with the pump parameter, it is possible to control the dynamics of the system by keeping all the other parameters fixed. This is an indication that it may be possible to control the dynamics from CW to chaos only changing a single parameter.

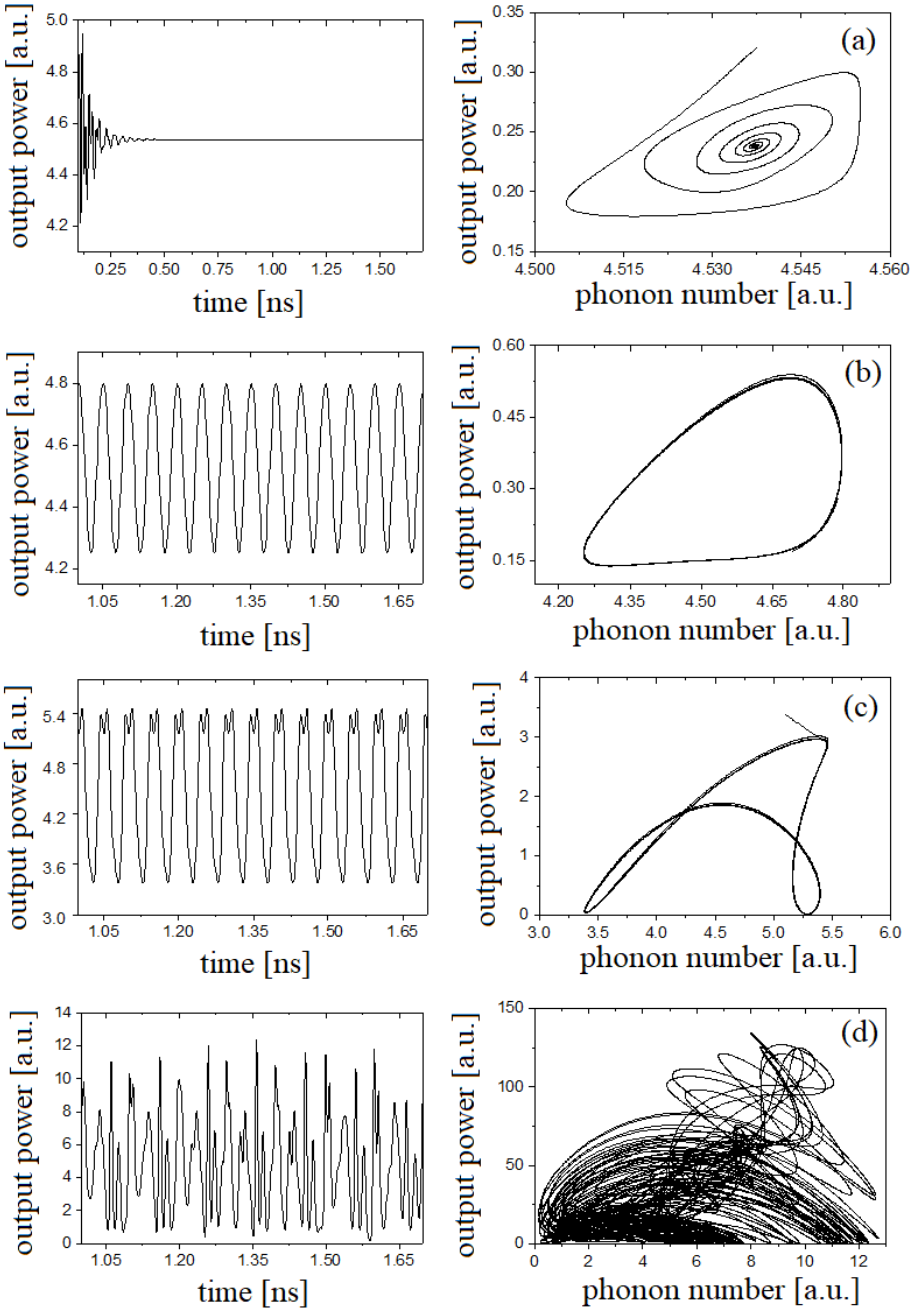

Figure 2. Time traces of the output photons power (left), and phase portrait (right) for $\alpha = 8$, $\Gamma = 2.5$, $\varphi = 3\pi/2$ and various values of modulation index: a) m = 0, b) m = 0.1, c) m = 0.5, d) m = 0.9.

In what follows the dynamics of the system (1)-(4) is presented for an increase of parameter α to $\alpha = 15$, i.e. increase of phonon rate losses. As was expected an increase of α from 5 to 15 lead to a more complex dynamics even for m = 0 (see Figure 3). As one can see, for m = 0, the time evolution of the emitted photons describes a regime of periodic waves with the phase portrait as a complicated limit cycle.

For an increase of modulation index parameter to m = 0.9 in the system new harmonics appears and the phase portrait becomes more complex. Thus, with the help of parameter α one can transform periodic regime to quasi-chaotic.

One can conclude that the dynamic of system is strongly dependent on both parameters α and m.

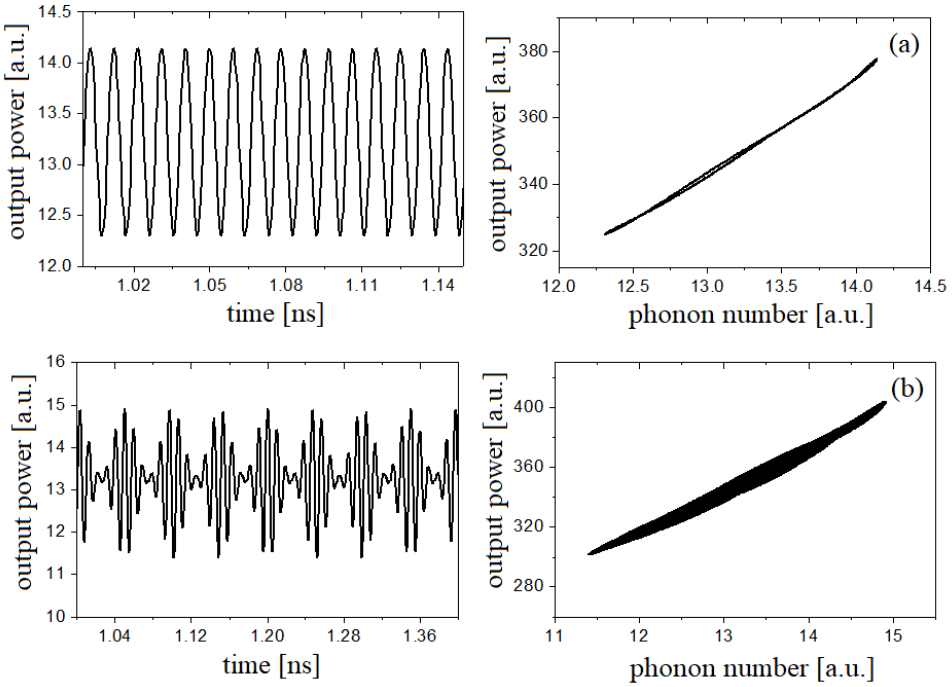

Figure 3. Time traces of the output photons power (left), and phase portrait (right) for $\alpha = 15$, $\Gamma = 2.5$, $\varphi = 3\pi/2$ and two values of modulation index: a) m = 0, b) m = 0.9.

The external phase can influence the evolution of output power. Thus, we change the phase from $\varphi=3\pi/2$ to $\varphi = \pi$ and vary the modulation pump from 0 to 0.9 for parameters as in Figure 2. As shown in Figure 4 for m = 0, periodic oscillations can be observed in the dynamics of the system, and with its increase of it to m = 0.9 strong chaotic oscillations appear. The phase trajectories describe a strange attractor for chaotic behavior is shown in Figure 4b.

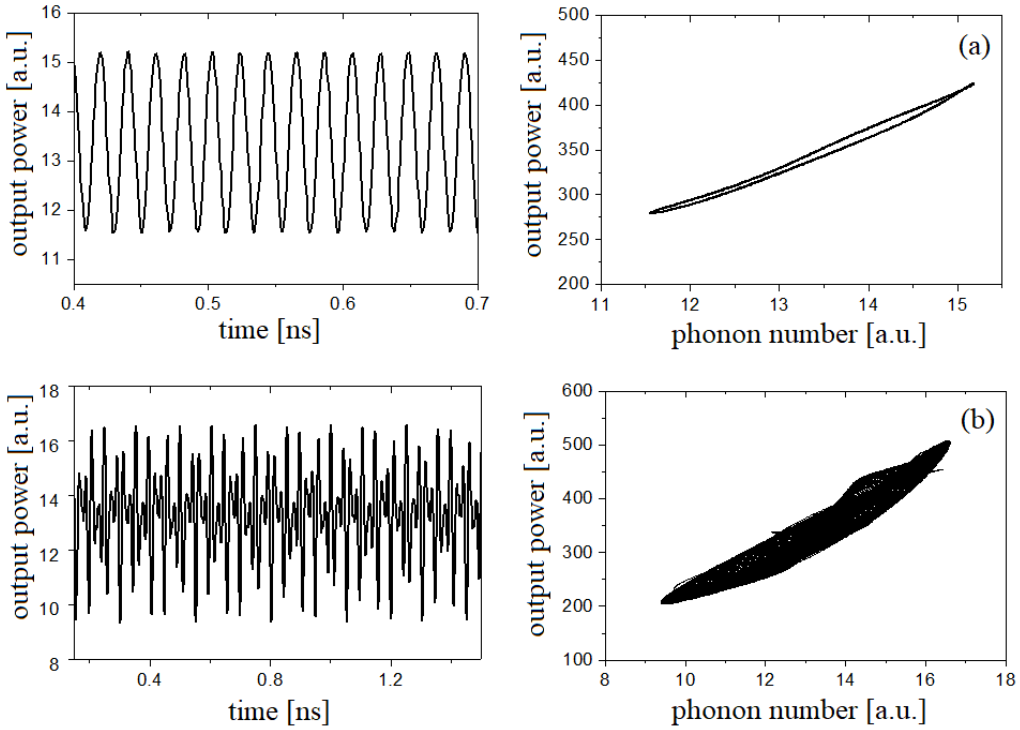

Figure 4. Time traces of the output photons power (left), and phase portrait (right) for $\alpha = 8$, $\Gamma = 10$, $\varphi = \pi$, and various values of modulation index: a) m = 0, b) m = 0.9.

Next, we describe the system dynamics in terms of bifurcation diagrams. Figure 5 shows bifurcation diagram, where feedback strength Γ is considered as bifurcation parameter. The diagram shows the dependence of photon number on the feedback strength for maximum (black) and minimum (red) values and for different pump parameter m. Each dot represents a peak of the output power for a fixed value of feedback strength.

Thus, for a given value of the feedback strength, the figure displays the values of all the local maximal (black) and minimal (red) of the time traces, calculated within 50 ns, of the emitted output power.

For $m = 0$, the systems starts from CW operation - region A in both Figures 5a and 6A, followed by periodic oscillations - region B in both Figures 5b and 6B.

The regions C and D (Figure 5a and Figures 6C and 6D) are characterized by chaotic waves. An increase of m to 0.1 results in a small change in the bifurcation diagram (see Figure 5b). When $m = 0.5$ the region of CW disappears (see Figure 5c) and the behavior becomes more complicated. For $m = 0.9$, in the bifurcations diagram chaotic regimes are obtained (see Figure 5d and Figures 6E and 6F).

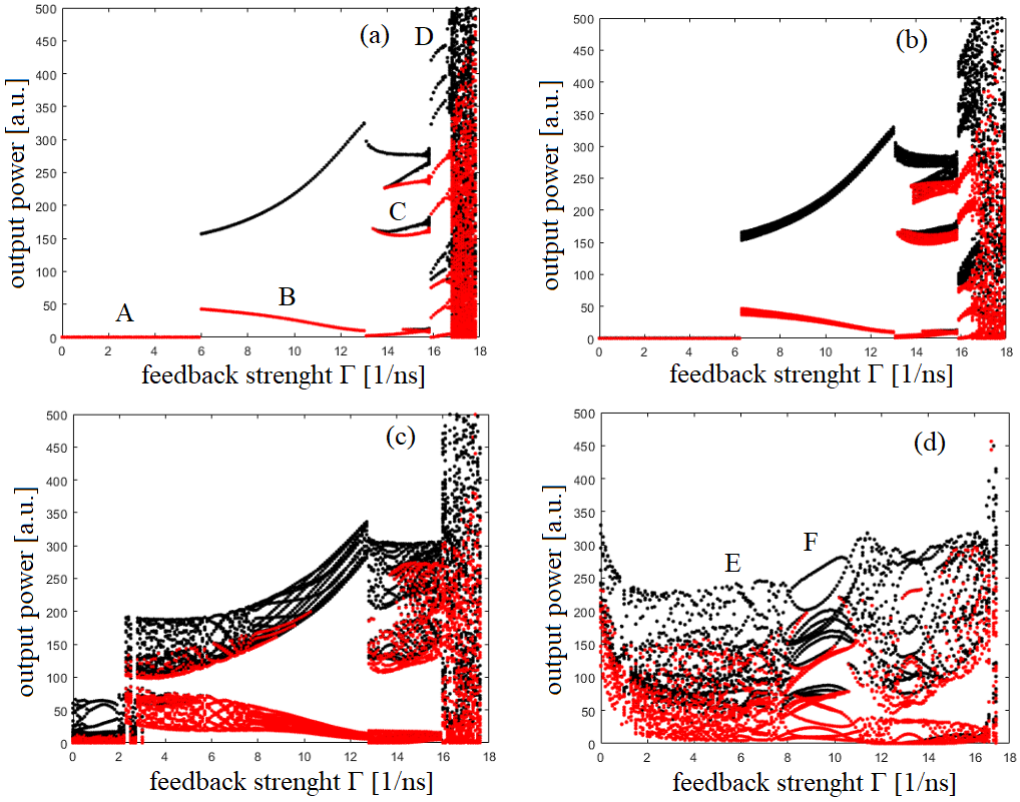

Figure 5. Numerical bifurcation diagram of the output power for amplitude of the optical feedback as bifurcation parameter, where: $\alpha = 8$, $\varphi = 3\pi/2$, a) $m = 0$, b) $m = 0.1$, c) $m = 0.5$, d) $m = 0.9$.

Thus, a scenario compatible with that of quasiperiodic route to chaos is observed. Thus, the influence of external optical feedback on the dynamics of emitted Fröhlich photons and phonons is very sensitive to external feedback parameters and can influence the system stability.

We can control the dynamics of the system via two main parameters the feedback strength of external feedback and modulation pump index.

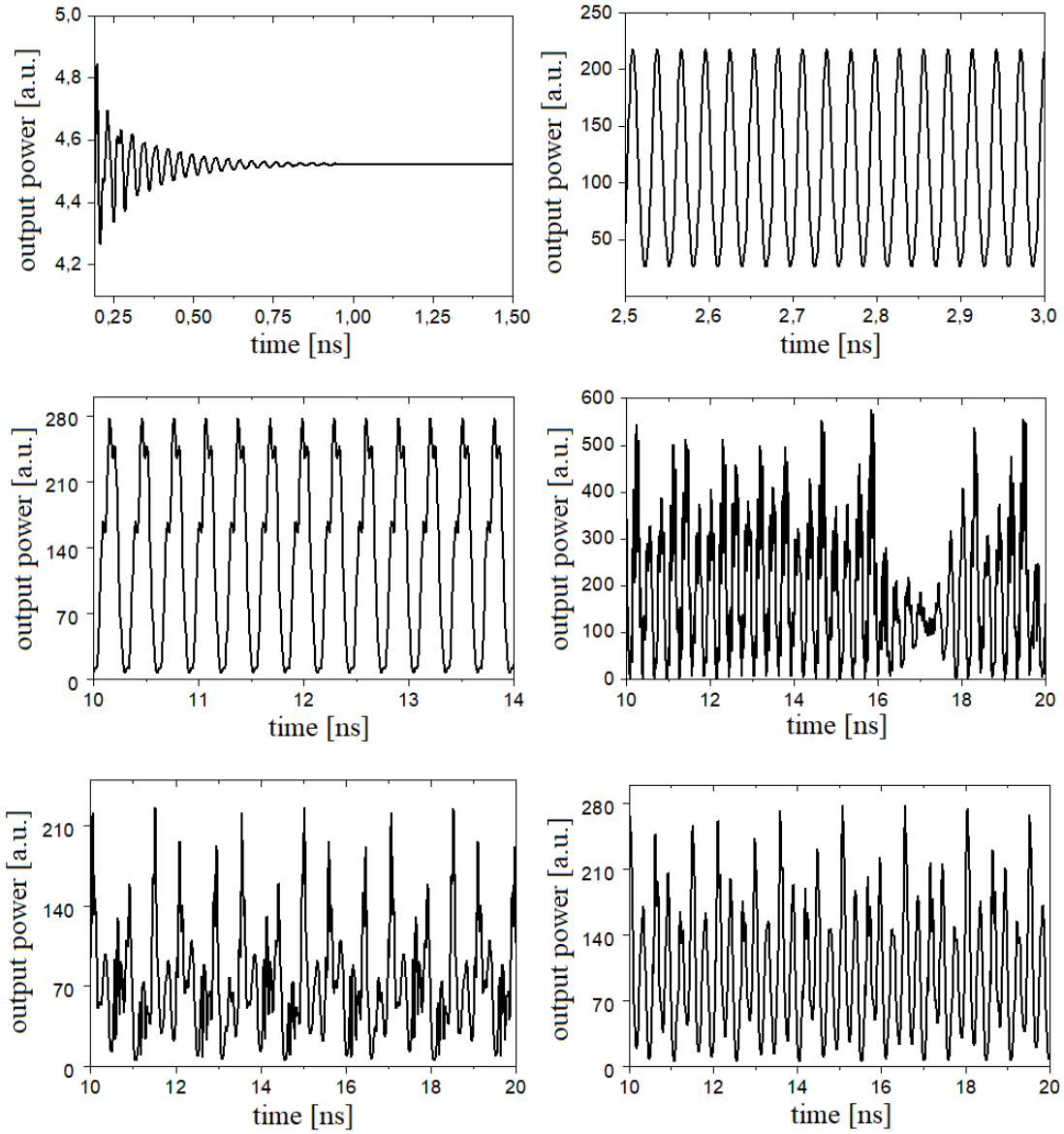

Figure 6. Time traces of the output photons power for $\alpha = 8$, $\varphi = 3\pi/2$ and various values of modulation index: (A) m = 0, Γ = 4; (B) m = 0, Γ = 10; (C) m = 0, Γ = 15; (D) m = 0, Γ = 17; (E) m = 0.9, Γ = 5; (F) m = 0.9, Γ =10.

5. Conclusions

In this paper we report a model for generation and control of chaotic behavior of Fröhlich photons and phonons in a biological medium. The dynamics of condensed dipole-active Bose phonons and internal Fröhlich photons is influenced by external optical feedback. Thus, the dynamics of systems can exhibit regimes of continuous CW, periodic oscillations, period doublings, chaotic regimes for certain values of the system parameters. An important goal of this study is the influence of modulation parameter of external pumping on the dynamics of the system.

In the absence of modulation pump parameter, m, the evolution of the system for certain fixed parameters tends to a stable stationary state, and the phase trajectories describe a stable focus. A small increase of m contributes to the appearance of a periodic oscillation in the system, and the phase portrait of trajectories show a limit cycle. For moderated and large values of modulation parameter, one can observe the occurrence of quasi-periodic

pulsations as well as strong chaotic regimes. Thus, the transition of the system from stable states to periodic oscillations, from periodic regime to quasi-periodic pulsations as well as from quasi-periodic pulsations to chaotic behavior is possible only via a single variable parameter.

The parameter α that characterizes the phonon rate losses also influence the dynamics of the emitted photons and phonons. For large values of *m*, the model shows a strong chaotic oscillations regime and the phase trajectories describe strange attractors. The same regimes, i.e., chaotic oscillations and strange attractors can be obtained under the influence of external feedback amplitude and phase.

The dynamics of the systems was also described and in terms of bifurcation diagrams, considering feedback strength Γ as bifurcation parameter. Thus, with our model we can control the dynamics of the system via two main parameters the feedback strength of external feedback and modulation pump parameter.

Acknowledgments: This work was supported by the project 020402 "*Development of technologies and investigation of the properties of layered semiconductor compounds, hybrid nanostructures and laser sources*".

Conflicts of Interest: The authors declare no conflict of interest.

References

1. D'Arco, A.; Di Fabrizio, M.; Dolci, V.; Petrarca, M.; Lupi, S. THz pulsed imaging in biomedical applications. *Condens. Matter* 2020, 5(2), 25.
2. Akinori, I.; Stefano, L.; Augusto, M. Terahertz as a frontier area for science and technology. *Condens. Matter* 2021, 6(3), 23.
3. Ramundo-Orlando, A. Effects of Millimeter Waves Radiation on Cell Membrane - *A Brief Review. J Infrared Milli Terahz Waves* 2010, 31, pp. 1400–1411.
4. Sarika, S.; Neeru, K. Health Implications of Electromagnetic Fields, Mechanisms of Action, and Research Needs. *In: Advances in Biology* 2014, 24 p.
5. Kojima, M.; Tsai, CY.; Suzuki, Y. Ocular Response to Millimeter Wave Exposure Under Different Levels of Humidity. *J Infrared Milli Terahz Waves* 2019, 40, 574–584.
6. Le Pogam, P.; Le Page, Y.; Habauzit, D. et al. Untargeted metabolomics unveil alterations of biomembranes permeability in human HaCaT keratinocytes upon 60 GHz millimeter-wave exposure. *Sci Rep* 2019, 9, 9343.
7. Torgomyan, H.; Trchounian, A. Bactericidal effects of low-intensity extremely high frequency electromagnetic field: an overview with phenomenon, mechanisms, targets and consequences. *Crit Rev Microbiol.* 2013, 39(1), pp. 102-11.
8. Davies, A.G.; Linfield, E.H.; Johnston, M.B. The development of terahertz sources and their applications. *Physics in Medicine and Biology* 2002, 47(21), pp. 3679-3689.
9. Globus, T.R.; Woolard, D.L.; Khromova, T.; Crowe, T.W.; Bykhovskaia, M.; Gelmont, B.L.; Hesler, J.; Samuels, A.C. THz-Spectroscopy of Biological Molecules. *J Biol Phys.* 2003, 29(2-3), pp. 89-100.
10. Li, X.-H.; Tang, J.-T.; Liao, Y.-P.; Jin, H.-K.; Zhou, J.-M.; Wang, G.-H.; Wang, H. Millimeter wave in the treatment of acute radiation-induced cervical skin ulcers. *J. Clin. Rehab. Tissue Eng.* 2008, 12, pp. 663-666.
11. Zaytsev, I.; Dolganova, I.N.; Chernomyrdin, N.V.; Katyba, G.M.; Gavdush, A.A.; Cherkasova, O.P.; Komandin, G.A.; Shchedrina, M.A.; Khodan, A.N.; Ponomarev, D.S. The progress and perspectives of terahertz technology for diagnosis of neoplasms: *A review. J. Opt.* 2020, 22, 013001.
12. Yang, X.; Zhao, X.; Yang, K.; Liu, Y.; Liu, Y.; Fu, W.; Luo, Y. Biomedical Applications of Terahertz Spectroscopy and Imaging. *Trends Biotechnol.* 2016, 34, pp. 810–824.
13. Son, J.H.; Oh, S.J.; Cheon, H. Potential clinical applications of terahertz radiation. *J. Appl. Phys.* 2019, 125, 190901.
14. Titova, L.V.; Ayesheshim, A.K.; Golubov, A.; Rodriguez-Juarez, R.; Woycicki, R.; Hegmann, F.A.; Kovalchuk, O. Intense THz pulses down-regulate genes associated with skin cancer and psoriasis: a new therapeutic avenue? *Sci Rep.* 2013, 3, 2363.

15. Fëdorov, V.I.; Serdyukov, D.S.; Cherkasova, O.P.; Popova, S.S.; Nemova, E.F. The influence of terahertz radiation on the cell's genetic apparatus. *J. Opt. Technol.* 2017, 84, pp. 509–514.
16. Frohlich, H. Bose condensation of strongly excited longitudinal electric modes. *Phys. Lett, A* 1968, 26, pp. 402-403.
17. Geletyuk, V.I.; Kazachenko V.N.; Chemeris, N.K.; Fesenko, E.E. Dual effects of microwaves on single Ca2+-activated K+ channels in cultured kidney cells. *FEBS Letters* 1995, 359, pp. 85-88.
18. Zhadobov, M.; Saileau, R.; Viè, V. Interactions between 60-GHz millimeter waves and artificial biological membranes: dependence on radiation parameters. *IEEE Tras. MW Theory and Tec.* 2006, 54, pp. 2534-2542.
19. Bolterauer, H.; Tuszyński, J.A. Fröhlich and Davydov regimes in the dynamics of dipolar oscillations of biological membranes. *Phys. Rev. A,* 1991, 44, 1366.
20. Ciobanu, N.; Rusu, S.; Tronciu, V. Dynamical behavior of Bose-condensed dipole-active phonons and internal Fröhlich photons in biological media. *In: E-Health and Bioengineering Conference (EHB)*, Iasi, Romania, 2015, pp. 1-4.
21. Gubceac, N.; Ciobanu, N.; Tronciu, V. Control dynamics of the generated Frohlich photons by biological system. In: *E-Health and Bioengineering Conference (EHB),* Iasi, Romania, 2022, pp. 1-4.
22. Sola, I.J.; Martín, J.C.; Álvarez, J.M. Nonlinear response of a unidirectional erbium-doped fiber ring laser to a sinusoidally modulated pump power. *Optics Communications* 2002, 212 (4–6), pp. 359-369.
23. Jordi, T.-A.; Quintero-Quiroz, C.; Masoller, C. Comparing the dynamics of periodically forced lasers and neurons. *New Journal of Physics* 2019, 21, 103039.
24. Masoliver, M.; Masoller, C.; Zakharova, Z. Control of coherence resonance in multiplex neural networks. *Chaos, Solitons & Fractals* 2021, 145, 110666.
25. Radziunas, M.; Little, DJ.; Kane, DM. Numerical study of optical feedback coherence in semiconductor laser dynamics. *Opt Lett.* 2019, 44(17), pp. 4207-4210.

Citation: Gubceac, N.; Ciobanu, N.; Tronciu, V. Generation and control of chaotic behaviour of photons and phonons in biological media. *Journal of Engineering Science*. 2025, XXXII (1), pp. 80-89. https://doi.org/10.52326/jss.utm.2025.8(2).07.

Publisher's Note: JES stays neutral with regard to jurisdictional claims in published maps and institutional affiliations.

Submission of manuscripts: jes@meridian.utm.md

Journal of Engineering Science *Vol. XXXII, no. 1 (2025), pp. 90 - 110*
Fascicle *Architecture, Civil and Environmental Engineering* *ISSN 2587-3474*
Topic *Environmental Engineering* *eISSN 2587-3482*

https://doi.org/10.52326/jes.utm.2025.32(1).08
UDC 620.952:621.311.238

EXPLORING THE ENERGY GENERATION POTENTIAL OF JATROPHA CAKE IN A BIOREFINERY: AN OPTIMIZATION STUDY

Khadijah Nasir [1], ORCID: 0009-0002-3816-2067,
Toyese Oyegoke [1,2 *], ORCID: 0000-0002-2026-6864

[1] *CAD-Engineering of Processes and Reactive Materials Group, Chemical Engineering Department, Faculty of Engineering, Ahmadu Bello University, Zaria, Nigeria.*
[2] *Green Science Forum - Modeling & Simulation, Pencil Team, Ahmadu Bello University, Zaria, Nigeria.*
* Corresponding author: Toyese Oyegoke, *OyegokeToyese@gmail.com*

Received: 01. 06. 2025
Accepted: 02. 28. 2025

Abstract. Waste management and energy access remain critical challenges globally, especially in developing countries where poor waste management and unreliable power supply exacerbate environmental and socio-economic issues. This study aims to explore the potential of using Jatropha cake as a sustainable bioenergy source in gas-turbine power plants to address these challenges. Using a Central Composite Design (CCD) approach, the study evaluates the effects of compressor efficiency, turbine efficiency, heat transfer coefficients, and heat transfer area on power generation from Jatropha cake, modeled using the DWSim simulation package. The findings show that an open-loop gas-turbine configuration with a compressor efficiency of 83.92% and turbine efficiency of 98% can generate a maximum power output of 174235 kW. In contrast, the closed-loop configuration, optimized with a heat exchanger (HX) at 120 W/m²K heat transfer coefficient and 1000 m² heat transfer area, yields 74375.70 kW. The results suggest that the open-loop configuration is more efficient, offering significantly higher power generation. This study highlights the viability of Jatropha cake as a bioenergy resource, providing a promising solution for improving power supply in energy-deficient communities while contributing to sustainable waste management practices.

Keywords: *Biomass, Bioenergy, Biorefinery, Jatropha, Alternative Energy, Environment.*

Rezumat. Gestionarea deșeurilor și accesul la energie rămân provocări critice la nivel global, în special în țările în curs de dezvoltare, unde gestionarea deficitară a deșeurilor și alimentarea cu energie electrică nesigură amplifică problemele de mediu și socio-economice. Acest studiu își propune să exploreze potențialul utilizării turtei de Jatropha ca sursă durabilă de bioenergie în centralele electrice cu turbine pe gaz pentru a aborda aceste provocări. Folosind o abordare de tip Central Composite Design (CCD), studiul evaluează efectele eficienței compresorului, eficienței turbinei, coeficienților de transfer de căldură și suprafeței de transfer de căldură asupra generării de energie din turta de Jatropha, modelată folosind pachetul de simulare DWSim. Rezultatele arată că o configurație cu turbină pe gaz în buclă deschisă, cu o eficiență a compresorului de 83,92% și o eficiență a turbinei de 98%, poate genera o putere maximă de 174235 kW. În schimb, configurația în buclă închisă, optimizată

cu un schimbător de căldură (HX) la un coeficient de transfer de căldură de 120 W/m²K și o suprafață de transfer de căldură de 1000 m², produce 74375,70 kW. Rezultatele sugerează că configurația în buclă deschisă este mai eficientă, oferind o generare de energie semnificativ mai mare. Acest studiu evidențiază viabilitatea turtei de Jatropha ca resursă bioenergetică, oferind o soluție promițătoare pentru îmbunătățirea alimentării cu energie în comunitățile cu deficit energetic, contribuind în același timp la practici durabile de gestionare a deșeurilor.

Cuvinte cheie: *Biomasă, Bioenergie, Biorafinărie, Jatropha, Energie alternativă, Mediu.*

1. Introduction

Waste management has continued to be a subject of concern across the globe, irrespective of a country's classification, whether developed, developing, or underdeveloped [1–6]. The issue continues to attract attention toward finding better approaches for minimizing waste or transforming waste into valuable products or applications, such as biofuels, bio-based chemicals, or bioenergy development.

Many research efforts have focused on exploring measures for adding value to waste globally generated across communities [1,5,7]. Literature reports indicate a continuous trend of rising waste generation [2], suggesting that more attention should be given to research exploring initiatives for transforming waste into valuable chemicals and energy, which is vital.

Most developing countries that also suffer from poor waste management are also faced with inconsistent and interrupted power supply from their governments [2,8-12]. A large number of residents in such communities rely on locally generated power through solar power technology or resort to the use of biomass energy (i.e., firewood burning), which is environmentally unfriendly [2]. As a result, the significance of exploring the potential for bioenergy generation from waste in such communities would go a long way in addressing the energy supply problems they face. Some studies in the literature have explored the potential of transforming bagasse [9,13], sawdust [14,15], maize cob [16], and many other biomass sources for bioenergy generation in these communities. The literature indicates that these explorations have resulted in significant useful power generation [9,17–23]. However, attempts to explore the use of Jatropha cake in the literature are limited, and its application in running a power plant using either an open- or closed-loop gas-turbine power plant configuration has not yet been fully explored.

Hence, this study provides computational insight into the potential of using Jatropha cake for power generation, with optimization of the power generation capacity using both open- and closed-loop gas-turbine power plants. The study employs a process modeling and simulation approach, using an open-source process simulator (DWSim package). The findings reveal the achievable power generation capacity using Jatropha cake and the implications of compressor and turbine efficiency, including heat exchanger heat transfer area and coefficient, on the turbine feed stream temperatures and overall power generation capacity.

2. Materials and Methods

2.1. Computational details and Strategy

This research employed the use of DWSim [24] simulator in the modeling and simulation of the process of energy generation from Jatropha cake. In the study, it was resolved to use of the chosen simulator (DWSim) [25], since it was free and requires no need to purchase license. The Peng Robinson model [26] was chosen as the thermodynamic package for determination of accurate physical and transport properties and phase behavior. For the simulation of process plant, the stage-wise procedure shown in Figure 1 was adopted.

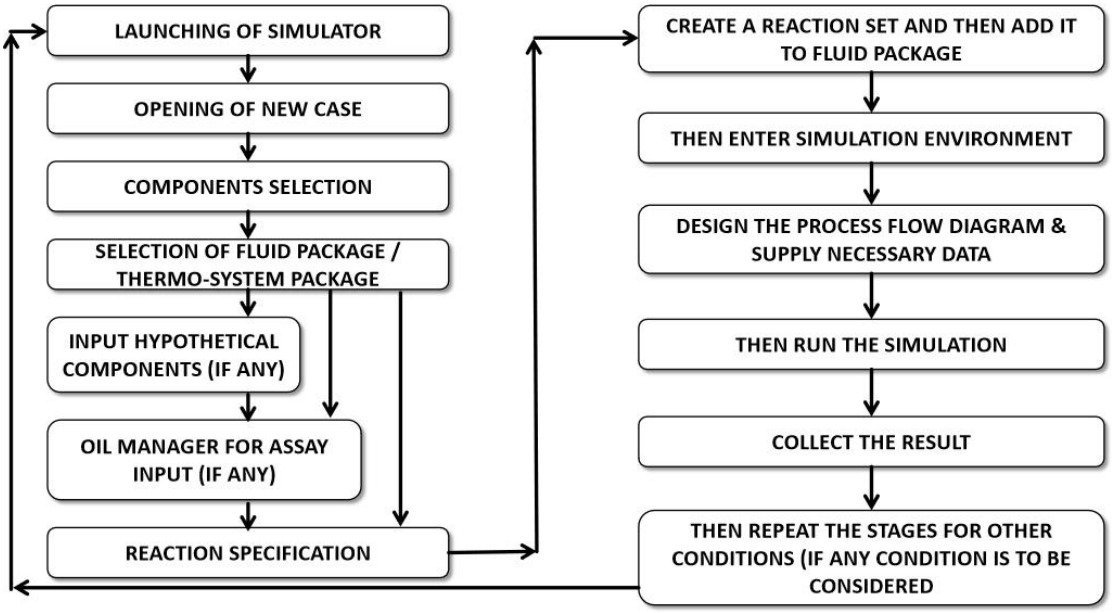

Figure 1. Flow Chart for Process Simulation (adopted from [27]).

In the modeling of the power plant, the study employs the use of the chemical composition data reported in the literature to model the Jatropha cake as the feedstock for the power generation process. However, in the study, the presence of the extractives was neglected (that is, approximated to be zero per cent weight) due to their insignificant percentage by weight reported and their volatility in the presence of high temperature. In a nutshell, the modeled values were normalized (in absence of percent for extractives) to 100%. These compositions are presented in Table 1.

Table 1

Jatropha cake composition

Component	Composition in % weight		
	Literature [28] Value	**Simulation Modeled Value**	**Normalized Value**
Cellulose	53.50	53.50	56.30
Hemicellulose	16.60	16.60	17.50
Lignin	24.90	24.90	26.20
Extractives	5.00	0.00	0.00

Table 2 presents the components selected from the DWSim compound database and those not available on the database (hypothetical compounds). The hypothetical compounds are created using their various properties such as their normal boiling points, molecular weights, molecular formulas and many other data gotten from literature [27].

Table 2

Hypothetical compounds and their properties

Compound	Specified Properties
Cellulose	Chemical Formula: $(C_6H_{10}O_5)_n$ where n = 100 units Molecular Weight$^{(E)}$,
Hemicellulose	Chemical Formula: $(C_5H_8O_4)_n$ where n = 10 units Molecular Weight$^{(E)}$
Lignin	Chemical Formula: $(C_{31}H_{34}O_{11})_n$ where n = 10 units Molecular Weight$^{(E)}$,

Note: E - estimated property.

Table 3

Components involved in the simulation process

Compound	Chemical formula	CAS number	Process application
Oxygen	O_2	7782-44-7	Combustor inlet
Carbon dioxide	CO_2	124-38-9	Combustor outlet
Water	H_2O	7732-18-5	Combustor outlet
Cellulose	$(C_6H_{10}O_5)_n$	9004-34-6	Feedstock
Hemicellulose	$(C_5H_8O_4)_n$	9014-63-5	Feedstock
Lignin	$(C_{31}H_{34}O_{11})_n$	9005-53-2	Feedstock

Note: CASnumber – Chemical Abstracts Service number.

The modeling of these compounds was done using the compound creator study option. Table 3 gives a summary of the modeled hypothetical compounds and properties inputted while modelling the compounds.

Table 4

Equipment used for modeling the open loop power plant

Equipment	Model	Operating condition
Air compressor	Compressor	Pressure ratio: 9.5, efficiency of 95%
Combustor	Mixer	Pressure calculation: maximum inlet
	Gibbs reactor	Calculation mode: adiabatic
Turbine	Expander	Outlet pressure: 1 atm, efficiency: 95%

Table 5

Equipment used for modeling the closed loop plant

Equipment	Model	Operating condition
Air compressor	Compressor	Pressure ratio: 9.5, efficiency of 95%
Combustor	Mixer	Pressure calculation: maximum inlet
	Gibbs reactor	Calculation mode: adiabatic
Air compressor 2	Compressor	Outlet pressure: 20 atm, efficiency: 95%
Heating Heat exchanger	Heating heat exchanger	Heat transfer coefficient: 100 W/m^{2}K
		Heat transfer area: 1000 m^2
Turbine	Expander for generator	Outlet pressure: 1 atm, efficiency: 98%
Cooling Heat exchanger	Cooling heat exchanger	Heat transfer coefficient: 100 W/m^{2}K
		Heat transfer area: 1000 m^2

Various equipment is needed for the modeling of the process plants were identified and modeled using the relevant data provided in Table 4 and 5 for both the open and closed loop case. Although, equipment like combustors were modeled as a combination mixer and Gibb reactor since DWSim Gibb reactor does not allow one to charge in more than one inlet stream. Details of the equipment model across the plants are presented in Table 4 for the open loop and Table 5 for the closed loop.

2.2. Design of Experiment for the Optimization of the Power Generation

In the study, the experiment was designed with the use of Design Expert version 6.0.6 employing response surface methodology (central composite design) and was run 13 times, whose output was later employed in the optimization of the power generation process conditions. Open-loop process was use to understand the impact of compressor and turbine efficiency on power generation for open-loop (PG_O) and syngas temperature (T_{S4}), while

closed-loop one was used to understand the impact of heat transfer coefficient and area on the power generation for closed-loop (PG_C).

Table 6

Design for compressor and turbine efficiency impact on PGo and T_{S4}

Response Variable	Variable Name	Units	Obs.	Study Type	Experiments	Initial Design
Y1	Power Gen.	kW	13	Response Surface	13	Central Composite
Y2	Syngas Temp.	K	13			
Factor Variable	**Variable Name**	**Units**	**Low Actual (L_A)**	**High Actual (H_A)**	**Low Coded (L_C)**	**High Coded (H_C)**
A (coded)	Comp. Eff. (actual)	%	39.75	79.25	-1	1
B (coded)	Turb. Eff (actual)	%	39.75	79.25	-1	1

Note: HPHT – high pressure high temperature stream; A and B – factor variables (in a normalized form with no unit); Y1 and Y2 – response variables; Obs. – number of observations; Comp. Eff. – compressor efficiency, %; Turb. Eff. – turbine efficiency, %.

For the determination of the coded values (otherwise known as the normalized form of the independent or factor variables assessed in the study) of the turbine and the compressor efficiencies for the different variations, equation 1 below is used.

$$y = \frac{(x-L_A)(H_C-L_C)}{(H_A-L_A)} + L_C, \quad (1)$$

where: x is value in actual form; y-value in coded form; L_A - low actual value; H_A - high actual value; L_C - low coded value, H_C- high coded value.

Table 7

Design summary with no blocks for impact of heat transfer coefficient and heat transfer area on HPHT gas stream temperature (T_{S5}) and power generated for closed-loop (PG_C)

Response Variable	Variable Name	Units	Obs.	Study Type	Experiments	Initial Design
Y1	HPHT Temp.	K	13	Response Surface	13	Central Composite
Y2	Power generated	kW	13			
Factor Variable	**Variable Name**	**Units**	**Low Actual (L_A)**	**High Actual (H_A)**	**Low Coded (L_C)**	**High Coded (H_C)**
A (coded)	Ht Trns. Coeff. (actual)	W/m^2K	28.87	120	-1	1
B (coded)	Ht Trns. Area (actual)	m^2	179.86	1000	-1	1

Note: HPHT – high pressure high temperature stream; A and B – factor variables (in a normalized form with no unit); Y1 and Y2 – response variables; Obs. – number of observations; Ht Trns. Coeff. – heat transfer coefficient, W/m2K; Ht Trns. Area - heat transfer area, m^2.

For the first case, the factors compressor and turbine efficiencies were varied in order to determine the optimal response variables (i.e., the power generation and syngas temperature) and the experiments were run 13 times. The variations of the factors were

limited to a range between 39.75% (less efficient) and 79.25% (more efficient). This design summary is presented in Table 6.

For the second case, the HPHT temperature and power generated were the responses recorded from variation of the factors which are the heat transfer area and heat transfer coefficient. After 13 runs with the factors limited between a range of 28.87 W/m^{2}K (small) to 12087 W/m^{2}K (bigger) for heat transfer coefficient and 179.86 m^2 (small area) to 1000 m^2 (large area) for the heat transfer coefficient. The design summary is presented in Table 7.

3. Results

3.1. Process Flow Diagram for Modelling of the Gas-Turbine Power Plant

In this section, we presented the various process power plant that we explored in our study using both the process flow diagram (PFD) and block flow diagrams (BFD). The processes explored in the use of gas-turbine power plant include the open-loop and closed-loop process technologies.

3.1.1. Open Loop Process

Following the process flow diagram and block flow diagrams presented in Figures 2 and 3, we presented the block flow employed in the modeling of the open-loop gas-turbine power plant, which was successfully modeled in a DWSim package show in the process flow diagram, in Figures 2 and 3.

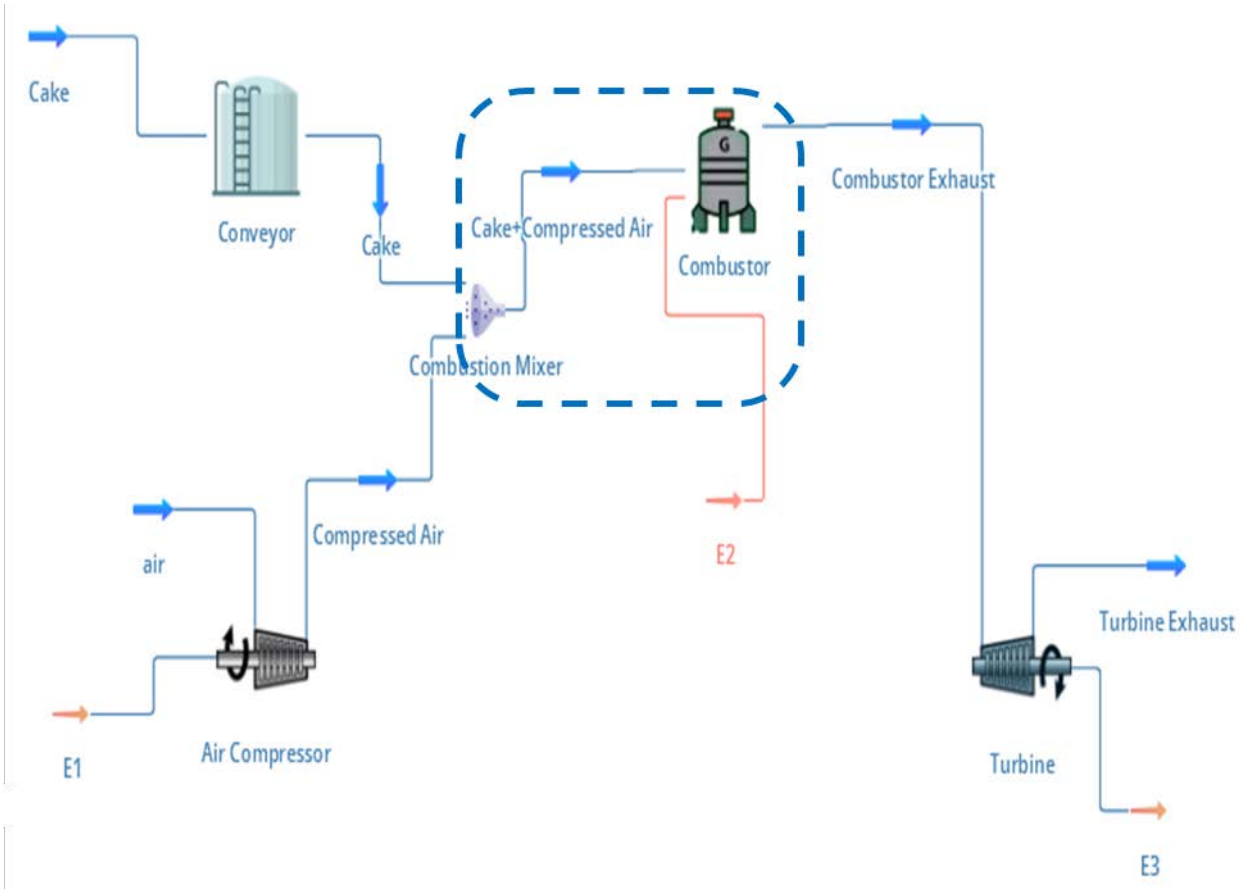

Figure 2. Biomass-fueled open-loop gas-turbine power plant (Process flow diagram).

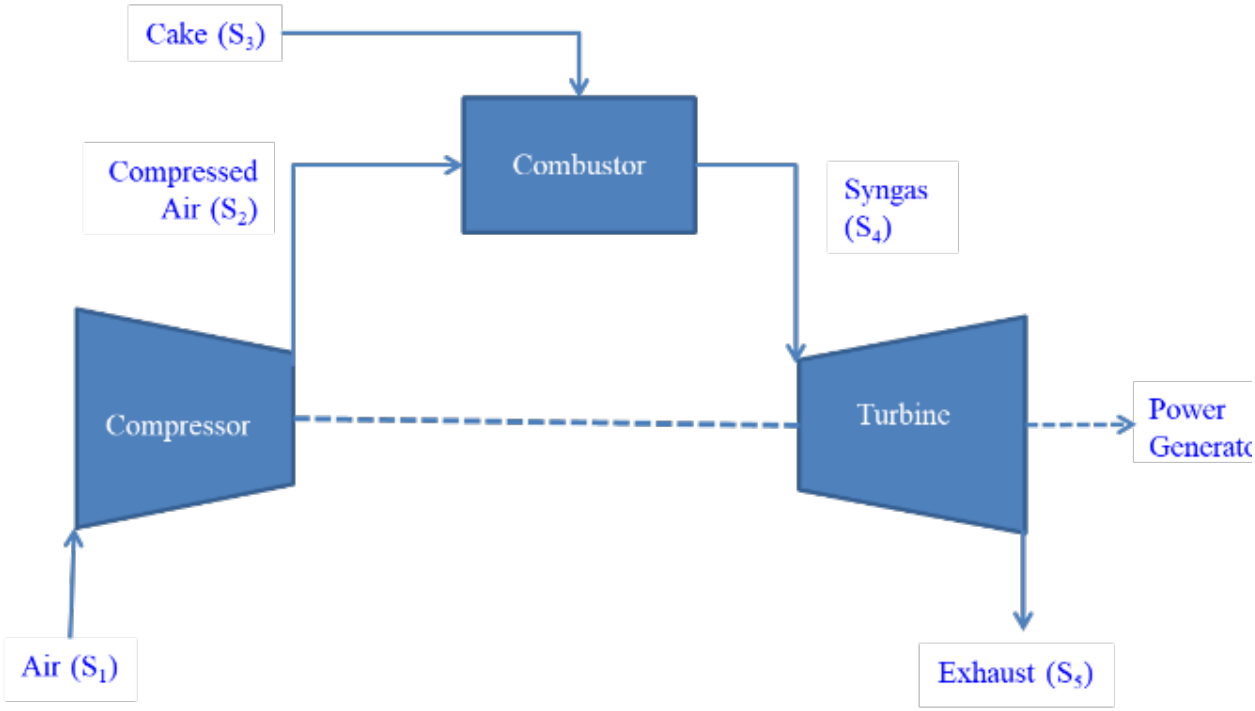

Figure 3. Biomass-fueled open-loop gas-turbine power plant (Block flow diagram).

The process entails series of process equipment like conveyor, compressor, turbine, and combustor (a reacting chamber) as shown in Figures 2 and 3. The power plant deployed the use of the Jatropha cake (that is, the residue of the Jatropha oil extraction process), where the conveyor was employed to transport and feed the combustor while the air is fed via the use of compressor.

After which, the cake is combusted in the presence of sufficient air to produce the high-pressure syngas as its exhaust, which is later used in driving the power plant turbine to generate the power or energy.

3.1.2. Closed-Loop Process

The process flow diagram and block flow diagram used in modeling the closed-loop gas turbine power plant in the DWSim package were shown in Figure 4. The process consisted of various pieces of equipment, including a conveyor, compressor, turbine, combustor (a reaction chamber), heat exchangers, and a working fluid (such as helium, nitrogen, or argon), as shown in Figure 4. Jatropha cake, a residue from the Jatropha oil extraction process, was used as the feed.

The conveyor transported the feed to the combustor, while air was supplied via the compressor. In the presence of sufficient air, the cake underwent combustion in the combustor, producing high-pressure syngas at a high temperature, which then became the combustor exhaust.

This exhaust was used to heat the working fluid (which was introduced into the system via the compressor) to an appropriate temperature using a heat exchanger.

After the heat is transferred from the combustor exhaust to the working fluid, the working fluid, which is at high pressure and temperature, is used to drive the power plant gas turbine. After power generation, the exhaust from the turbine, which contains the working fluid at lower pressure and temperature, is cooled in another heat exchanger using a cooling water stream and then recycled for reuse or re-circulation.

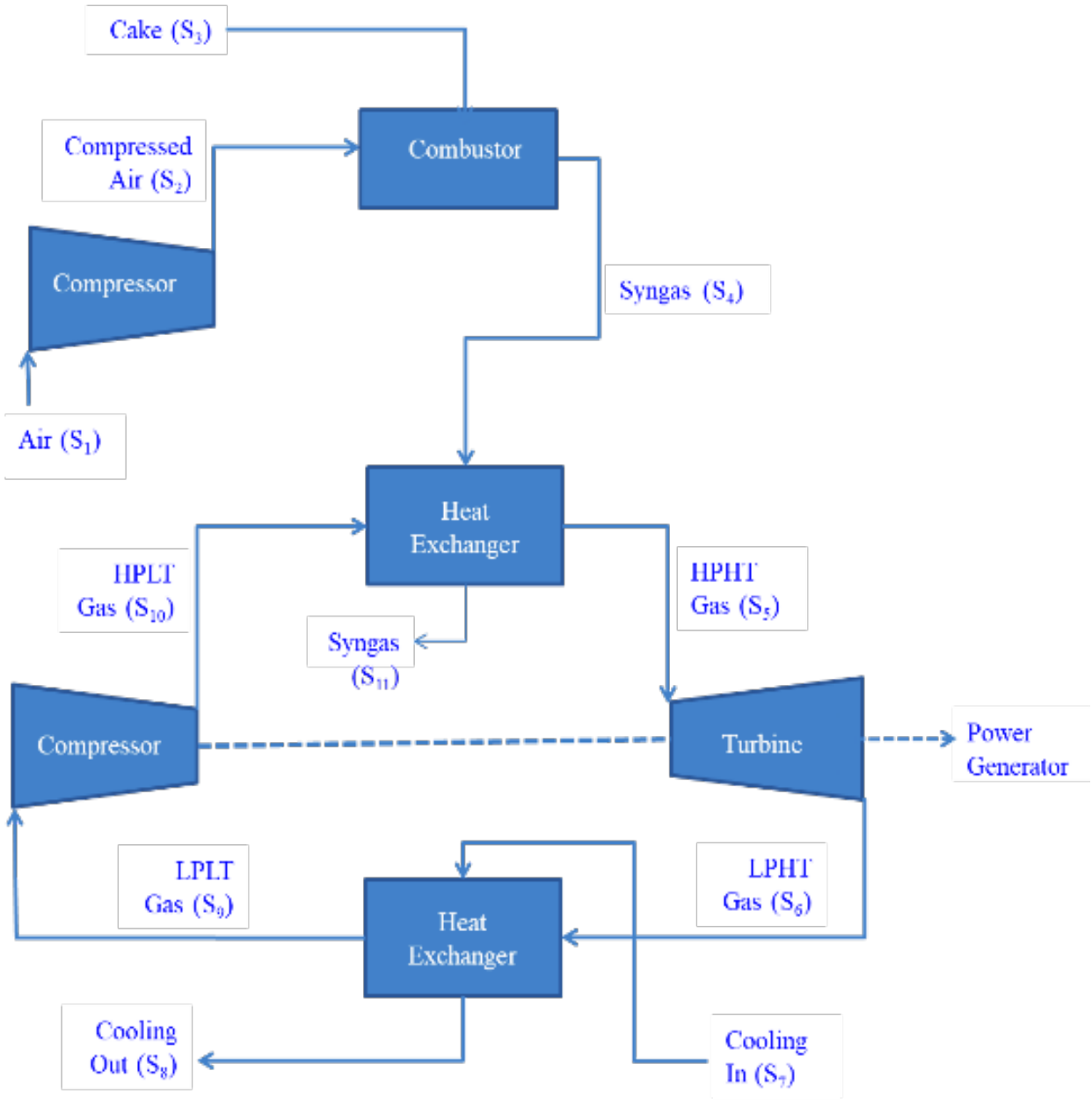
Cake (S_3)
Compressed Air (S_2)
Combustor
Compressor
Syngas (S_4)
Air (S_1)
Heat Exchanger
HPLT Gas (S_{10})
HPHT Gas (S_5)
Syngas (S_{11})
Compressor
Turbine
Power Generator
LPLT Gas (S_9)
LPHT Gas (S_6)
Heat Exchanger
Cooling Out (S_8)
Cooling In (S_7)

a)

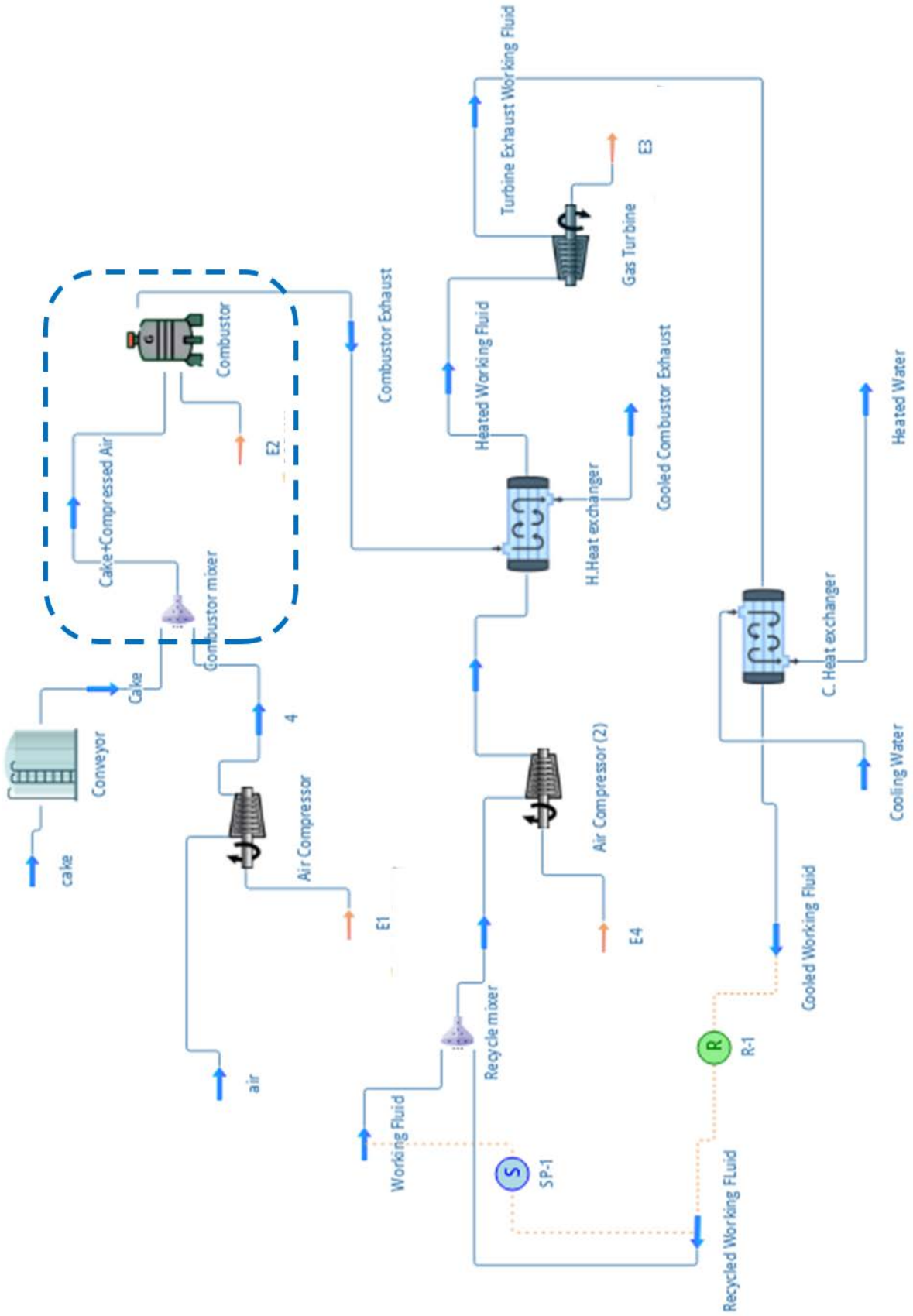

b)

Figure 4. Biomass-fueled closed-loop gas-turbine power plant: a) block flow diagram and b) process flow diagram for the process plant.

.

3.2. Impact of Compressor and Turbine Efficiency on Power Generation

3.2.1. Open Loop Gas-turbine Power Plant

a. Model screening analysis for the prediction of power generated

The results obtained from our analysis of the biomass-based gas-turbine power plant for the development of the PG_O prediction model are presented in Table 8. In the analysis, we evaluated the suitability of using linear, two-factor interaction (2FI), quadratic, and cubic models to predict power generation based on relevant independent variables (factors).

Table 8

Model summary statistics for the analysis of variance (ANOVA) and other statistical analysis parameters for the prediction of power generation for open loop (PG_O)

Source	SS	DF	MS	F Value	P-value	RSqr.	Adj. RSqr.	Pred. RSqr.
Linear	1.70E+10	2	8.52E+09	376.34	< 0.0001	0.9869	0.9843	0.9742
2FI	5.90E+06	1	5.90E+06	0.24	0.6353	0.9872	0.9830	0.9719
Quadratic	2.11E+08	2	1.05E+08	73.14	< 0.0001	0.9994	0.9990	0.9959
Cubic**	9.11E+06	2	4.55E+06	23.59	0.0028	0.9999	0.9999	0.9964
Residual	9.65E+05	5	1.93E+05					
Total	9.53E+10	13	7.33E+09					

Note: SS – sum of square; DF – degree of freedom; MS – mean square; F Value – F test result; P-value – significance test; RSqr. – Rsquare value; Adj. RSqr. – adjusted Rsquare value; Pred. RSqr. – predicted Rsquare value; (**) – aliased model (that is, unsuitable model due to the failure of the model to distinguish effect of two or more variables in its model).

As shown in Table 8, the ANOVA analysis indicates that both the linear and quadratic models are suitable for predicting the amount of power generated, based on their P-values, which were found to be less than 0.05, in agreed with related report [29] that indicate that P-values less than 0.05 is insignificant. Additionally, these models exhibited higher values for their SS and MS compared to the cubic and 2FI models, which had higher P-values. Further analysis of the top-rated models (linear and quadratic) was conducted using R-squared values, as shown in Table 8. The results confirmed that both models are highly reliable, with R-squared values greater than 95%. However, the quadratic model was rated higher due to its superior P-value and R-squared value, which further validated its predictions in agreement with the interpretation presented in the literature [21,30].

b. Model analysis for the prediction of power generated for open-loop (PG_O)

The quadratic model developed for predicting PG_O is presented in the following equation (in coded form of the factors explored in the study):

$$PG_O = 80723.20 + 15793.88A + 43372.29B - 5428.24A^2 + 173.56B^2 - 1214.83AB, \text{ (kW)} \quad (2)$$

where: A is compressor efficiency (Comp. Eff. no unit) and B is turbine efficiency (Turb. Eff. non unit).

The analysis of the most suitable model (quadratic) shows that the constant term (also known as the average) is 80723 kW. Among the factors, B has the most significant effect on power generation, as indicated by its higher coefficient (43372.29). In contrast, A has a lesser effect, as shown by its lower coefficient (15793.88). In general, the interaction terms (A^2, B^2, and A*B) were found to have a smaller effect on power generation compared to the single-factor effects (A and B). This conclusion is based on the higher coefficients reported for the single-factor terms (A and B) compared to the interaction terms (A^2, B^2, and A*B).

Findings from this quadratic analysis further explain why the linear models demonstrated good prediction capabilities in Table 8 (as discussed in the previous section). These results confirm that compressor and turbine efficiencies have a predominantly linear relationship with power generation. However, the quadratic model reveals that the inclusion of non-linear terms, such as A^2 and B^2, significantly improves prediction accuracy, as evidenced by the results in Tables 8 and 9.

Table 9

ANOVA and other statistical analysis parameters for response surface quadratic model for the prediction of Power Generated for open-loop (PG_O)

Source	SS	DF	MS	F Value	Prob > F	Statistic Parameter	Value
Model	1.73E+10	5	3.45E+09	2399.28	< 0.0001	RSqr.	0.9994
A	2.00E+09	1	2.00E+09	1386.91	< 0.0001	Adj RSqr.	0.9990
B	1.51E+10	1	1.51E+10	10459.13	< 0.0001	Pred RSqr.	0.9959
A^2	2.05E+08	1	2.05E+08	142.46	< 0.0001		
B^2	2.10E+05	1	2.10E+05	0.15	0.7141		
AB	5.90E+06	1	5.90E+06	4.10	0.0825		
Residual	1.01E+07	7	1.44E+06				
Lack of Fit	1.01E+07	3	3.36E+06				
Pure Error	0	4	0				
Cor Total	1.73E+10	12					

Note: SS – sum of square; DF – degree of freedom; MS – mean square; F Value – F test result; P-value – significance test; RSqr. – Rsquare value; Adj. RSqr. – adjusted Rsquare value; Pred. RSqr. – predicted Rsquare value; A – compressor efficiency; B – turbine efficiency.

Further analysis of the model in Table 9 indicates that the B^2 (quadratic factor) and interaction term (A*B) in the quadratic model have no significant impact on the amount of power generated by the power plant using Jatropha cake as feedstock due to its P-value that is higher than 0.05, which confirms it to be insignificant following the literature [31,32].

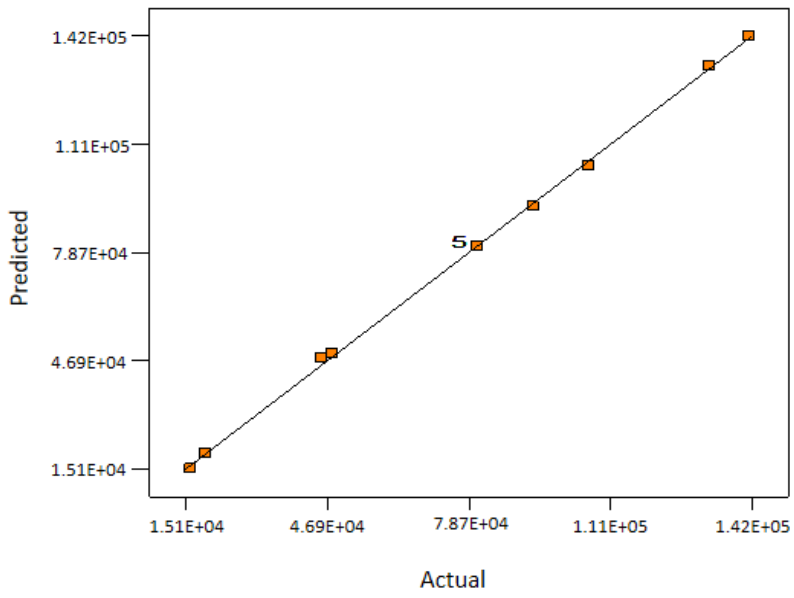

Figure 5. A plot of predicted vs. actual value of PG_O.

Conversely, other terms, including A, B, and the quadratic effect of A, were found to have a more significant influence on the power output of the evaluated process. Additionally, Figure 5 further emphasizes the accuracy of the quadratic model, demonstrating a strong alignment between the actual and predicted values.

3.2.2 Impact of Compressor and Turbine Efficiency on Syngas(S_4) Temperature

a. Screening analysis for the syngas (S4) temperature model

The results obtained from the analysis of the biomass-based gas-turbine power plant for the development of the syngas temperature model is presented in Table 10. In the analysis, the suitability of using various models (including linear, two-factor interaction (2FI), quadratic, and cubic models) for predicting the syngas temperature based on relevant independent variables was evaluated.

Table 10

Model summary statistics for the analysis of variance (ANOVA) and other statistical analysis parameters for the prediction of syngas (S_4) Temperature.

Source	SS	DF	MS	F Value	Prob>F	RSqr.	Adj. RSqr.	Pred. RSqr.
Linear	6.15E+04	2	3.07E+04	47.08	< 0.0001	0.904	0.8848	0.8118
2FI	0	1	0	0	1	0.9040	0.8720	0.7887
Quadratic	6.26E+03	2	3.13E+03	79.77	< 0.0001	0.9960	0.9931	0.9713
Cubic**	2.48E+02	2	1.24E+02	23.50	0.0029	0.9996	0.9991	0.9752
Residual	26.39	5	5.28					
Total	1.21E+08	13	9.30E+06					

Note: SS – sum of square; DF – degree of freedom; MS – mean square; F Value – F test result; P-value – significance test; RSqr. – Rsquare value; Adj. RSqr. – adjusted Rsquare value; Pred. RSqr. – predicted Rsquare value; A – Compressor efficiency; B – Turbine efficiency; (**) - aliased model (that is, unsuitable model due to the failure of the model to distinguish effect of two or more variables in its model).

The results in Table 10, showing the ANOVA analysis, reveal that both the linear and quadratic models are suitable for predicting the syngas temperature. This conclusion is based on the low P-values (less than 0.05) and the higher SS and MS values compared to the other models (cubic and 2FI), which had higher P-values, in accordance with statistical interpretation reported in the literature [30]. Further analysis of the two best-rated models (linear and quadratic) was conducted using the R-squared values. As observed from Table 10, both models are highly reliable, with R-squared values greater than 95%. Although the quadratic model was rated higher due to its superior P-value and R-squared value, making it the most suitable model, which agrees with the literature report [30,33].

b. Model development and analysis for the prediction of syngas (S4) temperature (Ts_4)

The quadratic model developed for predicting the Ts_4 is presented in the following equation (both in coded and actual form of the factors explored in the study):

$$Ts_4 = 3030.29 - 87.67A + 2.500E\text{-}003B + 29.60A^2 - 0.91B^2 + 5.000E\text{-}003AB, \text{(K)} \quad (3)$$

where: A is compressor efficiency (Comp. Eff no unit) and B is turbine efficiency (Turb. Eff no unit).

The analysis of the quadratic model shows that the constant term is 3030.29 K. The factors with the most significant effect on the Ts_4 are A with a coefficient of 87.67 and the interaction term A^2 with a coefficient of 29.60. These factors have higher coefficients

compared to the other factors, which are B, and the interaction terms B^2 and A*B, with coefficients of 2.500E-003, 0.91, and 5.000E-003, respectively. The findings made also aligns with the trend of the P-values report for each factor in relation with the literature report [29,32], which states P-values greater than 0.05 confirm B, B^2, and A*B insignificant. The negative sign of the factor A coefficient implies that as the value of A increases, the response variable (Ts_4) decreases initially but the positive value of the coefficient of A^2 suggests that further increase in A will lead to an increase in $T_{s4.}$

Table 11

ANOVA and other statistical analysis parameters for response surface quadratic model for the prediction of syngas (S_4) Temperature (Ts_4).

Source	SS	DF	MS	F Value	Prob > F	Statistic Parameter	Value
Model	67749.3	5	13549.86	345.55	< 0.0001	RSqr.	0.9960
A	61493.59	1	61493.59	1568.23	< 0.0001	Adj RSqr.	0.9931
B	5.00E-05	1	5.00E-05	1.275E-06	0.9991	Pred RSqr.	0.9713
A2	6094.77	1	6094.77	155.43	< 0.0001		
B2	5.74	1	5.74	0.15	0.7134		
AB	1.00E-04	1	1.00E-04	2.550E-06	0.9988		
Residual	274.48	7	39.21				
Lack of Fit	274.48	3	91.49				
Pure Error	0	4	0				
Cor Total	68023.79	12					

Note: SS – sum of square; DF – degree of freedom; MS – mean square; F Value – F test result; P-value – significance test; RSqr. – Rsquare value; Adj. RSqr. – adjusted Rsquare value; Pred. RSqr. – predicted Rsquare value; A – compressor efficiency; B – turbine efficiency.

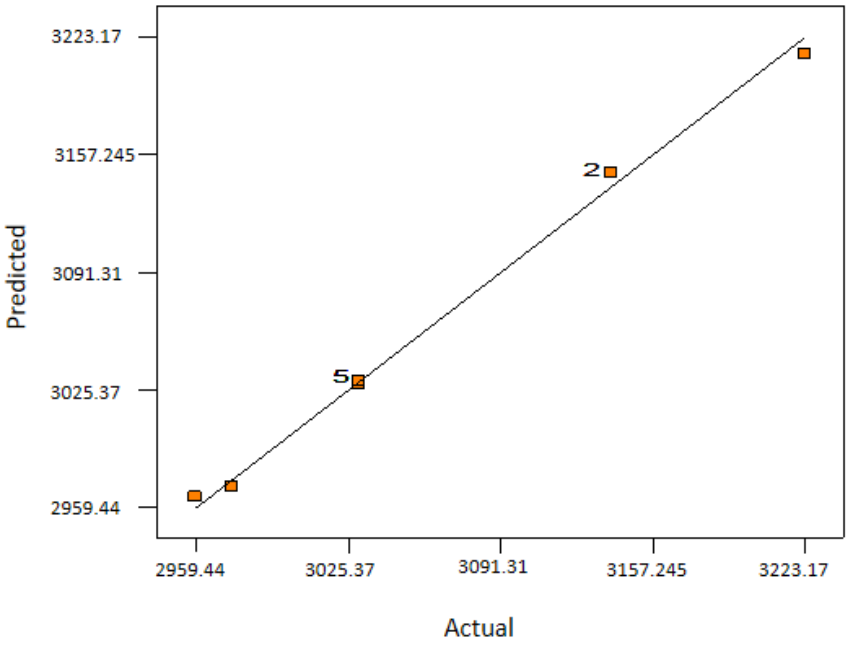

Figure 6. A plot of predicted vs. actual value of Syngas (S_4) Stream Temperature (T_{S4}).

Results of the quadratic model analysis confirm that compressor efficiency has a predominantly linear relationship with the Ts_4. From further analysis of the model in Table 11, it is observed that factors associated with A have the most significant effect on Ts_4, while factors associated with B have very little effect on the Ts_4. This is further justified by the

position of the stream (S4), as the stream is positioned before the turbine therefore the turbine parameters have no effect on Ts_4. Additionally, the accuracy of the quadratic model is further emphasized in Figure 6, which depicts a strong alignment between the actual and predicted values.

3.2.3. Optimization Criteria, Solution, and Validation

In the search for better conditions to produce improved power generation, we used the criteria stated in Table 12 for optimizing the power generation capacity, while constraining the compressor and turbine efficiencies to a specified range presented in Table 12, and keeping the Jatropha cake feed quantity constant.

Table 12

Criteria for Optimizations

Name	Goal	Lower Limit	Upper Limit	Lower Weight	Upper Weight	Importance
Comp. Eff.	In range	20	98	1	1	3
Turb. Eff	In range	20	98	1	1	3
Power Gen.	Maximize	16283	200000	1	1	3
S_4 Temp.	In range	2959.44	3223.17	1	1	3

Note: S4 Temp. – stream S4 temperature; Comp. Eff. – compressor efficiency Turb. Eff. – turbine efficiency; Power Gen. – power generated.

Table 13

Results for Optimization and Validation

Solution	Comp. Eff. (%)	Turb. Eff (%)	Power Gen. (kW)	S_4Temp. (T_{S4}) (K)	Desirability
Optimized	83.92	98	174235	2963.70	0.86
Validated	83.92	98	174518	2965.77	-

Note: S4 Temp. – stream S4 temperature; Comp. Eff. – compressor efficiency Turb. Eff. – turbine efficiency; Power Gen. – power generated.

Using a numerical approach to optimize the power generation with the constraints stated in Table 12, the optimum Ts_4, compressor efficiency (Comp. Eff.), and turbine efficiency (Turb. Eff.) in the Jatropha cake-to-power process yielded an optimum power output of 174,235 kW and an Ts_4 of 2963.70 K, as shown in Table 13, with a desirability of 86%. The comparison of the optimized solution and the validation results for the optimum power generated shows good agreement with an insignificant difference. The findings suggest that running the power plant turbine and compressor below the confirm optimum efficiency could results to a much more lower power output in the said plant.

3.3. Impact of Heat Transfer Coefficient and Heat Transfer Area on Closed-Loop Gas-turbine Power Plant

3.3.1. Impact of Heat Transfer Coefficient and Heat Transfer Area on Heat Exchanger Heated Stream Temperature

a. Screening analysis for the prediction model for HPHT gas (S5) stream temperature (*Ts_5*)

The results obtained from our analysis of the biomass-based closed-loop gas-turbine power plant for the development of the *Ts_5* model are presented in Table 14. The evaluation of the suitability of using linear, quadratic, two-factor interaction (2FI), and cubic models for predicting the *Ts_5* was carried out in the analysis.

Table 14

Model summary statistics for the analysis of variance (ANOVA) and other statistical analysis parameters (Note: **aliased model)

Source	SS	DF	MS	F Value	P-value	RSqr	Adj. RSqr	Pred. RSqr
Linear	1.55E+05	2	77251.37	69.85	< 0.0001	0.9332	0.9198	0.8647
2FI	6846.57	1	6846.57	14.63	0.0041	0.9746	0.9661	0.9332
Quadratic	3222.18	2	1611.09	11.38	0.0063	0.9940	0.9897	0.9574
Cubic**	990.94	2	495.47	25650.74	< 0.0001	1	1	1
Residual	0.097	5	0.019					
Total	1.21E+07	13	9.29E+05					

Note: SS – sum of square; DF – degree of freedom; MS – mean square; F Value – F test result; P-value – significance test; RSqr. – Rsquare value; Adj. RSqr. – adjusted Rsquare value; Pred. RSqr. – predicted Rsquare value; (**) – aliased model (that is, unsuitable model due to the failure of the model to distinguish effect of two or more variables in its model).

As presented in Table 14, the ANOVA analysis indicates the suitability of both the linear and quadratic models for predicting the Ts_5. This suitability is based on the P-values, which were found to be less than 0.05, in agreement with the reports [29,31] in the literature. Furthermore, the values of the SS and MS were higher for these models compared to the other models (cubic and 2FI).

Using the R-squared values of the identified best-rated models (linear and quadratic), the reliability was confirmed, with both models exhibiting an R-squared value greater than 90%. Although both models exhibited R-squared values above 90%, the quadratic model had the higher value, which rated it as the most suitable model for prediction.

b. Model analysis for the prediction of HPHT gas (S5) stream temperature (Ts_5)

The quadratic model developed for predicting the Ts_5 is presented in the following equation (in coded form of the factors explored in the study):

$$Ts_5 = 976.91 + 90.38A + 105.56B - 13.92A^2 - 18.09B^2 + 41.37AB, \text{(K)} \quad (4)$$

where: A is the heat transfer coefficient (Ht. Trns. Coeff. no unit) and B is the heat transfer area (Ht. Trns. Area no unit).

Analysis of the quadratic model shows that the constant term (also known as the average) is 976.91 K. It is evident from the coefficients of the various factors that B, with a higher coefficient of 105.56, has the most significant effect on the Ts_5, in contrast to the A with a coefficient of 90.38.

In comparison to the single factors A and B, the interaction terms A^2, B^2, and A*B, with coefficients of 13.92, 18.09, and 41.37 respectively, have a lesser effect on the Ts_5. The findings from this quadratic model indicate the linear relationship between the heat transfer coefficient (A) and heat transfer area (B) with the Ts_5. Moreover, the model also shows that the inclusion of non-linear terms, such as A^2 and B^2, significantly improves the prediction accuracy, as seen in Tables 14 and 15.

Upon further analysis of the quadratic model in Table 15, it is evident that the quadratic factors AA and BB and the interaction term A*B have no significant impact on the Ts_5. the other terms which include A and B showed greater significance on the Ts_5.

Table 15

ANOVA and other statistical analysis parameters for response surface quadratic model for the prediction of HPHT Gas (S_5) Stream Temperature.

Source	SS	DF	MS	F Value	P-value	Statistic Parameter	Results
Model	1.65E+05	5	32914.3	232.48	< 0.0001	RSqr.	0.994
A	65354.81	1	65354.81	461.62	< 0.0001	Adj RSqr.	0.9897
B	89147.93	1	89147.93	629.68	< 0.0001	Pred RSqr.	0.9574
A^2	1347.35	1	1347.35	9.52	0.0177		
B^2	2276.93	1	2276.93	16.08	0.0051		
AB	6846.57	1	6846.57	48.36	0.0002		
Residual	991.04	7	141.58				
Lack of Fit	991.04	3	330.35				
Pure Error	0	4	0				
Cor Total	1.66E+05	12					

Note: SS – sum of square; DF – degree of freedom; MS – mean square; F Value – F test result; P-value – significance test; RSqr. – Rsquare value; Adj. RSqr. – adjusted Rsquare value; Pred. RSqr. – predicted Rsquare value; A – Heat transfer coefficient (Ht. Trns. Coeff.), B - Heat transfer area (Ht. Trns. Area).

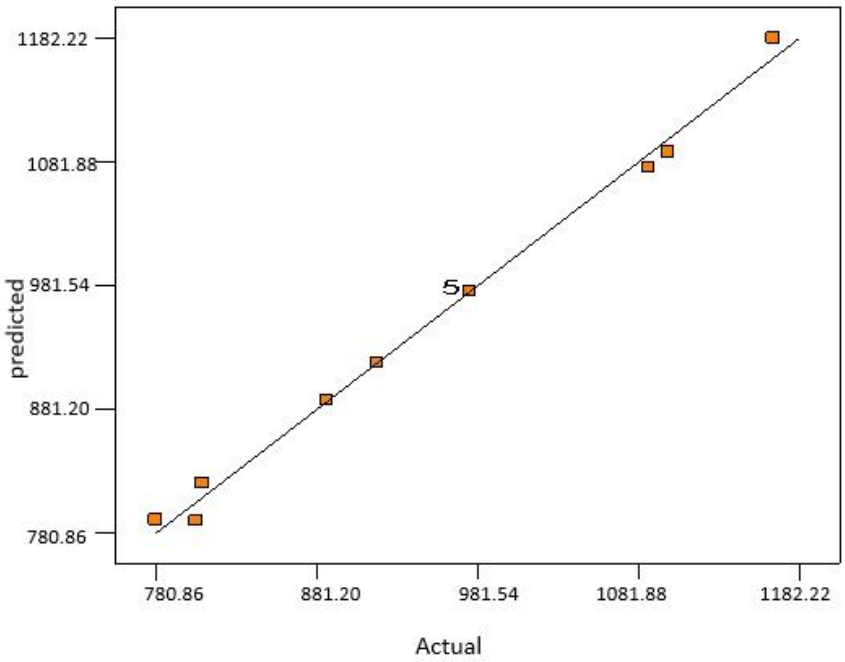

Figure 7. A plot of predicted vs. actual value of HPHT Gas (S_5) Stream Temperature.

The accuracy of the quadratic model is further emphasized in Figure 7 which shows the alignment between the actual and predicted values.

3.4. Impact of Heat Transfer Coefficient and Heat Transfer Area on Power Generation

3.4.1. Screening analysis for the prediction model for the power generated for closed-loop (PG_C)

The results obtained from the analysis of the biomass-based gas-turbine power plant for the development of the power generation prediction model is presented in Table 16 Evaluation of the suitability of using linear, two-factor interaction (2FI), quadratic, and cubic models for predicting power generation using relevant independent variables (factors) was carried out in this analysis.

Table 16

Model summary statistics for the analysis of variance (ANOVA) and other statistical analysis parameters for the prediction of power generated for closed-loop (PGc)

Source	SS	DF	MS	F Value	P-value	RSqr	Adj. RSqr	Pred. RSqr
Linear	9.92E+09	2	4.96E+09	69.86	< 0.0001	0.9332	0.9198	0.864
2FI	4.54E+08	1	4.54E+08	15.99	0.0031	0.9759	0.9679	0.9365
Quadratic	1.95E+08	2	9.74E+07	11.19	0.0066	0.9943	0.9902	0.9592
Cubic**	6.09E+07	2	3.04E+07	4518.85	< 0.0001	1	1	0.9998
Residual	33686.48	5	6737.3					
Total	1.44E+10	13	1.11E+09					

Note: SS – sum of square; DF – degree of freedom; MS – mean square; F Value – F test result; P-value – significance test; RSqr. – Rsquare value; Adj. RSqr. – adjusted Rsquare value; Pred. RSqr. – predicted Rsquare value; (**) – aliased model (that is, unsuitable model due to the failure of the model to distinguish effect of two or more variables in its model).

Table 16 shows the ANOVA analysis, which indicates that both the linear and quadratic models, with P-values less than 0.05, are suitable for predicting the amount of power generated. This was due to its P-value that is higher than 0.05, which confirms it to be insignificant following the literature [31,32]. Upon further analysis, their SS and MS values also exhibited higher values. The best-rated models were chosen based on a comparison of their various R-squared values. From this comparison, it is evident that the quadratic model exhibited the higher R-squared value among the best-rated models, in accordance with the literature [33,34] interpretation for higher R-squared value. For this reason, the quadratic model was chosen.

3.4.2. Model analysis for the prediction of power generated for closed-loop (PG_C)

The quadratic model developed for the prediction of PG_C is presented in Equation (in coded form of the factors explored in the study):

$$PG_C = 21940.90 + 22915.61*A + 26734.57*B - 3427.62*A^2 - 4444.07*B^2 + 10656.33*A*B, \text{(kW)} \quad (5)$$

where: A is Heat transfer coefficient (Ht. Trns. Coeff. no unit) and B is heat transfer area (Ht. Trns. Area no unit).

The analysis of the quadratic model shows that the constant term is 21940.90 kW and although both factors A and B have high and close values, the factor with the greater effect on the power generated is the B due to its higher coefficient (26734.57). By comparing the coefficients, the interaction terms A^2, B^2 and A*B were found to have less effect on the power generated compared to the single-factors A and B.

Table 17

ANOVA and other statistical analysis parameters for response surface quadratic model for the prediction of power generated for closed-loop (PG_C)

Source	Sum of Squares	DF	Mean Square	F Value	P-value	Statistic Parameter	Value
Model	1.06E+10	5	2.11E+09	242.85	< 0.0001	RSqr	0.9943
A	4.20E+09	1	4.20E+09	482.69	< 0.0001	Adj RSqr	0.9902
B	5.72E+09	1	5.72E+09	656.98	< 0.0001	Pred RSqr	0.9592
A^2	8.17E+07	1	8.17E+07	9.39	0.0182		
B^2	1.37E+08	1	1.37E+08	15.79	0.0054		
AB	4.54E+08	1	4.54E+08	52.19	0.0002		
Residual	6.09E+07	7	8.70E+06				

Continuation Table 17

Lack of Fit	6.09E+07	3	2.03E+07
Pure Error	0	4	0
Cor Total	1.06E+10	12	

Note: SS – sum of square; DF – degree of freedom; MS – mean square; F Value – F test result; P-value – significance test; RSqr. – Rsquare value; Adj. RSqr. – adjusted Rsquare value; Pred. RSqr. – predicted Rsquare value; A – heat transfer coefficient (Ht. Trns. Coeff.); B - heat transfer area (Ht. Trns. Area).

Further analysis from Table 17 reveals that all the factors have a significant effect on the amount of power generated from the plant using Jatropha cake as feedstock. Further emphasis on the accuracy of the model is demonstrated in Figure 8, where a strong alignment between actual and predicted value is observed.

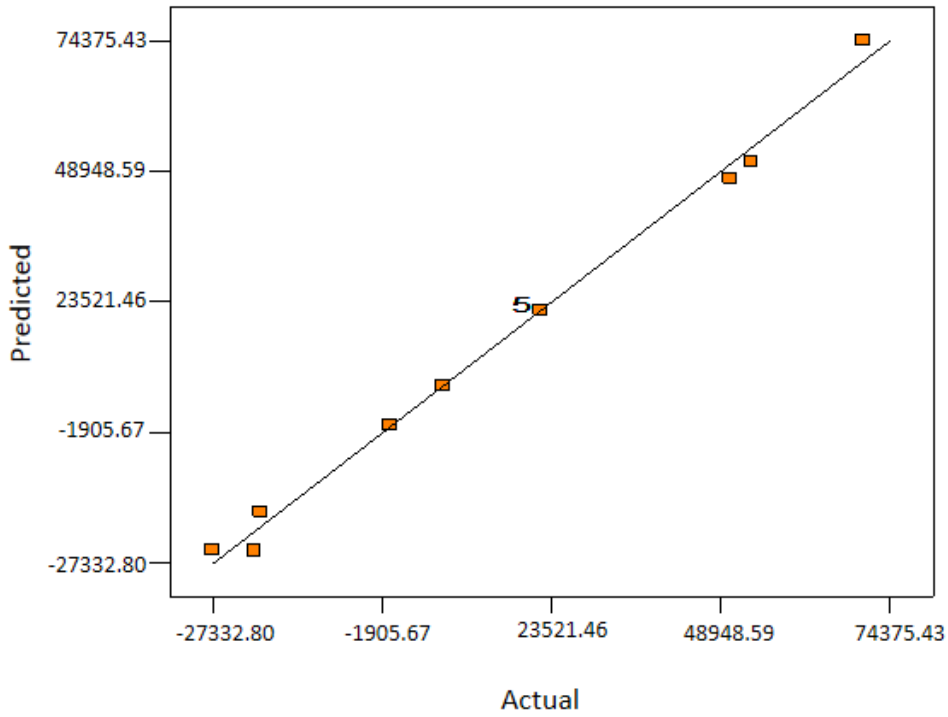

Figure 8. A plot of predicted vs. actual value of Power Generated.

3.4.3. Optimization Criteria, Solution, and Validation

The criteria employed for the optimization of power generation capacity are presented in Table 18. While keeping the Jatropha cake feed quantity constant, the heat transfer coefficient and heat transfer area were constrained to a specified range presented in the Table 18.

Table 18

Criteria for Optimizations

Name	Goal	Lower Limit	Upper Limit	Lower Weight	Upper Weight	Importance
Ht Trns. Coeff.	is in range	28.87	120	1	1	3
Ht Trns. Area	is in range	179.86	1000	1	1	3
Outlet Temp.	is in range	780.857	1500	1	1	3
Power generated	maximize	-27332.8	200000	1	1	3

Note: Ht Trns. Coeff. – heat transfer coefficient, W/m^{2}K; Ht Trns. Area - heat transfer area, m^2; Outlet Temp. – heating heat exchanger outlet temperature, K.

Table 19

Results for Optimization and Validation

Solution	Ht Trns. Coeff. (W/m^2K)	Ht Trns. Area (m^2)	Outlet Temp. (K)	Power generated (kW)	Desirability
Optimized	120	1000	1182.22	74375.7	0.447
Validated	120	1000	1166.08	70336.5	-

Note: Ht Trns. Coeff. – heat transfer coefficient; Ht Trns. Area – heat transfer area; Outlet Temp. – heating heat exchanger outlet temperature from raising the gas from a lower temperature (LT) to higher temperature (HT).

A numerical approach was employed in the optimization of the power generation using the constraints stated in Table 18. The optimum conditions were found to yield an outlet temperature of 1182.22 K and power generation of 74375.7 kW, respectively, with a desirability of 45%. The optimized and validated solution results show good agreement, with an insignificant difference in both outlet temperature (1182.22 and 1166.08) and power generated (74375.7 and 70336.5 kW). The findings made from the study suggest that the heat exchanger use in the power plant would be produced higher power out if sufficient transfer area of less than 1000 m^2 is made available and material with minimum heat transfer coefficient of 120 kW/m^2K for the heat transfer process.

5. Conclusions and Recommendations

In this study, a central composite design (CCD) approach was utilized to evaluate the effects of compressor efficiency, turbine efficiency, heat transfer coefficients, and heat transfer area (in a heat exchanger) on power generation in a prospective gas-turbine bio-power plant. The process was successfully modeled using the DWSim simulation package to simulate power generation from Jatropha cake. The study examined the effects of compressor and turbine efficiency using an open-loop gas-turbine power plant configuration, while the effects of heat transfer coefficient and area were analyzed using a closed-loop gas-turbine power plant configuration to identify optimal conditions.

The findings indicate that using a compressor with 83.92% efficiency and a turbine with 98.00% efficiency in an open-loop power plant would yield a maximum power output of 174235.0 kW from Jatropha cake. Additionally, the assessment of heat transfer area and coefficient in a closed-loop configuration revealed that values of 1000 m^2 and 120 W/m^2K, respectively, represent the optimal conditions for maximizing power generation to 74375.70 kW from Jatropha cake. These results were obtained through optimization studies carried out using the CCD design approach.

In a nutshell, the study therefore demonstrates that employing a compressor with a minimum efficiency of 83.92% and a turbine with a minimum efficiency of 98% in a gas-turbine power plant (open or closed-loop) would yield a promising power output using Jatropha cake. Furthermore, in a closed-loop system, where a heat exchanger (HX) is required, using an HX with a heat transfer coefficient of 120 W/m^2K and a heat transfer area of 1000 m^2 would result in significantly higher power generation. The deployment of these optimal conditions would substantially enhance power generation yield.

Further work could explore a modified form of the closed-loop gas-turbine power plant, which would introduce an additional turbine between the combustor and heat exchanger of the looped section of the power plant to determine whether this configuration could lead to an even higher power generation capacity.

Acknowledgments: The authors do acknowledge the support of the other research team members like Abdullahi Jibrin and Suleiman Omeiza Suleiman during the study.

Conflicts of Interest: The authors declare no conflict of interest.

References

1. Mishra, K.; Siwal, S.S.; Nayaka, S.C.; Guan, Z.; Thakur, V.K. Waste-to-chemicals: Green solutions for bioeconomy markets. *Science of The Total Environment* 2023, 887, 164006. https://doi.org/10.1016/J.SCITOTENV.2023.164006.
2. Oyegoke,T.; Oyegoke, F.A.;, Fasanya, O.O.; Gambo, I.A. State of Agro-wastes Management in Nigeria : Status, Implications, and Way Forward. *Waste Recovery and Management* 2023, 1, pp. 241–272. https://doi.org/10.1201/9781003359784-14.
3. Eze, W.U.; Oyegoke, T.; Gaiya, J.D.; Umunakwe, R.; Onyemachi, D.I.; Eze, W.U.; Oyegoke. T.; Gaiya, J.D.; Umunakwe, R.; Onyemachi, D.I. Review of personal protective equipment and their associated wastes, life-cycle and effective management during the Covid-19 pandemic in developing nations. *Clean Technologies and Recycling* 2022, 2, pp. 1-31. https://doi.org/10.3934/CTR.2022001.
4. Vinti, G.; Vaccari, M. Solid Waste Management in Rural Communities of Developing Countries: An Overview of Challenges and Opportunities. *Clean Technologies* 2022, 4, pp. 1138–1151. https://doi.org/10.3390/CLEANTECHNOL4040069.
5. Igwebuike, C.M.; Oyegoke, T. Decarbonizing our environment via the promotion of biomass methanation in developing nations: a waste management tool. *Pure & Applied Chem* 2024, 96(5), pp. 651-670. https://doi.org/10.1515/PAC-2023-1109/MACHINEREADABLECITATION/RIS.
6. Karić, N.; Maia, A.S.; Teodorović, A.; Atanasova, N.; Langergraber, G.; Crini, G.; Ribeiro, A.R.L.; Đolić, M. Bio-waste valorisation: Agricultural wastes as biosorbents for removal of (in)organic pollutants in wastewater treatment. *Chemical Engineering Journal Advances* 2022, 9, 100239. https://doi.org/10.1016/j.ceja.2021.100239.
7. Oyegoke, T. Green fuels: concepts, benefits, and studies in Nigeria. *Bulgarian Chemical Communications* 2022, 54, pp. 29–39. https://doi.org/10.34049/bcc.54.1.5458.
8. Igwebuike, C.M.; Awad, S.; Olanrewaju, Y.A.; Andrès, Y. The prospect of electricity generation from biomass in the developing countries. *International Journal of Smart Grid and Clean Energy* 2021, 10, pp. 150–156. https://doi.org/10.12720/SGCE.10.2.150-156.
9. Oyegoke, T.; Jibril, B.E. Design and Feasibility Study of a 5 MW Bio-Power Plant in Nigeria. *IJRER* 2016, 6, pp. 1498–1505.
10. Demirbas, A.H.; Demirbas, I. Importance of rural bioenergy for developing countries. *Energy Convers Manag* 2007, 48, pp. 2386–2398. https://doi.org/10.1016/J.ENCONMAN.2007.03.005.
11. Khan, S.; Nisar, A.; Wu, B.; Zhu, Q.L.; Wang, Y.W.; Hu, G.Q.; He, M.X. Bioenergy production in Pakistan: Potential, progress, and prospect. *Science of The Total Environment* 2022, 814, 152872. https://doi.org/10.1016/J.SCITOTENV.2021.152872.
12. Arndt, C.; Henley, G.; Hartley, F. Bioenergy in Southern Africa: An opportunity for regional integration? *Dev South Afr* 2019, 36, pp. 145–154. https://doi.org/10.1080/0376835X.2018.1447363.
13. Jeremiah, M.; Kabeyi, B.; Olanrewaju, O.A. Bagasse Electricity Potential of Conventional Sugarcane Factories. *Journal of Energy* 2023, 21, 5749122. https://doi.org/10.1155/2023/5749122.
14. Owebor, K.; Otuagoma, S.O.; Eyenubo, O.J.; Uranta, A.G.; Ukrakpor, F.E.; Ezewu, K.; Ebisine, E.E. Technical Analysis of Sawdust-to-Power: A Paradigm Shift in Waste Management in a Typical Developing Economy. *Journal of Energy & Power Tech* 2023, 5, pp. 1–18. https://doi.org/10.21926/JEPT.2304033.
15. Veeyee, K.F.; Bup, N.D.; Boldor, D.; Elambo, N.G. Potentials of sustainable electricity production from sawdust by small-scale wood transformation units: a case study in Cameroon. *Intl Journal of Energy & Env Eng* 2021, 12, pp. 101–114. https://doi.org/10.1007/S40095-020-00362-0/METRICS.
16. Zhou, Q.; Cai, W.; Zhang, Y.; Liu, J.; Yuan L, Yu F, Wang X, Liu M. Electricity generation from corn cob char though a direct carbon solid oxide fuel cell. *Biomass Bioenergy* 2016, 91, pp. 250–258. https://doi.org/10.1016/J.BIOMBIOE.2016.05.036.
17. Ibrahim, H.A.; Ayomoh, M.K.; Bansal, R.C.; Gitau, M.N.; Yadavalli, V.S.; Naidoo, R. Sustainability of power generation for developing economies: A systematic review of power sources mix. *Energy Strategy Reviews* 2023, 47, 101085. https://doi.org/10.1016/J.ESR.2023.101085.
18. Bagherian, M.A.; Mehranzamir, K.; Rezania, S.; Abdul-Malek, Z.; Pour, A.B.; Alizadeh, S.M. Analyzing utilization of biomass in combined heat and power and combined cooling, heating, and power systems. *Processe*s 2021, 9(6), 102. https://doi.org/10.3390/pr9061002.

19. Abbas, T.; Issa, M.; Ilinca, A.; El-Ali, A. Biomass Combined Heat and Power Generation for Anticosti Island: A Case Study. *Journal of Power & Energy Eng* 2020, 08(3), pp. 64-87. https://doi.org/10.4236/jpee.2020.83005.
20. Yaqoob, H.; Teoh, Y.H.; Ud, D.Z.; Sabah, N.U.; Jamil, M.A.; Mujtaba, M.A.; Abid, A. The potential of sustainable biogas production from biomass waste for power generation in Pakistan. *J Clean Prod* 2021, 307, 127250. https://doi.org/10.1016/J.JCLEPRO.2021.127250.
21. Amirrud, M.M.; Shahin M. Sensitivity and Uncertainty Analysis of Economic Feasibility of Establishing Wind Power Plant in Kerman, Iran. *RERA* 2020, 1, pp. 247–260.
22. Aslam, Z.; Li, H.; Hammerton, J.; Andrews, G.; Ross, A.; Lovett, J.C. Increasing Access to Electricity: An Assessment of the Energy and Power Generation Potential from Biomass Waste Residues in Tanzania. *Energies* 2021, 14, 1793. https://doi.org/10.3390/EN14061793.
23. Oliveira, M.O.; Somariva, R.; Ando, J.O.; Neto, J.M.; Bretas, A.S.; Perrone, O.E.; Reversat, J.H. Biomass electricity generation using industry poultry waste. *RE&PQ Journal* 2012, 1, pp. 1650-1654. https://doi.org/10.24084/repqj10.791.
24. Navarro-Pérez, D.; Moreno-Diaz, J.C.; Simeone-Barrientos, P. Emergency Remote Teaching in Process Simulation using DWSim: A Case Study from Diq-Umag, Chilean Patagonia. *Ciência e Tecnologia para o Desenvolvimento Ambiental, Scientia et Technica* 2023, 27, pp. 130-140. https://doi.org/10.37572/edart_27022376724.
25. Coyle, B.; Henderson, M.; Chan Jin, L.J.; Boyd, M.A.; Berner, L.T.; Tangsriwong, K.; Lapchit, P.; Kittijungjit, T.; Klamrassamee, T.; Sukjai, Y.; Laoonual, Y. Modeling of chemical processes using commercial and open-source software: A comparison between Aspen Plus and DWSIM. *IOP Conf Ser Earth Environ Sci* 2020, 463, 012057. https://doi.org/10.1088/1755-1315/463/1/012057.
26. Lopez-Echeverry, J.S.; Reif-Acherman, S.; Araujo-Lopez, E. Peng-Robinson equation of state: 40 years through cubics. *Fluid Phase Equilib* 2017, 447, pp. 39-71. https://doi.org/10.1016/j.fluid.2017.05.007.
27. Oyegoke, T.; Dabai, F. Techno-economic feasibility study of bioethanol production from a combined cellulose and sugar feedstock in Nigeria: 1-modeling, simulation and cost evaluation. *NIJOTECH* 2018, 37, pp. 913–20. https://doi.org/10.4314/njt.v37i4.8.
28. Sharma, R.; Sheth, P.N.; Gujrathi, A.M. Kinetic modeling and simulation: Pyrolysis of Jatropha residue de-oiled cake. *Renew Energy* 2016, 86, pp. 554–562. https://doi.org/10.1016/J.RENENE.2015.08.066.
29. Oyegoke, T.; Owolabi, O.A.; Bamigbala, O.A.; Geoffrey, T.T. Sensitivity Analysis of Selected Project Parameter on the Feasibility of Converting Maize Cob to Bioethanol as a Means of Promoting Biorefinery Establishment in Nigeria. *IJRER* 2022, 12, pp. 259–72. https://doi.org/10.20508/IJRER.V12I1.12621.G8413.
30. Aguinis, H.; Vassar, M.; Wayant, C. On reporting and interpreting statistical significance and p values in medical research. *BMJ Evid Based Med* 2021, 26, pp. 39–42. https://doi.org/10.1136/BMJEBM-2019-111264.
31. Di Leo, G.; Sardanelli, F. Statistical significance: p value, 0.05 threshold, and applications to radiomics—reasons for a conservative approach. *Eur Radiol Exp* 2020, 4, pp. 1–8. https://doi.org/10.1186/S41747-020-0145-Y/METRICS.
32. Andrade, C. The P Value and Statistical Significance: Misunderstandings, Explanations, Challenges, and Alternatives. *Indian J Psychol Med* 2019, 41, 215. https://doi.org/10.4103/IJPSYM.IJPSYM_193_19.
33. Chicco, D.; Warrens, M.J.; Jurman, G. The coefficient of determination R-squared is more informative than SMAPE, MAE, MAPE, MSE and RMSE in regression analysis evaluation. *PeerJ Comput Sci* 2021, 7, pp. 1–24. https://doi.org/10.7717/PEERJ-CS.623/SUPP-1.
34. Hamilton, D.F.; Ghert, M.; Simpson, AHRW. Interpreting regression models in clinical outcome studies. *Bone Joint Res* 2015, 4, 153. https://doi.org/10.1302/2046-3758.49.2000571.

Citation: Nasir, K.; Oyegoke, T. Exploring the energy generation potential of Jatropha cake in a biorefinery: An optimization study. *Journal of Engineering Science*. 2025, XXXII (1), pp. 90-110. https://doi.org/10.52326/jss.utm.2025.8(2).08.

Submission of manuscripts: jes@meridian.utm.md

Journal of Engineering Science *Vol. XXXII, no. 1 (2025), pp. 111 - 124*
Fascicle *Architecture, Civil and Environmental Engineering* *ISSN 2587-3474*
Topic *Environmental Engineering* *eISSN 2587-3482*

https://doi.org/10.52326/jes.utm.2025.32(1).09
UDC 620.95:634.5

COMPARATIVE EVALUATION OF ENERGY POTENTIAL AND COMPOSITION OF WALNUT, HAZELNUT, AND ALMOND RESIDUES FOR SOLID BIOFUEL PRODUCTION

Grigore Marian, ORCID: 0000-0002-9975-2522,
Alexandru Banari*, ORCID: 0000-0001-9132-610X

Technical University of Moldova, 168 Stefan cel Mare Blvd, Chisinau, Republic of Moldova
* Corresponding author: Alexandru Banari, *alexandru.banari@sfc.utm.md*

Received: 02. 18. 2025
Accepted: 03. 24. 2025

Abstract. Interest in renewable energy, particularly biomass-derived energy, has significantly increased in recent decades. As one of the most readily available resources in the Republic of Moldova, biomass energy plays an essential role in the country's evolving national energy framework. This study aims to evaluate the quality of tree biomass generated by nut trees, specifically walnut, hazelnut, and almond, considering its potential use as raw material for solid biofuel production. A comprehensive qualitative and quantitative assessment was conducted, focusing on calorific value, ash content, volatile matter content, and the concentrations of C, H, S, N, and Cl—key components contributing to pollutant emissions (CO, CO_2, NO_x, SO_2, etc.). The findings highlight that nut residues meet quality standards for solid biofuels derived from non-woody biomass, showcasing their significant potential for sustainable energy production.

Keywords: Nucifera Biomass, Solid Biofuels, Walnut, Hazelnut, Almond, Energy Potential.

Rezumat. Interesul pentru energiile regenerabile, în special pentru cea obținută din biomasă a crescut în mod semnificativ în ultimele decenii. Fiind una din sursele cu disponibilitate mare în Republica Moldova energia din biomasă joacă un rol important în noul cadru energetic național. Scopul acestui studiu a fost de a estima calitatea biomasei vegetale pomicole generate de nuciferi, având în vedere potențialul utilizării acesteia ca materie primă pentru producerea biocombustibililor solizi. S-au efectuat estimarea calitativă și cantitativă a reziduurilor de nuc, alun și migdal ținând cont de valoarea calorifică, conținutul de cenușă și materii volatile, conținutul de C, H, S, N și Cl) care sunt constituenți ai factorilor poluanți (CO, CO_2, NO_x, SO_2 etc.). Rezultatele demonstrează că reziduurile nucifere pot îndeplini standardele de calitate pentru biocombustibilii solizi pe bază de biomasă nelemnoasă, cu un potențial semnificativ pentru producerea de energie durabilă.

Cuvinte cheie: *Biomasă nucifere, Biocombustibili solizi, Nuc, Alun, Migdal, Potențial energetic.*

1. Introduction

In the current global context, marked by the depletion of conventional energy resources, the ongoing energy crisis, the increasingly pronounced impact of climate change, and the identification and effective use of renewable energy sources have become a key priority for the Republic of Moldova.

To encourage the continuous development of renewable energy, the Republic of Moldova has implemented a series of policies and strategies highlighting its commitment to sustainability. Among these, the Energy Strategy of the Republic of Moldova until 2030 [1] and the Energy Strategy of the Republic of Moldova until 2050 [2] stand out as essential documents. These strategies aim to achieve essential objectives such as ensuring energy security, improving energy efficiency, and diversifying energy sources. A central aspect of these initiatives is the promotion of renewable energy, including biomass-derived energy, as a means to reduce dependency on energy imports. This approach not only strengthens national energy independence but also supports the transition to a more sustainable and resilient energy system. The use of biomass as a fuel source represents a promising solution for meeting global energy demands, providing significant economic and environmental benefits. As a renewable resource, biomass has gained significant popularity worldwide, particularly among energy-import-dependent countries such as the Republic of Moldova [3]. Despite its potential, the biomass sector faces certain challenges, including ensuring the consistent quality of raw materials [4–6].

In Europe, concerns regarding biomass quality and sustainability, as well as its impact on the performance of solid biofuels, have been a focal point of policy development. These issues were formally addressed with the adoption of Directive 2009/28/EC, which promotes the use of energy from renewable sources, where biomass playing a pivotal role [7]. According to various authors [8–11], the quality of biomass is a critical factor in ensuring the quality of the final product. Biomass used as raw material for producing solid biofuels consists of a highly heterogeneous range of biogenic materials from diverse origins, including agriculture, forestry, wood processing industries, and the food industry. This variability poses significant challenges for standardization and predicting its impact on the quality of the final product [8, 12–14].

Among the existing types of biomass, orchard-derived biomass stands out as one of the most promising options with considerable potential in the Republic of Moldova [15–17]. Being available in various forms – both dedicated and residual – it offers relatively stable and predictable energy production [18]. This study aims to analyze the quality and potential of orchard biomass generated from nut trees, considering its potential use as raw material for the production of solid biofuels. The research hypothesis suggests that residues generated from nut tree cultivation could serve as a viable resource for manufacturing solid biofuels with properties that comply with ENplus standards.

Nut trees play an important role in global agriculture, including in the Republic of Moldova, given their nutritional and economic value. Nuts are highly appreciated on international markets, offering competitive prices, which encourage local producers to expand cultivated areas [19, 20]. *Nut trees* share significant common features as woody plants that produce hard-shelled fruits, which allow for extended storage and provide effective protection against external factors. In this context, a study conducted on biomass from various fruit tree species in intensive plantations in Croatia revealed that hazelnuts generate the highest residue yield among nut trees, producing 1,848 kg/ha, followed by almonds with 1.627 kg/ha, and walnuts with only 538.5 kg/ha [21]. However, the same author highlights that almonds, despite their lower planting density, yield the largest amount of biomass per tree (5.81 kg), positioning them as a highly attractive option for using residues in thermal energy production. In addition to residues from tree pruning and maintenance, nut trees generate a significant amount of biomass in the form of endocarps (the hard, woody shells

protecting the seeds). The literature identifies various methods for transforming these residues into energy sources. For instance, studies demonstrate that pelletizing almond shells can yield fuels with high calorific value, suitable for use in thermal plants and electricity generation [22]. Beyond energy production, almond shells have industrial applications, including the preparation of activated carbon, abrasive stones, and fine linoleum blends [23]. Walnut and hazelnut shells present promising potential as raw materials for producing particle boards [24]. Beyond their traditional use as fuel, walnut shells have found innovative applications in the food industry, specifically as a substrate in the acetic fermentation process for producing white wine vinegar. This method involves washing and drying the shells at controlled temperatures to prepare them for inoculating acetic bacteria. This approach highlights the sustainability of utilizing walnut shells as active biological materials in processes that yield high-quality food products [25]. The research was conducted at the Scientific Laboratory of Solid Biofuels (LSBCS) of Technical University of Moldova using validated standard methods. Biomass samples were collected from various agricultural households across the Republic of Moldova. The results confirmed the initial hypothesis, demonstrating that plant residues from nut trees represent a sustainable and reliable raw material for producing solid biofuels, meeting the qualitative requirements specified in the SM EN ISO 17225:2021 standards.

2. Materials and Methods

The investigation methodology was based on a systematic study conducted at the LSBCS of UTM, accredited by the National Accreditation Center of the Republic of Moldova [26]. The research was carried out in two distinct phases. In the first phase, biomass quantities from various walnut, hazelnut, and almond varieties were estimated. Experimental samples were collected from multiple locations: the Voinești Nursery in Voinescu village, Hâncești district; the CC Dumbrava Veche SRL in Radeni village, Straseni district; and various individual farms in Truseni commune, Chisinau municipality. Figure 1 presents sequences from the biomass sampling process.

Figure 1. Sequences of walnut biomass sampling in Truseni commune, Chisinau municipality**.**

Samples were coarsely shredded on-site immediately after collection using a *Murena* branch shredder and weighed with an accuracy of 10.0 g using the ACFN balance. The weighed samples were packed in polyethylene bags and transported to the LSBCS on the same day, where their moisture content at the time of harvest was determined. In the second phase, the residue mixtures from various walnut, hazelnut, and almond varieties collected across different regions of Moldova were analyzed for their calorific value, ash content, volatile matter content, and elemental composition, including carbon (C), hydrogen (H), nitrogen (N), sulfur (S), and chlorine (Cl).

Sample collection was performed in accordance with the requirements of the SM EN ISO 18135:2017 standard, while sample preparation followed the guidelines outlined in SM EN ISO 14780:2017/A1:2020.

The collected samples were conditioned by grinding using a Retsch SM 100 mill equipped with a 1 mm mesh sieve (Figure 2a). The grinding process was performed at a rotor speed of 1500 min^{-1}, ensuring uniform particle size reduction while minimizing excessive dust formation.

The gross calorific value of the biomass was determined at constant volume using an IKA C6000 isoperibolic calorimeter (Figure 2c). The methodology for calculating the net calorific value, reported on a dry basis and adjusted for a predetermined moisture level, is detailed in our previous work [27].

Moisture content was assessed by measuring the weight loss of the biomass after heating at 105 ± 2 °C in a UNB 500 - Memmert oven (Figure 2f), in accordance with the SM EN ISO 18134-1:2017 standard. The resulting moisture content was reported on a dry basis, applying the calculation method described in [28].

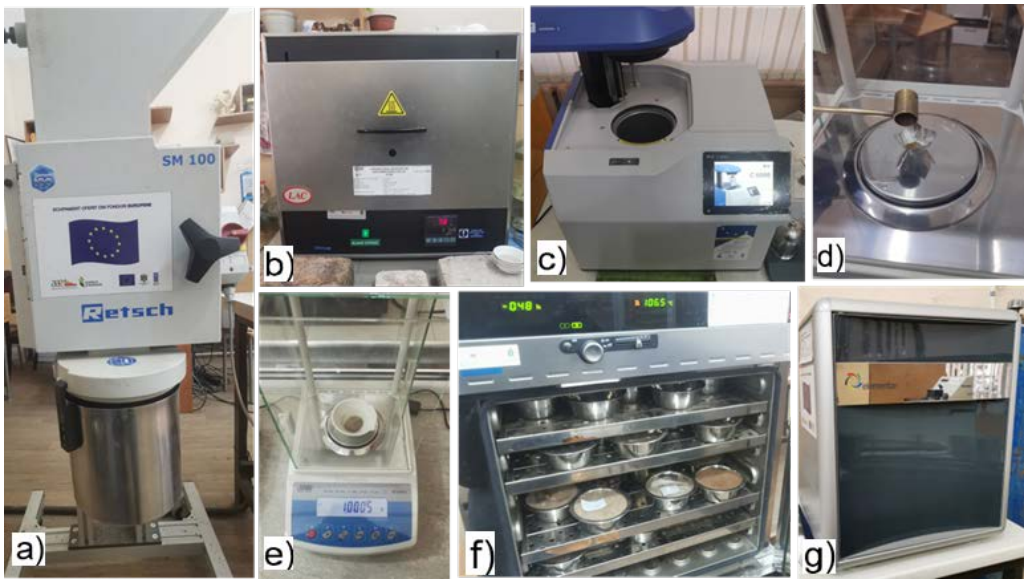

Figure 2. Equipment used for testing: a) Retsch SM 100 mill; b) LAC LH 06/13 muffle furnace; c) IKA C6000 isoperibolic calorimeter; d) Sample weighing; e) AS220/C2 analytical electronic balance; f) UNB 500-Memmert oven; h) Vario MACRO cube elemental analyzer.

The ash content of the samples was determined by incinerating approximately one gram of each sample. The samples, placed in crucibles, were progressively heated following this procedure:

- heated to 250 ± 10 °C at a rate of +5 °C/min for 50 min;

- maintained at 250 ± 10 °C for 60 min, then gradually heated to 550 ± 10 °C over 60 min;

- held at 550 ± 10 °C for 120 min, then cooled to an ambient temperature. Chemical analysis of the samples was performed using the Vario MACRO cube CHNS Cl elemental analyzer (Figure 2h). Detection and quantitative analysis were carried out using a thermal conductivity detector. The results were processed using EAS software, which enabled data display, monitoring, recording, and analysis for chemical element characterization.

All tests were repeated five times, and the standard deviation and confidence intervals were determined. The corresponding tables present the average values from these repetitions.

Figure 3. Biomass samples prepared according to SM EN ISO 14780:2017 requirements: a) hazelnut original fruits and endocarp; b) almond original fruits and endocarp; c) walnut kernel and endocarp; d) hazelnut branches; e) shredded hazelnut endocarp; f) shredded walnut endocarp.

3. Results

In the Republic of Moldova, the most important nut species are walnut (*Juglans regia* L.), hazelnut (*Corylus avellana* L.), and, to a lesser extent, almond (*Prunus dulcis*). In recent years, the area of nut plantations has increased significantly, reaching a total of 39.1 thousand hectares, of which 26.8 thousand hectares are productive plantations [29]. Walnut dominates, accounting for about 95% of the plantations, followed by hazelnut (~3%) with almond and other nut species making up the remainder. It is noteworthy that hazelnut and almond cultivation are experiencing a significant upward trend.

Table 1 presents data on the total nut yield for 2022–2023, categorized by type, highlighting the role of individual households in production. These households contribute approximately 60–65% of the total yield, indicating that the majority of nut production occurs at the individual level.

Table 1

The global walnut harvest in the Republic of Moldova for the reference years, thousand tons [29]

2022				2023			
HhAC	AE	SFF	IHh	HhAC	AE	SFF	IHh
19.1	6.5	0.9	11.7	21.2	4.9	0.9	15.4

Note: HhAC- households of all categories; AE - agricultural enterprises; SFF - small family farms; IHh - individual households.

Walnuts are the most widely consumed dried fruit worldwide and are considered both economically and ecologically significant, with diverse applications in the medical, nutritional, agricultural, and industrial sectors [30]. Native to the Old World, walnuts have been cultivated in Europe since 1000 BC, with their origin spanning an extensive region from the Balkans to the western Himalayan range [20]. This species is well-adapted to temperate-continental climates and offers numerous valuable qualities, including health benefits, use in the furniture industry, and an essential role as a forest tree for preventing and controlling soil erosion [31].

Today, walnuts are commercially grown in various regions worldwide, including North Africa, East Asia, the United States, western South America, and Southern Europe, especially in countries such as Romania and the Republic of Moldova [32]. In the Republic of Moldova, walnut orchards include both traditional local varieties, such as *Pescianski, Cazacu,* and *Calarasi*, as well as imported ones. Modern plantations are primarily dominated by French varieties like *Fernor* and *Franquette*, American varieties like *Chandler*, or those developed at the Voinesti nursery, including *Carpatica* and *Ovata*. All of these varieties are listed in the Republic of Moldova's Plant Variety Catalog and are authorized for cultivation within the national agri-food sector [33].

In rural households, the walnut tree has been a common feature. Production traditionally focused on harvesting walnut kernels, the edible part of the fruit, which accounted for 20% to 60.3% of the total weight, with an average of 42.70% [23]. Shells from kernel processing were abundantly available and traditionally used for heating stoves. Due to their high calorific value, walnut shells provided a practical and economical solution for individual households.

The walnut tree's longevity of 200 to 300 years ensures a continuous biomass yield without the need for frequent replanting [23].

Hazelnuts, native to Europe and Asia Minor, are cultivated for their nuts, used both for direct consumption and in the food industry. Rich in minerals and vitamins, hazelnuts offer tonic, energetic, and digestive benefits, making them a valuable source of essential nutrients [34]. In Moldova, the main varieties grown include Tonda Gentile, Fertile de Coutard (Barcelona), Nocchione, and Tonda Francescana (B). These varieties thrive in areas with moderate rainfall and possess a shallow root system, which makes them sensitive to drought.

Hazelnuts can be cultivated with either a single trunk or multiple trunks, depending on growers' preferences and objectives. Single-trunk forms facilitate mechanical harvesting and optimal light exposure, while multi-trunk forms allow for gradual regeneration by replacing old shoots with new ones. A hazelnut bush typically produces approximately 3-7 kg of green biomass. According to authors' analysis and the study [35], the average biomass per plant was 4.17 kg of fresh material, highlighting the significant potential of hazelnuts as a sustainable biomass source. This biomass mainly results from periodic pruning of branches

and shoots during maintenance and care operations, as well as residual materials from nut harvesting.

The almond tree, native to the arid regions of the Middle East and Central Asia, grows naturally along the Mediterranean coast, in China, and India [36]. Recently, several almond varieties have been adapted for cultivation in the southern regions of the Republic of Moldova. These include local varieties such as Meteor, Victoria, Alb Moldovenesc, Hramov Standard, and Pervenet Hramova (sold by SRL Dumbrava Veche); Tuono (an Italian variety noted for late blooming and resistant to late frosts); Nonpareil (a Californian variety famous for its large, sweet almonds); and Nocchione (an Italian variety known for medium-sized fruits and high productivity).

Almond trees can be shaped like traditional trees or managed as large bushes. During pruning and processing, almonds yield significant amounts of plant biomass, which can be converted into raw material for producing densified solid biofuels. The edible kernel of almonds accounts for approximately 20-40% of the entire nut, including the shell and outer husk, with this ratio varying depending on the variety and growing conditions [37]. This biomass, including shells and husks, can be a valuable source for bioenergy production, making almonds not only a nutritional commodity but also a sustainable option for solid biofuels.

Overall, the amount of plant biomass resulting from pruning nut trees is influenced by several factors, including:

- Crop type (different nut species produce varying amounts of biomass based on their growth characteristics and branching patterns).
- Tree age and size (older and larger trees typically generate more woody material than younger, smaller trees, as their growth produces more biomass).
- Harvesting technology (the use of specialized equipment can optimize biomass collection by reducing labor costs and improving efficiency).

Pruning type (maintenance pruning produces less biomass than regeneration or formative pruning) [38]. There are three main types of nut tree pruning: formative, maintenance, and rejuvenation [39], specific to each group of nut trees, producing different amounts of residual biomass.

Table 2 shows the results regarding the biomass quantities obtained from cultivating various walnut, hazelnut, and almond varieties. To better reflect real-world conditions, where biomass collection does not involve sorting by varieties or species, average values for different nut groups were determined. The dispersion and confidence intervals were also calculated to provide a more accurate representation of biomass yield across different conditions.

The analysis of nut residue potential, as summarized in Table 2, was conducted using samples collected from orchards over 10 years of age. Each biomass sample comprised a mixture of one-year-old and perennial shoots. Sampling procedures followed the methodology described in [40].

Tree selection was performed according to SM EN ISO 18135:2017 standard. Specifically, trees in a specific area of the plantation were assigned a two-digit identifier: the first digit denoting the row number and the second digit indicating the tree's position within the row. The quartering method was employed to ensure a representative selection of samples.

Table 2

The amount of residues generated by different varieties of walnut, hazelnut, and almond trees

Variety of fruit trees	Average number of trees, trees /ha	Average biomass quantity, kg/tree	Biomass quantity, kg/ha	Moisture content at harvest, %wt	Biomass quantity adjusted to 10%wt, kg/ha	Average nut yield in shell, kg/ha	Average endocarp/kernel ratio, %	Endocarp quantity, kg/ha
Walnut								
Pescianski	200	9.63	1926.0	46	1155.6	1750	56	980
Ovata	200	8.41	1682.0	48	971.8	2200	48	1056
Fernor	250	8.52	2130.0	43	1349.0	2800	48	1344
Franquette	200	9.16	1832.0	47	1078.8	2000	57	1140
Chandler	250	8.35	2087.5	42	1345.3	2500	44	1100
Mean	***220.0***	***8.81***	***1931.5***	***45.2***	***1180.1***	***2250.0***	***50.6***	***1124.0***
Standard Deviation	***27.4***	***0.56***	***184.3***	***2.6***	***165.9***	***412.3***	***5.6***	***136.6***
Confidence Interval	***24.0***	***0.49***	***161.6***	***2.3***	***145.4***	***361.4***	***4.9***	***119.7***
Hazelnut								
Tonda Francescana	820	4	3436	44	2138	2290	56	1282
Tonda Gentile	500	4	2080	43	1317	2240	55	1232
Barcelona	500	4	2070	42	1334	2190	57	1248
Fertile de Coutard	820	4	2968	45	1814	2210	52	1149
Nocchione	820	4	3091	46	1855	2090	53	1108
Mean	***692.0***	***4.0***	***2729.1***	***44.0***	***1691.6***	***2204.0***	***54.6***	***1203.9***
Standard Deviation	***175.3***	***0.3***	***621.2***	***1.6***	***356.6***	***74.0***	***2.1***	***72.7***
Confidence Interval	***153.6***	***0.2***	***544.5***	***1.4***	***312.6***	***64.9***	***1.8***	***63.8***
Almond								
Meteor	350	7.8	2730	48	1577	2500	78	1950
Alb Moldovenesc	280	8.6	2408	52	1284	1800	77	1386
Tuona	350	7.4	2590	58	1209	2200	69	1518
Nanparil	400	6.3	2520	54	1288	2400	68	1632
Victoria	280	8.2	2296	43	1454	2400	66	1584
Mean	***332.0***	***7.7***	***2508.8***	***51.0***	***1362.5***	***2260.0***	***71.6***	***1614.0***
Standard Deviation	***51.7***	***0.9***	***166.7***	***5.7***	***149.9***	***279.3***	***5.5***	***209.4***
Confidence Interval	***45.3***	***0.8***	***146.1***	***5.0***	***131.4***	***244.8***	***4.8***	***183.5***

Note: wt - percentage by weight.

The results indicate significant variability in the amount of vegetal biomass resulting from pruning operations across the studied nut trees species. Hazelnuts produced the largest amount of vegetal residues, averaging 2729.1±544.5 kg/ha, while walnuts yielded the lowest, with an average of 1931.5±161.6 kg/ha. For endocarp residues, almonds recorded the largest

quantity, averaging 1614±183.5 kg/ha, whereas walnuts had the smallest amount, with an average of 1124±119.7 kg/ha.

To fully assess the potential of nut residues as raw materials for biofuel production, their thermochemical characteristics were analyzed. The following Table presents the results of the analysis of the main characteristics of nut residues, which are of interest for evaluating their energy applications. A comparative evaluation of these characteristics (see Table 3) highlights significant differences in residue quality, especially in ash content, which ranged from 1.4% for hazelnut branches and shoots to 5.5% for walnut branches. In terms of calorific value, walnut branches recorded the lowest energy potential ($q_{Pnet\ M=10\%}$ = 15501.1 J/g), while almond branches demonstrated the highest ($q_{Pnet\ M=10\%}$ = 15968.4 J/g). Additionally, walnut branches exhibited the highest sulfur and nitrogen content among the tested samples, posing potential environmental challenges during combustion.

Table 3

Average results of characteristics of vegetable biomass generated from nut trees

Biomass origin		q_{Vd}, J/g	$q_{Vnet\ d}$, J/g	$q_{Pnet\ M=10\%}$	A, %	M rec., %	MV, %	C, %	N, %	H, %	Cl, %	S, %	O, %
Walnut	branches	18823	17494.9	15501.1	5.5	46.9	77.9	48.8	0.62	6.11	0.04	0.08	38.89
	endocarp	20083	18757.3	16637.3	0.9	11.0	79.0	45.9	0.18	6.07	0.03	0.04	46.89
Hazelnut	branches	19119	17771.7	15750.3	1.4	44.5	80.2	47.5	0.57	6.18	0.05	0.07	44.26
	endocarp	20297	18941.2	16802.7	0.9	10.9	77.1	45.2	0.19	6.21	0.03	0.05	47.42
Almond	branches	19421	18014.1	15968.4	2.4	44.6	79.7	51.2	0.54	6.48	0.05	0.04	39.30
	endocarp	19856	18462.0	16371.5	1.6	12.7	78.4	49.7	0.29	6.41	0.04	0.04	42.01

Note: A – ash content on a dry basis; MV – volatile matter content; q_{Vd},– higher calorific value measured at constant volume; $q_{Vnet\ d}$, J/g lower calorific value at constant pressure; $q_{Pnet\ M=10\%}$,– lower calorific value at constant pressure calculated for a moisture content of 10%.

All residues in the form of branches and shoots require conditioning through drying, as their moisture content at harvest significantly exceeds the recommended values for pellet and briquette processing [41].

In contrast, endocarp residues generated by all studied nut species can be processed directly without prior conditioning through drying due to their low moisture content, which ranges from 10.9% for hazelnut to 12.7% for almond. These moisture values fall within the recommended limits for raw materials used in the production of densified solid biofuels [41]. Notably, walnuts, hazelnuts, and almonds the endocarp residues can also be used directly, without densification, in both traditional stoves and most modern thermal power plants [42]. Comparing the data obtained in this study with the requirements outlined in the SM EN ISO 17225 standards, it can be concluded that biomass derived from walnut pruning is suitable exclusively for the production of pellets and briquettes classified as non-woody biomass products, blends, and biomass mixtures. Specifically, walnut pruning biomass is categorized as A for pellets and A2 for briquettes, while branches from hazelnut and almond trees meet the criteria for use as raw material in the production of A2-grade wooden briquettes.

Synthesizing the data presented in Tables 2 and 3, the energy potential of biomass generated by nut tree species was calculated per hectare of plantation area. The analysis of nut biomass energy potential considered several perspectives, each playing an essential role for resource evaluation and efficient planning for solid biofuel production. These perspectives

include the theoretical potential, the available potential, and the economic potential, which some authors refer to as the sustainable implementation potential.

The theoretical energy potential (TEP) represents the total energy available in the biomass produced, without considering any limiting factors such as collection efficiency or losses during processing. It provides a maximum estimate based on the total amount of biomass generated by agricultural activities. The TEP is calculated based on the calorific value of the biomass and assumes its complete utilization [43]. For example, if all agricultural residues were collected and 100% utilized, this potential would reflect the total energy contained in those residues. The theoretical energy potential calculated for one hectare of nut plantations was determined using the following equation:

$$TEP = m_{b.M=10\%} \cdot q_{p.net.M-10\%}, \quad (1)$$

where: $m_{b.M=10\%}$ - the average amount of biomass converted to a moisture content of 10%; $q_{p.net.M-10\%}$ - the net calorific value of biomass at a moisture content of 10%, calculated at constant pressure.

The available energy potential (AEP) is lower than the theoretical energy potential, being defined as the part of the theoretical potential available for energy production, limited by constraints related to the use of this biomass for non-energy purposes, the efficiency of the technological process, etc. [44]. For example, not all biomass can be harvested from the field, as part of it must be left for ecological purposes to maintain soil fertility. The available energy potential was determined as the product of theoretical energy potential and the availability coefficient (A). This coefficient, which reflects these limitations, is commonly accepted in the literature for fruit trees and is set at a value of 0.8 [40, 43, 45].

The sustainable energy potential for implementation (SEPI) represents the portion of the available energy potential that can be profitably utilized, considering the costs associated with biomass collection, processing, and usage, as well as technical and sustainability factors. This potential depends on economic, technological, and policy factors [46, 47] and also factors such as transport and storage losses [40]. For example, if the costs of biomass harvesting and processing exceed the value of the energy produced, this biomass will not be considered part of the economic potential, as it would not be financially viable for energy production.

The sustainable energy potential for implementation was calculated using the following equation:

$$SEPI = AEP \cdot (1 - k_{il}), \quad (2)$$

where: k_{il} - implementation loss coefficient.

The analysis of these three types of energy potential is essential for developing efficient strategies for utilizing agricultural biomass in solid biofuel production. The theoretical potential offers a broad overview, representing the maximum energy available from biomass without considering practical constraints. The available potential reflects the real-world limitations, such as biomass losses during collection and processing, as well as competition with non-energy uses. Finally, the SEPI assesses the economic and technical feasibility of utilizing the biomass, considering the costs involved and the market context. Together, these potential types guide the planning and implementation of biomass-based energy projects, ensuring both practicality and profitability.

Figure 4 illustrates the energy potential of biomass from three types of nut trees—walnut, hazelnut, and almond—categorized into two distinct types of biomass: woody biomass (WB) and endocarp biomass (EB). This differentiation allows for a clearer comparison of the energy potential of each biomass type, providing insights into their respective contributions to the overall energy potential of the nut tree residues.

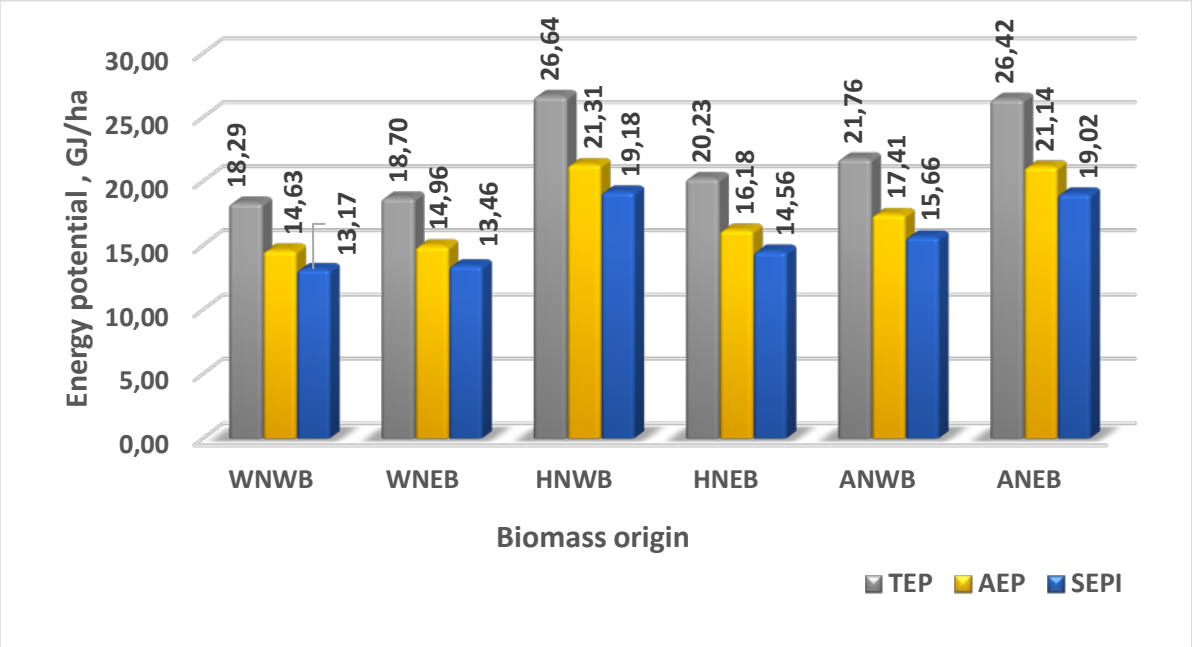

Figure 4. Energy potential of biomass generated by nut trees: TEP - theoretical energy potential; AEP - available energy potential, SEPI - sustainable energy potential of implementation; WNWB - walnut woody biomass; WNEB - walnut endocarp biomass; HNWB – hazelnut woody biomass; HNEB - hazelnut endocarp biomass; ANWB - almond woody biomass; ANEB - almond endocarp biomass.

When comparing the energy potential values across the types of biomass studied, significant differences emerge between woody biomass and endocarp, with hazelnut woody biomass yielding the highest energy values, followed by walnut and almond biomass, which exhibit slightly lower values.

The highest energy potential can be harnessed from processing almond residues, with a total SEPI of 34.69 GJ/ha, closely followed by hazelnut residues, with a total SEPI of 33.75 GJ/ha. Walnut residues, however, have the lowest energy potential, with a total SEPI of 26.64 GJ/ha.

These findings emphasize the importance of evaluating different types of energy potential when planning biomass utilization. Specifically, TEP offers a maximum estimate of energy capacity, while the AEP and SEPI reflect how practical and economic constraints shape the actual biomass availability for energy production.

4. Conclusions

1. Nut tree residues, including branches and endocarps, represent a sustainable and valuable source of biomass for solid biofuel production in the Republic of Moldova.

2. Endocarps, characterized by low moisture and ash content, are suitable for direct use in energy production without requiring drying or pre-conditioning.

3. Among the studied residues, hazelnut exhibited the highest calorific value (20.297 J/g), followed by walnut (20.083 J/g) and almond (19.856 J/g).

4. The energy potential of nut tree biomass is influenced by practical and economic factors, with almond residues demonstrating the highest energy yield per hectare of plantation.

5. The proper use of walnut tree residues effectively aligns with renewable energy strategies, contributing to energy independence and reducing reliance on imported energy sources.

These findings highlight the significant role of nut tree residues as a renewable energy resource, advocating their integration into sustainable biomass utilization strategies.

Acknowledgments: The authors gratefully acknowledge the financial support provided by the Government of the Republic of Moldova and the National Agency for Research and Development under project no. 23.70105.7007.08, contract no. 7/08R. This work was also supported by the technical and logistical assistance of project no. 20.80009.5107.15, "Development and implementation of good practices for sustainable agriculture and climate resilience / GREEN/020407."

Conflicts of interest: The authors declare no conflict of interest.

References

1. Government Decision Resolution No. 958 on the Energy Strategy of the Republic of Moldova until 2030. 2007. Available online: https://www.legis.md/cautare/getResults?doc_id=68103&lang=ro (accessed on 29.12.24) [in Romanian].
2. The Energy Strategy of the Republic of Moldova until 2050. (n.d.). Available online: https://energie.gov.md/sites/default/files/concept_strategia_enenergetica_act._-clean_1.pdf (accessed on 21.01.25) [in Romanian].
3. Capuano, L. International energy outlook 2020 (IEO2020). Available online: https://www.eia.gov/outlooks/ieo/pdf/ieo2020.pdf (accessed on 21.01.25).
4. Ciolacu, F.; Ianuș, G.; Marian, G.; Munteanu, C.; Paleu, V.; Nazar, B.; Istrate, B.; Gudîma, A.; Daraduda, N. A Qualitative Assessment of the Specific Woody Biomass of Fruit Trees. *Forests* 2022, 13 (3), 405. https://doi.org/10.3390/f13030405.
5. Marian, G.; Banari, A.; Gudima, A.; Nazar, B.; Pavlenco, A. Improving the quality of pellets produced from white buckchin biomass through the formation of blends. *The Agri-Food Sector – Achievements and Perspectives* 2022, pp. 119-121. Available online: https://ibn.idsi.md/sites/default/files/imag_file/119-121_35.pdf [in Romanian].
6. Tilvikiene, V.; Kadziuliene, Z.; Liaudanskiene, I.; Zvicevicius, E.; Cerniauskiene, Z.; Cipliene, A.; Raila, A. J.; Baltrusaitis, J. The quality and energy potential of introduced energy crops in northern part of temperate climate zone. *Renewable Energy* 2020, 151 (40), pp. 887–895. https://doi.org/10.1016/j.renene.2019.11.080.
7. Directive 2009/28/EC of 23 April 2009 on the promotion of the use of energy from renewable sources and amending and subsequently repealing. Directives 2001/77/EC and 2003/30/EC - 2012, (October), 515–578. Available online: https://faolex.fao.org/docs/pdf/eur88009.pdf (accessed on 20.12.24)
8. Toscano, G.; De Francesco, C.; Gasperini, T.; Fabrizi, S.; Duca, D.; Ilari, A. Quality Assessment and Classification of Feedstock for Bioenergy Applications Considering ISO 17225 Standard on Solid Biofuels. *Resources* 2023, 12(6), 69. https://doi.org/https://doi.org/10.3390/resources12060069.
9. Nath, B.; Chen, G.; Bowtell, L.; Mahmood, R. A. M. Assessment of densified fuel quality parameters: A case study for wheat straw pellet. *Journal of Bioresources and Bioproducts* 2023, 8 (1), pp. 45–58. https://doi.org/10.1016/j.jobab.2022.10.001.
10. Thiffault, E.; Barrette, J.; Blanchet, P.; Nguyen, Q. N.; Adjalle, K. Optimizing quality of wood pellets made of hardwood processing residues. *Forests* 2019, 10 (7), 607. https://doi.org/10.3390/f10070607.
11. Bosona, T.; Gebresenbet, G.; Olsson, S. O. Traceability system for improved utilization of solid biofuel from agricultural prunings. *Sustainability* 2018, 10(2), 258. https://doi.org/10.3390/su10020258.
12. Williams, C. L.; Emerson, R. M.; Tumuluru, J. S. Biomass Compositional Analysis for Conversion to Renewable Fuels and Chemicals. Available online: https://www.intechopen.com/chapters/52751 (accessed on 21.01.25).
13. Marian, G.; Ivanova, T. A.; Gudîma, A.; Nazar, B.; Malai, L.; Marian, T.; Pavlenco, A. Biomass Resources from

Vineyard Residues for the Production of Densified Solid Biofuels in the Republic of Moldova. *Agronomy* 2024, 14(10), 2183. https://doi.org/10.3390/agronomy14102183.
14. Libutti, A.; Cammerino, A. R. B.; Monteleone, M. Management of residues from fruit tree pruning: A trade-off between soil quality and energy use. *Agronomy* 2021, 11 (2), 236. https://doi.org/10.3390/agronomy11020236.
15. Braga D.; Hlusov, V. Study on assessing the potential for utilizing solid biomass in centralized heating systems in the Republic of Moldova. 2024. Available online: https://www.undp.org/ro/moldova/publications/studiu-privind-evaluarea-posibilitatilor-de-valorificare-biomasei-solide-sistemele-de-alimentare-centralizata-cu-energie-termica (accessed on 15.01.25) [in Romanian].
16. Gudîma, A.; Marian, G.; Pavlenco, A. The current state of research on the influence of production variables on the quality of densified biofuels in pellet form. *Meridian Ingineresc* 2017, 1, pp. 51-60 Available online: https://ibn.idsi.md/sites/default/files/imag_file/51_60_Stadiul%20actual%20al%20cercetarilor%20cu%20privire%20la%20influenta%20variabilelor%20de%20productie.pdf [in Romanian].
17. Crucean, Ş. The main diseases and pests of nut crops in agroecosystems, 59. Available online: https://ibn.idsi.md/sites/default/files/imag_file/59_7.pdf (accessed on 16.01.25) [in Romanian].
18. Cimpoieş, Gh.; Popa, S.; Rîbinţev, I.; Marian, G.; Andriuca, V.; Macari, A.; Mîrza S.; Zbancă, A. *Cultivation and exploitation of sea buckthorn*. Print CARO, Chisinau, Republic of Moldova, 2024, 380 p. ISBN: 380 978-9975-180-91-7 [in Romanian].
19. National Strategy for Agricultural and Rural Development for the years 2023-2030. 2023 Available online: https://cancelaria.gov.md/sites/default/files/document/attachments/864_maia.pdf (accessed on 13.01.25) [in Romanian].
20. Taha, N. A.; Al-Wadaan, M. A. Significance and use of walnut, Juglans regia Linn: A review. *Advanced Journal of Microbiology Research* 2021, 15 (1), pp. 1–10.
21. Bilandzija, N.; Voca, N.; Kricka, T.; Matin, A.; Jurisic, V. Energy potential of fruit tree pruned biomass in Croatia. *Spanish Journal of Agricultural Research* 2012, 10 (2), 292–298. https://doi.org/10.5424/sjar/2012102-126-11.
22. Baum, R.; Wajszczuk, K.; Pepliński, B.; Wawrzynowicz, J. Potential for agricultural biomass production for energy purposes in Poland: A review. *Contemporary Economics* 2013, 7 (1), 63–74. https://doi.org/10.5709/ce.1897-9254.74.
23. Cociu, V. *Walnut*. Ministry of Agriculture and Forestry, Bucharest, Romania, 1980, 167 p. [in Romanian].
24. Barbu, M. C.; Sepperer, T.; Tudor, E. M.; Petutschnigg, A. Walnut and hazelnut shells: Untapped industrial resources and their suitability in lignocellulosic composites. *Applied Sciences* 2020, 10 (18), 6340. https://doi.org/10.3390/APP10186340.
25. Boiştean, A.; Chirsanova, A.; Gaina, B.; Siminiuc R. Process for producing vinegar from white wine (57). Patent No: MD 1517(13)Y of 04/30/2021. 2021.
26. MOLDAC. Decision No. 160 of 16.09.2024. Available online: https://acreditare.md/register/laboratorul-stiintific-de-biocombustibili-solizi-din-cadrul-ip-universitatea-tehnica-a-moldovei/ (accessed on 30.01.25).
27. Marian, G.; Gelu, I.; Gudima, A.; Nazar, B.; Istrate, B.; Banari, A.; Pavlenco, A.; Daraduda, N. Calorific Value of Pellets Produced From Raw Material Collected From Both Sides of the River Prut. *Journal of Engineering Science* 2023, 29 (4), pp. 126–137. https://doi.org/10.52326/jes.utm.2022.29(4).10.
28. Marian, G.; Ianuş, G.; Istrate, B.; Gudima, A.; Nazar, B.; Pavlenco, A.; Banari, A.; Daraduda, N. A Qualitative Assessment of the Specific Woody Biomass of Fruit Trees. *Forests* 2022, 13 (3), 405. https://doi.org/10.3390/f13030405.
29. Statistical data bank. Available online: https://statbank.statistica.md/PxWeb/pxweb/ro/40%20Statistica%20economica/40%20Statistica%20economica__16%20AGR__AGR020/AGR020070.px/ (accessed on 16.12.24).
30. Fordos, S.; Abid, N.; Gulzar, M.; Pasha, I.; Oz, F.; Shahid, A.; Khan, M. K. I.; Mousavi Khaneghah, A.; Aadil, R. M. Recent development in the application of walnut processing by-products (walnut shell and walnut husk). *Biomass Conversion and Biorefinery* 2023, 13 (16), pp. 14389–14411. https://doi.org/10.1007/s13399-023-04778-6.
31. Sota, V.; Benelli, C.; Myrselaj, M.; Kongjika, E.; Gruda, N. S. Short-Term Conservation of Juglans regia L. via Synthetic Seed Technology. *Horticulturae* 2023, 9(5), 559. https://doi.org/10.3390/horticulturae9050559.
32. Pîntea, M. Walnut cultivation (*Juglans regia* L.): Biological and production aspects. *Academus* 2015, 1, pp. 119–123. Avaible online: http://akademos.asm.md/files/Cultivarea nucului.pdf [in Romanian].
33. Machidon, M. The plant variety catalogue for the year 2024. Available online:

https://cstsp.md/uploads/files/Catalog%202024.pdf (accessed on 23.12.24) [in Romanian].
34. Roşca, I.; Mîţu, V.; Mîrza, A. *Genus Corylus* L. importance for culture in the Republic of Moldova. *Journal of Botany* 2020, 12 (1) pp. 109-122 [in Romanian].
35. Acampora, A.; Civitarese, V.; Sperandio, G.; Rezaei, N. Qualitative characterization of the pellet obtained from hazelnut and olive tree pruning. *Energies* 2021, 14 (14), 4083. https://doi.org/10.3390/en14144083.
36. Dadu, C.; Donea, V.; Onica, E.; Donea, E.; Oboroc, I. The Common Almond (Amygdalus communis L.) – A species with potential for the Republic of Moldova. *Pomicultura, Viticultura şi Vinificaţia* 2022, 88 (2), pp. 62-72 [in Romanian].
37. Prgomet, I.; Goncalves, B.; Domínguez-Perles, R.; Pascual-Seva, N.; Barros, A. I. R. N. A. Valorization challenges to almond residues: Phytochemical composition and functional application. *Molecules* 2017, 22 (10), 1774. https://doi.org/10.3390/molecules22101774.
38. Borkowska, A.; Maj, G.; Klimek, K. E.; Kapłan, M. The Determination of Woody Biomass Resources and Their Energy Potential from Hazelnut Tree Cultivation. *Energies* 2024, 17 (18), 4536. https://doi.org/10.3390/en17184536.
39. Silvestri, C.; Santinelli, G.; Pica, A. L.; Cristofori, V. Mechanical pruning of european hazelnut: Effects on yield and quality and potential to exploit its by-product. *European Journal of Horticultural Science* 2021, 86 (2), pp. 189–196. https://doi.org/10.17660/eJHS.2021/86.2.9.
40. Pavlenco, A.; Marian, G.; Gudîma, A. The energy potential of agricultural residues: a case study for the northern development region, Republic of Moldova. *Ştiinţa Agricolă* 2018, 2 (2), pp. 141-148. Available online: https://ibn.idsi.md/sites/default/files/imag_file/141-148-compressed.pdf [in Romanian].
41. Marian G. Solid Biofuels: Production and Properties. In: *The Energy and Biomass Project in the Republic of Moldova*, Bons Office, Chişinău, 2016, 172 p. [in Romanian].
42. Alfattani, R.; Shah, M. A.; Siddiqui, I. H.; Ashraf, M. A.; Alnaser, I. Bio-char characterization produced from walnut shell biomass through slow pyrolysis: Sustainable for soil amendment and an alternate bio-fuel. *Energies* 2022, 15 (1), 1. https://doi.org/10.3390/en15010001.
43. Pence, I.; Kumas, K.; Siseci Cesmeli, M.; Akyüz, A. Detailed analysis of Türkiye's agricultural biomass-based energy potential with machine learning algorithms based on environmental and climatic conditions. *Clean Technologies and Environmental Policy* 2024, 26, pp. 4177–4195.
44. Fitri, H.; Gürdil, G. A. K.; Demirel, B.; Cevher, E. Y.; Roubík, H. Biomass potential from agricultural residues for energy utilization in West Nusa Tenggara (WNT), Indonesia. *GCB Bioenergy* 2023, 15 (11), pp. 1405–1414. https://doi.org/10.1111/gcbb.13100.
45. Gudîma, A. Assessment of agricultural residue utilization for energy purposes: a case study for soroca district, Republic of Moldova. *Meridian Ingineresc* 2017, 1, pp. 26-29. Available online: http://repository.utm.md/bitstream/handle/5014/291/MI_2017_1_pg_26_29.pdf?sequence=1&isAllowed=y [in Romanian].
46. Bryan, B. A.; Ward, J.; Hobbs, T. An assessment of the economic and environmental potential of biomass production in an agricultural region. *Land Use Policy* 2008, 25 (4), pp. 533–549. https://doi.org/10.1016/j.landusepol.2007.11.003.
47. Portugal-Pereira, J.; Soria, R.; Rathmann, R.; Schaeffer, R.; Szklo, A. Agricultural and agro-industrial residues-to-energy: Techno-economic and environmental assessment in Brazil. *Biomass and Bioenergy* 2015, 81, pp. 521–533. https://doi.org/10.1016/j.biombioe.2015.08.010.

Citation: Marian, G.; Banari, A. Comparative evaluation of energy potential and composition of walnut, hazelnut, and almond residues for solid biofuel production. *Journal of Engineering Science*. 2025, XXXII (1), pp. 111-124. https://doi.org/10.52326/jss.utm.2025.8(2).09.

Submission of manuscripts: jes@meridian.utm.md

Journal of Engineering Science *Vol. XXXII, no. 1 (2025), pp. 125 - 135*
Fascicle *Food Engineering* *ISSN 2587-3474*
Topic *Food Technologies and Food Processes* *eISSN 2587-3482*

https://doi.org/10.52326/jes.utm.2025.32(1).10
UDC 641.5:633.18

THE IMPACT OF STORAGE CONDITIONS ON THE MICROBIOLOGICAL AND ORGANOLEPTIC QUALITY OF COOKED RICE

Anna Vîrlan *, ORCID: 0009-0000-7983-9340,
Rodica Siminiuc, ORCID: 0000-0003-4257-1840

Technical University of Moldova, 168, Stefan cel Mare Blvd, Chisinau, Republic of Moldova
* Corresponding author: Anna Vîrlan, *anna.virlan@doctorat.utm.md*

Received: 03. 04. 2025
Accepted: 03. 30. 2025

Abstract. Cooked rice, owing to its high moisture content and rich nutritional profile, is particularly prone to microbiological contamination, especially under suboptimal storage conditions. This study investigated the effects of three distinct storage regimes—room temperature, refrigeration, and freezing—on the microbiological and organoleptic quality of cooked rice, with the objective of identifying safe consumption windows and minimizing quality degradation. Microbiological assessments were carried out in accordance with relevant ISO standards, while sensory evaluation was performed using a descriptive scoring method by a trained panel. The findings revealed that rice stored at room temperature became microbiologically unsafe after 24 hours. In contrast, refrigeration maintained microbiological safety up to day five, and freezing preserved overall stability for up to three months. However, sensory quality deteriorated progressively under all conditions, with the most pronounced alterations observed in samples frozen for over 90 days. These results underscore the critical role of appropriate storage conditions in ensuring food safety and preserving sensory attributes. While the study does not propose technological innovations, it provides a practical framework by integrating microbiological and sensory evaluations into a reproducible model applicable in both educational and professional settings.

Keywords: *cooked rice, storage conditions, refrigeration, freezing, microbiological analysis, sensory evaluation, food safety.*

Rezumat: Orezul gătit, datorită conținutului său ridicat de umiditate și profilului său nutrițional bogat, este deosebit de predispus la contaminare microbiologică, în special în condiții suboptime de depozitare. Acest studiu a investigat efectele a trei regimuri distincte de depozitare — temperatura camerei, refrigerare și congelare — asupra calității microbiologice și organoleptice a orezului gătit, având ca obiectiv identificarea ferestrelor de consum sigur și minimizarea degradării calității. Evaluările microbiologice au fost realizate în conformitate cu standardele ISO relevante, iar evaluarea senzorială a fost efectuată utilizând o metodă descriptivă de scor de către un panel instruit. Rezultatele au evidențiat că orezul păstrat la temperatura camerei a devenit nesigur din punct de vedere microbiologic după 24 de ore. În schimb, refrigerarea a menținut siguranța microbiologică până în ziua a cincea, iar congelarea a asigurat stabilitatea generală pentru o perioadă de până la trei luni. Totuși, calitatea senzorială s-a deteriorat progresiv în toate condițiile, cele mai pronunțate modificări

fiind observate în probele congelate mai mult de 90 de zile. Aceste rezultate subliniază rolul esențial al condițiilor adecvate de depozitare în asigurarea siguranței alimentare și conservarea caracteristicilor senzoriale. Deși studiul nu propune inovații tehnologice, el oferă un cadru practic prin integrarea evaluărilor microbiologice și senzoriale într-un model reproductibil, aplicabil atât în mediul educațional, cât și în cel profesional.

Cuvinte-cheie: *orez gătit, condiții de depozitare, refrigerare, congelare, analiză microbiologică, evaluare senzorială, siguranța alimentelor*.

1. Introduction

Rice is one of the most widely consumed foods globally, serving as an essential source of carbohydrates, proteins, and micronutrients for more than half of the world's population [1]. It is also often cooked in advance and stored for later consumption, which can significantly influence both its nutritional value and food safety [2].

The quality of cooked rice is affected by factors such as temperature, humidity, and storage duration, which directly influence the development of microflora and the occurrence of physicochemical changes [3]. Due to its high-water content and carbohydrate-rich composition, cooked rice becomes a favorable substrate for microbial growth, especially when stored at room temperature [4]. The presence of pathogenic agents such as *Bacillus cereus* is well documented in the literature under these conditions and is frequently associated with foodborne illnesses [5].

On the other hand, refrigeration and freezing are effective methods for slowing microbial growth, but they can negatively impact the sensory properties of the product through processes such as starch retrogradation, texture modification, and flavor loss [6]. Studies indicate that prolonged storage can lead to changes in consistency, aroma, and appearance, affecting the overall acceptability of the product [7,8].

In this context, the present study aims to analyze the impact of storage conditions on the microbiological and organoleptic quality of cooked rice. The study compares three experimental conditions (room temperature, refrigeration, and freezing) to determine optimal storage intervals from the perspective of food safety and sensory acceptability.

2. Materials and Methods

The following materials were used in the study:

- Round-grain rice groats (*Bunetto* brand, code SM 1004), commercially available, with fine granulation and a high starch content, suitable for preparing a liquid-consistency porridge.
- Purified, still drinking water (*OM* brand), certified in accordance with the FSSC 22000 standard.
- Cooked rice, obtained according to the protocol described below, portioned and stored in sterile containers.
- Experimental samples of cooked rice, cooled and subsequently stored under different temperature regimes for varying durations.
- Culture media and laboratory reagents, used for microbiological analyses, in accordance with the ISO standards referenced in Section 2.4.

2.1.2. Protocol for Thermal Processing

The cooking process was conducted under standardized conditions, as outlined in Table 1.

Table 1

Standardized boiling conditions applied to cooked rice samples

Parameter	Specification
Type of rice	Round-grain rice
Water-to-rice ratio	2:1
Cooking vessel	Stainless steel pot, 22 cm diameter
Final consistency	Liquid (soft porridge)
Cooking method	Boiling on stovetop, uncovered
Boiling temperature	100°C

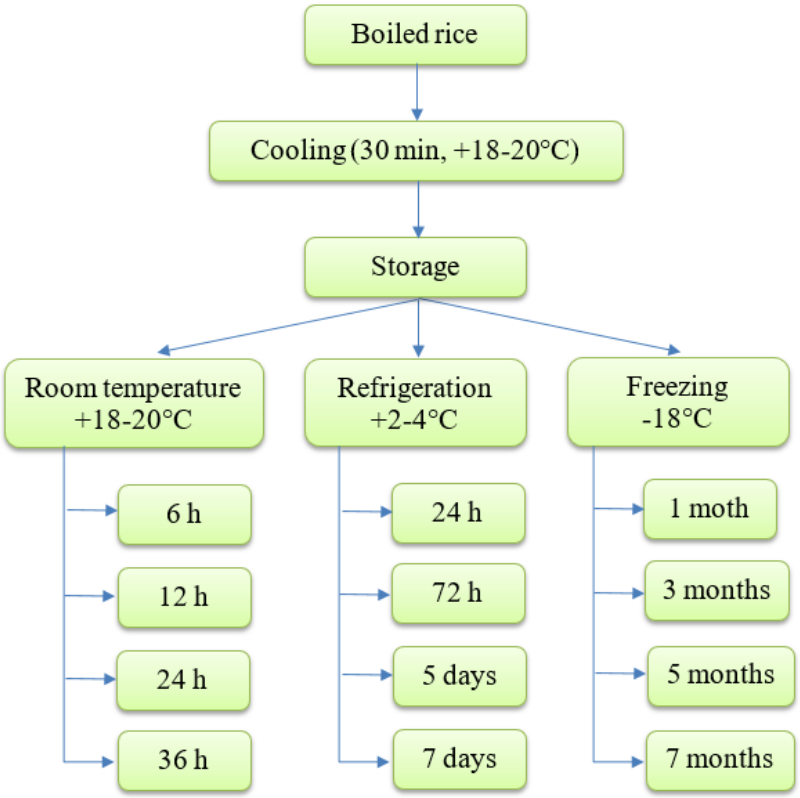

Figure 1. Storage Scheme of Boiled Rice Based on Thermal Regime.

After boiling, the rice was left to cool for 30 minutes at room temperature (+18...+20°C) in a hygienic environment, uncovered, to allow for texture stabilization.

2.1.3. Storage Protocol

Cooked rice samples were divided into equal batches and stored in sterile, airtight containers. Three temperature regimes were used for storage, as follows:

- Room temperature (+18...+20°C): 6 hours, 12 hours, 24 hours, and 36 hours.
- Refrigeration (+2...+4°C): 24 hours, 72 hours, 5 days, and 7 days.
- Freezing (−18°C): 1 month, 2 months, 3 months, and 5 months.

The batches were subsequently evaluated from both microbiological and organoleptic perspectives at each time point. The storage process is illustrated schematically in Figure 1.

2.2. Laboratory Equipment and Materials

The following equipment and consumables were used in the experiment, all compliant with good laboratory practice requirements (Table 2) [9,10].

Table 2

Equipment and consumables used for the preparation, storage, and analysis of cooked rice samples

Equipment	Model / Brand	Country of Origin	Purpose
Precision scale	Kern FCB 6K1	Germany	Accurate weighing of ingredients and sample portions
Microwave oven	Samsung MG23K3575AS	South Korea	Uniform reheating of samples (if applicable)
Laboratory refrigerator	Liebherr TP 1410	Germany	Storage of samples at controlled temperature (+2…+8 °C)
Vertical freezer	Liebherr GP 1486	Germany	Storage of samples at −18 °C
Bacteriological incubator	Unspecified model	-	Incubation of Petri dishes at 30 °C and 37 °C
Laminar flow microbiological cabinet	Unspecified model	-	Aseptic handling during inoculation
Digital thermometer	Unspecified model	-	Temperature monitoring during sample storage
Culture media (PCA, VRBL, XLD, Baird-Parker)	Merck, Bio-Rad	Germany, France	Microbiological determinations in accordance with ISO standards [11,13–15]

All disposable materials were sterilized prior to use or supplied in a sterile state. The culture media were prepared according to the manufacturers' instructions [11] and used in compliance with the ISO standards specific to each type of analysis [12-15].

2.3. Sample Storage Protocol

After boiling, the rice was allowed to cool at room temperature (+18…+20°C) for 30 minutes, uncovered, under controlled hygienic conditions. The samples were then portioned into sterile, single-use food-grade plastic containers, sealed tightly, and properly labeled.

According to the analytical objectives, the samples were divided into three experimental batches, each subjected to a distinct storage regime:

- At room temperature (+18…+20 °C): evaluation was performed after 6, 12, 24, and 36 hours.
- Under refrigeration (+2…+4 °C): samples were analyzed after 24 hours, 72 hours, 5 days, and 7 days.
- Under freezing (−18 °C): evaluation was conducted after 1 month, 2 months, 3 months, and 5 months.

All samples were stored in designated spaces, without significant variations in temperature or exposure to light. Storage was carried out without opening the containers until the time of microbiological and organoleptic testing.

The overall structure of the experimental design is illustrated schematically in Figure 1.

2.4. Analytical Methods

To assess the influence of storage conditions on product quality, the cooked rice samples were analyzed from both microbiological and organoleptic perspectives, in accordance with internationally recognized protocols. The analytical methods were systematically applied to all experimental batches in parallel, using equipment and materials compliant with food safety standards.

2.4.1. Microbiological Analysis

Microbiological determinations were carried out in accordance with international ISO standards, using both selective and non-selective culture media, as specified in Table 3. All samples were processed under aseptic conditions, employing a laminar flow microbiological cabinet and sterile materials. Results were expressed in colony-forming units (CFU/g), and interpretation was performed in compliance with Regulation (EC) No 2073/2005 on microbiological criteria for foodstuffs.

Table 3

Applied microbiological methods and incubation conditions

Target Microorganism	Culture Medium	Incubation Conditions	Reference Standard
Total viable count (TVC)	Plate Count Agar (PCA)	30 °C for 72 h	ISO 4833-1:2013 [13]
Enterobacteriaceae	Violet Red Bile Glucose Agar (VRBL)	37 °C for 24 h	ISO 21528-2:2017 [14]
Salmonella spp.	Xylose Lysine Deoxycholate Agar (XLD)	37 °C for 24 h	ISO 6579-1:2017 [15]
Staphylococcus aureus (coagulase-positive)	Baird-Parker Agar	37 °C for 48 h	ISO 6888-1:2021 [16]

2.4.2. Organoleptic Evaluation

The organoleptic analysis was conducted in accordance with the SR ISO 6658:2017 standard on sensory analysis methodology, using the descriptive scoring method. The evaluation was carried out in a dedicated, well-lit room, free of extraneous odors, and maintained at a constant ambient temperature.

The tasting panel consisted of 10 individuals aged between 22 and 60 years, previously familiarized with the analyzed product and the scoring methodology. Each participant received coded samples of cooked rice from all experimental batches, served in single-use containers at the optimal temperature for tasting.

The reference attribute was overall sensory quality, assessed based on four criteria: visual appearance, aroma, taste, and texture. Each criterion was rated on a scale from 1 (unsatisfactory) to 5 (excellent). The final score was expressed as the arithmetic mean of the ratings given by all panelists for each criterion and each individual sample.

Samples were presented in random order to minimize psychological bias. Between samples, panelists used still water to cleanse the palate.

3. Results and Discussion

3.1. Evolution of Microbial Load Depending on Storage Regime and Duration

The evolution of the microbiological quality of cooked rice was analyzed based on the applied storage conditions and the duration of storage. The analyses focused on the presence and

dynamics of mesophilic aerobic and facultative anaerobic flora, coliforms, *Staphylococcus aureus* bacteria, and *Salmonella spp.* strains, for each of the experimental batches evaluated.

Under room temperature storage conditions (+18...+20°C), an increase in mesophilic aerobic flora was observed as early as the first 12 hours, from <10 CFU/g to 3.4×10^2 CFU/g. After 24 hours, the values exceeded the acceptable limit (1.1×10^3 CFU/g), reaching 2.1×10^3 CFU/g at 36 hours. The detailed evolution of the microbial load is presented in Table 4. During this period, coliforms, *Staphylococcus aureus*, and *Salmonella spp.* we're not detected.

Table 4

Microbiological Results for Cooked Rice Stored at Room Temperature

Admissible Limit (According to Regulation EC No. 2073/2005)	**Mesophilic Aerobic and Facultative Anaerobic Bacteria (CFU/g)**	**Coliform Bacteria (in 0.01 g of product)**	**Staphylococcus aureus (in 1 g of product)**	**Salmonella spp. (in 25 g of product)**
	⩽ 1.0×10^3	**Absence**	**Absence**	**Absence**
Storage Duration	<10	Not detected	Not detected	Not detected
6 hours	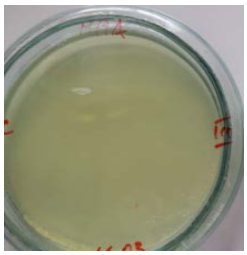			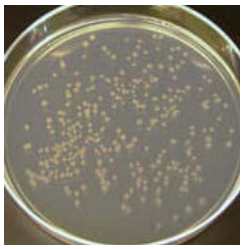
12 hours	3.4×10^2 	Not detected 	Not detected 	Not detected 
24 hours	1.2×10^3 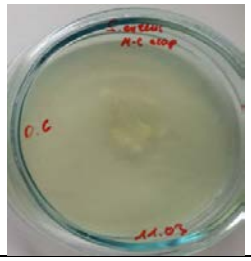	Not detected 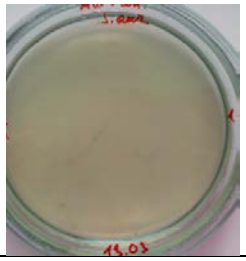	Not detected 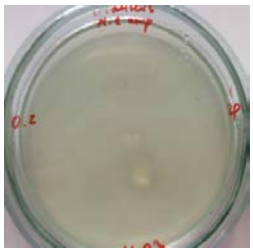	Not detected 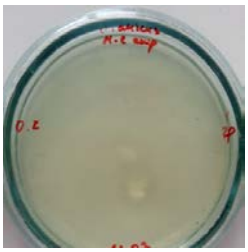
36 hours	2.1×10^3 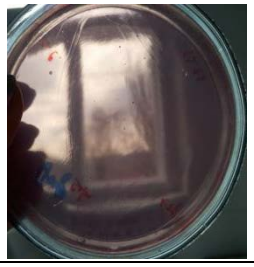	Not detected 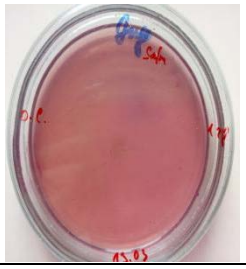	Not detected 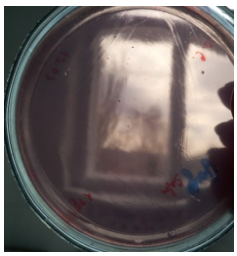	Not detected 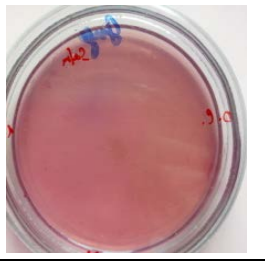

Under refrigeration conditions (+2…+4 °C), the evolution of the microbial load was significantly slowed. Values remained within admissible limits until the fifth day; however, on the seventh day, the critical threshold (1.5×10^3 CFU/g) was exceeded, and coliform colonies appeared, indicating the onset of spoilage. No pathogenic microorganisms were detected during this period.

Under freezing conditions (−18 °C), the samples remained microbiologically stable up to the third month. After this period, the bacterial load began to gradually increase, reaching 2.5×10^3 CFU/g by the fifth month, thus exceeding the maximum admissible limit. Throughout the entire freezing period, no presence of coliforms, *Salmonella spp*., or *Staphylococcus aureus* was detected (Table 5).

Table 5

Microbiological Results for Cooked Rice Stored Under Refrigeration and Freezing Conditions

Storage Regime	Storage Duration	Mesophilic Aerobic and Facultative Anaerobic Bacteria (CFU/g)	Coliform Bacteria (in 0.01 g of product)	*Staphylococcus aureus* (in 1 g of product)	*Salmonella* spp. (in 25 g of product)
Refrigeration (+2…+4°C)	24 h	<10	Not detected	Not detected	Not detected
Refrigeration (+2…+4°C)	3 days	5.0×10^2	Not detected	Not detected	Not detected
Refrigeration (+2…+4°C)	5 days	8.0×10^2	Not detected	Not detected	Not detected
Refrigeration (+2…+4°C)	7 days	1.5×10^3	Detected	Not detected	Not detected
Freezing (−18°C)	1 month	<10	Not detected	Not detected	Not detected
Freezing (−18°C)	2 months	<10	Not detected	Not detected	Not detected
Freezing (−18°C)	3 months	4.5×10^2	Not detected	Not detected	Not detected
Freezing (−18°C)	5 months	2.5×10^3	Not detected	Not detected	Not detected

The obtained results highlight the essential role of storage temperature in controlling the development of spoilage microflora in cooked rice. The rapid increase in mesophilic flora at room temperature is correlated with favorable conditions for bacterial growth (high humidity, neutral pH, and optimal temperature for development). These findings are consistent with previous studies, which indicate accelerated spoilage of rice-based preparations left at ambient temperature for more than 6–12 hours [17,18].

The microbiological stability observed under refrigeration up to day five is a positive outcome; however, the presence of coliforms on day seven confirms that refrigeration slows but does not entirely inhibit bacterial growth. Freezing, while effective in maintaining a low microbial load in the medium term, does not completely prevent long-term bacterial proliferation—likely due to the reactivation of bacteria after thawing and structural degradation of the samples.

The systematic absence of major pathogenic agents (*Salmonella spp.* and *Staphylococcus aureus*) may indicate good hygiene practices during preparation and handling, but this cannot be generalized beyond controlled laboratory conditions.

These data support the practical recommendation to consume cooked rice within 24 hours if stored at room temperature, within 5 days if refrigerated, or within 3 months if frozen—under optimal hygienic conditions.

3.2. Evolution of Organoleptic Characteristics Depending on Storage Conditions

The sensory analysis aimed to assess how the appearance, aroma, taste, and texture of cooked rice change depending on the storage regime and duration. The evaluation was performed by a panel of 10 trained individuals, using a five-point scale for each sensory attribute, where 5 represented excellent quality and 1 indicated an unacceptable product.

Storage at room temperature. After 12 hours, the samples were rated as having acceptable sensory characteristics. However, starting from 24 hours, a clear decline in organoleptic quality was observed, particularly in terms of aroma and taste, which received average scores of 2.8 and 2.5, respectively. After 36 hours, all four attributes scored below 2, with the appearance becoming wet and unattractive, the texture sticky, and the aroma noticeably altered (Figure 2. Results of the sensory evaluation of cooked rice stored at room temperature).

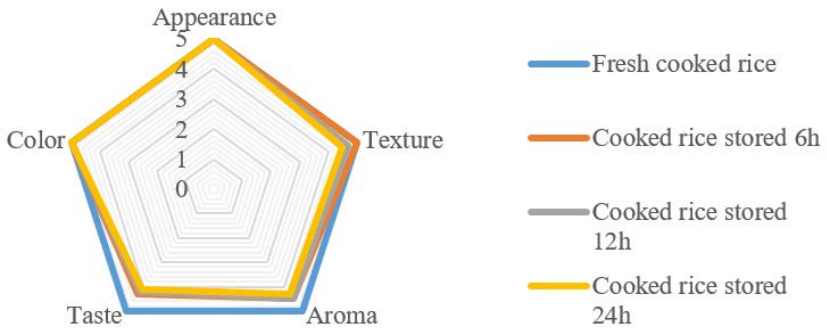

Figure 2. Results of the sensory evaluation of cooked rice stored at room temperature.

Refrigeration Regime (+2...+4 °C). Samples stored under refrigeration and evaluated after 24 hours maintained good sensory quality, with scores above 4 for all attributes. Slight declines were observed on days three and five, particularly in aroma and taste. After 7 days, the taste was considered slightly altered, and the texture was perceived as wetter compared to fresh samples. The scores decreased to average values between 2.9 and 3.2 (Figure 3. Results of the sensory evaluation of cooked rice stored under refrigeration conditions).

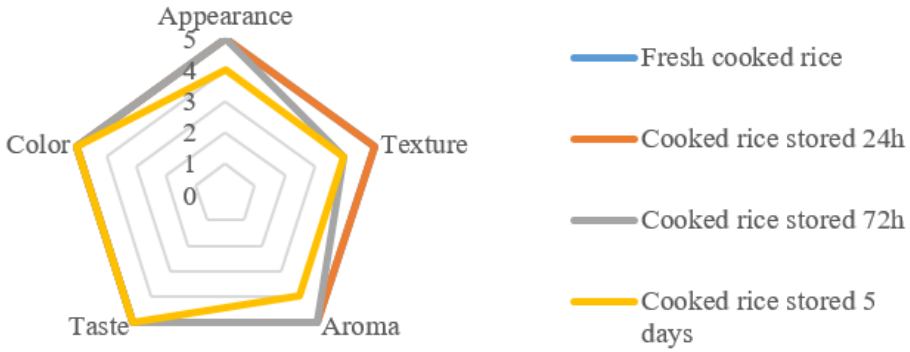

Figure 3. Results of the sensory evaluation of cooked rice stored under refrigeration.

Freezing Regime (–18 °C). Freezing allowed for the preservation of sensory characteristics for up to two months, with scores ranging between 4.0 and 4.5. In the third month, the panel observed a decline in texture and a slight loss of flavor, while in the fifth month, the changes were pronounced: the texture became soft and watery, the taste was bland, and the overall appearance was unsatisfactory. Scores dropped below 3 for all attributes, indicating advanced deterioration (Figure 4).

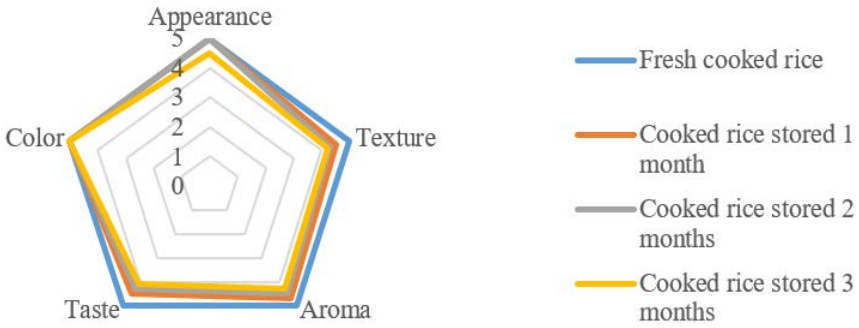

Figure 4. Results of the sensory evaluation of cooked rice stored at freezing temperature (–16...–18 °C).

The obtained data suggest that sensory changes are influenced by physicochemical reactions occurring during storage, particularly starch retrogradation and moisture migration. The results are consistent with previous research [19,20], which showed that rice-based foods are highly sensitive to textural and aromatic alterations during cold storage. Freezing best preserves the sensory profile during the initial months; however, cumulative negative effects become clearly noticeable after 90 days, especially in terms of taste and texture.

Considering these observations, it is recommended that cooked rice be consumed within 24 hours if stored at room temperature, within 3–5 days under refrigeration, and within a maximum of 2 months if frozen, in order to ensure acceptable sensory quality.

4. Conclusions and Recommendations

The results obtained in this study highlight the significant influence of storage conditions on the microbiological and organoleptic quality of cooked rice.

From a microbiological perspective, it was found that rice becomes unsafe for consumption after 24 hours of storage at room temperature due to the exceeding of permissible limits for mesophilic flora. Under refrigeration, microbiological safety is maintained up to the fifth day, while freezing ensures microbiological stability up to the third month. The presence of coliforms on day seven (refrigeration) and the increase in mesophilic load in the fifth month (freezing) indicate the onset of spoilage.

The sensory analysis confirmed the gradual degradation of organoleptic quality, reflected in the loss of aroma and taste, as well as changes in texture. The most affected samples were those stored under freezing conditions for more than 90 days, where starch retrogradation led to compacted texture and diminished flavor.

Based on the results obtained, the following maximum storage durations for cooked rice are recommended:

- up to 24 hours at room temperature (+18...+20 °C);
- up to 5 days under refrigeration (+2...+4 °C);
- up to 3 months under freezing (–18 °C), in sterile containers with no intermediate opening.

The results provide valuable scientific support for optimizing cooked rice storage practices, contributing to reduced food waste and increased consumer safety. These findings are relevant not only for households but also for catering units, public institutions, and operators in the food industry.

Although the study does not propose methodological or technological innovations, its merit lies in its practical synthesis of the effects of storage conditions on a widely consumed food, under controlled laboratory conditions. The work offers a simple model for combined microbiological and sensory evaluation, with didactic and practical applicability, which can be used in educational activities as well as to guide consumers toward safer storage practices.

Acknowledgments. The authors gratefully acknowledge the support provided by the Institutional Project 020405 "Optimizing food processing technologies in the context of the circular bioeconomy and climate change" (Bio-OpTehPAS), implemented at the Technical University of Moldova.

Conflicts of Interest: The authors declare no conflict of interest.

References

1. Juliano, B.O. *Rice: Chemistry and Technology*, 2nd ed. American Association of Cereal Chemists, St. Paul, MN, USA, 1985, pp. 1–17.
2. Kaur, B.; Ranawana, V.; Henry, J. The Glycemic Index of Rice and Rice Products: A Review, and Table of GI Values. *Crit. Rev. Food Sci. Nutr.* **2016**, *56*, pp. 215–236.
3. Zhou, Z.; Robards, K.; Helliwell, S.; Blanchard, C. Effect of Storage Temperature on Cooking Behaviour of Rice. *Food Chem.* **2007**, *105*, pp. 466–470.
4. International Rice Research Institute (IRRI). *Rice Grain Quality and Marketing*. IRRI, Los Baños, Philippines, 1985, pp. 16–17.
5. Kramer, J.M.; Gilbert, R.J. Bacillus cereus and Other Bacillus Species. In: *Foodborne Bacterial Pathogens*; Doyle, M.P., Ed. Marcel Dekker. New York, USA, 1989, pp. 21–70.
6. Perdon, A.A.; Siebenmorgen, T.J.; Buescher, R.W.; Gbur, E.E. Starch Retrogradation and Texture of Cooked Milled Rice during Storage. *J. Food Sci.* **1999**, *64*, pp. 828–832.
7. Champagne, E.T.; Bett-Garber, K.L.; McClung, A.M.; Bergman, C. Sensory Characteristics of Diverse Rice Cultivars as Influenced by Genetic and Environmental Factors. *Cereal Chem.* **2004**, *81*, pp. 237–243.
8. World Health Organization (WHO). *Foodborne Disease Outbreaks: Guidelines for Investigation and Control*; WHO: Geneva, Switzerland, 2008, 157 p.
9. International Organization for Standardization. *Microbiology of the food chain — General requirements and guidance for microbiological examinations*. ISO 7218:2007. ISO: Geneva, Switzerland, 2007.
10. European Parliament and Council. Directive 2004/10/EC of the European Parliament and of the Council of 11 February 2004 on the harmonisation of laws, regulations and administrative provisions relating to the application of the principles of good laboratory practice and the verification of their applications for tests on chemical substances. *Off. J. Eur. Union* **2004**, *L50*, pp. 44–59.
11. Merck KGaA. Technical Information for Culture Media: PCA, VRBL, XLD, and Baird-Parker Agar. Available online: https://www.sigmaaldrich.com (accessed on 9 April 2025).
12. International Organization for Standardization. *Microbiology of the food chain — Horizontal method for the enumeration of microorganisms — Part 1: Colony count at 30 degrees C by the pour plate technique*. ISO 4833-1:2013. ISO: Geneva, Switzerland, 2013.
13. International Organization for Standardization. *Microbiology of the food chain — Horizontal method for the detection and enumeration of Enterobacteriaceae — Part 2: Colony-count technique*. ISO 21528-2:2017. ISO: Geneva, Switzerland, 2017.
14. International Organization for Standardization. *Microbiology of the food chain — Horizontal method for the detection, enumeration and serotyping of Salmonella — Part 1: Detection of Salmonella spp.* ISO 6579-1:2017. ISO: Geneva, Switzerland, 2017.

15. International Organization for Standardization. *Microbiology of the food chain — Horizontal method for the enumeration of coagulase-positive staphylococci (Staphylococcus aureus and other species) — Part 1: Technique using Baird-Parker agar medium*. ISO 6888-1:2021. ISO: Geneva, Switzerland, 2021.
16. International Organization for Standardization. *Microbiology of the food chain — Horizontal method for the enumeration of coagulase-positive staphylococci (Staphylococcus aureus and other species) — Part 1: Technique using Baird-Parker agar medium*. ISO 6888-1:2021. ISO: Geneva, Switzerland, 2021.
17. Ahmed, T.; Riaz, M.; Hussain, M.; Akhtar, S.; Niaz, B.; Amjad, M. Microbiological Safety of Rice Dishes Stored at Ambient Temperature: A Public Health Concern. *J. Food Saf.* 2019**,** *39,* e12651.
18. Li, Y.; Chen, M.; Zhang, H.; Liu, D. Microbial Changes and Quality Deterioration in Ready-to-Eat Rice During Room Temperature Storage. *Food Control* 2022, *137,* 108986.
19. Zhao, Y.; Huang, Z.; Ma, X.; Shen, Q. Starch Retrogradation and Quality Changes in Cooked Rice During Storage. *J. Cereal Sci*. 2021, *98,* 103193.
20. Martín-Peláez, S.; Cano-Lamadrid, M.; Hernández, F.; Sendra, E. Changes in Aroma and Texture of Rice-Based Foods During Cold Storage. *Foods* 2020, *9,* 1218.

Citation: Vîrlan, A.; Siminiuc, R. The impact of storage conditions on the microbiological and organoleptic quality of cooked rice. *Journal of Engineering Science*. 2025, XXXII (1), pp. 125-135. https://doi.org/10.52326/jss.utm.2025.8(2).10.

Submission of manuscripts: jes@meridian.utm.md

Journal of Engineering Science *Vol. XXXII, no. 1 (2025), pp. 136 - 150*
Fascicle *Food Engineering* *ISSN 2587-3474*
Topic *Food Industry and Management* *eISSN 2587-3482*

https://doi.org/10.52326/jes.utm.2025.32(1).11
UDC 633.1:664

CURRENT AND PROSPECTIVE DIRECTIONS IN THE USE OF THE GRAIN CROPS TRITICALE

Daria Suhovici [1], ORCID: 0009-0000-7112-691X,
Sergiu Paiu [1*], ORCID: 0009-0008-0931-8521,
Iurie Rumeus [1,2], ORCID: 0000-0002-6392-7343,
Olga Boeștean [1], ORCID: 0000-0002-0390-3550,
Georgiana Gabriela Codină [3], ORCID: 0000-0002-6575-0078,
Aliona Ghendov-Mosanu [1], ORCID: 0000-0001-5214-3562

[1] *Technical University of Moldova, 168 Stefan cel Mare Blvd., Chisinau, Republic of Moldova*
[2] *Cahul State University "Bogdan Petriceicu Hasdeu", 1 Independence Square, Cahul, Republic of Moldova*
[3] *"Stefan cel Mare" University, 720229 Suceava, Romania*
* Corresponding author: Sergiu Paiu, *sergiu.paiu@doctorat.utm.md*

Received: 01. 18. 2025
Accepted: 02. 28. 2025

Abstract. Triticale is a young crop that combines the main qualities of its ancestors - rye and wheat. This grain crop has a higher quality amino acid composition, which allows its use as raw material not only for special-purpose food products, but also for the feed industry. It is also less demanding of weather conditions and is resistant to various diseases, which allows increasing the grain harvest per hectare of crops. Breeding triticale varieties that combine high protein content with good biological quality is an important task for researchers. First of all, triticale is a grain crop, which allows expanding the range of foods and improving their nutritional value, since these products are in demand among consumers. Deficiency of protein and dietary fiber in the population's diet is still a pressing problem today. Triticale, in turn, can solve a number of problems associated with malnutrition, which makes research in this area promising and worthy of attention.

Keywords: *triticale, wheat, rye, chemical composition, protein, food, quality.*

Rezumat. Triticale este o cultură tânără care combină principalele calități ale strămoșilor săi - secara și grâul. Această cultură de cereale are o compoziție de aminoacizi de calitate superioară, ceea ce permite utilizarea sa ca materie primă nu numai pentru produsele alimentare de specialitate, ci și pentru industria furajelor. De asemenea, este mai puțin pretențios față de condițiile meteorologice și este rezistent la diferite boli, ceea ce permite creșterea recoltei de cereale la hectar de cultură. Creșterea soiurilor de triticale care combină conținutul ridicat de proteine cu o bună calitate biologică este o provocare importantă pentru cercetători. Studiul realizat a demonstrat o posibilă extindere a gamei de produse alimentare și îmbunătățirea valorii lor nutritive, deoarece aceste produse sunt solicitate în rândul consumatorilor. Deficitul de proteine și fibre alimentare din alimentația populației rămâne încă o problemă actuală a zilelor noastre. Triticale, la rândul său, poate rezolva o serie de

probleme asociate malnutriției, ceea ce face ca cercetările în această direcție să fie promițătoare și să merite atenție.

Cuvinte cheie: *triticale, grâu, secară, compoziția chimică, proteine, alimente, calitate*.

1. Introduction

Particular interest in triticale as a valuable crop is caused by its hybrid features, combining the qualitative characteristics of rye and wheat. Despite the well-known successes of wheat breeding in developing new varieties that combine high productivity, good nutritional qualities, resistance to lodging, responsiveness to fertilizers and other valuable characteristics, it still has a weak expression of a number of important characteristics, first of all, this is insufficient resistance to the action of some unfavorable soil, climatic and environmental factors [1]. Practitioners note that the beneficial qualities of rye are poorly expressed in wheat. Wheat is very sensitive to temperature drops, excess salt, does not tolerate increased soil acidity, is more susceptible to fungi, needs organic and mineral fertilizers to a greater extent, etc. In addition, due to the ability to form a large number of spikelets in an ear (up to 50-60, with 20-25 in wheat), rye has higher potential and grain productivity [2]. The triticale ear is a combinatorial coalescence of morphological features of rye and wheat plants on which the yield depends: multi-spikelet ear (in rye), and multi-flowered ear (in wheat).

It should also be noted that protein deficiency and undernourishment in the world are increasing every year and can reach 30% in Central Africa and South Asia [3]. The data presented allow us to conclude that a fairly large part of the world's population suffers from protein deficiency - a disease that is a consequence of the imbalance between the formation and breakdown of protein. The alimentary cause of its occurrence is protein deficiency in the diet [4]. The European Union (EU) is mainly self-sustaining in agricultural area, due to its conventional policy of agriculture. Nevertheless, the EU livestock farming is severely relying on imports of proteins that are plant-based for cattle fodder. The connection between import of protein and clearcutting, if we look at it one way, and the major greenhouse gases from cattle raising, if we look at it another way, are also providing significant importance to the use of plant proteins in human nourishment. For a large number of adults living in Europe, the main source of protein is animal products such as meat and eggs, although plant sources are becoming increasingly popular [5].

The most popular source of vegetable protein for the population of the Republic of Moldova (RM) is bread and other bakery products and groceries. Bread consumption per person per year in Europe is about 58 kg. Although consumption of baked products varies greatly across the continent, in most countries the average consumption is 50 kg per capita. Examples of great bread consumers are Germany and Austria, with an average of 80 kg but in the RM the figure reaches 107 kg in 2023, while the United Kingdom and Ireland are at the bottom of the list with an annual consumption lower than 50 kg [6]. However, the nutritional value of traditional bread varieties does not fully meet the requirements of nutritionology, since the necessary balance of proteins and carbohydrates is not observed. As is known, without protein, a product cannot be considered complete, since it is what supplies our body with the necessary amino acids. The World Health Organization (WHO) sets the Safe Level of Protein intake at 0.83 g/kg/day [7].

The relevance of this work is that proteins of plant origin are currently the main resources of food and fodder protein and will not lose their importance in the near future.

Many scientists point to the primary importance of the amino acid composition of grain proteins as the most important factor in their food and feed value [8]. As is known, bread made from wheat flour is poor in the most important essential amino acid – lysine. Therefore, it is necessary to search for ways to increase the nutritional value of bread by expanding the raw material base of bakery production. In recent years, the grain crop triticale – an artificial hybrid of rye and wheat – has been increasingly recognized [9,10]. The new cereal crop has high potential yields and a number of valuable nutritional properties. Its amino acid composition is characterized by a significant content of glutamic acid, proline and a higher level of lysine, compared to wheat. All this contributes to the rapid spread of triticale culture across countries and continents and its gradual introduction into the flour-milling, baking, feed and even alcohol industries. However, despite the ongoing research on the creation, improvement and perfection of triticale crop selection, the technological features of triticale grain have still not been sufficiently studied, which does not allow for the expansion of mass production of flour and other products from this grain variety.

2. Features of triticale grain crop

Triticale is a young crop in evolutionary terms, synthesized by crossing chromosome complexes - wheat and rye. And only a little more than 30 years ago the first varieties were introduced into production. Today, its sown areas in the world amount to more than 3 Mha. The largest areas of triticale are in Poland (840 kha), Germany (537 kha), China (550 kha), Australia (400 kha), Ukraine (130 kha), in Russia they amount to 220 - 250 kha [11,12]. The interest of agricultural producers and processors in the new crop is steadily growing, the areas of its cultivation are expanding. The special interest in the crop is explained by the high potential of more complete protein content, better digestibility compared to wheat, high yield, resistance to unfavorable soil and climatic conditions, fungal and viral diseases, high winter hardiness, and reduced demands on soil fertility [13-15].

Figure 1. Triticale varieties obtained at the Institute of Genetics, Physiology and Environmental Protection, Moldova State University [22].

The term triticale arose from a combination of the generic names of the parent species of wheat - *Triticum* and rye - *Secale*. At first, this constant-intermediate hybrid was called *Triticosecale rimpau*, but the most widely used name was *Triticale*, which was proposed in his

work by E. Oehler [16]. Modern varieties have been created by breeders using complex methods and genetic tools, although there are known cases of spontaneous emergence of triticale under the influence of unusual conditions during vegetation [17-20].

Today, the triticale grain crop has ceased to be a botanical curiosity and, in modern conditions, successfully competes with traditional cereals, since the nutritional value of the grain has significant advantages over other crops [21]. For several decades, it has been used in production mainly for grain fodder and green fodder. However, in recent years, breeders have been working hard to create and introduce grain varieties suitable for obtaining flour for the purpose of baking bread and flour confectionery products, Figure 1 [22].

2.2. Morphology of grain crops and their selection

There are two main types of plants according to the vegetation period: winter and spring triticale. Winter triticale can differ greatly in morphological features depending on the origin of the parental forms. The morphology of triticale grain is intermediate [23]. There are 30 to 40 spikelets in an ear. The best grain-forage varieties of triticale exceed both rye and wheat in spikelet length and the number of spikelets in an ear. Ripening triticale ears often exceed 15 cm in length and are usually awned. Triticale grains are yellowish-brown, exceeding wheat grains in length, reaching 10-12 mm in length and up to 3 mm in width [24].

An important task in breeding any grain crop is to create varieties that have ecological plasticity, high productivity and grain quality, and resistance to abiotic and biotic stress. Currently, triticale breeding has achieved significant success in the field of creating highly productive varieties.

Breeding triticale for quality is associated with a number of difficulties, such as the large phenotypic variability of quantitative traits characterizing grain quality [25]. One of the main and difficult tasks is selection for a high level of protein, with high quality. To solve such a problem, biochemical technological assessment and genetic analysis of the selection material are necessary [26-29]. One of the real and promising ways of creating high-protein forms is to search for genomes that have factors of high protein content with good quality. For this purpose, it was proposed to involve the rye genome and the A genome of wheat [30,31]. Such data allow us to assume that one of the reserves for increasing the protein content is to increase the dose of the A genome in triticale.

3. Biochemical composition of triticale

The general chemical composition of triticale grain is typical for cereal grains, a characteristic feature of which is a high content of carbohydrates and protein. It should be noted that the chemical composition of triticale grain varies widely depending on the variety, production zone, agroecological and meteorological conditions [32,33].

Protein is an important building material for our body. Every cell of the body consists of it, it is part of all tissues and organs. In addition, a special type of protein plays the role of enzymes and hormones in a living organism.

3.1. Protein-proteinase complex of triticale grain

The special interest in wheat-rye amphidiploids observed recently is explained by the ability of the crop to accumulate a significant amount of protein of high biological value in the grain [34]. The amount of protein in any grain is the ratio of the endosperm to the pericarp and aleurone layer, however, in the newest varieties of triticale, which have well-formed grain, the amount of protein is equal to or slightly higher than in soft wheat varieties.

The special value of triticale grain protein is its high lysine content, which is 15-30% higher than that of wheat, a nearly ideal amino acid balance, and a lower content of antinutrients than that of other crops. The use of triticale protein to increase biological value is preferable to the use of other sources [35,36].

Triticale grain contains: 12.1 - 14.0% water, 12.8 - 15.1% proteins, 68.8 - 71.44% carbohydrates, 1.07 - 1.7% fat, 13.1 – 16.0% dietary fiber, and 1.5 - 2.0% ash [3,22,37,38]. The grain endosperm consists of 26-28% water-soluble proteins, 7-8% salt-soluble proteins, 25-20% alcohol-soluble proteins, and 18-20% acetic acid-soluble proteins. Most authors note that the total protein content in the grain of wheat-rye amphidiploids is higher than that of rye and wheat [39,40].

The nutritional value of protein depends on its content of essential amino acids. Studies conducted in the commonwealth of independent states (CIS) countries and abroad have shown that triticale protein is characterized by a well-balanced amino acid composition, as convincingly demonstrated by the following data, presented in Table 1 [41].

Table 1

Content of some amino acids in wheat, rye and triticale grains, % of total protein content

Name	Wheat	Rye	Triticale
Lysine	3.00	4.09	3.50
Histidine	2.25	2.25	2.35
Arginine	4.36	4.79	5.22
Glutamic acid	31.18	24.95	29.93
Proline	9.46	11.00	12.01

In terms of the content of amino acids lysine, aspartic, glutamic acids, threonine, alanine, valine, tyrosine, triticale grain proteins occupy an intermediate position between the proteins of wheat and rye. According to Bugstaller, triticale contains 14% more protein, 35% more methionine and 15 % more cysteine than wheat [42].

The combination of high protein content with the productivity of the best triticale varieties provides a high protein yield per hectare, 25-45% higher than that of wheat and rye. Two hectares of crops of the best triticale varieties are equivalent in protein yield to three hectares of wheat [43]. Significant variability in the protein and lysine content of triticale grain compared to wheat indicates the possibility of further improvement of quality in this indicator in parallel with selection for increased productivity and improved grain density [44].

3.2. Carbohydrate-amylase complex of triticale grain

The most important component of triticale grain is starch. Unlike its ancestors, triticale has a lower starch content in the grain. However, in terms of nitrogen, ash, fat and phosphorus content, triticale starch is practically no different from the starch of the parent forms. Only a lower amylose content is noted.

In terms of the shape of starch grains, triticale occupies an intermediate position between the parent forms, rye starch is characterized by the smallest size of starch grains with a content of fine fraction, and wheat - the largest. Triticale grain accumulates up to 5% of sugars, only an insignificant amount is accounted for by monosaccharides, and mainly fructosides predominate, the amount of which is close to rye. The amount of alcohol-soluble carbohydrates in triticale significantly exceeds that of wheat and is comparable to rye. Alcohol-soluble sugars accumulate up to 3%, of which oligosaccharides make up about 70%, fructose 0.1-7.0%, glucose - 1.9-5.0%, sucrose – 2.0-3.0%, maltose - 4-8% [45].

It should be remembered that immature triticale grain has a low starch content. This phenomenon is associated with high activity of α-amylase, which is of great importance for the technology of processing grain into flour for baking purposes. The presence of such a factor leads to defective bread. As is known, α-amylase is active in wheat only at the time of germination, unlike rye, where it is active even in a state of full ripeness [46].

3.3. Lipids of triticale grain

Many biochemical processes occurring during storage and processing, as well as the nutritional value of grain, largely depend on the characteristics of the lipid complex. As is known, along with the energy role, lipids perform functional and structural roles. It should be noted that the composition of triticale lipids is very complex and is not an intermediate form between wheat and rye. Free lipids contain 83-89% of non-polar components, mainly triglycerides. Bound lipids contain 61-73% of polar and 27-39% of non-polar components. The main components of polar groups are fatty acids - palmitic, stearic, linoleic and linolenic [47]. Their content in grain is affected by the growing region.

The synthesis of polyunsaturated fatty acids in the human body is limited, and since the lipids of triticale contain an increased content of linoleic acid, we can talk about the increased biological value of the crop. Native lipids of grain crops contain tocopherols (vitamin E), which are in an active form in vegetable oils. They are represented by the α-form, which indicates a low antioxidant activity of their lipids. Studies have revealed a high content of phospholipids in the fraction of bound lipids of triticale, which brings this crop closer to rye [47].

3.4. Micronutrients of grain

The question of the role of mineral substances and vitamins in cereal grains in supplying the human body with these substances, as well as the question of protein composition, is of particular relevance given the relatively large share of grain products in human nutrition.

Triticale grain and its milled products are a good source of such minerals as potassium, phosphorus, magnesium, sodium, copper, zinc and iron [48]. It is noted that triticale flour has an increased content of phosphorus, magnesium and iron compared to whole-grain wheat flour.

The vitamin composition of triticale (thiamine, riboflavin, biotin, folic acid, pantothenic acid) is at the same level as wheat. However, in general, its composition is better than that of rye, with the exception of nicotinic acid [49,50].

When grinding grain, mineral substances are distributed unevenly among the milled products. The greatest amount of phosphorus, iron, and manganese is contained in the bran of torn systems, which are characterized by the highest ash content (5.03-5.38%). A positive relationship was noted between the content of protein, phosphorus and manganese. It was found that the content of mineral substances in triticale flour is usually lower than in bran. Thus, it can be said that the mineral composition of triticale is at the same level as wheat, but in general the composition is better than that of rye [51].

4. Usage of triticale in bakery

The daily human diet includes grain products: bread, bakery and pasta, of particular interest is the use of whole grain flour, which contains a significant amount of fiber, all essential amino acids, vitamins, as well as micro- and macroelements such as magnesium,

calcium, potassium, sodium, iron, phosphorus, copper, zinc and selenium while having a low-cost price [52].

According to statistics, in RM the population actively consumes bakery and other flour products, in particular those made from premium and first grade wheat flour, due to their affordability, wide range and high energy value, Table 2.

Table 2

Average food consumption in the Republic of Moldova by categories [53]

Category	2021	2022	2023
Bread and flour products, kg/person	116.7	112.1	107.3
Meat products, kg/person	54.2	54.0	54.5
Dairy products, L/person	232.3	230.3	225.0
Vegetables, pumpkin and their processed products, kg/person	124.1	116.3	117.1
Fruits, berries and their processed products, kg/person	69.8	71.0	70.3

Insufficient balance of the chemical composition of such products is a problem of both quantitatively and qualitatively insufficiency of vitamins A, B, E, H, PP, dietary fiber, micro- and macronutrients in the diet [54].

One of the possible solutions is to use new raw material sources of plant origin. Triticale grain has an increased content of amino acids, including lysine, valine, leucine, etc. Therefore, triticale is the most promising for expanding the range of everyday food products. Triticale flour can be used to produce unfermented products such as waffles, muffins, gingerbread, cookies. There is sufficient data on the technology of their preparation in this area [55,56].

4.1. Flour and flour mixes

Traditional wheat and rye-wheat bread, which is the most popular among the population, has insufficient nutritional value and an imbalance of essential nutrients. The chemical composition of bread is not entirely complete in biological terms. Bread does not have a high enough protein content, and bread proteins are poor in essential amino acids, primarily lysine, tryptophan and methionine, and bread also lacks calcium salts and a number of vitamins [57].

Triticale grain has unique properties that are due to the predecessors of this crop. The whiteness of the flour and the presence of gluten proteins conventionally classify the grain as a wheat crop, and the high activity of amylolytic enzymes and the balance of proteins - as a rye crop. Due to its high frost resistance, as well as resistance to many diseases, triticale does not require treatment with additional plant protection products and the use of fertilizers. Despite the advantages of the crop in terms of nutritional value and the presence of gluten proteins, triticale grain is not in demand by the flour-milling industry as a raw material. The explanation for this is the difficulty of milling such grain according to the wheat type [58].

Today, triticale flour is mainly used as an improver and substitute for enzyme preparations, due to the high autolytic activity of flour. Methods have been developed to improve the quality and increase the nutritional value of rye and wheat bread with low amylase activity, gas and sugar-forming capacity. Various technological solutions are proposed for the possibility of using triticale flour as the main raw material for bakery production [57,58]. Flour is produced in three grades: sifted, peeled and wholemeal, in

accordance with the rules for organizing and conducting technological processes at flour mills and in compliance with approved sanitary norms and rules.

The researchers also proposed a method for obtaining triticale-rye-flax flour, according to which the initial raw material is first purified, then a grinding mixture is made from prepared triticale grain, rye grain and flax seeds in a ratio of 5.0:4.3:0.7. The need to enrich bakery flour with polyunsaturated fatty acids is justified by the fact that the human body cannot synthesize ω-3 and ω-6 fatty acids due to the lack of an enzyme system [59]. The invention will make it possible to obtain food flour with a rich content of mineral elements, water-soluble and fat-soluble vitamins, tocopherols and polyunsaturated fatty acids.

Table 3

Chemical composition of the control sample and triticale-rye-flaxseed flour with increased fat and protein content [59]

Name	Moisture content, %	Fat content, %	Protein content, %	Ash content, %
Original wheat flour	14.9	1.12	11.9	0.74
Triticale-rye-flaxseed flour	13.4	4.37	13.9	3.27

Analysis of the data in Table 3 shows that the resulting products are characterized by a high content of protein and fat, which allows them to be located as a high-lipid flour mixture in the production of a wide range of bakery and flour confectionery products, including functional products.

4.2. Bread

Attempts have been made over time to use triticale in the production of bread, biscuits and various pastas, but the prevalence of its use in food production remains low. The main reasons for this are the weak gluten system, high amylolytic activity and low stability of the technological properties of triticale grain [60]. Although triticale is characterized by high α-amylase activity and weak dough rheological properties, some varieties can produce bread of acceptable quality [61].

Studies have shown that the addition of 20-25% triticale flour improved wheat bread, especially from ordinary flour with low gluten quality due to the higher activity of amylases and proteases and high gluten extensibility. More recently, researchers have shown that a mixture of up to 50% triticale flour with wheat flour produced bread with a quality similar to that of wheat flour [62]. Baking bread from triticale flour in Hungary under industrial conditions has shown that sifted flour, but with a lower ash content, and rye type with an ash content of 0.9% give a high-quality bread, intermediate in its properties between wheat and rye. It was observed that mixing wheat and triticale flour in a ratio of 1:1 has a positive effect on the rheological properties. It is recommended to add triticale flour up to 30% to bake wheat bread. Bread with triticale flour is similar to wheat bread in appearance and crumb color and has good taste and aromatic properties [62].

A number of studies were conducted by Kharkov researchers to develop a technology for producing bakery products from triticale flour. When making bread from hulled and wholemeal triticale flour, the products were of unsatisfactory quality, with a sharp sour taste, dense crumb, and cracks in the upper crust. It was also shown that the method of producing bread from triticale flour cannot fully correspond to the methods used for making bread from

rye and wheat flour. Therefore, a concentrated lactic acid leaven with low acidity was added to the dough kneading. In addition, intensive kneading of the dough was excluded. Thus, new types of bakery products with increased biological and nutritional value using triticale flour are currently being actively developed [63]. Triticale bread had a specific taste and pleasant aroma, retained freshness for a long time. Systematic consumption of even 100 g of bread per day will allow the body to receive a significant share of the recommended average daily intake of essential amino acids, vitamins B, PP [64].

Ghendov-Mosanu et al. investigated the quality of different triticale varieties (Ingen 35, Ingen 33, Ingen 93, Ingen 54, Ingen 40, Fanica and Costel) grown in the RM from the point of view of the flour, dough, and bread quality characteristics. Triticale flours were analyzed for physicochemical quality and CIELab color parameters. It was demonstrated that triticale flours were suitable for bakery. According to the sensory data, all bread samples except those obtained from the Costel variety were of very good quality [22].

4.3. Biscuit and shortbread semi-finished products

One of the stable segments of the world market remains the confectionery market, which in recent years has been characterized by a constant increase in production and consumption volumes. The trend in recent years is an increase in consumer demand for healthy food products. These include functional confectionery products, including fortified ones [65].

Since triticale flour has a low gluten quality, but a high nutritional value, the possibility of its use in the production of flour confectionery products has been investigated. The effect of triticale flour on the quality of biscuit and shortbread semi-finished products has been studied [66]. In the recipes of these products, premium wheat flour was replaced by triticale flour in amounts of 20, 40, 60, 80 and 100%. Samples of finished products were analyzed in terms of sensory and physicochemical quality. As the dose of triticale flour increased, the color of the crumb of the finished product acquired a grayish hue, and the samples were characterized by uneven porosity and light compaction. The moisture content of the finished product in all experimental variants fluctuated insignificantly and remained within the limits provided by the standard (25±3%). The height of the semi-finished product slightly decreased with the increase in the dose of triticale flour from 2.6 cm to 2.2 cm [66].

4.4. Pasta

Triticale grain is a raw material for the flour and cereal industry. In addition, there is an increase in demand for products with increased biological value and functional food products, which include products with a high content of protein, vitamins, minerals [67]. To solve this problem, it is possible to use flour from modern varieties of triticale grain, which will increase the nutritional value of pasta and expand the range. Flour for the production of pasta is produced mainly in special flour mills from hard and soft high-vitreous wheat [68,69]. As a result of comprehensive studies of the physicochemical characteristics of triticale grain and the determination of the technological properties of its processed products, taking into account their quality indicators, a technology for the production of pasta flour from triticale grain has been developed, and the main technological parameters of the production process have been determined [69].

The versatility of the developed method lies in the possibility of obtaining the final product with the intended use in the form of semolina for culinary purposes or flour for the production of pasta, depending on the milling properties (vitreosity, grain hardness) [70].

Comparison of the developed method with the method for producing pasta flour from durum wheat during triticale grain processing showed that the general structure of technological operations and the selected equipment modes allow increasing the yield of semolina with a more uniform structure by size; extracting the endosperm part of higher quality grain with high efficiency; conducting an effective enrichment process, and reducing energy costs for obtaining the final product by reducing the technological process.

The quality of gluten affects the elasticity, strength (fragility), and roughness of pasta products. When producing pasta, they focus on the quality of gluten corresponding to weak groups I and II (60 - 90 units of the device IDK). Too weak gluten produces raw products prone to crushing and sticking, and strong gluten can lead to an increase in breakage and roughness of the finished product [71]. The data on the quality of gluten obtained from triticale grain indicate their compliance with weak groups I and II and also indicate a possible "strengthening" effect on the produced pasta.

Ribbon pasta is pasta formed in the form of threads that have an oval shape in cross section. During the studies, the obtained samples of pasta have pleasant organoleptic properties and are able to hold the shape of the product, among the disadvantages it is possible to highlight the dark shade of the cooked pasta. There is an insignificant difference in the coefficient of cooking, in the sample produced from flour of triticale grain of the "Bereket" variety, which indicates better dimensional stability [67]. It is also necessary to study and select additional ingredients to improve the appearance of the finished product, by adding wheat or rice flour, which will also improve the physicochemical quality indicators of the finished product. Thus, it is possible to expand the range of pasta products attractive to the consumer and endowed with increased biological value.

5. Alternative uses of triticale

Many researchers have proven that the nutritional value of food products containing substances of only animal or plant origin is low [72-75]. The use of plant raw materials in the production of milk, in addition to enriching it with functional ingredients, increases digestibility and allows you to get food products that meet human physiological norms. In recent years, scientists have been improving the technology of dairy products of high nutritional and biological value, the range of which is constantly expanding. One of the prospects for expanding the range of functional fermented milk products is the use of sources of natural biologically active substances. Such enrichments include grain crops [72].

5.1. Adding triticale culture to yogurt

The effect of triticale grains on the sensory properties, nutritional and biological value of a new yogurt with the addition of triticale grains was studied. Crushed triticale grains were used as a filler [72]. It was shown that the presence of 1.5% triticale grains in yogurt influenced the taste and smell, being very pleasant. The taste was slightly specific to triticale grains, the consistency was uniform. The taste and smell of the sample with 2% triticale grains, unlike the previous sample, had a slightly floury taste. The mixture was evenly distributed in the product volume. The consistency was uniform. The specific taste and smell of triticale grains in the 5% yogurt sample was very clearly visible. The mixture of triticale grains was unevenly distributed in the product volume, the consistency was uneven. During the sensory analysis, yogurt with 1.5% and 2% triticale received 4.8 and 4.6 points out of 10 for taste and smell. Thus, the introduction of ground triticale grains into the yogurt production recipe enriches the product with vitamins, microelements and dietary fiber, increases its shelf

life, improves sensory properties and does not require changes in the technological process of product production. Given the good taste properties and chemical composition of triticale grains, the production of yogurt with plant components allows improving its nutritional and biological properties and expanding the range of fermented milk products in the functional direction [72].

5.2. Using infrared radiation (IR) to make ready-to-eat breakfast

Currently, one of the areas of development of grain processing technology is the production of new types of products that do not require long cooking. These are, for example, baby and dietary food, ready-to-eat breakfast cereals. The application of infrared (IR) rays is especially promising in the production of such products. Dry breakfast cereals from cereal raw materials obtained by IR processing are widely used in the population's nutrition [73]. At the same time, it is necessary to address the issue of expanding the raw material base for the production of ready-to-eat breakfast cereals, in particular, using triticale grains. Various rational ways of IR processing of triticale grains to obtain a new product with high nutritional value and high content of dietary fiber in the form of flakes have been investigated. IR-processed triticale cereal flakes can be used as a ready-to-eat product in the form of dry breakfast cereals [74].

Slow heating of the grain resulted in its gradual drying. The moisture contained inside the grain was removed from it without damaging the grain structure. Rapid heating of triticale grains resulted in the evaporation of moisture inside the grain, which led to an increase in the water vapor pressure inside the triticale grain [75]. The grain “explodes” from the inside, leading to the destruction of the structural framework of the grain. The use of short-wave IR radiation of 0.9–1.1 μm for treatment of triticale grains ensures uniform heating of the grain throughout its volume. Treatment of triticale grains with IR rays, which causes the grain to “explode” from the inside, significantly affects the state of all grain components, affecting protein, carbohydrate and lipid complexes. The nature and depth of changes depend on the IR treatment modes. The carbohydrate complex of triticale grains, and primarily starch, undergoes the greatest changes as a result of IR treatment. Since water vapor fills the entire intermolecular volume, all starch granules of triticale grains are destroyed. The peeling of grains is accompanied by additional destruction of starch and an increase in the amount of dextrins in the product. Intensification of IR treatment leads to an increase in the amount of crumbs when flattening the grains. Immediately after IR processing, triticale grains are flattened into flakes while hot. The technology of obtaining a new food product from whole triticale grains allows for the preservation of fiber, which is explained by the presence of triticale grain husks during IR processing [76]. Thus, a new product in the form of triticale grain flakes was obtained, which has a high nutritional value and a high content of dietary fiber. It has a good appearance, a pleasant smell and taste, practically does not require cooking and is made available by simply adding boiling water or milk and can be used as a dry breakfast.

6. Conclusion

Triticale is a grain crop that undoubtedly has a promising future. At the present stage, it is already rightfully considered a viable commercial grain crop used in the production of human food and feed. The growing interest in the crop is caused by its great potential, as it is adapted to the conditions of all regions where wheat and rye grow. Increasing aridity, the

manifestation of other abnormal phenomena of climate and agriculture create conditions for greater preference for triticale in agricultural production compared to other cereals. In such situations, the advantage of new hexaploid triticale varieties becomes especially obvious. Being a hybrid, triticale embodied in its genome the highest ecological plasticity of winter rye.

Triticale combines the best features and properties of the parent species: it has large grain, contains a higher mass fraction of protein, and significantly exceeds other grain crops in terms of total protein yield per hectare. Breeding triticale varieties that combine high protein content with good biological quality is a difficult task due to the instability of the quantity and quality of protein in grain depending on the place of grain cultivation. In order to improve the biological quality of triticale protein, it is necessary to use wheat and rye varieties with high nutritional and feed value.

The above allows us to draw a conclusion about the advisability of further in-depth studies of the technological properties of triticale grain and flour in order to determine valuable and promising varieties for their effective use in the production and expansion of the range of bakery products. As well as continuing research in the field of developing technologies for dietary, therapeutic and prophylactic food products from triticale flour. When developing technologies and recipes for bakery products from triticale flour, it should be remembered that the production should be based on the principle of suppressing excess enzymatic hydrolysis of starch under the action of amylases during dough fermentation and bread baking, as well as increasing the initial acidity of the dough. The results of breeding, biochemical and technological studies presented in the monograph showed high efficiency of triticale production and its use for food and industrial purposes, which allows us to transfer this crop from the ranks of "scientific" to the category of industrial crops. And the scientific achievements obtained in this area of research should become the basis for further scientific forecasting in the work of breeders, agronomists and technologists.

Acknowledgments. This work was supported by a grant from the Ministry of Research, Innovation and Digitization, CNCS-UEFISCDI, project number PN-IV-P8-8.3-ROMD-2023-0078, within PNCDI IV and Institutional Project 020405 “Optimizing food processing technologies in the context of the circular bioeconomy and climate change”, Bio-OpTehPAS, being implemented at the Technical University of Moldova.

Conflicts of Interest: The authors declare no conflict of interest.

References

1. Filip, E.; Woronko, K.; Stępień, E.; Czarniecka, N. An Overview of Factors Affecting the Functional Quality of Common Wheat (*Triticum aestivum* L.). *International Journal of Molecular Sciences* 2023, 24, 7524.
2. Celestina, C.; Hunt, J.; Brown, H.; Huth, N.; Andreucci, M.; Hochman, Z.; Kohout, M. Scales of development for wheat and barley specific to either single culms or a population of culms. *European Journal of Agronomy* 2023, 147, 126824.
3. Jiang, W.; Zhao, Y.; Wu, X.; Du, Y.; Zhou, W. Health inequalities of global protein-energy malnutrition from 1990 to 2019 and forecast prevalence for 2044. *Public Health* 2023, 225, pp. 102-109.
4. Auerman, L.Ya. *Tekhnologiya hlebopekarnogo proizvodstva.* Professiya, Sankt-Peterburg, Rossiya, 2005, 416 p.
5. Albaladejo Román, A. EU feed autonomy: Closing the gaps in European food security. Available online: https://www.europarl.europa.eu/thinktank/en/document/EPRS_BRI(2023)739328 (accessed on 15.09.2024).
6. Bakery: European market, consumer trends, and innovation. Available online: https://www.ahfesproject.com/research/bakery-european-market-consumer-trends-and-innovation/ (accessed on 15.09.2024).

7. World Health Organization; Food and Agriculture Organization; United Nations University Protein and amino acid requirements in human nutrition. *WHO Technical Report Series* 2007, 935, 265 p.
8. Sokol, N.V. Biologicheskaya i pishchevaya cennost' hleba s pektinom iz muki sorta Veda. *Novye tekhnologii* 2009, 4, pp. 49-52.
9. Mesta-Corral, M.; Gómez-García, R.; Balagurusamy, N.; Torres-León, C.; Hernández-Almanza, A.Y. Technological and Nutritional Aspects of Bread Production: An Overview of Current Status and Future Challenges. *Foods* 2024, 13*,* 2062. https://doi.org/10.3390/foods13132062
10. Goryanina, T.A.; Medvedev, A.M. Baking grain quality of winter triticale, winter wheat and winter rye. *Grain Economy of Russia* 2020, 67, pp. 28-32.
11. Grabovec, A. I. Selekciya geksaploidnyh tritikale na povyshennuyu ekologicheskuyu plastichnost' i produktivnost'. *Evolyuciya nauchnyh tekhnologij v rastenievodstve* 2004, 2, pp. 12-19.
12. Tutel'yan, V.A.; Popova, T.S. *Novye strategii v lechebnom pitanii*. Medicina, Moskva, Rossiya, 2002, 144 p.
13. De Zutter, A.; Landschoot, S.; Vermeir, P.; Van Waes, C.; Muylle, H.; Roldán-Ruiz, I.; Haesaert, G. Variation in potential feeding value of triticale forage among plant fraction, maturity stage, growing season and genotype. *Heliyon 2023*, 9(1), e12760.
14. Biel, W.; Kazimierska, K.; Bashutska, U. Nutritional value of wheat, triticale, barley and oat grains. *Acta Scientiarum Polonorum Zootechnica 2020*, 19, pp. 19-28.
15. Gaviley, O.V.; Katerynych, O.O.; Ionov, I.A.; Dekhtiarova, O.O.; Griffin, D.K.; Romanov, M.N. Triticale: A General Overview of Its Use in Poultry Production. *Encyclopedia* 2024, 4, pp. 395–414.
16. Mergoum, M.; Gómez-Macpherson, H. Triticale improvement and production. *FAO Plant production and protection paper* 2004, 179, 172 p.
17. Randhawa, H.S.; Bona, L.; Graf, R.J. Triticale breeding - Progress and prospect. *Triticale* 2015, pp. 15-32.
18. Shimko, V.E.; Gordej, I.A. Geneticheskie osnovy sozdaniya i ispol'zovaniya samofertil'nyh linij ozimoj rzhi v selekcii na geterozis. *Molekulyarnaya i prikladnaya genetika* 2009, 10, pp. 69-79.
19. Grabovec, A.I. Metody i rezul'taty selekcii ozimoj tritikale na Donu: Tritikale. *Genetika, selekciya, agrotekhnika, ispol'zovanie zerna i kormov* 2010, 4, pp. 27-30.
20. Mujahid Alam, P.; Stephen, B.; Katherine, F. Emerging Trends in Wheat (*Triticum* spp.) Breeding: Implications for the Future. *Frontiers in Bioscience-Elite* 2024, 16(1), 2.
21. Oettler, G. The fortune of a botanical curiosity–Triticale: past, present and future. *The Journal of Agricultural Science* 2005, 5, pp. 329-346.
22. Ghendov-Mosanu, A.; Popa, N.; Paiu, S.; Boestean, O.; Bulgaru, V.; Leatamborg, S.; Lupascu, G.; Codină, G.G. Breadmaking Quality Parameters of Different Varieties of Triticale Cultivars. *Foods* 2024, 13, 1671.
23. Li, C.Y.; Li, W.H.; Lee, B.; Laroche, A.; Cao, L.P.; Lu, Z.X. Morphological characterization of triticale starch granules during endosperm development and seed germination. *Canadian Journal of Plant Science* 2011, 91(1), pp. 57-67.
24. Sokol, N.V. *Tritikale-kul'tura hlebnaya*. Palamarium Academic Publishing, Saarbrücken, Germany, 2014, 137 p.
25. Trini, J.; Maurer, H.P.; Neuweiler, J.E.; Würschum, T. Identification and Fine-Mapping of Quantitative Trait Loci Controlling Plant Height in Central European Winter Triticale (×*Triticosecale* Wittmack). *Plants* 2021, 10, 1592.
26. Bukreeva, G.I.; Kovtunenko, V.Ya. Hlebopekarnoe kachestvo zerna tritikale Krasnodarskoj selekcii. In: *Tezi dopovidej naukovo-prapktichnoi konferencii, Naukove zabespechennya virobnictva zerna tritikale i produktiv jogo pererobki*, 2005, pp. 4-35.
27. Kamanova, S.; Yermekov, Y.; Shah, K.; Mulati, A.; Liu, X.; Bulashev, B.; Ospankulova, G. Review on nutritional benefits of triticale. *Czech Journal of Food Sciences* 2023, 41(4), pp. 248-262.
28. Cui, L.; Xu, L.; Wang, H.; Fan, X.; Yan, C.; Zhang, Y.; Jiang, C.; Zhou, T.; Guo, Q.; Sun, Y.; et al. Evaluation of Dual-Purpose Triticale: Grain and Forage Productivity and Quality Under Semi-Arid Conditions. *Agronomy* 2025, 15, 881.
29. Makarska, E.; Ciolek, A.; Kociuba, W. Composition of gluten proteins and quality parameters of winter triticale hybrids. *Polish Journal of food and nutrition sciences* 2008, 58(3), pp. 341-344.
30. Han, G.; Yan, H.; Li, L.; An, D. Advancing wheat breeding using rye: a key contribution to wheat breeding history. *Trends in Biotechnology* 2025*,* 2, 14 p.
31. Li, G.; Wang, L.; Yang, J.; He, H.; Jin, H., Li, X.; Wang, D. A high-quality genome assembly highlights rye genomic characteristics and agronomically important genes. *Nature genetics* 2021, 53(4), pp. 574-584.
32. Donchenko, L.V. *Vysokie tekhnologii APK*. KGAU, Krasnodar, Rossiya, 2006, 384 p.
33. Zhu, F. Triticale: Nutritional composition and food uses. *Food Chemistry* 2018, 241, pp. 468-479.

34. Donchenko, L. V.; Sokol, N. V. Analiz himicheskogo sostava tritikale i ee vozmozhnosti v hlebopechenii. In: *Sbornik dokladov mezhdunarodnoj nauchnoj prakticheskoj konferencii «Pishchevye produkty 21 veka»* 2001, 1, pp. 123-136.
35. Muhova, A.; Stefka, D. Protein, lysine and methionine content in the grain of triticale grown under organic system. *Scientific Papers, Series A: Agronomy* 2020, pp. 158-164.
36. Jørgensen, H.; Thomsen, S. T.; Schjoerring, J. K. The potential for biorefining of triticale to protein and sugar depends on nitrogen supply and harvest time. *Industrial Crops and Products* 2020, 149, 112333.
37. Rakha, A.; Åman, P.; Andersson, R. Dietary fiber in triticale grain: Variation in content, composition, and molecular weight distribution of extractable components. *Journal of Cereal Science* 2011, 54(3), pp. 324-331.
38. Ghendov-Mosanu, A.; Ropciuc, S.; Dabija, A.; Saitan, O.; Boestean, O.; Paiu, S.; Rumeus, I.; Leatamborg, S.; Lupascu, G.; Codină, G.G. Effect of Brewers' Spent Grain Addition to a Fermented Form on Dough Rheological Properties from Different Triticale Flour Cultivars. *Foods* 2025, 14, 41.
39. Moskal, K.; Kowalik, S.; Podyma, W.; Łapiński, B.; Boczkowska, M. The Pros and Cons of Rye Chromatin Introgression into Wheat Genome. *Agronomy* 2021, 11, 456. https://doi.org/10.3390/agronomy11030456
40. Kenijz, N.V.; Sokol, N.V. Vliyanie razlichnyh krioprotektorov na reologiyu testa dlya polufabrikatov. *Molodoj uchenyj* 2014, 10, pp. 147-150.
41. Kazakov, E.D.; Karpilenko, G.P. *Biohimiya zerna i zernoproduktov*. GIORD, Sankt-Peterburg, Rossiya, 2005, 512 p.
42. Koryachkina, S.; Kuznecova, E.; Cherepnina, P. Ispol'zovanie zerna tritikale v tekhnologii zernovogo hleba. *Hleboprodukty* 2007, 5, pp. 38-40.
43. Silko, S.N.; Sokol, N.V.; Donchenko, L.V. Ispol'zovanie pektina s cel'yu uluchsheniya kachestva hleba. *Uspekhi sovremennogo estestvoznaniya* 2005, 5, pp. 60-61.
44. Auelbek, A.; Aimenova, Z.; Abai, G.; Usenova, U.; Daulbaj, A. Physical and chemical properties of triticale grain. *Internauka* 2019, 3, pp. 6-8.
45. Rosell, C. M.; Koehler, P. Chemistry of Cereal Grains. *Handbook on Sourdough Biotechnology* 2023, pp. 25-66.
46. Singh, K.; Kayastha, A. M. α-Amylase from wheat (*Triticum aestivum*) seeds: its purification, biochemical attributes and active site studies. *Food chemistry* 2014, 162, pp. 1-9.
47. Kan, A. Characterization of the fatty acid and mineral compositions of selected cereal cultivars from Turkey. *Records of Natural Products* 2015, 9(1), 124.
48. Codină, G.G.; Ursachi, F.; Dabija, A.; Paiu, S.; Rumeus, I.; Leatamborg, S.; Lupascu, G.; Stroe, S.-G.; Ghendov-Mosanu, A. Physicochemical Properties, Polyphenol and Mineral Composition of Different Triticale Varieties Cultivated in the Republic of Moldova. *Molecules* 2025, 30, 1233.
49. Gricenko, S. A. *Razrabotka tekhnologii hleba funkcional'nogo naznacheniya na osnove muki tritikale*. Krasnodar, Rossiya, 2003, 24 p.
50. Garutti, M.; Nevola, G.; Mazzeo, R.; Cucciniello, L.; Totaro, F.; Bertuzzi, C.A.; Caccialanza, R.; Pedrazzoli, P.; Puglisi, F. The Impact of Cereal Grain Composition on the Health and Disease Outcomes. *Front Nutr*. 2022, 25(9), 888974.
51. Hoseney, R. C. *Principles of cereal science and technology*. AACC International PRESS, MN, USA, 2010, 280 p.
52. Belopuhov, S. L.; Novikova, A. V.; Tolmacheva, T. A. Perspektivy pererabotki semyan maslichnogo l'na. *Innovacii v sel'skom hozyajstve i ekologii* 2020, 7, pp. 15-28.
53. Statistical data bank: Social statistics. Available online: https://statistica.gov.md/ro (accessed on 18.09.2024).
54. Chertov, E.D.; Magomedov, G.O.; Zacepilina, N.P.; Reprynceva, T.A.; Dorsosockaya, E. O.; Lygin, V.V.; Cheshinskij, V. L. Sbivnye hlebobulochnye izdeliya dlya pitaniya shkol'nikov. *Hleboprodukty* 2014, 11, pp. 58-60.
55. Magomedov, G.O.; Olejnikova, A.Ya.; Saevyakova, T.A. *Tekhnologiya muchnyh konditerskih izdelij*. Uchebnoe posobie, Moskva, Rossiya, 2009, 296 p.
56. Tertychnaya, T. N. Teoreticheskie i prakticheskie aspekty primeneniya tritikale v proizvodstve hlebobulochnyh i muchnyh konditerskih izdelij povyshennoj pishchevoj cennosti. *Vestnik VGAU* 2010, Voronezh, Russia, 341 p.
57. Donchenko, L.V.; Kruglyakova, S.A.; Roslyakov, Yu.F.; Sokol, N.V. Vliyanie pektinovyh veshchestv na kachestvo hleba iz muki tritikale. In: *Nauchno-prakticheskaya konferenciya «Molodye uchenye-pishchevym i pererabatyvayushchim otraslyam APK», tekhnologicheskie aspekty proizvodstva* 2000, pp. 37-46.
58. Erkinbaeva, R.K. Mikrobiologicheskie sposoby povysheniya kachestva hleba iz muki tritikale. *Introdukciya mikroorganizmov v okruzhayushchuyu sredu* 1994, pp. 120-128.
59. Kandrokov, R.H. Sposob polucheniya tritikalevo-rzhano-l'nyanoj muki. *Patent* 2021, RU 2761559 C1.
60. Woś, H.; Brzeziński, W. Triticale for food. *Quality driver Springer* 2015, pp. 213-232.

61. Fraś, A.; Gołębiewska, K.; Gołębiewski, D.; Mańkowski, D. R.; Boros, D.; Szecówka, P. Variability in the chemical composition between triticale grain, flour and bread. *Journal of Cereal Science* 2016, 71, pp. 66-72.
62. Pena. R.J.; Amaya, A. Milling and breadmaking properties of wheat-triticale blends. *Journal of the Science of Food and Agriculture* 1992, 60, pp. 483–487.
63. Tertychnaya, T.N.; Krechetova, S.V.; Derkanosova, N.M. Optimizaciya receptury hleba povyshennoj pishchevoj cennosti na osnove tritikale. *Hlebopechenie Rossii* 2003, 1, pp. 16-18.
64. Babaeva, B.S. Tritikale-poleznyj gibrid. *Nauka i molodyozh': novye idei i resheniya* 2016, pp. 433-435.
65. Tertychnaya, T.N. Ispol'zovanie tritikalevoj muki v proizvodstve keksa. *Hranenie i pererabotka sel'hozsyr'ya* 2008, 2, p. 70.
66. Kondratenko, R.G.; Nazarenko, E.A.; Erkinbaeva, R.K. Perspektiva ispol'zovaniya muki tritikale v konditerskoj promyshlennosti. *Pishchevaya promyshlennost'* 2000, 3, p. 36.
67. Novikova, A.A.; Tolmacheva, T.A.; Merkur'ev, N.V. Izuchenie kachestva makaronnyh izdelij iz muki zerna tritikale. *Biotekhnologicheskie priemy proizvodstva i pererabotki sel'skohozyajstvennoj produkcii* 2021, pp. 197-202.
68. Sarkar, A.; Fu, B.X. Impact of Quality Improvement and Milling Innovations on Durum Wheat and End Products. *Foods* 2022, 11, 1796. https://doi.org/10.3390/foods11121796.
69. Sissons, M. Role of durum wheat composition on the quality of pasta and bread. *Foods* 2008, 2, pp. 75–90.
70. Urubkov, S.A.; Smirnov, S.O. Perspektivnye tekhnologicheskie resheniya proizvodstva makaronnoj muki iz zerna tritikale, i primenenie produktov ego pererabotki pri izgotovlenii makaronnyh izdelij. *Hranenie i pererabotka zerna - nauchno prakticheskij zhurnal* 2014, 2(179), pp. 34-38.
71. Smirnov, S.O.; Urubkov, S.A. Razrabotka universal'noj tekhnologii proizvodstva makaronnoj muki ili krupki iz zerna tritikale. *Tritikale* 2016, pp. 202-217.
72. Lemekhova, A.A. Kislomolochnye produkty s prorostkami zlakovyh kul'tur. *Molochnaya promyshlennost'* 2012, 10, pp. 58-61.
73. Krasnova, Yu.V.; Butova, S.N.; Gun'kin, V.A.; Pureckij, A.A.; Suslyanok, G.M. Sposob proizvodstva pektinsoderzhashchego produkta iz shelushenyh semyan podsolnechnika. *Patent* 2017, RF № 2619241.
74. Gun'kin, V.A.; Suslyanok, G. M. Sposob proizvodstva hlop'ev iz shelushenogo zerna ovsa. *Patent* 2014, RF № 2504214.
75. Butova, S.N.; Gun'kin, V.A.; Pureckij, A.A.; Suslyanok, G.M. Sposob proizvodstva pektinsoderzhashchego produkta iz zerna l'na. *Patent* 2017, RF № 2619385.
76. Gun'kin, V.A.; Suslyanok, G.M.; Vani, D.A. Poluchenie gotovogo zavtraka v vide hlop'ev iz zerna tritikale. *Health, Food & Biotechnology* 2019, 1(3), pp. 47-56.

Citation: Suhovici, D.; Paiu, S.; Rumeus, Iu.; Boeștean, O.; Codină, G.G.; Ghendov-Mosanu, A. Current and prospective directions in the use of the grain crops triticale. *Journal of Engineering Science*. 2025, XXXII (1), pp. 136-150. https://doi.org/10.52326/jss.utm.2025.8(2).11.

Submission of manuscripts: jes@meridian.utm.md